# ‘Next generation’ chromatographic media for biopharmaceutical manufacturing

By
Johannes Christian Mohr

A thesis submitted to
The University of Birmingham
for the degree of
DOCTOR OF PHILOSOPHY

School of Chemical Engineering
The University of Birmingham
January 2019

# Instead of a dedication

Toute la joie silencieuse de Sisyphe est là. Son destin lui appartient. Son rocher est sa chose. De même, l'homme absurde, quand il contemple son tourment, fait taire toutes les idoles. Dans l'univers soudain rendu à son silence, les mille petites voix émerveillées de la terre s'élèvent. Appels inconscients et secrets, invitations de tous les visages, ils sont l'envers nécessaire et le prix de la victoire. Il n'y a pas de soleil sans ombre, et il faut connaître la nuit. L'homme absurde dit oui et son effort n'aura plus de cesse. S'il y a un destin personnel, il n'y a point de destinée supérieure ou du moins il n'en est qu'une dont il juge qu'elle est fatale et méprisable. Pour le reste, il se sait le maître de ses jours. À cet instant subtil où l'homme se retour- ne sur sa vie, Sisyphe, revenant vers son rocher, contemple cette suite d'actions sans lien qui devient son destin, créé par lui, uni sous le regard de sa mémoire, et bientôt scellé par sa mort. Ainsi, persuadé de l'origine tout humaine de tout ce qui est humain, aveugle qui désire voir et qui sait que la nuit n'a pas de fin, il est toujours en marche. Le rocher roule encore.
Je laisse Sisyphe au bas de, la montagne! On retrouve toujours son fardeau. Mais Sisyphe enseigne la fidélité supérieure qui nie les dieux et soulevé les rochers. Lui aussi juge que tout est bien. Cet univers désormais sans maître ne lui paraît ni stérile ni futile. Chacun des grains de cette pierre, chaque éclat minéral de cette montagne pleine de nuit, à lui seul, forme un monde. La lutte elle-même vers les sommets suffit à remplir un cœur d'homme.
Il faut imaginer Sisyphe heureux.
(Camus, 1942)

All Sisyphus' silent joy is contained therein. His fate belongs to him. His rock is his thing. Likewise, the absurd man, when he contemplates his torment, silences all the idols. In the universe suddenly restored to its silence, the myriad wondering little voices of the earth rise up. Unconscious, secret calls, invitations from all the faces, they are the necessary reverse and price of victory. There is no sun without shadow, and it is essential to know the night. The absurd man says yes and his effort will henceforth be unceasing. If there is a personal fate, there is no higher destiny, or at least there is but one which he concludes is inevitable and despicable. For the rest, he knows himself to be the master of his days. At that subtle moment when man glances backward over his life, Sisyphus returning toward his rock, in that slight pivoting he contemplates that series of unrelated actions which becomes his fate, created by him, combined under his memory's eye and soon sealed by his death. Thus, convinced of the wholly human origin of all that is human, a blind man eager to see who knows that the night has no end, he is still on the go. The rock is still rolling.
I leave Sisyphus at the foot of the mountain! One always finds one's burden again. But Sisyphus teaches the higher fidelity that negates the gods and raises rocks. He too concludes that all is well. This universe henceforth without a master seems to him neither sterile nor futile. Each atom of that stone, each mineral flake of that night-filled mountain, in itself forms a world. The struggle itself toward the heights is enough to fill a man's heart.
One must imagine Sisyphus happy.

“Jojo, wenn du die Chaosarmee jetzt nicht umbringst, dann ist die am Ende ja gar nicht tot?!“ - T. Ahlich (2015)

# Thesis abstract

Novel ways to produce bilayered chromatography adsorbent media featuring a functionalised core surrounded by an inert size exclusion layer for nanoplex purification were explored.

Surface functionalisation of anion exchange chromatography media via cold atmospheric pressure plasma etching and oxidation was investigated. Both, a dielectric barrier discharge plasma generation system and a fluidised bed underwater reactor produced bead samples with significantly reduced surface binding, while maintaining their core binding capacities.

A 3D visualisation method, allowing the study of the binding topography of the spatial distribution of pDNA and BSA adhered to Q ligands within particles was developed. This CLSM method revealed imperfections on the surface of adsorbents, providing additional binding sites for pDNA due to micro crevices.

Implementing beads with a more homogenous surface, restricted access media were produced via an AGE activation-partial bromination method. The thickness and homogeneity of the size exclusion layer was controlled via viscosity enhanced reaction diffusion balancing, yielding a distinct layer devoid of ligands. The particles did not show residual pDNA binding and selectivity of core vs surface binding increased by 100-fold cf. previous studies.

The commercial adsorbent Capto Core 700 was successfully implemented as a first capture step for pDNA purification from crude *E.coli* lysates.

# Acknowledgments

I would like to express my sincerest gratitude to Professor Owen Thomas for his patience, constant encouragement and guidance to find my way.

A very big thanks to Professor Daniel Bracewell and Dr James Walsh for their academic supervision and input to this work.

The Centre for Doctoral Training (CDT) for funding this project and embedding it in a larger community of fellow researchers.

Thank you to David Boylin, Elaine Mitchell and Dr Martina Modic for your help and advice with technical support and assistance with some of the experiments.

To all my research group colleagues at the Biochemical Engineering Department at the University of Birmingham, it was a pleasure to meet and work with you throughout my time in Birmingham.

Ich möchte meinen ganz speziellen Dank meiner Familie aussprechen. Ohne eure Nachsicht, Uneigennützigkeit, Energie und Vertrauen wäre ich heute nicht da wo ich bin.

Several other people that left without saying.

# Table of Contents

# Table of Figures

**Chapter 1 Introduction**



**Chapter 2 Materials and Methods**

**Chapter 3 Cold atmospheric pressure plasma etching and oxidation of AEC media for preparation of multifunctional bilayered supports**

**Chapter 5 Characterization of the commercial bilayered chromatography resin Capto® Core 700**

# List of Tables

# Abbreviations

| | |
|---|---|
| **AEC** | Anion Exchange Chromatography |
| **AGE** | Allyl Glycidyl Ether |
| **APGD** | Atmospheric pressure glow discharge |
| **BCA** | Bicinchoninic Acid |
| **BSA** | Bovine Serum Albumin |
| **CC700** | Capto Core 700 |
| **ccc** | Covalently Closed-Circular |
| **CEC** | Cation Exchange Chromatography |
| **CGMP** | Current Good Manufacturing Practice |
| **CIP** | Cleaning in Place |
| **CR** | Congo red |
| **CSLM** | Confocal Laser Scanning Microscopy |
| **ct** | Calf Thymus |
| **CV** | Column Volume |
| **DBD** | Dielectric Barrier Discharge |
| **DMSO** | Dimethyl Sulfoxide |
| **DOT** | Dissolved Oxygen Tension |
| **DPA** | Diphenylamine |
| **ds** | Double stranded |
| **EB** | Expanded Bed |
| **em** | Emission |
| **EMEA** | European Medicines Evaluation Agency |
| **ESEM** | Environmental Scanning Electron Microscope |
| **EtOH** | Ethanol |
| **EU** | Endotoxin Units |
| **ex** | Excitation |
| **FB** | Fluidised Bed |
| **FBR** | Fluidised Bed Reactor |
| **FDA** | Food and Drug Administration |
| **FF** | Fast Flow |
| **GuHCl** | Guanidine Hydrochloride |
| **HCP** | Host Cell Protein |
| **HIC** | Hydrophobic Interaction Chromatography |
| **HPLC** | High Performance Liquid Chromatography |
| **HSC** | Hematopoietic Stem Cell |
| **IEC** | Ion Exchange Chromatography |
| **IgM** | Immunoglobulin M |
| **kbp** | Kilo Base Pair |
| **LAL** | Limulus Amebocyte Lysate |
| **LB** | Luria Bertani |
| **LUT** | Look Up Table (for fluorescence correlation) |
| **M&M** | Materials and Methods |
| **MMC** | Mixed Mode Chromatography |
| **MO** | Methylene Orange |
| **MQW** | Milli-Q Water |
| **n** | Amount of substance (mol) |
| **NA** | Nucleic Acid |
| **NaCl** | Sodium Chloride |
| **oc** | Open Circular |
| **OD** | Optical density |
| **PCR** | Polymerase Chain Reaction |
| **pDNA** | Plasmid DNA |
| **PPG** | Polypropylene Glycol |
| **PSD** | Particle Size Distribution |
| **Q** | Quaternary Amine |
| **RAM** | Restricted Access Media |
| **ROI** | Region of interest |
| **ROS** | Reactive Oxygen Species |
| **SBV** | Settled Bed Volume |
| **sc** | Supercoiled |
| **SEC** | Size Exclusion Chromatography |
| **SLM** | Standard litres per minute |
| **TE** | Tris-EDTA |
| **QC** | Quality Control |
| **VE-RDB** | Viscosity Enhanced Reaction Diffusion Balancing |
| **WHO** | World Health Organization |

# Chapter 1 Introduction

## 1.1. Gene therapy and DNA vaccination

It is within the authors awareness that the following section concerning gene therapy is not directly interconnected with subsequent parts of this thesis, focussing on the practical implementation of a DSP unit operation for nanoplex purification. However, as nanoplex of choice throughout the study pDNA was chosen.
It is hence desired to give the reader an introductory overview over a promising field of application.

### 1.1.1. Overview

In medical terms, human gene therapy has been defined as the precise and intentional delivery of therapeutic genetic material into a patient's cells as a drug to treat disease.
Its impact on human healthcare in the future is promising and expected to offer a plethora of therapeutic options for treating and improving control over cancer and several devastating medical conditions (Kay, 2011).
Gene therapy as a way to cure genetic defects by replacing defective DNA with 'exogenous good DNA' was first conceptualised in the 1960s and early 1970s (Friedmann *et al.*, 1972). The first approved successful gene therapy in human was conducted in 1990, when Ashanti DeSilva was treated for severe combined immunodeficiency disorder. The 4-year-old girls' immune system could be partially restored using ex vivo gene transfer of a healthy adenosine deaminase gene copy into T-cells followed by reinjection of the altered cells into her blood stream (Anderson, 1990; Rosenberg *et al.*, 1990).
This and other early breakthroughs sparked scientific enthusiasm for gene therapy and conceptually similar pDNA vaccination using viral vectors as delivery vehicles. In 1999, Jesse Gelsinger died of an immune rejection response caused by viral vector associated toxicity, while participating in a clinical trial of a viral gene therapy agent designed to treat ornithine transcarbamylase deficiency. This incident tempered the rapid development of gene therapies and raised interest in non-viral vectors as potentially safer options, for gene delivery (Glover *et al.*, 2005; Wilson, 2009).

Despite the sorrowful 1999 setback, from 1989 to 2018, more than 2800 clinical trials associated with gene therapy were conducted (Edelstein, 2018) and in 2003 the first gene therapy product "Gendicine" was approved for clinical use in humans. It is a cancer gene therapy delivering the tumor suppressor gene p53 via a recombinant adenovirus and was approved by the Chinese Food and Drug Administration for the treatment of squamous cell carcinoma (Pearson *et al.*, 2004; Wilson, 2005). The first gene therapy treatment receiving approval in the Western World by the European Medicines Agency (EMA) was Glybera, designed for reversion of lipoprotein lipase deficiency (uniQure, 2012). Recently, in August 2017, the US Food and Drug Administration (FDA) approved the first form of human gene therapy in the US- Tisagenlecleucel (marketed as Kymriah) is an adaptive *ex-vivo* T-cell therapy (viral delivery) for B-cell acute lymphoblastic leukaemia (FDA, 2017b).

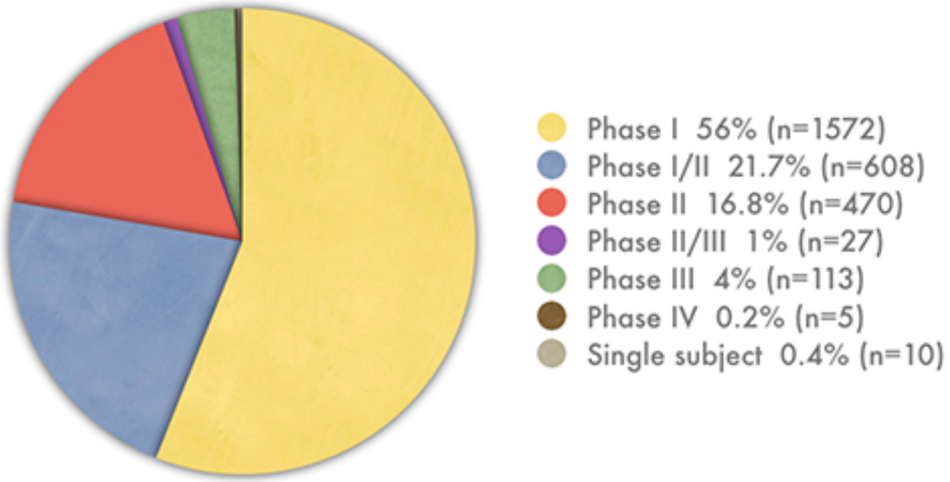


Figure 1-1 Gene therapy clinical trials worldwide in various development stages from 1989 to 2018 (Edelstein, 2018)

Generally, gene therapy aims to cure genetic disorders, caused by mutations in the gene sequence that if left uncorrected cause expression of ill phenotypes. These can either be hereditary in nature or caused by new mutations in the hosts gDNA.

These genetic defects can be repaired by making functional genes available to the cells by either: (i) replacing the mutated gene with a working copy (replacement therapy); (ii) addition of a working copy (supplement therapy); or (iii) inactivation of the malfunctioning gene ('knock-out') (Yang *et al.*, 1996).

In general, gene therapy could be applied to all human cell types (Parker *et al.*, 2003). Yet, somatic (non-reproductive) cells are generally safer than germ-line cells, due to their inability

to pass genomic alterations on to future generations, therefore limiting potential off-target effects to the treated individual rather than its offspring.

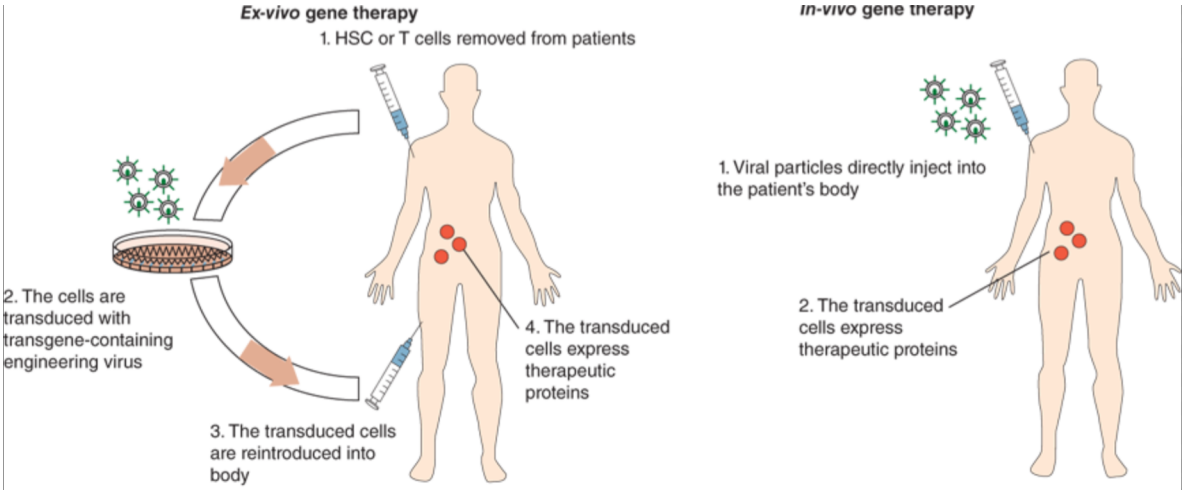


Figure 1-2 Ways genetic material can be administered to the human body for gene therapy; (image retrieved from (Kaushansky *et al.*, 2016))

For the delivery of therapeutic genetic material, scientists have explored two different types of strategies: '*ex vivo*' and '*in vivo*' (Figure 1-2). In the *ex vivo* route of administration cells are extracted either from the patient (autologous) or from a different host (allogenic), transduced with the therapeutic genetic material, optionally multiplied in a laboratory and (re-) administered to the patient. Modifying cells outside the human body is generally preferred as it allows for harsh transfection conditions (e.g. electroporation etc.) to be used and limits genetic alteration to the target cell population. However, these techniques are limited to cells amenable to surgical removal and re-administration (i.e. blood cells, skin cells) and often fail for cell types requiring embedding in intricate functional networks for their function (i.e. neurons). In contrast, *in vivo* techniques work by directly injecting carriers of therapeutic genetic material into the body.

### 1.1.2. Gene delivery systems

Common for most different ways to introduce therapeutic genes into patients, the success of gene therapy as a therapeutic treatment of diseases remains a delivery challenge to date (Gonçalves *et al.*, 2017). Ideally, delivery of exogenous DNA is cell type specific and provides a precise amount of genetic material being delivered to each cell, allowing for gene expression but avoiding toxicity (Mali, 2013). Further, the ideal gene delivery vehicle accommodates foreign DNA of sufficient size for the target application, achieves ample levels of long-lasting transgene expression and is non-immunogenic (Gardlik *et al.*, 2005; Shillitoe, 2009).

The plethora of gene delivery approaches can be divided into three main categories, non-viral delivery strategies such as (i) physical methods and (ii) chemical carriers as well as (iii) viral vector based strategies (i.e. gene transfer via viral vectors is called transduction cf. transfection for non-viral vectors (Biceroglu *et al.*, 2005; Ramamoorth *et al.*, 2015).

### 1.1.3. Non-viral delivery strategies

Poor toxicological profiles associated with viral vectors have sparked interest in non-viral vectors in clinical gene therapy (Akhtar, 2005). Other incentives for non-viral vector delivery techniques are mainly associated with the lack of immune responses, as well as comparatively easy manufacturing and assembly (Merdan *et al.*, 2002).

In depth discussion about non-viral delivery vectors for gene therapy, highlighting advantages and disadvantages of each technique are plentiful in the literature, the following paragraphs hence aim to provide a brief overview over the most commonly applied methods (Parker *et al.*, 2003; Patil *et al.*, 2005; Mali, 2013; Ramamoorth *et al.*, 2015; Altwaijry *et al.*, 2018).

Physical methods employ physical force to introduce genetic material into cells, by countering the membrane barrier.

Initially the use of naked plasmid DNA for systemic gene delivery was discarded as unrealistic due to rapid DNA degradation by endogenous nucleases. However, direct injection of pDNA into a patient's blood stream constitutes the simplest way to introduce genetic material to host cells (Parker *et al.*, 2003). Needle injections of naked pDNA have been employed for gene therapy applications in tissues such as muscle, skin, liver and solid tumours, however, rapid degradation by endonucleases yield very low efficiencies.

Particle bombardment (i.e. gene gun) aims to deliver DNA coated heavy metal particles with the aid of high velocity. The necessary speed is hereby evoked via high voltage electronic discharges, gas pressure discharge or spark discharges (Al-Dosari *et al.*, 2009; Aravindaram *et al.*, 2009).

Electroporation utilises an electrostatic field causing an electric potential difference greater than the trans-membrane pressure of the cell, leading to transient breakdown of the membrane. The formation of pores allows genetic material to be incorporated into the cell before it regenerates (reversible). Irreversible electroporation uses high power electric fields to permanently disrupt cell membranes. The technique has been successfully used in cancer treatment for destroying cancer cells via electroporation or utilising the created pores as an entry point for gene delivery (Au *et al.*, 2013; Deipolyi *et al.*, 2014). The method has emerged as a reliable tool for pDNA delivery intradermally, intratumoural, intramuscularly, as well as 'ex vivo' (Regnier *et al.*, 2000; Zhang *et al.*, 2002; Shirley *et al.*, 2014).

In sonoporation, genetic material is incorporated into micro-bubbles and administered to patients. Subsequent application of ultrasound waves cause localised, temporary permeability of the cell membrane via cavitation, allowing uptake of genetic material in close proximity (Newman *et al.*, 2007).

Delivery via the use of photoporation is in concept similar to electroporation. Single laser pulses shoot holes into cell membranes leading to uptake of genetic material through transient pores. The technique is still in an early experimental stage, lacking documented clinical application (Li *et al.*, 2007; Ramamoorth *et al.*, 2015).

Magnetofection couples therapeutic genes to magnetic nanoparticles which can be kept at the target site via strong external magnets. Following enzymatic cleavage of crosslinking molecules in the complex, DNA molecules are released. The technique mostly finds application *'in vitro'* (Dobson, 2006). Other physical methods include hydroporation and mechanical massage (Herweijer *et al.*, 2007; Su *et al.*, 2012)

In contrast to physical transfection methods, chemical transfection introduces the gene of interest via the use of inorganic particles or lipid-, polymer- or peptide-based vectors (Su *et al.*, 2012). Among other inorganic particles, the use of calcium phosphate, calcium chloride,

silica, gold, magnetic compounds and fullerenes are the most applied methods (Al-Dosari *et al.*, 2009; Mali, 2013).

Most chemical vectors condense DNA via electrostatic interactions, protecting the molecule from nucleases of the host, while DNA complexation reduces the charge repulsion of the cell membrane and DNA, aiding delivery into the cells (McCrudden *et al.*, 2013). Non-viral vectors can complex large DNA molecules in addition to targeting of specific tissues due to the use of targeting ligands (Altwaijry *et al.*, 2018).

Liposomes as a chemical formulation comprise of a phospholipid bilayer, forming a spherical vesicle around the genetic material (Allen, 1997). Cationic lipids bind strongly to DNA molecules encapsulated inside, providing protection against nuclease degradation (lipoplex). The positive net charge of the liposome aids transport of the pDNA product to target cells through the blood stream (Gregoriadis *et al.*, 2000).

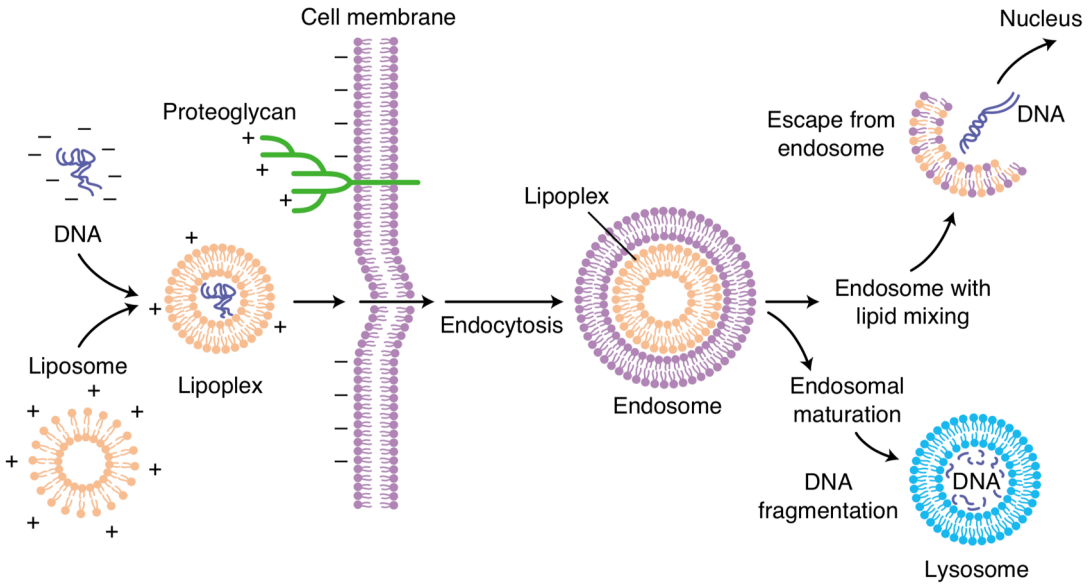


Figure 1-3 Lipoplex-mediated transfection and endocytosis (Parker *et al.*, 2003)

The internalization mechanism of lipoplexes is thought to be mediated by endocytosis (Figure 1-3). Although the majority of endosomes fuse with lysosomes degrading the DNA, some will be released into the cytoplasm where they can travel to and fuse with the nucleus, culminating in gene expression (Parker *et al.*, 2003). Linking neutral colipids such as dioleoylphosphatidylethanolamine (DOPE) or cholesterol to the liposomes improves

transfection through the cell membrane by promoting endosomal escape and release of pDNA into the cytoplasm (Fasbender *et al.*, 1997).

Polymersomes are synthetic versions of liposomes, made of amphiphilic copolymers (Figure 1-4). Polycationic polymers readily complex pDNA molecules, condensing them in the process due to their high avidity (Brenner *et al.*, 2014). Several different copolymers have been used to form nanoparticle-DNA complexes, with polylysine and polyethylenimine being the most significant candidates (Cherng *et al.*, 1999). Similar to the protection granted by liposomes, polymerosomes protect the enclosed NA against degradation until its release into the cytoplasm. However, delivery via synthetic polymers offers several advantages over liposome formulations such as enhanced mechanical strength, plasmid storage capacity and blood circulation time (Krishnamoorthy *et al.*, 2014; Yin *et al.*, 2014). However, both lipids as well as cationic polymers show inherent toxicity to the host, limiting applicable dosage sizes (Lv *et al.*, 2006).

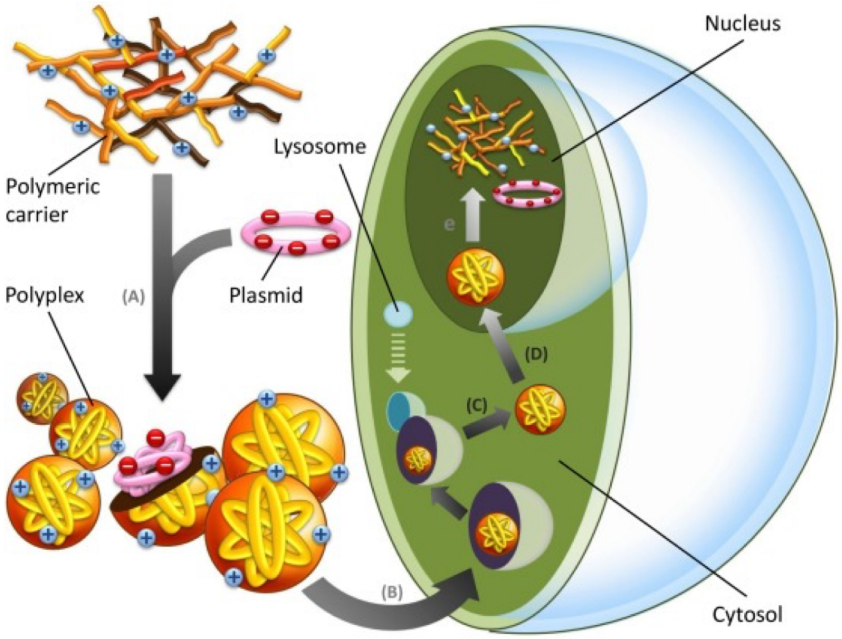


Figure 1-4 Intracellular gene delivery mediated by a polymeric gene carrier; therapeutic nucleic acid is mixed with a cationic polymers to form polyplex particles which can enter target cells by endocytosis; major processes include electrostatic interactions (A), cellular internalization (B), endosomal escape (C), nuclear translocation (D) and polyplex dissociation (E) (image adapted from (Lai *et al.*, 2018))

### 1.1.4. Viral delivery vectors

Recombinant, replication-defective viral vectors were the first molecular tools used to enable efficient, nontoxic gene transfer into human somatic cells (Kotterman *et al.*, 2015)

Despite recent advances made in the development of non-viral based strategies, viral vectors are still by far the most commonly used delivery methods in clinical trials (Figure 1-5) (Ginn *et al.*, 2018). Selection of viral system of choice is typically based on safety considerations, target cell specificity and availability of permissive cells (Wu *et al.*, 2000).

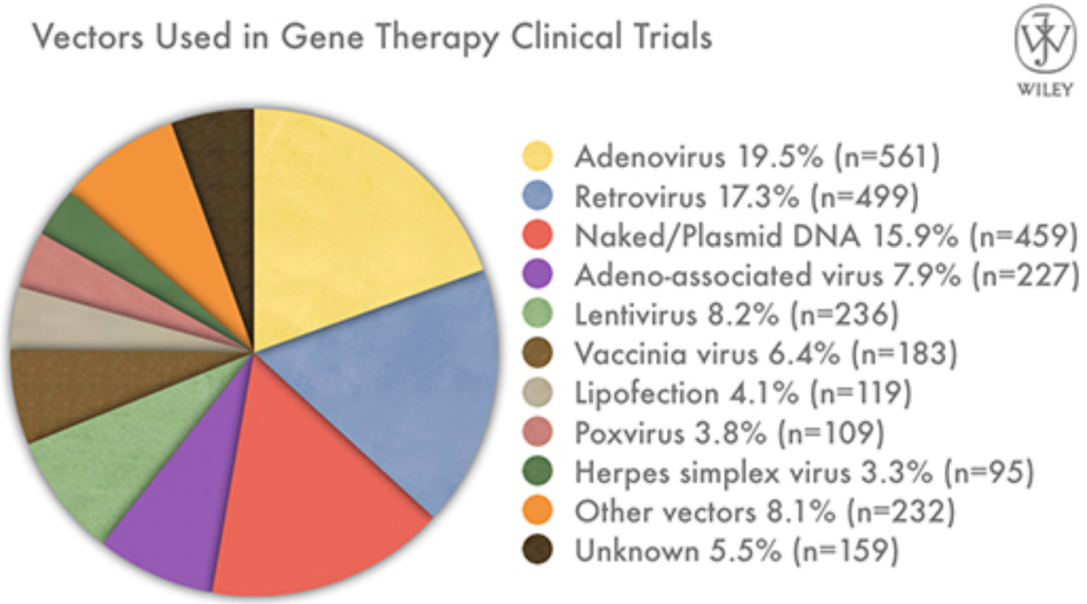


Figure 1-5 Gene therapy vectors currently used in clinical trials (data retrieved from the Journal of Gene Medicine; http://www.abedia.com/wiley/vectors.php; last modified August 2018; accessed December 2018)

Gene delivery via viral vectors has several advantages over chemical and physical methods, such as high transduction efficiency and targeting precision *in vivo* (Selvam *et al.*, 2006). Furthermore, physical and chemical methods demand repeated dosage applications, whereas fewer (single) administrations may be sufficient for viral delivery methods (Xi *et al.*, 2003).

The main disadvantages for the application of viral vectors as gene delivery vehicles are associated with safety concerns (immunogenicity and insertional mutagenesis), size limitations for therapeutic DNA constructs, as well as manufacture and quality control (Phillips, 2001).

Among other criteria for categorisation, viral delivery can be divided into (i) integrating and (ii) non- integrating viral vectors.

In order to replicate, viruses introduce their genetic material into (human) host cells by tricking its cellular machinery to use the viral genome as a blueprint for replication. Integrating viruses hereby insert their genome at a specific spot in the genome. Scientists have utilised this property by altering viruses to transduce therapeutic genes instead of their own. Elimination of obligate viral genes has led to replication deficient viruses causing reduced biosafety concerns as they require complementation of helper genes for successful replication only possible in laboratory environment. (Mali, 2013). Among other integrating viral vectors, retroviruses (such as lentiviruses), and adeno-associated-virus have shown the most promising transduction results in clinical trials (Verma, 2013; Yin *et al.*, 2017).

Retroviruses can either be replication-competent or replication-defective. The biggest limitations for the use of retroviruses as gene delivery vehicles are the limited size of the gene insert they can accommodate (between 8-10 kbp for replication defective retroviruses), and the requirement for cells to be actively dividing for transduction (Coffin *et al.*, 1997). The theoretical fear of insertional mutagenesis causing leukaemia or cancer became reality when 20% of patients involved in a gene therapy clinical trial aiming to treat X-linked severe combined immunodeficiency, using a retroviral formulation in 2002, developed leukaemia (Hacein-Bey-Abina *et al.*, 2002).

Adeno-associated virus is a small virus causing only a mild immune response in human patients and is generally seen as non-pathogenic. It can infect both, dividing and non-dividing cells, leading to long and stable gene expression (Nussbaum *et al.*, 2015). These features make adeno-associated viruses attractive candidates for gene delivery, however, size limitations of the gene insert (up to 5 kbp) severely hamper their application potential.

Among the group of non-integrating viral vectors, adenovirus is the most widely studied. Following infection, the adenoviral genome remains in the nucleus without integrating into chromosomal DNA. In most tissue types the duration of transgene expression is limited as the effects are prone to disappear after cell division (transient gene expression).

Table 1-1 compares the most important viral delivery vectors and non-viral delivery strategies, highlighting their advantages and restrictions (Mountain, 2000; Dunbar *et al.*, 2018).

Table 1-1 Advantages and disadvantages of different gene delivery vectors (adapted from (Mountain, 2000))

| Vector | Advantages | Disadvantages |
|---|---|---|
| **Adenovirus** | Very high transfection efficiency ex vivo and in vivo<br>Transfects proliferating and non-proliferating cells<br>Substantial clinical experience acquired<br>Efficient retargeted transfection demonstrated | Repeat dosing ineffective owing to strong immune responses<br>Insert-size limit of 7.5 kb<br>Manufacture, storage, quality control (QC) are moderately difficult<br>Short duration of expression |
| **Retrovirus** | Fairly prolonged expression<br>High transfection efficiency ex vivo<br>Substantial clinical experience ex vivo<br>Low immunogenicity | Low transfection efficiency in vivo<br>Insert-size limit of 8 kb<br>Transfects only proliferating cells<br>Safety concern of insertional mutagenesis<br>Manufacture, storage, QC are extremely difficult |
| **Lentivirus** | Transfects proliferating and non-proliferating cells<br>Transfects haematopoietic stem cells | Safety concerns from immunodeficiency virus origins<br>Manufacturing, storage, QC are extremely difficult<br>Insert-size limit of 8 kb<br>No clinical experience |
| **AAV** | Efficiently transfects a wide variety of cells in vivo<br>Very prolonged expression in vivo<br>Low immunogenicity | Insert-size limit of 4.5 kb<br>Manufacture, QC are very difficult<br>Little clinical experience<br>Safety concern of insertional mutagenesis<br>Repeat dosing affected by neutralizing antibody responses |
| **Naked pDNA** | Manufacturing, storage, QC are simple and cheap<br>Very low immunogenicity<br>Clinical efficacy demonstrated in critical limb ischaemia<br>Very good safety profile | Very short duration of expression in most tissues<br>Very inefficient transfection ex vivo and in vivo<br>Retargeting transfection very difficult |
| **Cationic lipids** | Relatively simple manufacturing, storage, QC<br>Efficient transfection ex vivo<br>Low immunogenicity<br>Good safety profile | Inefficient transfection in vivo<br>Very short duration of expression<br>Little clinical experience<br>Retargeting transfection difficult |
| **Condensed DNA particles** | Relatively simple manufacturing, storage, QC<br>Efficient transfection ex vivo<br>Low immunogenicity<br>Good safety profile<br>Retargeted transfection demonstrated | Inefficient transfection in vivo<br>Very short duration of expression<br>No clinical experience |

### 1.1.5. DNA vaccination

In addition to treating diseases, plasmids can be used as DNA vaccines for genetic immunization against several ailments. Vaccines have changed the quality and span of human life since their discovery and many diseases such as polio and tuberculosis have been eradicated in the western world, due to the availability of respective vaccines. Many more previously epidemic maladies can nowadays be contained and controlled due to the introduction of their vaccine.

These traditional vaccines work by presenting the patient's immune system with an immunogenic antigen via oral gavage or direct injection and causing an immune reaction leading to immunological memory. These antigens are typically attenuated or dead pathogens. There is also another way to present the body with a well-defined antigen: have the body transiently express said antigen in its own cells – this is called DNA vaccination.

Plasmids are well suited for use in vaccinations as, opposed to applications in gene therapy techniques, patient immunity does not require long-term, sustained expression of the transduced antigen and instead can be accomplished in short-term gene expression. To invoke an immune response, pDNA is injected into (predominantly) muscle tissue, where it is translated into an antigen protein. Plasmids as therapeutic agents in vaccination work differently than traditional vaccines, as they can stimulate the human immune system to produce both humoral and cellular responses, including the production of cytotoxic T lymphocytes (Phillips, 2001).

In comparison to traditional types of vaccination such as live attenuated viruses, weakened bacterial strains, modified endotoxins, viruses etc., pDNA vaccines are considered safe for administration and tolerated by human hosts. Further advantages over conventional vaccines based on viral formulations include moderate storage conditions and ease of large-scale production development (Ferreira *et al.*, 2000b). The main disadvantage of DNA vaccines cf. their viral counterparts, are low efficiency that, as a result, make the use of large dosages (up to several milligrams per full treatment) a necessary requirement (Ferreira *et al.*, 2000b).

Several pDNA vaccines have been approved for their use in veterinary medicine (Jorge *et al.*, 2017), however, to date no vaccine has been approved for the use in humans. Several diseases with complex etiologies such as cancer, neurodegenerative diseases such as Alzheimer's and

Parkinson's disease are being target by researchers and clinicians (Patil *et al.*, 2005; Yang *et al.*, 2014). In addition, pDNA vaccination techniques targeting ZIKA virus (Kudchodkar *et al.*, 2018), Dengue Virus (Danko *et al.*, 2018), human papillomavirus (Cheng *et al.*, 2018), AIDS and tuberculosis (Bruffaerts *et al.*, 2014) as well as many other diseases are currently being developed. Furthermore, DNA vaccines have also been investigated as a means to prevent allergic responses through desensitisation (Horner *et al.*, 2001). Currently the two most common approaches for delivery of pDNA vaccines are injection of DNA in saline buffers by hypodermic needle and delivery via the use of gene guns (Aravindaram *et al.*, 2009).
Experts estimate that annual production and purification of many kilograms or even tons of pDNA could become a necessity to satisfy future needs for large scale pDNA vaccination applications (Aldridge, 2006).

This demand puts the pressure on engineers to develop scalable, cost-effective methods capable of large scale pDNA production and purification that meet pharmacological purity standards.

## 1.2. Production and purification of plasmid DNA formulations

Many different nanoplex systems have been explored as gene therapy vectors for the delivery of pDNA to target cells. However, all of those processes require highly purified pDNA and plasmids have become an indispensable tool for the biotechnological industry, crucial for the production of pharmaceutical proteins, antibodies, vaccines, enzymes and molecular diagnostic tools (Prazeres *et al.*, 2014). This work centres around the production and formulation of naked pDNA for therapeutic applications.

The introduction of respective DSP techniques and unit operations, presented in the following paragraphs, hence focusses on their implementation for pDNA purification.

### 1.2.1. Structure and physicochemical properties of pDNA

For the development of a successful production and purification method of pDNA, an understanding of its structure and properties is imperative, to be able to exploit them for various purification strategies.

Plasmid DNA is a small, circular DNA molecule spatially separated from host cell chromosomal DNA, that can replicate autonomously within a suitable host. For that reason, it bears at least one sequence that serves as origin of replication initiating the replication (Brown, 2010).

Most commonly, plasmids can be found as double stranded (ds) DNA ring structures in bacteria, where they carry at least one specialised gene responsible for conditional characteristics in the cell (e.g. antibody resistances; adaptive metabolic functions, allowing the host to survive on different nutrient sources; ability to metabolise otherwise toxic compounds) (Casali, 2003). This characteristic is often used in laboratory applications, as it allows for bacterial selection within a culture, via antibiotic resistance genes carried by pDNA (Nethe-Jaenchen, 2001).

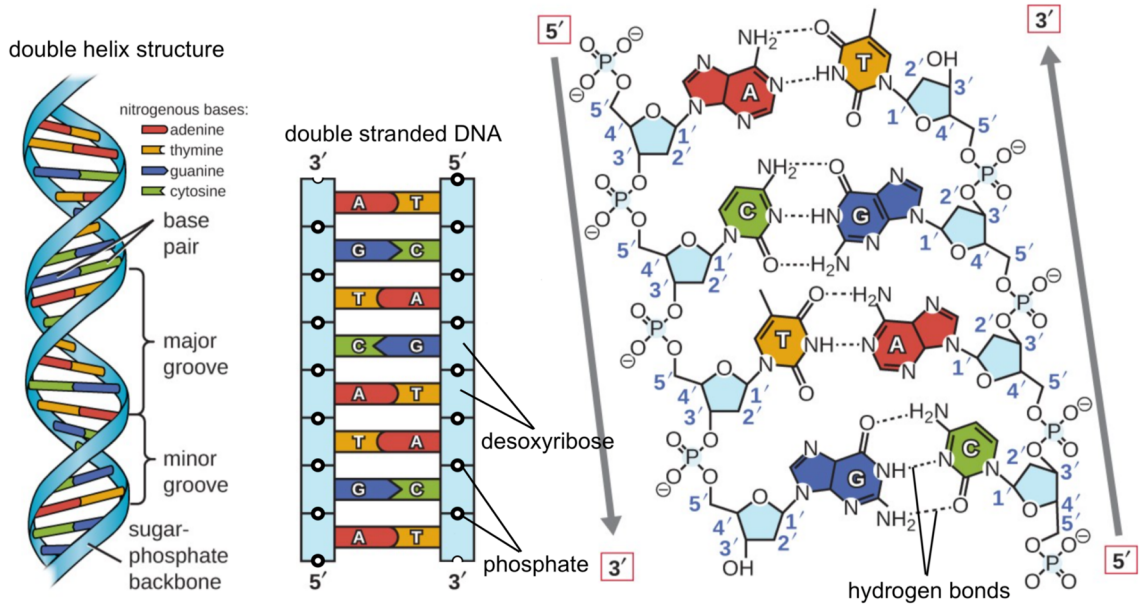


Figure 1-6 Structure of DNA (adapted and extended from (Lumen, 2018))

Its primary structure consists of a linear sequence of nucleotides, covalently linked together by phosphodiester bonds (Figure 1-6). Each nucleotide comprises of three components; a nitrogenous base (either adenine, guanine, cytosine or thymine), a 2-desoxyribose and at least one phosphate group (Lodish, 2000). DNA is a polymer comprising of repeating nucleotides, forming two helical chains, linked together via hydrogen bonding (secondary structure) (Watson *et al.*, 1953). These chains are coiled around the same axis with a diameter of ~2 nm and stabilised via base-stacking forces of aromatic nucleobases (AT and GC) in the hydrophobic centre of the molecule (Yakovchuk *et al.*, 2006).

The exterior of DNA is hydrophilic due to phosphate groups forming the backbone structure of the molecule. The phosphate groups are negatively charged at pH > 4, making the DNA molecule as a whole bear a partial negative charge (Sinden, 1994). pDNA has different conformations in which it occurs; these are mainly open circular (oc), linear and supercoiled/ covalently closed-circuit (sc/ccc) and its isoform has a large impact on the molecules spatial uptake (radius of gyration; ).

Table 1-2 Radius of gyration and M values from SLS analysis of sc, oc, and linear isoforms of 5.76, 9.80, and 16.8 kbp plasmids in 10 mM $Na_2$ EDTA-200 mM NaCl (Latulippe *et al.*, 2010)

| | Plasmid isoform | | | | |
|---|---|---|---|---|---|
| | | | Linear | | |
| Plasmid DNA size (kbp) | Supercoiled $R_G$ (nm) | Open-circular $R_G$ (nm) | $R_G$ (nm) | Experimental $M$ (Da) $\times 10^{-6}$ | Calculated[a] $M$ (Da) $\times 10^{-6}$ |
| 5.76 | $102 \pm 2$ | $130 \pm 3$ | $174 \pm 2$ | $3.67 \pm 0.26$ | 3.81 |
| 9.80 | $117 \pm 3$ | $157 \pm 5$ | $213 \pm 3$ | $6.50 \pm 0.60$ | 6.49 |
| 16.8 | $169 \pm 4$ | $193 \pm 5$ | $242 \pm 3$ | $10.7 \pm 0.2$ | 11.1 |

[a]Calculated molecular weight ($M$) determined using 662 Da per base pair.

In order to reduce the free Gibbs energy of the molecule, DNA contorts around itself in space, forming supercoils (Figure 1-7). Supercoiling (in nature) is important for a number of reasons, such as compaction of the molecule to limit its spatial uptake and regulation of access to the genetic code. Supercoiling furthermore increases the stability of the molecule via enhanced base exposure, leading to an increased net-charge compared to other conformations (Almeida *et al.*, 2015). Disruption of hydrogen bonding may cause unfolding and ultimately loss of the supercoiled (sc) isoform, however anchor base pairs prevent the separation of double strands and aids renaturation of sc conformation, given the pH does not raise above 12.5 (Diogo, 1999).

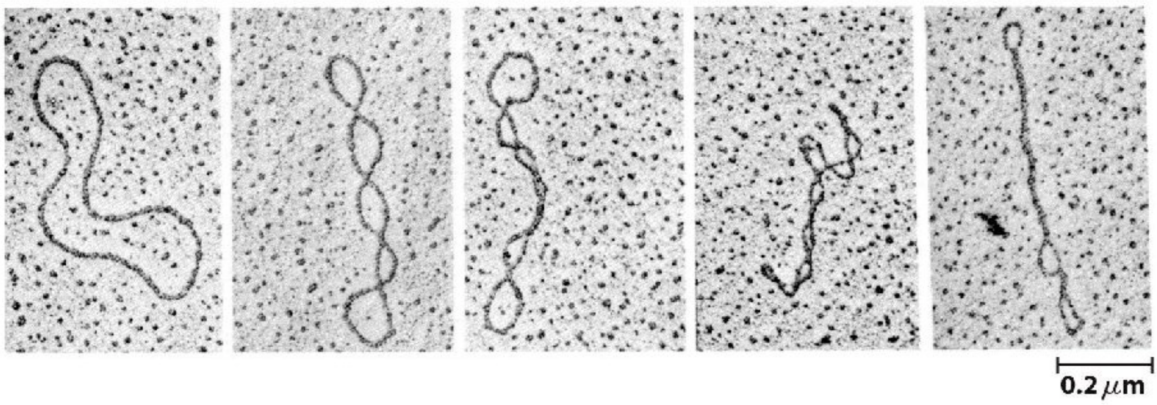


Figure 1-7 SEM images of pDNA; molecule on the far left is in oc conformation, with the level of supercoiling increasing from left to right (Kornberg *et al.*, 1992)

Other isoforms of pDNA occurring in cell lysates include open circular (single strand nick) and linear pDNA (result of a double strand nick, cleaving both phosphodiester bonds on opposite sides of the double strand, causing the molecule to unwind) (Thomas, 2008; Li *et al.*, 2011). Due to its length and circular nature of the molecule, knots or multimers (catenanes,

concatamers) can occur (Summers, 2009; Higgins *et al.*, 2015). Sizes of pDNA intended for vaccination range typically from 3-15 kilo base pairs (kbp), with estimations that sizes will increase in the future (Levy *et al.*, 2000). Although stable in solution, pDNA is shear sensitive and known to suffer structural damage when exposed to mechanical stress (Zhang *et al.*, 2007).

### 1.2.2. Industrial scale production of pharmaceutical grade pDNA

Since their application in gene therapy and use in vaccination, the demands for therapeutic pDNA formulations have increased tremendously over the past decades (Xenopoulos *et al.*, 2014).

From an industrial point of view, sc pDNA is the most desirable isoform of pDNA due to its stability, bioavailability (therapeutically most active form), eminent antigenicity and the fact that it is the isoform thought to be most effective at transferring gene expression (Prazeres *et al.*, 2001; Stadler *et al.*, 2004; Sousa *et al.*, 2012). The quality of pDNA formulations is as a result judged by their sc content, with the FDA specifying a minimum of 80% supercoiling for pDNA vaccines (FDA, 2007), with a quality of over 90% being recommended.

When developing a manufacturing process for pDNA formulations, it is important to comply with all quality specifications posed by the different regulatory agencies (such as European Medicines Evaluation Agency (EMEA), World Health Organization (WHO), Food and Drug Administration (FDA) and others, depending on the targeted market (Epstein, 1996). Beside regulatory constraints controlling the level of contaminants in final formulations, manufacturers are also being held responsible to comply with Current Good Manufacturing Practice (CGMP) to ensure high industrial manufacturing standards (WHO, 2007; FDA, 2017a; MHRA, 2017).

Table 1-2 Example of purity requirements for a pDNA vaccine, the required testing method is added in brackets (Prather et al., 2003) adapted from (Sagar, 2003)

| Contaminant | Purity requirement |
|---|---|
| **Endotoxin level (assessed by Limulus amebocyte lysate (LAL) test)** | <0.5 endotoxin units (EU)/mg pDNA |
| **Host cell protein (HCP) (Bicinchoninic acid (BCA) Assay)** | <1% |
| **gDNA (qPCR)** | <1% |
| **sc conformation of the product** | >90% |
| **RNA (HPLC ribose assay)** | <0.1% |

Outside of regulatory constraints, a production process for pDNA manufacturing needs to be economically viable. The choice of which unit operations to incorporate hence needs to be made with care, aiming to reduce the overall number of process steps to a minimum while maximizing plasmid yield in each (Figure 1-8). In a very broad sense, the production of therapeutic pDNA can be considered a three-step process, comprising of upstream manufacturing (vector design, transformation, fermentation and cell harvest), cell lysis and purification/ formulation (Figure 1-9) (Urthaler *et al.*, 2005a; Huber, 2008).

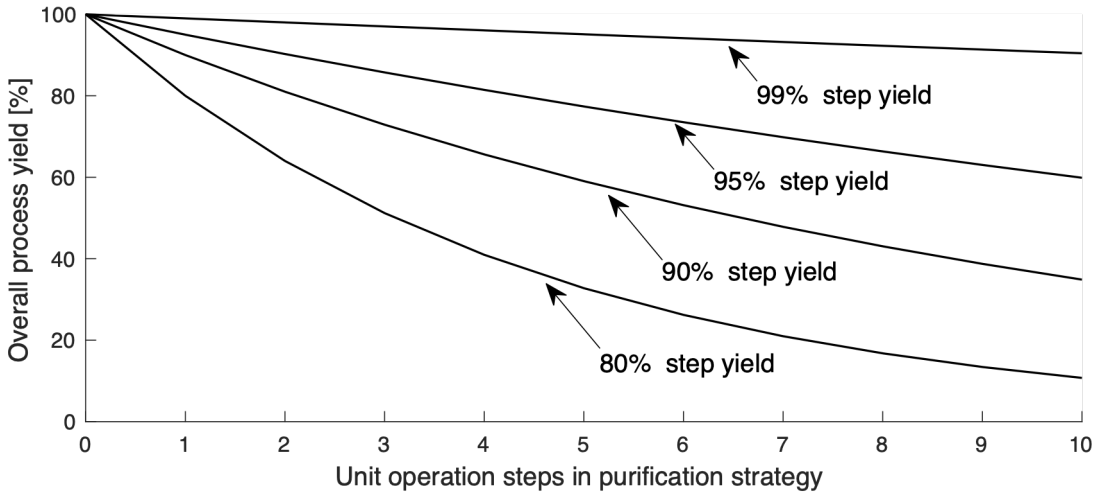


Figure 1-8 Even high single step yields can add up to significant product losses, threatening economic viability of a production strategy if too many unit operations are implemented

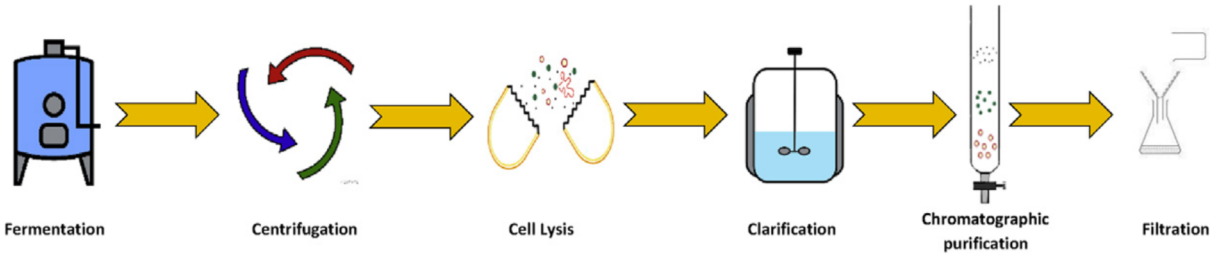


Figure 1-9 General structure of the production and formulation steps incorporated for pDNA manufacturing (Abdulrahman *et al.*, 2018)

On a commercial scale, pDNA is produced via biosynthesis in *E. coli* K12 strains (such as DH5α*),* a bacterial host that has been used extensively for bio-manufacturing of therapeutic proteins and pDNA (Carnes *et al.*, 2006).

Historically yields have been very low (<200 mg/L) however, recent advances in upstream protocols, have gradually led to increasing product titres, enabling cost effective plasmid

manufacture (Listner *et al.*, 2006; Singer *et al.*, 2009). Currently titres up to 2 g/L are achievable in optimised production facilities (Williams *et al.*, 2009).

The industrial scale production has been reviewed in depth in other studies (Swartz, 2001; Prather *et al.*, 2003; Williams *et al.*, 2009), in this work the main focus was put on purification of pDNA from *E. Coli* lysates.

### 1.2.3. Cell disruption and clarification/ pre-purification

In an initial solid-liquid separation step, the high-density fermentation broth is collected via centrifugation (Tinnes *et al.*, 1992) or microfiltration (Riesmeier *et al.*, 1989). In addition to concentrating the slurry, this harvest step aims at removing most of the used up fermentation broth, which otherwise can interfere with some purification techniques (Prather *et al.*, 2003).

The pDNA product is still locked inside the host bacteria (intracellular), thus purpose of cell lysis is to release the pDNA molecules from the biomass into the surrounding buffer (Abdulrahman *et al.*, 2018). This enables the pDNA to be isolated from lysate components.

Several different techniques have been employed to liberate pDNA from cells.

Mechanical cell disruption of *E. coli* can cause significant damage to sc pDNA (Levy *et al.*, 1999; Lengsfeld *et al.*, 2002)). This shear sensitivity renders cell lysis unit operations used for DSP of other biopharmaceutical products impracticable and calls for other process design solutions (Carlson *et al.*, 1995; Levy *et al.*, 1999). However, a recent study highlights bead milling as an efficient disruption method of *E. coli* for the release of pDNA on a small scale (92% recovery of sc pDNA) (Padilla-Zamudio *et al.*, 2017).

For industrial applications, alkaline lysis, based on chemical disruption of the cell membrane, is still the most prevalently used method for cell disruption (Birnboim *et al.*, 1979; Prather *et al.*, 2003; Abdulrahman *et al.*, 2018).

Thermal lysis, relies on lysozyme digestion, breaking down the peptidoglycan in cell walls, followed by membrane dissociation via boiling of the lysate (Holmes *et al.*, 1981).

Following cell lysis, solid-liquid separation for the removal of cell debris and conditioning of lysate in preparation for subsequent chromatographic purification is implemented. Due to its ease of use, centrifugation has been a mainstay for clarification of crude lysates in the laboratory and preparative scales (Lahijani *et al.*, 1996; Prazeres *et al.*, 1998; Ferreira *et al.*, 1999).

However, centrifugation cannot be scaled to meet industrial demands while maintaining low shear energy input and is not suitable for large scale production feeds of pDNA containing lysates (Ferreira *et al.*, 2000b). For large scale operations, filtration, using 5 μm pore diameter filters, has proven to be the most suitable option (Marquet *et al.*, 1995; Theodossiou *et al.*, 1997; Borujeni *et al.*, 2014). Transmembrane pressure build-up can be reduced by the use of filter aids, such as diatomaceous earth, which also help to reduce shearing of the gDNA precipitates and reduces RNA contamination due to specific binding (Horn *et al.*, 1996).

To further clarify the lysate and for volume reduction, several techniques are used. Protein levels can be reduced via addition of chaotropic 'salting-out' agents such as lithium chloride (Chakrabarti *et al.*, 1992), or ammonium acetate (Horn *et al.*, 1995), which have the additional advantage to precipitate high molecular weight RNA (Ferreira *et al.*, 1999).

Plasmid DNA can be precipitated using polyethylene glycol (PEG), further reducing the process volume while offering the opportunity for a buffer exchange step, conditioning the lysate for subsequent chromatographic purification (Silva-Santos *et al.*, 2017).

### 1.2.4. The use of chromatography in pDNA purification

Among other DSP operations, chromatography in its many forms is still the most applied method throughout the industry (Xenopoulos *et al.*, 2014). Its importance throughout different pDNA purification strategies as well as associated financial burdens, has made chromatography the assessment standard for the whole manufacturing process (Sousa *et al.*, 2012).

Chromatography, as a family of purification methods is based on the differential partitioning of the target product from its contaminants by exploiting differences in molecular properties. Consequently, the complex composition of the lysate and similarity of physical, chemical and structural properties that the target molecule shares with its contaminants in crude cell lysates needs to be taken into consideration for the development of an economically viable pDNA purification process (see Table 1-3)

Table 1-3 Physical, chemical, and structural similarities between pDNA and contaminants in *E. coli* lysate (Sousa et al., 2012)

| Parameter | oc pDNA | sc pDNA | gDNA | RNA | Endotoxins |
|---|---|---|---|---|---|
| **Size** | X | X | X | | X |
| **Negative charge** | X | X | x | X | X |
| **Hydrophobicity** | X | X | | | |
| **Bases exposition** | | X | | X | |
| **NA conformation** | Relaxed circular; double-stranded | Compact sc; Double-stranded | Denatured single/ double-stranded | Single-stranded | |

Chemical properties, such as charge and hydrophobicity, physical properties like molecular weight, radius of gyration, the accessibility of nucleotide bases to binding ligands as well as topological constraints based on the molecules conformation can all be exploited to selectively separate sc pDNA from contaminating impurities and other pDNA conformations (Ferreira *et al.*, 2000b).

One way to categorise chromatographic purification strategies is, (i) by the mode of interaction (hydrophobicity, size, net charge, etc.), or (ii) by mode of operation (frontal loading-, negative mode chromatography, expanded bed adsorption (EBA), etc.).

In adsorptive chromatography (ion exchange chromatography (IEC), hydrophobic interaction chromatography (HIC), affinity, etc.) the target product binds to ligands provided on the surface of a stationary phase. A reversion of attractive forces, by changing the environmental conditions, subsequently elutes bound moieties from the ligands on the basis of their strength of interaction. To this date, the majority of pDNA purification strategies still use beaded chromatography in frontal loading mode.

For the design and manufacturing of chromatographic media, several different materials have been explored. The three main families of materials are inorganic resins (such as porous silica, hydroxyapatite or sintered glass), synthetic organic polymers (polystyrene, methacrylate, polyacrylamide) or natural organic polymers (cellulose, dextran, amylose, agarose) (Leonard, 1997). Due to its mechanical and chemical stability, neutral charge, hydrophilic nature and biocompatibility, agarose based adsorbents have been extensively employed in chromatographic purifications of biomolecules (Ioannidis *et al.*, 2012).

The manufacturing of agarose based supports can be achieved by several methods including spray gelation, extrusion through membranes, or via agitation/ cooling-induced gelation of agarose solutions dropped in mineral oil (Egorov *et al.*, 1970; Jahanshahi *et al.*, 2003; Zhou *et al.*, 2007; Yan *et al.*, 2009). Pore size of the adsorbents can be controlled by adjusting the agarose content as well as ionic strength of the agarose solution (Ioannidis *et al.*, 2012).

To enhance mechanical rigidity of agarose supports, chemical cross-linking is employed (e.g. epichlorohydrin or divinylsulfone). Although cross-linking does not alter the macroporous nature of the media, undesired interactions with solutes in biological feeds (namely proteins) have been reported (Noel *et al.*, 1996).

Controlling the different parameters influencing the size and pore size distribution, make the formation of agarose based adsorbents a challenging process, with a high propensity for batch-to-batch variations (Gilbert, 2018). Advantages of agarose based beaded chromatography media as well as other natural occurring polymers are their very low unspecific adsorptivity as well as excellent flow properties due to the use of cross-linking chemistry enhancing their rigidity (Jungbauer, 2005).

The agarose based stationary phases are in subsequent steps functionalised by coupling ligands on the surface of the internal pores of the media, determining the mode of interaction with the mobile phase.

To provide an overview over different modes of interaction applied for pDNA purification, the following paragraphs discuss each mode in detail.

1.2.4.1. Ion exchange chromatography

Due to the similarity in net charge of pDNA and most of its contaminants, anion exchange chromatography (AEC) has proven itself to be the ion-exchange chromatographic operation of choice. Cation exchange chromatography (CEC) could be used pH dependently to rid the feed of proteins but falls short of selectively removing RNA and endotoxins, both carrying a negative net charge (Schromm *et al.*, 1998).

Together with size exclusion chromatography (SEC), AEC is the most widely applied chromatographic mode for pDNA purification (Abdulrahman *et al.*, 2018). It is based on a binding interaction of positively charged ligands on the stationary phase, such as quaternary amines (Chandra *et al.*, 1992), diethylaminoethyl (DEAE; (Müller, 1986)) and the negatively charged phosphate group on the backbone of pDNA (Figure 1-10).

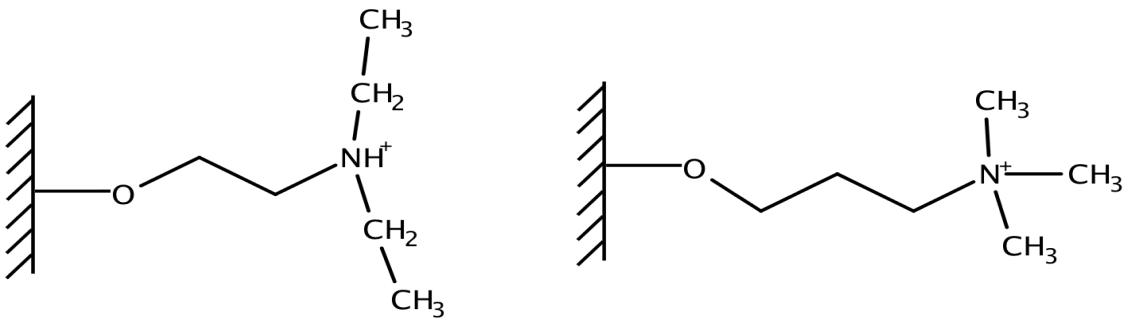


Figure 1-10 Chemical structures of two of the most widely applied AEC ligands; left: DEAE; right: Q

Bound molecules are subsequently eluted from the column via reversion of the attractive forces by applying a salt/ pH gradient. The binding strength of NA is gradually reversed, eluting different NA on the basis of their charge density, chain length, nitrogenous base composition and nucleotide sequence (Yamakawa *et al.*, 1996). Due to its compact nature and high charge density, sc pDNA binds more tightly to AEC columns and consequently elutes after other pDNA isoforms (Prazeres *et al.*, 1998), making it suitable for the separation of different pDNA

conformations from solution (Li *et al.*, 2011). To further enhance selectivity of the sc isoform over other conformations, addition of highly charged cationic additives such as urea, spermidine and sperime have been shown to selectively compact sc pDNA (Murphy *et al.*, 1999).

Most commercially available AEC media have been developed for the purification of protein bioproducts. However, the size difference between protein based and large plasmid products results in very poor binding capacities of pDNA to AEC resins (0.2-2 g/$L_{SBV}$ vs 10-100 g/$L_{SBV}$ in protein purification) (Prather *et al.*, 2003). With typical pore diameters of around 25 nm (for beaded resins of 6% agarose content (Hagel *et al.*, 1996b)) pDNA molecules are unable to diffuse into the internal pores of the media and hence binding is exclusively limited to the support surface (Ljunglof *et al.*, 1999).

Attempts have been made to enhance pDNA binding capacity via the addition of compacting agents aiming to reduce the radius of gyration of pDNA. However, increasing the capacity by 40% still barely utilises a fraction of binding area in comparison to a protein purification column (Colpan *et al.*, 1984; Murphy *et al.*, 1999; Murphy, 2003; Sagar, 2003).

The introduction of superporous/ perfusion beads increases the available binding area of conventional AEC media by crafting supports containing flow through pores (2-30 μm diameter). These pores allow pDNA to enter the beads via convective flow, with additional binding sites being provided by the pore walls, while at the same time allowing for increased flow velocities (Tiainen *et al.*, 2007c).

The limited availability of stationary phase for pDNA binding has led to the development of monolith stationary phases (Sousa *et al.*, 2011). These consist of a single piece of highly porous solid material (Tennikova *et al.*, 1993; Svec *et al.*, 1995), forcing the mobile phase through large ligand lined pores and in the process eliminating diffusion barriers found in classical column chromatographic operations (Urthaler *et al.*, 2005a).

While high levels of protein and NA clearance can be achieved, the selectivity of AEC for pDNA separation from other lysate components is hampered by its electrostatic mode of interaction (Lyddiatt *et al.*, 1998; Diogo *et al.*, 2005). Competitive binding makes co-elution of similarly charged contaminants such as high molecular weight RNA and endotoxins hard to avoid (Ferreira *et al.*, 2000b). Superior elution can be achieved using shallow salt gradients during

elution, however this compromises on process time (Lahijani *et al.*, 1996; Prazeres *et al.*, 1998).

Despite all efforts to enhance the separation efficiency of AEC, high purity standards in final pDNA formulations call for other purification steps, exploiting complimentary properties of the target molecule and its contaminants (Bellot *et al.*, 1993; Abdulrahman *et al.*, 2018).

1.2.4.2. Size exclusion chromatography

SEC (also referred to as 'gel filtration') fractionates different molecules in a feed on the basis of size. It is a non-adsorptive technique, where the lysate is loaded on a porous matrix with a broad pore size distribution (Figure 1-11). While large molecules cannot access small pores, their effective distance of travel through the column is comparatively short, causing them to elute first, while smaller molecules have a longer diffusional pathway, resulting in longer retention times (Ferreira *et al.*, 1997). Different pDNA isoforms are eluted as a function of their effective size (Potschka, 1991), with gDNA eluting first followed by linear and open circular (oc) pDNA (Moreau *et al.*, 1987). The compact structure of sc pDNA leads to a reduced size in comparison to other conformations and causes the molecule to elute last (Urthaler *et al.*, 2005b). Due to the significant difference in size, endotoxins, proteins and RNA can be separated easily from pDNA (Horn *et al.*, 1995).

The biggest disadvantages of the method are its very limited capacity and non-specificity for pDNA. For industrial purification of pDNA products, SEC is still used as a final polishing step, combining a rigorous removal of residual impurities with a buffer exchange step in preparation for formulation (Ghanem *et al.*, 2013). However, the implementation of a SEC step prior to further purification steps was reported to reduce endotoxin levels by as much as 8000 fold (Horn *et al.*, 1995).

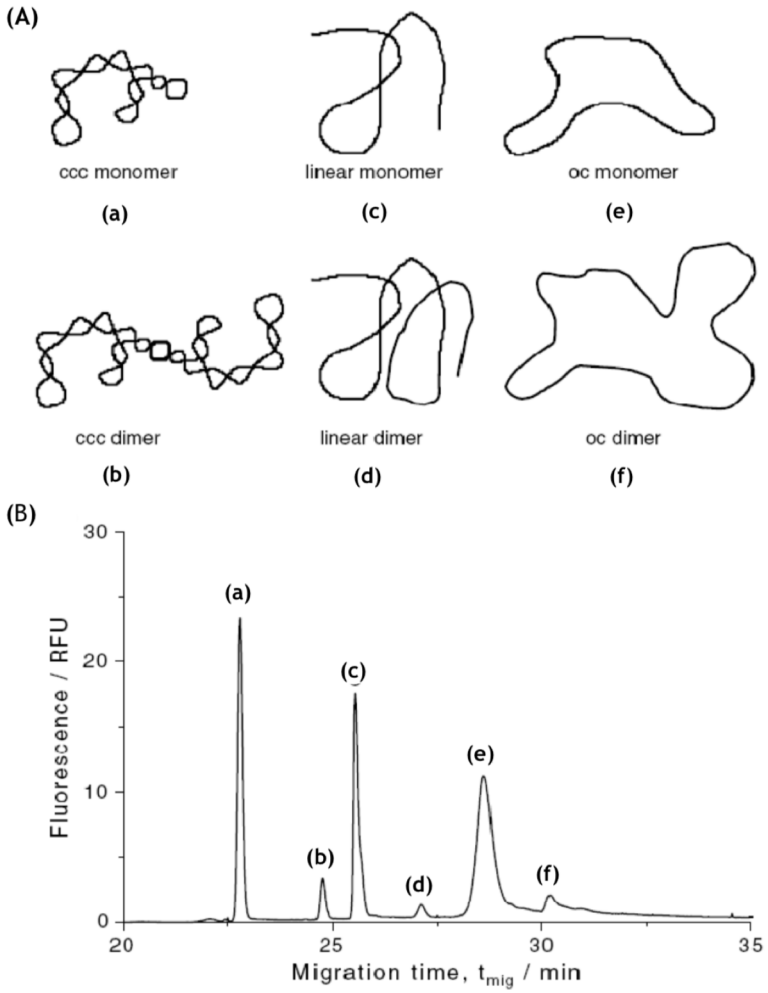


Figure 1-11 SEC for the separation of different pDNA isoforms; A: different pDNA isoforms; B: Topologic fractionation of a pDNA sample containing various isoforms with the use of capillary gel electrophoresis; adapted from (Schleef *et al.*, 2004)

Whilst not a SEC mode in the strict sense, slalom chromatography has been applied for size-fractionation of large (>5 kbp) pDNA molecules (Hirabayashi *et al.*, 2000). Although the retention mechanism is not yet fully understood, it has been suggested that the application of high flow rates results in a steep flow rate gradient in the crevices between microbeads. These forces cause pDNA molecules to extend and the resulting longer reorientation times increase their retention. Unlike in SEC, retention of NA is based on length rather than size, with hydrodynamic effects playing a pivotal role in the mechanism of separation (Diogo *et al.*, 2005).

1.2.4.3. Hydrophobic interaction chromatography (HIC)

HIC is a purification tool based around a difference in hydrophobicity of the components in the feed (Leonard, 1997), that has been applied for pDNA purification (Diogo *et al.*, 2000; Freitas *et al.*, 2009b; Pereira *et al.*, 2010).

The retention time of NA molecules in HIC columns is predominantly determined by their size, base composition and secondary structures (Colote *et al.*, 1986) In aqueous solution, DNA forms a double helix structure, exposing its hydrophilic phosphate backbone to the surrounding buffer, while keeping its aromatic bases tucked away inside the tertiary structure (Li *et al.*, 2005). While the double-stranded nature of NA is intact, its interaction with HIC ligands is very minimal. Binding of pDNA to HIC columns can be achieved via addition of 'salting-out' agents (e.g. ammonium sulphate). Following sample application, weakly bound molecules are washed off the column using a buffer of moderate salt concentration. Elution and separation of different pDNA isoforms is being carried out by gradually reducing the salt concentration. In a final step, strongly bound molecules (linear pDNA, denatured gDNA fragments, RNA) are stripped from the column and the column regenerated for future applications (McCue, 2014).

In an attempt to minimise the reliance on the hazardous ammonium sulphate, the use of potassium phosphate has been investigated, yielding 99% pDNA purity (Bonturi *et al.*, 2013). Despite a low recovery, the purity of the formulation is enough to meet international vaccine purity recommendations and the cleanliness, cost effectiveness and speed of the method make it a promising candidate for a single-step purification (Abdulrahman *et al.*, 2018). Unfortunately, the method was unable to distinguish between different pDNA isoforms.

Further single-step purification strategies for the formulation of sc pDNA have yielded 98% purity at 75% recovery (Bo *et al.*, 2013). However, a process involving the use of ammonium sulfate comes with regulatory constraints and is generally considered disadvantageous (Iuliano *et al.*, 2002).

1.2.4.4. Affinity chromatography (AC)

The principle of interaction in AC is based on biological macromolecules in a feed, interacting reversibly with immobilised ligands with high specificity through several different types of bonds and interactions (Ninfa *et al.*, 2010). It has the unique ability to purify biomolecules via exploiting their biological function or individual chemical structures due to the implementation of specific binding agents (Lowe *et al.*, 2001).

Separation of pDNA isoforms can be achieved by abusing the difference in the conformational structure of the molecules. Supercoiling of the NA chain adds torsional strain, which elevates both, the local charge density as well as base exposure in comparison to the oc conformation (Almeida *et al.*, 2015). Scientists have explored many different types of AC interaction for capturing sc pDNA; brief descriptions of some commonly applied methods are given below.

(i) Triple-helix affinity chromatography (THAC)

THAC is based on a triple-helix formation between a specific homopurine duplex sequence in the target pDNA and a pyrimidine oligonucleotide ligand covalently attached to the stationary phase (Schluep *et al.*, 1998; Sousa *et al.*, 2008b). Although it was reported that it is possible to purify sc pDNA by reducing gDNA, endotoxins and RNA in a single step operation, poor yield, enrichment of denatured pDNA and the requirement for long incubation times have limited the success of the technique (Wils *et al.*, 1997; Schluep *et al.*, 1998).

(ii) Immobilised metal affinity chromatography (IMAC)

IMAC relies of the interaction of charged CU(II) or Ni(II), immobilised onto a stationary phase, with exposed purine bases (adenine and guanine) on molecules in the lysate. As pDNA does not have any exposed purine bases in the sc isoform, the technique has been successfully applied for capturing endotoxins, RNA, and denatured DNA, while the target molecule is eluted in the flow through (Murphy *et al.*, 2003; Cano *et al.*, 2005; Tan *et al.*, 2007).

(iii) Protein/ amino acid–DNA affinity chromatography

Selecting amino acids and protein based ligands was initially based on the natural occurrence of different proteins and amino acids in biological organisms. These interactions mainly involve basic amino acids such as histidine or arginine (Sousa *et al.*, 2010a) and involves proteins presenting domains that recognise specific DNA sequences (Blanco *et al.*, 2005; Privalov *et al.*, 2007).

The use of arginine as a ligand promotes multiple different interactions with pDNA, including electrostatic and hydrophobic as well as biorecognition of nucleic acids. The strong specific biorecognition interaction of arginine with the sc pDNA isoform is based on higher availability and exposition of base pairs as a result of the increased degree of supercoiling cf. other pDNA isoforms (Sousa *et al.*, 2008a).

Similarly to arginine, the ability of histamine and agmantine has been exploited for specific recognition and purification of pDNA isoforms (Sousa *et al.*, 2014).

1.2.4.5. Multimodal/ mixed mode chromatography

Unlike traditional chromatographic techniques (IEC, HIC, etc.), in multimodal chromatography (MMC) the stationary phase interacts in more than one way with molecules in the mobile phase. While in single mode chromatography, weak secondary interactions may occur (e.g. weak electrostatic interactions observed in SEC (McLaughlin, 1989)), MMC actively exploits both interactions for the retention of molecules from the lysate (Yang *et al.*, 2011). Compared with other modes, higher selectivities can often be achieved in MMC due to the more specific nature of the resulting binding interactions (Matos *et al.*, 2014).

AC multimodal ligands such as histamine and agmantine have been explored recently for the purification of pDNA (Černigoj *et al.*, 2013; Sousa *et al.*, 2014; Bicho *et al.*, 2016). The imidazole ring in histamine exhibits hydrophobic properties while amino groups interact on the basis of electrostatic forces. Purification of a 5.17 kbp plasmid from other lysate components in a double elution from the same column yielded 97% sc pDNA at 98% purity (Černigoj *et al.*, 2013).

Although unable to distinguish between isoforms, the application of a monolith functionalised with octylamine was found to be an easier and simpler route of purification compared to HIC followed by AEC, reducing 99% of impurities at 80% recovery (Smrekar *et al.*, 2013).

Capto Adhere resin (containing a N-benzyl-n-methyl ethanolamine ligand showcasing properties of a strong AE ligand in conjuncture with hydrophobic interaction (Ma *et al.*, 2013)) was first used for the purification of pDNA from crude lysate by Matos et al. with little success (Matos *et al.*, 2014). However, Silva-Santos et al. used the resin for the selective formulation of pDNA isoforms from a pre-purified mixture of topoisomers, yielding purities of 91.8% and 92.3% oc and sc pDNA respectively (Silva-Santos *et al.*, 2016). Applying crude lysates to the

resin has in a subsequent study provided a successful baseline separation between isoforms in the lysate, however at the expense of yield (47%) (Silva-Santos *et al.*, 2017).

### 1.2.5. Facing the challenges of chromatographic pDNA purification/ Multifunctional and bilayered chromatography supports

The use of conventional chromatography for the purification of pDNA formulations is attributed to several challenges, inherent to the structural nature of beaded supports. The availability of binding sites for pDNA being limited to particle surfaces and, as a result low binding capacities of beaded supports have inspired researchers to find ways to improve chromatographic operations for pDNA purification. Reducing the size of target pDNA molecules using condensation agents leads to lower spatial uptake on the column; however, the problem of surface restricted binding resides (Murphy *et al.*, 1999; Murphy, 2003).

Changing the shape of the stationary phase from beaded media to a homogenous, single piece of porous solid into a monolith allows for excellent mass transfer and high binding capacities (Zöchling *et al.*, 2004; Saunders *et al.*, 2009). Low backpressure is the result of the rigid nature of the media, allowing for high operational flow rates (Jungbauer *et al.*, 2004). Forcing the lysate through specific pathways in the stationary phase via macropores, enhances ligand-lysate contact by convective flows, making the separation process in monolith columns non-diffusion limited (Josić *et al.*, 1999; Mihelič *et al.*, 2000; Josic *et al.*, 2001).

Functionalisation of monolithic base matrices with different ligands of interaction for pDNA purification, such as HIC, AEC and affinity ligands has been demonstrated in various publications, making it a promising alternative to beaded chromatographic media (Strancar *et al.*, 2002; Branovic *et al.*, 2004; Sousa *et al.*, 2011; Ongkudon *et al.*, 2013; Sousa *et al.*, 2014).

Membranes can be described as a monolith purification strategy with a very extreme aspect ratio comprising of very thin beds, providing very low pressure drops along the chromatographic unit and allowing for increased flow rates and consequently high throughput (Heath *et al.*, 1992; Zeng *et al.*, 1999; Endres *et al.*, 2003). Problems of the technique include large void volumes and difficult scalability (Urthaler *et al.*, 2005c).

EBA utilises the binding modes of traditional chromatography, while abandoning the classical set-up of beaded media tightly packed into columns. Instead the technique follows the design of a fluidised bed (Hjorth, 1997).

Due to the loose organization of the beads in the column, shear stress to the product is minimal and gentle sample handling guaranteed by design (Theodossiou *et al.*, 2000).

EBA has been used for pDNA recovery from crude *E. coli* feedstocks, however, limited pDNA binding capacities were reported (Thatcher *et al.*, 1997; Varley *et al.*, 1999; Ferreira *et al.*, 2000a). Binding capacity for EBA adsorbents in comparison to traditional AEC media can be improved by enhancing charge density on small beads in conjuncture with grafting polyethylene imine chains onto the surface, giving the adsorbents a higher surface area (Theodossiou *et al.*, 2000). Over recent years, interest in EBA techniques have declined, due to (still) limited binding capacities and problems associated with collapsing beds as a result of inter-particulate linking of adsorbents by long NA chains (Ferreira *et al.*, 2000a; Abdulrahman *et al.*, 2018).

Tentacle chromatography employs long tentacle-like polyelectrolyte chains with large linkers extending from the surface of supports to reduce interparticulate mass transfer during elution, whilst minimizing contact between the target product and the adsorbents stationary phase (Weitzhandler *et al.*, 1998; Ghanem *et al.*, 2013). The long chains allow for a higher binding capacity of the supports; however, scientific interest in the field has been low (Prather *et al.*, 2003).

The problem of surface restricted binding of pDNA can be partly overcome by the application of perfusion media (Ghanem *et al.*, 2013). This allows for higher processing flow rates as well as slightly enhanced pDNA capacity (Meyer, 2013). The internal structure of macroporous beads comprises of two differently sized pore types, namely flow through pores (6000-8000 Å) and diffusive pores (800-1500 Å), allowing for deeper penetration and binding of pDNA to the particles as well as quicker elution times (Deshmukh *et al.*, 2005; Tiainen *et al.*, 2007a; Arpanaei, 2008).

Reducing the bead size of adsorbents increases the relative binding surface available for pDNA. Such small beads however, suffer from high pressure backdrops due to the reduced interparticulate void volume. To maintain high flow rates, researchers have crafted rigid, non-porous adsorbent materials, however the enhanced flow velocities cause higher shear stress to the product (Sumita *et al.*, 1994; Tiainen *et al.*, 2007b).

Negative chromatography aims to bind contaminants from the load, while the target product elutes from the column in the flow through (Figure 1-12) (Lee *et al.*, 2014). One advantage of the method is that it circumvents the limited binding capacity of pDNA to traditional chromatographic media. Due to size limitations, pDNA can only adsorb to the outer surface of chromatography supports as the pore size of the porous media is too narrow for molecules to diffuse into and bind throughout the matrix (Grunwald *et al.*, 2001; Eon-Duval *et al.*, 2004; Gustavsson *et al.*, 2004).

The fragile nature of nanoplex bioproducts and the avoidance of binding in negative chromatography, have made this technique appealing to researchers, however the electrostatic similarities between pDNA and its contaminates in the feed make adaptation of the technique for pDNA purification challenging outside of affinity based purification strategies (Caramelo-Nunes *et al.*, 2014).

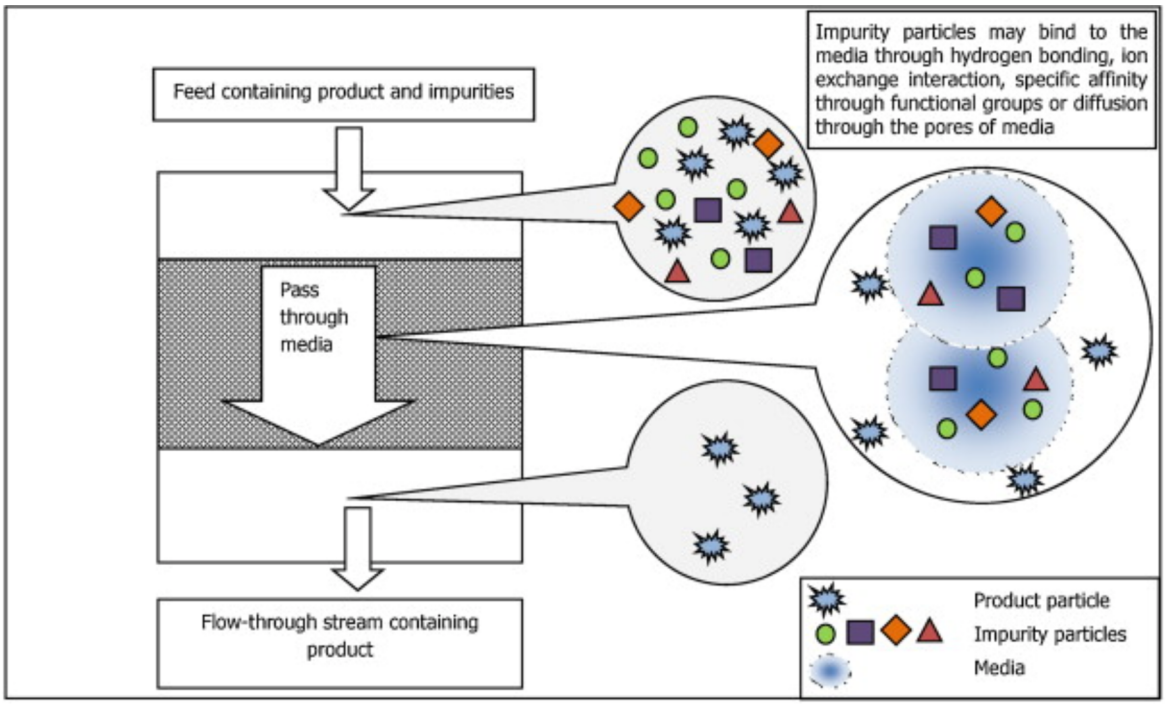


Figure 1-12 Working principle of negative mode chromatography, the stationary phase interacts only with the contaminants in the feed, allowing the target molecule to pass through the column in flow through mode; adapted from (Lee *et al.*, 2014)

Implementation of negative adsorption chromatography for the separation of large biomolecules from smaller contaminants, possessing similar surface chemistries, calls for a different type of adsorbent architecture.

In order to be able to capture nanoplex molecules in the flow through while retaining contaminants in the column, a new type of adsorbents has been proposed. These beads possess a non-interactive exterior, preventing binding of large entities (such as pDNA), while providing binding ligands for interaction with smaller molecules inside the bead. To provide such an environment, bilayered chromatography supports surround a functionalised core with a porous shell allowing diffusional access of small molecules to pores inside the beads.

Such AEC-SEC media combines the strength of both the adsorptive capacity of AEC for small molecules, while the inert outer shell layer prevents adsorption of pDNA. This type of architecture allows for a 'one-column-one bead' separation; small contaminants have free access to the core, where they are retained due to electrostatic interaction with the ligands, while target pDNA molecules are prevented from interaction due to their size (Figure 1-13).

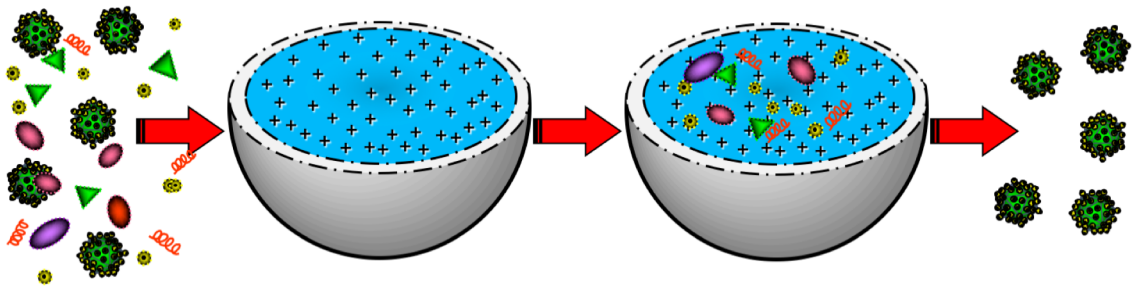

Figure 1-13 Working principle of AEC-SEC bilayered supports for the purification of nanoplex bioproducts (here VLPs) from small, chemically similar contaminants, exploiting size differences in conjuncture with electrostatic interactions in a single step operation (image courtesy by Dr E. Theodosiou)

Although separation media based on multilayer structures have found wide application in analytical techniques (high performance liquid chromatography (HPLC)), the use and development for media targeted for large scale production of nanoplex biomolecules is a comparatively new approach (Haginaka, 1991; Pinkerton, 1991; Hayes *et al.*, 2014; de Faria *et al.*, 2017). Several different manufacturing approaches have been explored to provide XEC/ SEC bilayered media (X- several modes of ligand interaction are conceivable, such as ionic, hydrophobic, multimodal, etc.) for the purification of large target products from smaller, chemically similar contaminants.

Coating an AEC Amberlite matrix by adsorbing negatively-charged, hydrophilic polyacrylic acid resulted in a bilayered structure that allowed capture of shikimic acid directly from the

fermentation media, while larger entities (such as cell debris) were excluded from interacting with the AEC core of the media, due to the cross-linked polymer coating (Dainiak *et al.*, 2002a). Another coating technique applied to an AEC Amberlite resin allowed for lactic acid to be adsorbed to the media while preventing various types of cells and cell debris from binding. The adsorbents were coated with a thin agarose layer followed by cross-linking to enhance stability of the bilayered structure (Viloria-Cols *et al.*, 2004).

Several prototype media for EBA purification of target proteins from complex feedstocks were manufactured by a three-phase-emulsion process. AEC, CEC and affinity core phases were coated by an agarose gel, reducing non-specific binding of cells and cell debris, while maintaining the core's ability for selective capturing of target proteins. The non-stick exterior was reported to reduce bead fouling and inter-particle cross-linking, leading to improved bed stability (Jahanshahi *et al.*, 2008). However, concerns about coating beaded media with agarose layers were reported. Casting of uniform, thin and mechanically robust agarose layers is challenging and as a result, particle volume increased by three-fold, compromising on bed expansion properties, binding capacity and intra-particle mass transfer (Arpanaei *et al.*, 2010).

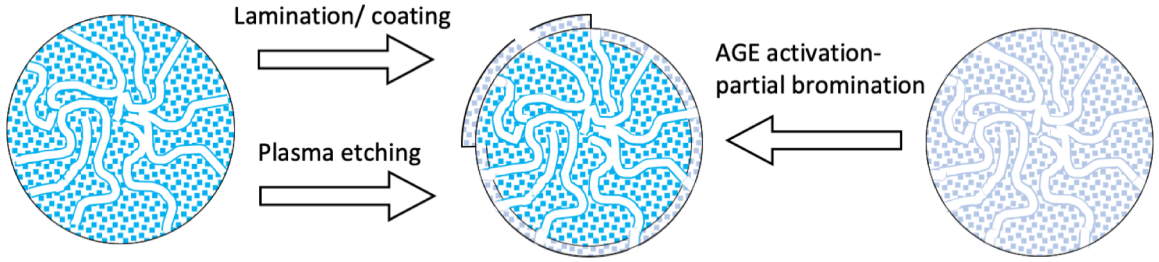


Figure 1-14 'Top down' (starting from fully derivatised AEC materials; Left) vs 'Bottom up' (build-up of functionality specifically inside the core of SEC materials; Right) approaches for the preparation of SEC-AEC bilayered media for packed bed chromatography

The first SEC-AEC bilayered media for pDNA purification in a packed column was first introduced by Gustavsson in 2004 (Gustavsson *et al.*, 2004). Instead of laminating/ coating pre-functionalised AEC supports, the researchers applied an allyl glycidyl ether (AGE) activation, partial bromination technique, based on several previously published patents (Bergstrom, 1997; Berg, 2003). Starting with the SEC base matrix Sephacryl S-500 HR (pore size 200 nm; predicted size cut-off 1 kbp), functionality was built into the particles in a three step 'bottom up' approach; (i) Allylation of support particles by reacting AGE with hydroxyl

groups throughout the surface of the agarose based stationary phase, (ii) partial bromination of an outer layer, followed by hydrolysis of allylated beads, (iii) coupling of the strong AEC ligand Q (quaternary amine) throughout the core of the supports.

Light micrographs of Congo red (CR) stained beads showcase a distinct separation of a charged core surrounded by a thin inert outer layer. The 'lid beads' were applied in a two-column strategy for pDNA purification of a 5.9 kbp plasmid from crude *E. coli* lysate with 89% yield, removing 99.5% of endotoxins and 96% HCP (Gustavsson *et al.*, 2004). The media was further used as part of an integrated pDNA purification strategy of a 6.1 kbp plasmid with 69% recovery (88% single process step yield) (Kepka *et al.*, 2004). Due to the spherical nature of chromatography supports, binding capacity of AEC-SEC media is strongly dependent on the amount of available binding sites distributed across the core (Table 1-5).

Table 1-4 Loss of volumetric binding capacity with increased thickness of SE layer for spherical beads of 100 µm diameter

| **Thickness of SE layer [µm]** | **Loss of core binding capacity [%]** |
|---|---|
| **2** | 10.4 |
| **4** | 20.1 |
| **6** | 29.1 |
| **8** | 37.3 |
| **10** | 44.9 |
| **12** | 51.9 |
| **14** | 58.2 |
| **16** | 64.0 |
| **18** | 69.2 |
| **20** | 73.9 |

In order to compromise binding space as little as possible, it is imperative for the production of bilayered supports via the AGE activation- partial bromination route, to keep the shell thickness as thin as possible. To achieve such thin non-adhesive layers, the diffusion pathway of bromine into the bead has to be as short as possible while maintaining a homogenous layer shape. The very fast convective transport of bromine in aqueous solution to the particles

surface, its high diffusion rate into the agarose media and its high reactivity with the AGE activated stationary support phase make control of the reaction challenging.

Two different options to balance the reaction and the diffusion rates of bromine with AGE activated supports have been investigated by Karnchanasri (Karnchanasri, 2012).

Enhancing the viscosity of support slurries via addition of sucrose slows down the convective transport of bromine, allowing it to surround the supports prior to diffusion/ reaction into the pores of AGE activated supports. By optimizing the reaction temperature, viscosity and addition of additives, SEC-AEC media on the basis of Sepharose CL-6B were produced. These supports yielded selectivity indices of up to 3.52 in static pDNA/ bovine serum albumin (BSA) binding studies (loss of surface vs core binding, see Chapter 3 for definition of SI) for 10% bromine addition at room temperature with 64% (w/v) sucrose.

Loading the supports into a column, the media was used to effectively purify a 27.4 kbp and a 4.1 kbp plasmid directly from cleared *E. coli* feedstocks. Controlling the RDB by heating the reaction vessel via microwave irradiation during the partial bromination step led to an almost complete elimination of surface charge (SI= 57.4) (Karnchanasri, 2012). Plasma irradiation treatment of material surfaces is a well-established technology that is used for the modification of surface properties at the 'nano-scale' (Fisher, 2002).

Plasma treatment of material surfaces has several advantages; (i) low operational temperatures (room temperature); (ii) shallow 'nano-scale' modifications can be achieved, without changing the bulk properties; (iii) modification of various types and compositions of surfaces; and (iv) no generation of large amounts of toxic by-products (Schram *et al.*, 1987). Plasma modifications have been used to induce surface modifications in biopurification materials including analytical chromatography beaded supports (Haginaka, 1991; Sudo *et al.*, 1998; Souverain *et al.*, 2004) and membrane materials (Ulbricht *et al.*, 1995; Chen *et al.*, 1999; Pieracci *et al.*, 1999; Pieracci *et al.*, 2000; Liu *et al.*, 2004).

The application of low temperature glow discharge plasma irradiation treatments for modification of AEC media surfaces has been demonstrated to prepare bilayered chromatography supports with a non-adsorptive surface (Arpanaei *et al.*, 2010). Plasma technology was hereby used in two different ways; (i) plasma etching was used to remove the strong AEC ligand quaternary amine from the surface of Q Hyper Z, replacing it with polar,

oxidizing, oxygen containing groups ('plasma etching and oxidation'); (ii) coating surface exposed Q ligands under a thin polymer layer, by providing appropriate monomers (vinyl acetate, pyrrolidone, safrole), using argon as the carrier gas ('plasma polymerization coating'). Both media were found to have substantial changes to the structural nature of the particles surfaces and reduced pDNA and sonicated ct DNA binding capacities cf. untreated Q Hyper Z. Under static binding conditions, these plasma etched beads showed loss of ~53% of 'surface' DNA binding, while losing just 9.3% of 'core' protein binding capacity. Dynamic EBA studies showed that the 10% breakthrough capacity of the media with respect to DNA binding had fallen significantly (up to 80%) after plasma etching, while protein binding capacities were unchanged cf. untreated Q Hyper Z. Furthermore, prior issues with bed contractions due to inter-particle-cross-linking of adsorbents by DNA were completely eradicated.

Many common chromatography adsorbents such as Sepharose and Sephacryl have a soft hydrogel structure. Under aqueous condition at atmospheric pressure, water accounts for >90% of the support volume and plays a pivotal structural role. Under low pressure conditions, water is easily evaporated from the pores of these hydrogels, resulting in a loss of support structure, rendering low pressure plasma treatments unsuitable for etching of hydrogel materials. Q Hyper Z is a rigid material composed of stable porous zirconium oxide beads filled with a high charge-density, cross-linked hydrogel (Pall Life Sciences, 2006), targeted for EBA chromatography, that can withstand the dry state necessary for the plasma system employed by Arpanaei. The extension of these low temperature, low pressure plasma treatments to beaded hydrogel chromatographic support materials is hence hindered, by the low pressure (~10 Pa) at which the plasma treatment was carried out. Low temperature plasma can be generated at atmospheric pressure using atmospheric pressure glow discharge (APGD) approaches (Kanazawa *et al.*, 1988; Xiaogui *et al.*, 2012). Modification of polymeric surfaces using APGD treatment has been demonstrated in a number of studies (Temmerman *et al.*, 2005; Choi *et al.*, 2006; Pappas *et al.*, 2006; Walsh *et al.*, 2007), indicating that APGD may be a suitable candidate for plasma etching of soft chromatography adsorbent surfaces.

Olszewski et.al. utilised APGD plasma etching treatments for the selective modification of soft hydrogel supports surfaces (Olszewski *et al.*, 2013). Instead of etching the support media in a desiccated or semi-dry state, the use of a custom built fluidised bed reactor (FBR) system

allowed for treatment in situ, generating reactive oxygen species (ROS) inside plasma filled bubbles travelling upwards through an aqueous support suspension.

Plasma etching was able to significantly reduce the static surface binding capacity of treated Q Sepharose FF (up to 70% loss of pDNA binding capacity) at the expanse of a small loss of core binding capacity (loss of ~10% BSA capacity), when using He-$O_2$ as a carrier gas (Knake *et al.*, 2008; Park *et al.*, 2010). Treatment of Q Sepharose Fast Flow (FF) media by using pure $O_2$ plasmas yielded very poor selectivities of surface vs core binding reduction. This was seen as a result of thermal damage to the media, resulting from contact of single supports with intensely hot plasma filaments during the treatment.

However, the ease of application to modify soft hydrogel support media in their aqueous (native) state has considerable application potential for the field of packed bed chromatography (Olszewski *et al.*, 2013).

Although initial uptake of restricted access media (RAM) application for nanoplex purification was slow, several companies have been working on the manufacturing of multifunctional chromatography adsorbent materials over the last years. In 2012 GE Healthcare launched the first commercial MMC/ SEC media Capto Core 700 (CC 700), for the intermediate purification and polishing of viruses and other large biomolecules (GE Healthcare Life Sciences, 2012).

The media comprises of a cross-linked agarose stationary phase, whose core is functionalised with the MMC ligand octylamine, employing hydrophobic and electrostatic modes of interaction for the selective and efficient capture of impurities. The core is surrounded by an agarose shell of approximately 5 μm thickness with a molecular size cut-off of 700 kDa, preventing large biomolecules from passing through the shell and interacting with the core.

Further multifunctional adsorbents with options to modulate different properties and vary multiple parameters in designing a separation protocol, including porosity, bead size, layer thickness, pore size distribution, type of ligand, and ligand concentration have been heralded (Glaser, 2013).

However, to date, only one more material utilizing the ‘core bead technology’ of GE Healthcare has been released to the market in Capto Core 400. The media has a similar targeted application cf. Capto Core 700 (CC700), however a slightly higher agarose content reduces the size cut-off of the media to 400 kDa (GE Healthcare, 2018c).

Cunha introduced a prototype of an EBA core-shell media based on agarose using the MMC octylamine ligand. The media was integrated in DSP of hMSC, where it improved the washing efficiency more than 10-fold, recovering ~70% of cells after global processing, without compromising characteristics of the target cells, with cell viability above 95% (Cunha *et al.*, 2016).

In 2018, BioToolomics introduced a 'Negative chromatography Antibody Purification' technology based on bilayered adsorbents. The company offers a library of MMC ligands for the specific capture of different impurities and provides a platform technology for the development of more efficient and cost-effective purification processes (BioToolomics, 2018).

## 1.3. Aims of this thesis

This study explores the preparation of multifunctional, bilayered chromatography supports for nanoplex purification, in a single negative chromatography mode purification step, creating a SE shell surrounding a charged core.

Early successes applying plasma etching and oxidation techniques to selectively modify the chemical exterior of beaded chromatography supports have yielded encouraging results treating EBA media with low pressure Helium plasmas to reduce the pDNA binding capacity while maintaining BSA adsorption. Expanding on the idea of using ROS to etch away functional ligands, this study aims to in situ modify the surfaces of agarose hydrogel adsorbents in their native wet state. To selectively eliminate surface binding ligands, cold atmospheric pressure plasma is generated in a novel custom build fluidized bed reactor. The main aim of chapter three is to identify suitable plasma parameters to ideally eliminate all ligands on the surfaces of AEC beaded supports, exploring different parameters such as overall treatment time, power input, sample size etc.

Bilayered supports, manufactured via partial bromination followed by ligand coupling, applying reaction diffusion balancing to control the shape of the non-binding zone have shown significant reductions of pDNA binding capacity cf. fully brominated controls. However, with all preparations levelling out at a max of 80% pDNA binding reductions, the residual pDNA binding on the surface could not be explained. Exploring different visualisation tools, such as confocal laser scanning microscopy (CLSM), Environmental Scanning Electron Microscope (ESEM) and light microscopy this study aims to identify the origin of the residual binding sites and if possible adjust the manufacturing protocol to enhance selectivity by eliminating remaining surface charges.

With CC700 being the first marketed restricted access media for nanoplex purification, chapter five focusses on the characterization of the media. Furthermore, the medias suitability as a first capture step for pDNA purification from crude *E. coli* lysates in negative chromatography mode will be explored.

# Chapter 2 General Materials and Methods

This section introduces the materials and methodology used to conduct experiments throughout this project.

All the methods that were applied in more than one chapter of this work are listed below, where methods are 'exclusive' to one chapter, the methodology will be given in the respective section of the chapter. However, some of the methods presented here only give a general overview over the practical implementation due to the number of variables associated with some experiments (e.g. plasma operation).

When the actual methods differ from or require more specificity, complimentary remarks on the methodology were made in the respective experimental sections of the associated chapters. The inclusion of this section as a separate chapter was nonetheless chosen to aid readability and avoid repetition of similar but not identical practical executions.

## 2.1. Materials

The chromatography resins Q Sepharose FF, Capto Q, DEAE Sepharose FF, Capto Core 700, Sepharose Cl-6B were purchased from GE Healthcare Bio-Sciences (Uppsala, Sweden). Q Hyper Z was gifted by Pall Corporation (Portsmouth, UK). EMD Fractogel (M) DEAE was purchased from Merck (Darmstadt, Germany).

Helium (CP grade), oxygen (CP grade) and He-$O_2$ (99.5%-0.5% v/v) were obtained from BOC Speciality Gases (UK).

*E. coli* DH5α and plasmid IT14: pPR322-p170 was kindly provided by Dr Eirini Theodosiou (Applied Chemistry and Chemical Engineering, Aston University, Birmingham, UK).

For transformation and fermentation of pDNA, Luria Bertani (LB) broth, bacteriological agar, D-glucose, ampicillin, kanamycin, polypropylene glycol (PPG) Sodium hydroxide and antifoam were purchased from Sigma-Aldrich Company Ltd. (St. Louis, MO, USA).

For pDNA purification, QIAfilter Plasmid Giga Kits, QIAfilter Plasmid Mega Kits and QIAprep Spin MiniPrep Kits were purchased from Qiagen GmbH (Hilden, Germany). Propan-2-ol was purchased from Sigma-Aldrich Company Ltd. (St. Louis, MO, USA).

For phenol-chloroform extraction of nucleic acids and subsequent agarose gel electrophoresis, Phenol: Chloroform: Isoamyl alcohol (25:24:1) solution, 3 M sodium acetate

(pH 7.0), 100x Tris-EDTA (TE) (10 mM Tris-Cl; 1 mM EDTA; pH 7.5) buffer, agarose, (high gelling temperature), 6x Blue Orange gel loading dye, ethanol (absolute) and 10x TBE buffer were purchased from Sigma-Aldrich Company Ltd. (St. Louis, MO, USA). Lambda- HinD III marker was purchased from Thermo Scientific (Waltham, MA, USA). SYBR safe DNA gel stain (Invitrogen, CA, USA) was purchased from Life Technologies Ltd (Paisley, UK).

For Diphenylamine (DPA) assay, Diphenylamine, perchloric acid, acetaldehyde, glacial acetic acid and calf thymus DNA were purchased from Sigma-Aldrich Company Ltd. (St. Louis, MO, USA).

Pierce BCA Protein Assay Kit and Thermo Scientific EA Sterilin clear microtiter plates were purchased from Thermo Scientific (Rockford, IL, USA).

For the Orcinol assay, Orcinol, iron(III) chloride, hydrochloric acid, ribonucleic acid from baker's yeast (*S. cerevisiae)* were purchased from Sigma-Aldrich Company (St. Louis, MO, USA).

For static binding studies, BSA, 100x TE (10 mM Tris-Cl; 1 mM EDTA; pH 7.5) buffer were purchased from Sigma-Aldrich Company Ltd. (St. Louis, MO, USA). Hoechst dye 33258 was purchased from Molecular Probes, Invitrogen (Eugene, Oregon, USA). Sodium azide was purchased from Sigma-Aldrich Company Ltd. (St. Louis, MO, USA).

For fluorescent labelling and subsequent CLSM experiments, immersion oil and dimethyl sulfoxide (DMSO) were purchased from Sigma-Aldrich Company Ltd. (St. Louis, MO, USA). PD-10 desalting columns packed with Sephadex G-25 media were purchased from GE-Healthcare (Uppsala, Sweden).

Invitrogen Molecular Probes Cy5 dye was purchased from Thermo Scientific (Rockford, IL, USA). Syto 9 green fluorescent nucleic acid stain was purchased from Lifetechnologies (Eugene, Oregon, USA). VWR VistaVision Microscope Slides and VWR Micro Cover Glasses were purchased from VWR International Ltd (Lutterworth, Leicestershire, UK).

For DPD plasma treatment, the sample support cakes were prepared on XK 26 net rings (product 11530834; GE Healthcare; Buckinghamshire)

Milli Q water (MQW) was used in all experiment unless stated otherwise.

## 2.2. Instrumentation

Experiments were performed using the instrumentation below.

ÄKTA Explorer 100 system controlled by UNICORN 4.11 software; Tricorn 5/50 columns (GE Healthcare, Uppsala, Sweden)

Pearson Current Monitor 2877 (Pearson, California)

PSP-603 power supply (GW Instek; Farnell, Leeds, UK)

72-8710 Oscilloscope (Tenma; Farnell, Leeds, UK)

TTI TG 1000 function generator (AIM-TTI Instruments; Farnell, Leeds, UK)

Tektronix P5100 High Voltage Probe; Tektronix DPO4104 Digital Phosphor Oscilloscope (Tektronix, Oregon)

Tektronix DPO4104 Digital Phosphor Oscilloscope (Tektronix, Oregon)

Microtiter plate reader GloMax-Multi Detection System (Promega UK; Southampton; UK)

10 mm path length Suprasil quartz cuvette (Hellma Analytics, UK)

UVIKON 922 spectrophotometer (KONTRON Instruments, Bletchley, UK)

Evolution 300 spectrophotometer (Thermo Fisher, Madison, USA)

VM 20 vortex mixer (Chil Tern Scientific Instrumentation, London, UK)

The material of the purpose-built plug comprising of machinable Macor glass ceramic was purchased from UK Farnell (Leeds, England)

J2-21 centrifuge (Beckman, High Wycombe, UK)

Mastersizer 2000 (Malvern Instruments, Malvern, UK)

Philips XL-30 FEG Environmental SEM (FEI Company, OR, USA)

HetoVac Speed vacuum system (Thermo Fisher, Madison, USA)

blood rotor shaker SB1 (Stuart Scientific, Staffordshire, UK)

Olympus BX50 Light microscope equipped with a Moticam 800x600 PIX (Olympus UK& Ireland, Southend-on-Sea, UK)

Microcentrifuge, MiniStar silverline (VWR International, Lutterworth, Leicestershire, UK)

Fermac 360 fermenter (Electrolab Biotech Ltd, Tewkesbury, Gloucestershire, UK)

SHKE4000-8CE shake flask incubator (Thermo Scientific, Rockford, IL, USA)

Series 300 autoclave (LTE Scientific, Greenfield, UK)

## 2.3. Methods

### 2.3.1. Transformation of plasmid IT14: pPR322-p170

The high copy number plasmid IT14: pPR322-p170 (26.88 kbp) was introduced into competent *E. coli* DH5$\alpha$ cells via heat shock transformation, following a modified protocol from Nishimura (Nishimura *et al.*, 1990).

50 µL of competent *E. coli* cells (DH5$\alpha$) were thawed on ice and transferred into a microcentrifuge tube containing 100 pg of IT14: pPR322-p170 and incubated on ice for 30 min. The cells were treated with a heat pulse (42°C; 60 s) to induce uptake of the plasmid by the cells followed by immediate cooling on ice. The cells were diluted 10- fold in pre-warmed LB media (containing 100 µg/mL ampicillin) and incubated for 1 h (37°C) to assist the development of antibiotic resistance.

For the preparation of a cell bank, the cells were plated out on a selective agar plate (0.25% (w/v) LB broth; 0.15% (w/v) bacteriological agar; 100 µg/mL ampicillin) and incubated overnight (37°C). A single colony was transferred into 8 mL LB media (containing 100 µg/mL ampicillin) and incubated overnight on an incubator shaker (37°C; 200 rpm). Sterile glycerol (2 mL) was added and mixed thoroughly. The sample was aliquoted into 0.5 mL aliquots and stored in cryotube vials at -80°C.

### 2.3.2. Fermentation of IT14: pPR322-p170 containing cells

An individual colony of *E. coli* Dh5α containing the 26.88 kbp plasmid IT14: pPR322-p170 was obtained via culturing on selective agar plates overnight at 37°C (0.15% (w/v) bacteriological agar; 100 µg/mL ampicillin; MQW). A single colony was cultured in a shake flask (10 mL LB media; 100 µg/mL ampicillin in a 100 mL conical flask) overnight (37°C; 220 rpm) until $OD_{600}$ = 1- 1.5 was reached. This pre-inoculum (0.5 mL) was transferred into an inoculum flask (80 mL LB media; 100 µg/mL ampicillin in a 500 mL conical shake flask) and grown overnight until an $OD_{600}$ of around 3 was reached (37°C, 220 rpm).

For the production of the bulk of pDNA containing cells, the content of the inoculum flask was transferred to a 5 L fermenter (FerMac 360, Electrolab, Tewkesbury, UK) which was used in batch mode, using the following (starting) conditions; 4 L of LB media, 30 g/L glucose, 100 µg/mL ampicillin, PPG antifoam, 37°C, pH = 7, agitator speed 400 rpm, air flow rate

4 standard litres per minute (SLM). The pH was maintained constant using automated loop pumps providing either 2 M NaOH or 1 M $H_2SO_4$ respectively. The dissolved oxygen tension (DOT) was monitored and maintained above 50% via manual regulation of the air flow rate as well as automated regulation of the agitation speed. Temperature was kept constant using a built-in heating mantle and water cooling.

Cell growth was monitored hourly by measuring the $OD_{600}$ and after the cell growth had reached late exponential stage the fermentation was terminated.

An exemplified growth curve of the cells can be found in Appendix A-1.

The cells were then harvested via centrifugation (J2-21 centrifuge; 15,000 g; 15 min; 4°C), the supernatant was discarded and the cell pellets aliquoted and stored at -20°C.

### 2.3.3. Alkaline cell lysis and obtaining purified pDNA solution for static binding studies

For the production of high purity pDNA solutions, Qiagen Giga and Mega kits were used following the manufacturers protocol.

Cells were gently thawed on ice overnight and resuspended in 125 mL of resuspension buffer P1 (containing 100 μg/mL RNase A). Lysis buffer P2 was added (125 mL) and following mixing by 6 times inversion, the sample was incubated at room temperature (5 min). Prechilled neutralisation buffer P3 was added (125 mL), thoroughly mixed and incubated on ice (30 min). The broth was centrifuged in aliquots of 500 mL (10,000 g; 20 min; 4°C). The Qiagen® tip column was equilibrated (75 mL QBT buffer) before the supernatant of the sample was applied and washed with 600 mL QC buffer before the pDNA was eluded with 100 mL of elution buffer QF.

The pDNA was precipitated by adding 70 mL of propan-2-ol and centrifuged down (10,000 g; 30 min; 4°C). The supernatant was discarded and the pellet washed with 70% ethanol and re- centrifuged (10,000 g; 5 min; 4°C). The supernatant was carefully removed, the pellet air dried (up to 2 h) and resuspended in TE buffer (10 mM Tris-HCl; 1 mM disodium EDTA; pH 8.0). The purified pDNA solution was visualised by agarose gel electrophoresis and measured for pDNA concentration using DPA assay as well as $OD_{260}$.

The solution was aliquoted and stored at -20°C (1 mL; 50 μg/mL) until it was used in static binding studies.

For the production of cleared *E. coli* lysate for frontal loading column chromatography experiments, an alkaline cell lysis was performed as described by Gustavsson et al. (Gustavsson *et al.*, 2004); an adapted method first described by Birnboim (Birnboim *et al.*, 1979).

5 g of frozen cell paste was gently thawed in a refrigerator before it was resuspended and vortex mixed on a VM20 Vortex mixer (Chil Tern Scientific Instrumentation, London, UK) with 36 mL resuspension buffer (10 mM Tris-HCl; 61 mM glucose; 50 mM ETDA; pH 8). The suspension was transferred to a fresh vessel before 78 mL of lysis buffer (0.2 M NaOH; 1% (w/v) SDS) was added and gently inverted for 10 min before neutralizing the suspension by addition of 59 mL neutralization buffer (5°C; 3 M potassium acetate; glacial acetic acid; pH 5.5). The white precipitate containing genomic DNA, cell debris and potassium dodecyl sulfate was removed by centrifugation (10,000 g; 4°C; 30 min) and the supernatant was analysed for pDNA and RNA contents using DPA and Orcinol assay respectively. The solution was stored in a clean vessel at -20°C until usage.

### 2.3.4. Characterisation of pDNA

#### 2.3.4.1. Agarose Gel electrophoresis (with preliminary phenol chloroform extraction of nucleic acids)

Agarose Gel Electrophoresis was performed on a 0.8% (w/v) agarose gel (0.64 g high gelling temperature agarose; 80 mL TBE buffer; 12 μL SYBR stain). Samples were prepared on mixing tape (3 μL pDNA sample/Lambda- HinDIII marker; 3.5 μL 0.5X TBE buffer; 1.5 μL Blue orange loading dye 6x). The gel was run in horizontal mode (constant voltage, 75 V) using 0.5x TBE buffer as running buffer for 2.5 h.

The gels were imaged using a Uvitec Imaging System (Uvitec Alliance, Version 15.16 for Windows).

Due to the low concentrations of nucleic acid species in column chromatography fractions, a nucleic acid extraction was performed prior to loading the fractions on gel for electrophoresis: 200 μL of sample were added to 200 μL of phenol: chloroform: isoamyl alcohol solution (25: 24: 1) and inverted seven times to form an emulsion. The samples were centrifuged (10,000 g; 10 min) and the top phase collected. The sample was mixed with 40 μL of 3 M sodium acetate (0.2 μm filtered; pH 7) and 0.5 mL of ethanol (-20°C) and stored overnight

(-20°C). The samples were centrifuged (10,000 g; 10 min) and the supernatant carefully pipetted out and discarded. The nucleic acid pellet was washed with 0.5 mL of ice cold 70% (v/v) ethanol and centrifuged (10,000 g; 10 min). The supernatant was carefully decanted and the pellet left to air dry before dissolving it again in 20 µL TE buffer (10 mM Tris-HCl; 1 mM disodium EDTA; pH 8.0).

2.3.4.2. pDNA sequencing of pBR322-P170

A sample tube containing 1 mL pDNA solution (20 µg/mL in 10 mM Tris-HCl, 1 mM disodium EDTA, pH 8.0) was shipped to and the sequencing experiments were performed with the help of MSc Manuel Mohr (Department of Biosystems Science and Engineering; ETHZ).

Sequencing of the plasmid has been performed via Sanger capillary sequencing using the primers displayed in Table 2-1 The resulting sequencing stretches and their respective overlaps are presented in Figure 2-1.

It is a pPR322-based high copy number plasmid (45.79 kbp), containing a 22.800 kbp insert from *Saccharomyces cerevisiae* chromosome III at the BamHI site.

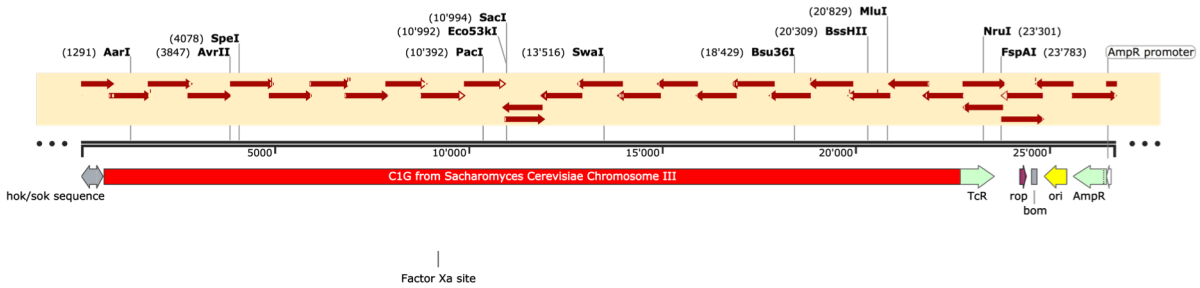


Figure 2-1 Linear plasmid map of the circular plasmid pBR322-P170: Top: common restriction endonuclease recognition sites are annotated (cleavage position in parenthesis) above the overlapping sequencing reads from the individual Sanger sequencing runs (dark red arrows). Bottom: Known features are annotated as different coloured blocks/ arrows depending on their orientation. Sequence map was created using Snapgene 3.1.4 software (GLS Biotech LLC)

Table 2-1 pDNA primer sequences of pBR322-P170

| Name | Sequence (5'-3') |
|---|---|
| **AmpStart (Microsynth standard)** | AAAACAGGAAGGCAAAATGC |
| **AmpStop (Microsynth standard)** | TCAGGCAACTATGGATGAAC |
| **Seq-Jo-001fwd** | GGATCTTCACCTAGATCC |
| **Seq-Jo-001rev** | TTTGTGATGCTCGTCAGG |
| **Seq-Jo-002fwd** | TACGCCGGACGCATCGTG |
| **Seq-Jo-002rev** | CGTATCGGTGATTCATTCTGC |
| **Seq-Jo-003fwd** | ATCTCCAGCAGCCGCACG |
| **Seq-Jo-003rev** | CCATACCCACGCCGAAAC |
| **Seq-Jo-004fwd** | AGCGGTATCAGCTCACTC |
| **Seq-Jo-004rev** | GATAGAGGCGCTAGTATG |
| **Seq-Jo-005fwd** | GTTCTTGACCTACCAGAAG |
| **Seq-Jo-005rev** | CACGTTTATTGCACACTC |
| **Seq-Jo-006fwd** | GAGAAATGCATCAGGCTG |
| **Seq-Jo-006rev** | GATGCATAGGATAGGTCG |
| **Seq-Jo-007fwd** | GGTTCTAACAATTCCTCC |
| **Seq-Jo-007rev** | GTGGCGCTGGTAATGATG |
| **Seq-Jo-008fwd** | GCTGAAAGGGATGGCTACG |
| **Seq-Jo-008rev** | GACCTAGATTCTCATAGAC |
| **Seq-Jo-009fwd** | CCTCTTCGTAGAATGCGG |
| **Seq-Jo-009rev** | CAAGAATACGCCAACAGC |
| **Seq-Jo-010fwd** | CGACACAGTTCATAACCG |
| **Seq-Jo-010rev** | GAAAAAGATCCTGGGGTG |
| **Seq-Jo-011fwd** | CCATCCTCATCCACTATAG |
| **Seq-Jo-011rev** | CCAGCGAGATTCTTATTTCG |
| **Seq-Jo-012fwd** | CACAGCGTTTCTGTGACC |
| **Seq-Jo-012rev** | GATCCTCACACTTACTCTGC |
| **Seq-Jo-013fwd** | CAATAGGACGAGGGAATC |
| **Seq-Jo-013rev** | GAGTTATTGCCCAGGTAGG |
| **Seq-Jo-014fwd** | TGATTGGAGAAAACACCG |
| **Seq-Jo-014rev** | CGTTTGTATCGCTATATGTACG |
| **Seq-Jo-015fwd** | GATCTCTTCGTGTAGTTGG |

### 2.3.5. Cold atmospheric pressure plasma treatment for in-situ modification of anion exchange chromatography media to create SEC-IEC adsorbents

#### 2.3.5.1. Plasma etching of chromatography supports at ambient temperatures

IEC adsorbents were treated in a custom-built fluidised bed reactor attached to an underwater plasma generation system (Figure 2-2).

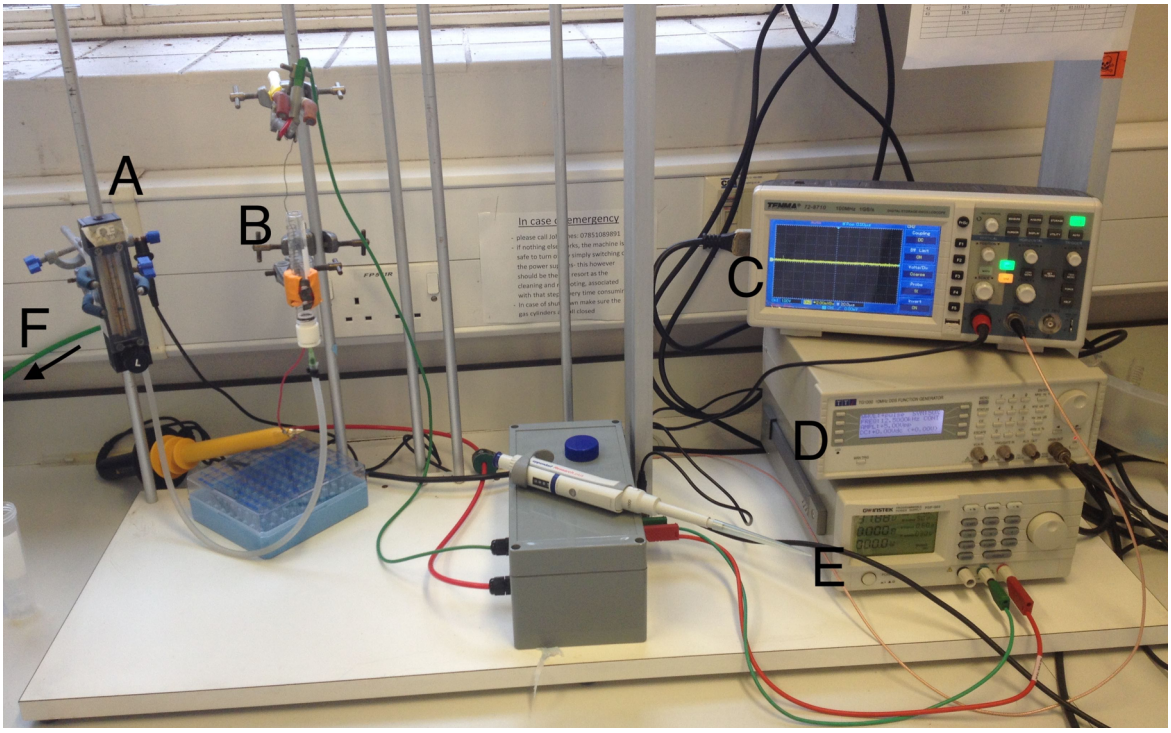


Figure 2-2 Set-up of the fluidised bed plasma reactor with associated periphery
A: gas flow meter; B: reaction vessel; C: oscilloscope; D: function generator; E: DC Power supply; F: gas cylinder (not shown)

In preparation for plasma treatment, adsorbents were washed and equilibrated in MQW and a 5x suspension (water: supports) was created. The suspension was vortex mixed on a VM 20 vortex mixer (Chil Tern Scientific Instrumentation, London, UK) and 5 mL (2.5 mL) was pipetted into a 15 mL Eppendorf tube and filled up with MQW to a total of 8 mL to create a 12.5% v/v (6.25% v/v) suspension and allowed to settle overnight (Figure 2-4 A).

For treatment, sample tubes were attached as shown in Figure 2-4 B; the purpose-built plug comprising of ceramic (machinable Macor glass ceramic (Figure 2-3; UK Farnell, Leeds, England)) and PTFE sealing rings plus a hollow electrode attached to a gas supply set to 0 SLM, was inserted into the open end of the sample tube (Figure 2-4 B).

To avoid the sample slurry flowing back into the gas line, the gas supply was opened. The tube was then inverted (Figure 2-4 C) and the tube tip was sliced off using a razorblade (Figure 2-4 D) to allow gas to exit during plasma operation. The second electrode was inserted from the top into the slurry, with the tip of the electrode 1 cm below the surface of the slurry (Figure 2-4 E). The upward flow of gas via the hollow syringe electrode at the base of the tube was set to the desired value, providing mixing of the sample slurry while equilibrating it with the respective carrier gas.

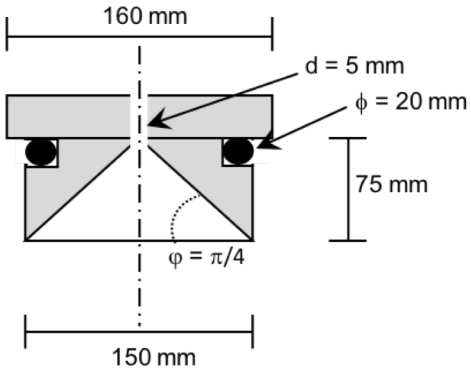


Figure 2-3 Custom built Macor ceramic plug of FBR

Frequency and flow rate were set to desired values and the slurry was treated for a set amount of time. During the plasma treatment, power input was kept constant by manually adjusting the voltage.

Current and voltage were measured with a Pearson Current Monitor 2877 (Pearson, California) and a Tektronix P5100 High Voltage Probe (Tektronix, Oregon). Signals were recorded on a Tektronix DPO4104 Digital Phosphor Oscilloscope (Tektronix, Oregon). Power was regulated and supplied using a PSP-603 power supply (GW Instek; UK Farnell, Leeds, UK). After the time of treatment had finished, the Power supply was cut and the slurry washed out of the reactor into a vacuum filter vessel. The supports were washed with 3X 150 mL of MQW and vacuum dried before gently scraping the sample cake off the filter and resuspending it in TE buffer (10 mM Tris-HCl; 1 mM disodium EDTA; pH 8.0; 10 mL total slurry volume, 10% slurrry).

Post treatment, each support sample was analysed in duplicate (results averaged) for its BSA and pDNA static binding capacities, to assess the reduction of core and shell binding levels respectively as described in 2.3.6.

Unless stated otherwise, all sample media were treated in MQW as surrounding buffer.

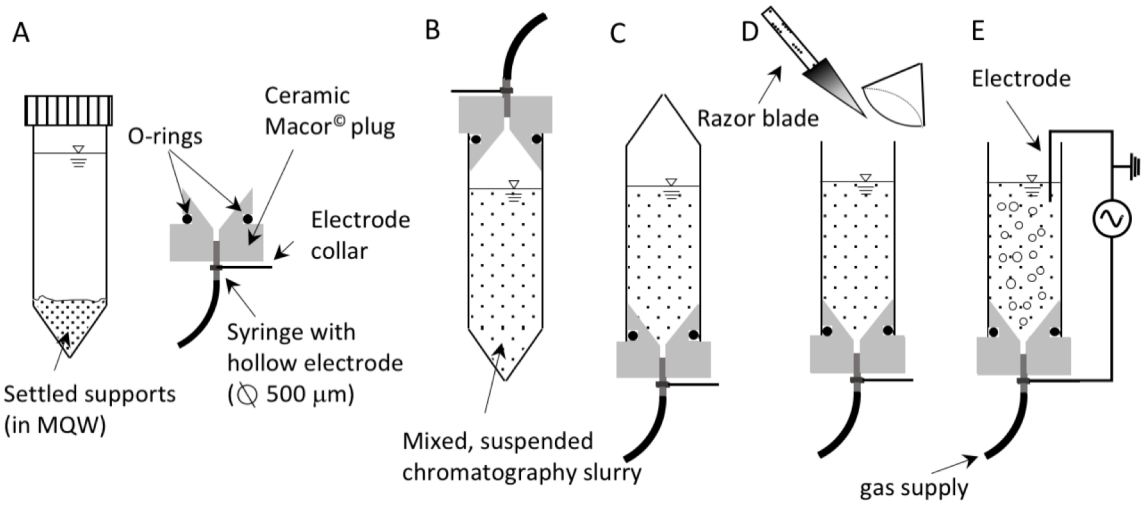


Figure 2-4 Sketch drawing of 'top down' fabrication process of cold atmospheric pressure plasma treatment for in-situ plasma etching and oxidation of chromatography supports to create SEC-IEC adsorbents
A: 15 mL Eppendorf tube with settled chromatography supports in MQW (left); purpose-built ceramic plug, supplied with PTFE O-rings with a hollow syringe attached to a gas supply and a copper electrode collar (right)
B: Vortex mixed Eppendorf tube with chromatography media slurry connected to the plasma apparatus (no gas flow)
C: Inversion of the set-up (start gas flow to prevent backflow of slurry into the gas supply line)
D: Slicing off the top of the Eppendorf tube with a razor blade allowing gas flow to mix slurry and equilibrate buffer with working gas
E: Insertion of electrode into the slurry; connection of electrical equipment, ready for plasma treatment operation

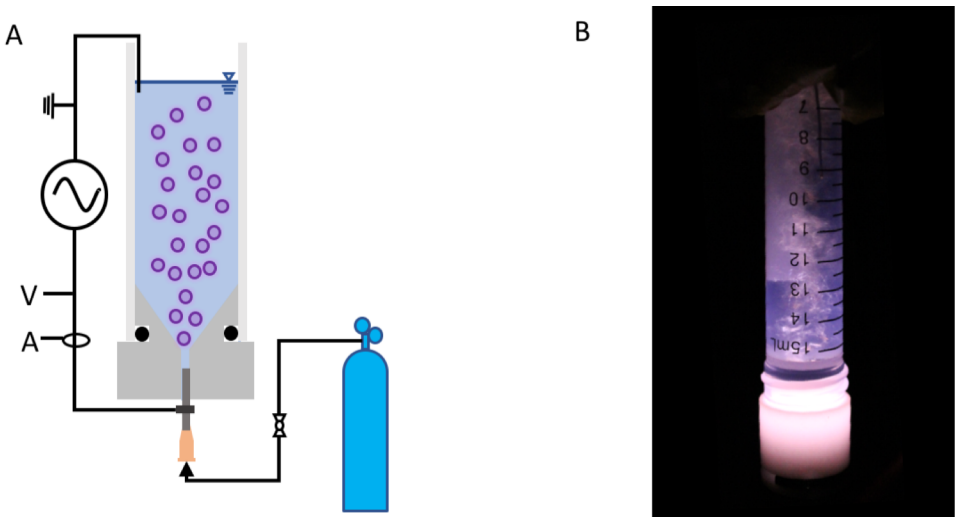


Figure 2-5 Fluidised bed plasma reactor under operational conditions

2.3.5.2. Plasma etching of chromatography supports after addition of a stirred ice bath

To investigate the influence of slurry temperature during plasma etching treatment, the reactor was modified by adding a stirred ice bath (Figure 2-6). The cooling tank was directly attached to an inverted 15 mL Eppendorf tube imposing several modifications to the operational work flow.

Instead of attaching the sample tube, inverting it and cutting off the tip of the tube, the gas flow through the reaction chamber was set and the slurry directly pipetted into the reactor vessel. To avoid interference with dissolved gas impurities in the sample buffer, the gas was allowed to flow through the slurry for one minute prior to application of voltage to the reactor. The plasma operation was then conducted as described above.

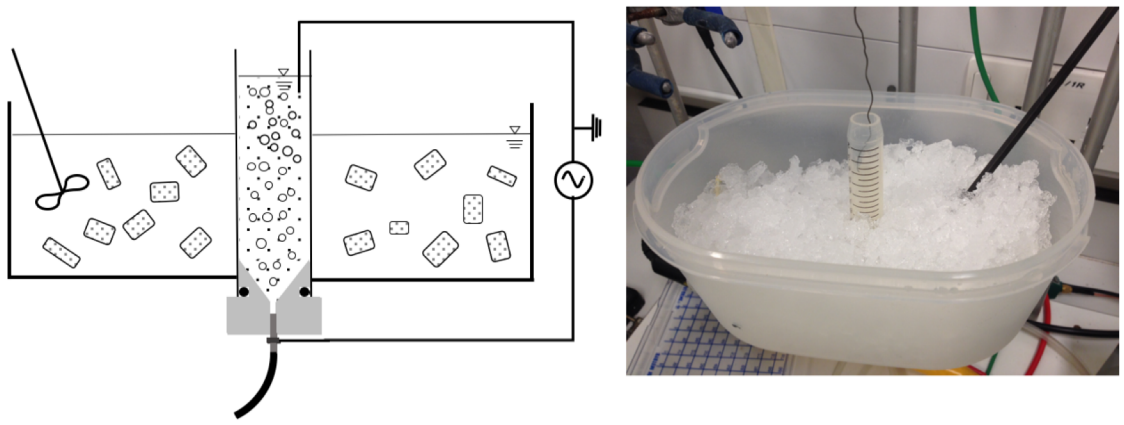

Figure 2-6 Modified reactor with the addition of a stirred ice bath to allow lower operational temperatures during the plasma treatment operation

## 2.3.6. Analysis of the binding properties of multifunctional chromatography supports

'Perfect' bilayered SEC-IEC chromatography supports (functionalised core surrounded by an inert size excluding outer shell) ideally have a very thin size excluding outer shell that prevents large nanoplexes to access and bind to the charged core of the supports as large non-adsorptive layers surrounding the charged core increase the dead volume of the media in a column chromatography operation.

In a 'top-down' approach for the manufacturing of such supports the aim has to be to create a thin outer shell while maintain full core functionality in order to avoid the loss of binding capacity. The lower limit for the thickness of the non-adsorptive layer is hereby the length of

the intermolecular forces that cause the nanoplex of interest to bind to the ligand of the support.

2.3.6.1. Static pDNA binding studies

Chromatography supports were washed in MQW and equilibrated in TE buffer (10 mM Tris-HCl; 1 mM disodium EDTA; pH 8.0) in a 10x suspension for ease and precision of sample handling. The supports were aliquoted into 750 μL (75 μL settled bed volume (SBV)) aliquots, allowed to settle and the supernatant was carefully pipetted out. The beads were incubated with 1.5 mL pDNA solution (concentration dependent on maximum binding capacity of respective media) on a blood rotor shaker SB1 (Stuart Scientific; Staffordshire; UK). Then the samples were centrifuged (2,000 g; 10 sec) and the supernatant was carefully pipetted out for quantification.

2.3.6.2. Static BSA binding studies

Chromatography supports were washed in MQW and equilibrated in TE buffer (10 mM Tris-HCl; 1 mM disodium EDTA; pH 8.0) in a 10x suspension for ease and precision of sample handling.

The supports were aliquoted into 750 μL (75 μL SBV) aliquots, allowed to settle and the supernatant was carefully pipetted out. The beads were incubated with 1.5 mL BSA solution (concentration dependent on maximum binding capacity of respective media) on a blood rotor shaker SB1 (Stuart Scientific; Staffordshire; UK) for 1 h. Then the samples were centrifuged (2,000 g, 10 sec) and the supernatant was carefully pipetted out for protein quantification.

### 2.3.7. Protein concentration measurements

#### 2.3.7.1. Bicinchoninic acid (BCA) assay for total protein concentration measurement

Total protein concentration in liquid samples was measured using the Pierce BCA Protein Kit following the manufacturers protocol:

The working reagent was prepared by mixing 50 parts of Reagent A (sodium bicarbonate; bicinchoninic acid; sodium tartrate in 0.1 M NaOH) to 1 part of Reagent B (4% cupric sulfate). Aliquots of 25 µL of sample were incubated with 200 µL of the working reagent on a plate rotor (37°C; 30 min; 200 RPM). Absorbance was measured after the plate was allowed to cool to room temperature on a GloMax-Multi Detection System (Promega UK; Southampton; UK) plate reader at 562 nm and compared to BSA standard curve for concentration determination.

#### 2.3.7.2. Spectrophotometric measurement of protein concentration

For small numbers of samples (highly pure BSA samples in TE buffer), a simple spectrophotometric assay was used. Protein solution (900 µL) was pipetted into a quartz cuvette (path length 10 mm; Suprasil, Hellma Analytics, UK) and the $OD_{280}$ was measured (Evolution 300, Thermo Fisher, Madison, USA). The protein concentration in solution was calculated according to Beer's Law (Beer, 1852):

$$A = \varepsilon * b * c$$

With A = Absorbance; c = concentration; $\varepsilon$ = molar extinction coefficient ($\varepsilon_{BSA}$= 6.6 (Fasman *et al.*, 1989)); b = path length

TE buffer (10 mM Tris-HCl; 1 mM disodium EDTA; pH 8.0) was used as a blank.

### 2.3.8. Nucleic Acid Quantification

Several different methods have been employed for pDNA quantification in solutions. Depending on sample purity requirements, simple optical density and fluorometric analyses methods were used, while DNA contents in *E. Coli* lysate fractions were analysed with DPA assay.

#### 2.3.8.1. Spectrophotometric analysis of pDNA concentration in solution

For small numbers of samples (highly pure pDNA in TE buffer, purified using Qiagen lysis as described in 2.3.3. ), a simple spectrophotometric assay was used. Plasmid DNA solution (800 μL) was pipetted into a quartz cuvette and absorbance was measured at $OD_{260}$. TE buffer (10 mM Tris-HCl; 1 mM EDTA; pH 8.0) was used as a blank, using a 10 mm path length quartz cuvette, the concentration of ds pDNA in solution and the optical density are linearly correlated for $OD_{260}$ = 0.1 - 1 and were calculated using the following equation (Barbas *et al.*, 2007):

$$c = OD260 * 50 \frac{\mu g\ [pDNA]}{mL\ [TE\ buffer]}$$

with c = concentration [$\mu g_{pDNA}/mL_{TE}$]

#### 2.3.8.2. Fluorometric quantification of pDNA content in aqueous solution using Hoechst dye 33258 ds DNA label

Hoechst dye 33258 is a known fluorescent label that is used for the quantification of DNA due to its fluorescent enhancement upon binding to A-T rich regions of ds DNA (Latt *et al.*, 1976; Loontiens *et al.*, 1990). The following microwell plate method is an adapted protocol by Rago et al. (Rago *et al.*, 1990).

Due to the light sensitivity of the dye, all experiments were conducted in a dark environment with all equipment wrapped in aluminium foil.

Hoechst dye 33258 was dissolved till oversaturation in a DMSO/MQW (1/4- v/v) solution, centrifuged (2,000 g; 20 s) and the saturated supernatant was pipetted out, centrifuged (2,000 g; 20 s) and the supernatant was pipetted out into a clean vessel to avoid undissolved dye in the solution.

Aliquots of 25 μL of Hoechst dye 33258 solution were mixed with 10 mL of TNE buffer (10 mM Tris; 2 M NaCl; 1 mM EDTA; 2 mM sodium azide; pH 7.4) to create the working reagent.

100 μL of working reagent were mixed with 100 μL of pDNA solution in a microwell plate and after 10 min incubation time the fluorescence intensity was measured (excitation/ emission (ex/em): 360/460 nm). The blank fluorescence of MQW was subtracted from each value.
Calf thymus DNA (in TE buffer; 10 mM Tris-HCl, 1 mM disodium EDTA, pH 8.0) was used to create a standard curve.
The fluorescence intensity counts are linearly correlated up to pDNA concentrations of at least 20 μg/mL (calf thymus (ct) DNA standard curve is depicted in Appendix A-2). As the binding specificity is strongly affected by the ionic strength of the surrounding buffer (Labarca *et al.*, 1980), all samples were kept in the same (TE) buffer environment without addition of further solutes.

2.3.8.3. Diphenylamine (DPA) assay to quantify pDNA concentrations

DPA assay is a colorimetric procedure to determine the concentrations of DNA in solution first described by (Burton, 1956). Total pDNA concentrations of column chromatography fractions were determined following a modified protocol (Gendimenico *et al.*, 1988), by mixing 175 μL of pDNA solution with 25 μL of 2 mg/mL BSA solution (in MQW) in a screw cap microcentrifuge tube before adding 200 μL of 0.4 M perchloric acid and mixing on a VM20 vortex mixer (Chil Tern Scientific Instrumentation, London, UK). The samples were incubated (0.5 h; at 4°C) and then centrifuged (10,000 g; 20 min). The supernatant was carefully pipetted out and discarded. The pellet was resuspended in 250 μL of 1 M perchloric acid by vortex mixing and incubated on a spinning heating block (70°C; 200 rpm; 30 min). Samples were allowed to cool to room temperature and mixed thoroughly with 500 μL of freshly prepared chromogenic reagent (prepared by mixing 200 parts of diphenylamine solution (1.5 g DPA dissolved in 100 mL glacial acetic acid and 1.5 mL of concentrated sulfuric acid) with 1 part of 2% (v/v) acetaldehyde). The samples were then incubated overnight on a heating block mixer (37°C; 18 h) and following incubation taken for $OD_{600}$ measurement (MQW was used as a blank). Calf thymus DNA solutions (in TE buffer; 10 mM Tris-HCl, 1 mM disodium EDTA, pH 8; concentrations determined by $OD_{260}$ measurements) were used to construct a standard curve for DNA concentration. Due to the hazardous nature of some of the compounds, the whole assay was performed in a fume cupboard.

#### 2.3.8.4. Orcinol assay for RNA quantification (Almog *et al.*, 1978)

Orcinol assay for RNA concentration measurement used in this study is based on a protocol first described by (Almog *et al.*, 1978).

Solution A was prepared by dissolving 100 mg of iron(III) chloride in 100 mL concentrated hydrochloric acid. Solution B was prepared by dissolving 300 mg of orcinol in 5 mL MQW. A working reagent was prepared by mixing 70 mL of solution A with 2.45 mL of solution B.

200 µL of the chromatography fraction sample containing RNA (diluted 1:2 with MQW) was mixed and incubated with 300 µL of freshly prepared working reagent in a water bath (95°C; 20 min). After cooling to room temperature, the samples were centrifuged (600 rpm; 15 min) and the supernatants were pipetted out for spectrophotometrical analysis at $OD_{665}$ (MQW used as blank).

RNA standards from baker's yeast (*S. cerevisiae*) were handled alongside the RNA samples at a concentration range of 0-100 µg/mL to construct a standard curve.

### 2.3.9. Ionic capacity measurements

Measurement of ionic capacity of beaded chromatography materials was conducted following a protocol by (Theodossiou *et al.*, 2002).

Chromatography supports (0.25 mL SBV in MQW) were incubated with 25 mL of 2 M NaCl for 1.5 h. To remove excess $Cl^-$ ions (from both the supernatant and unspecifically bound to supports), the supports were washed and drained five times with 50 mL MQW on a vacuum filter. The drained supports were subsequently transferred to 50 mL centrifuge tubes containing 25 mL of 0.1 M NaOH and incubated overnight on a blood tube rotator SB1. During the incubation with NaOH, excess $OH^-$ ions displace the $Cl^-$ ions on the beads, releasing them into the surrounding buffer. Supports were left to settle and 1 mL was taken for $Cl^-$ ion determination.

$Cl^-$ ion quantification was performed by either mixing 1 mL sample or calibration ladder solution with both 100 µL of 0.25 M ammonium iron (III) sulphate in 9 M $HNO_3$ and 100 µL of mercury (II) thiocyanate saturated in 96% ethanol. The sample was then mixed vigorously on a VM20 vortex mixer (Chil Tern Scientific Instrumentation, London, UK). The reaction was stopped after 5 min and the $OD_{460}$ was measured (UVIKON 922 spectrophotometer; KONTRON

Instruments, Bletchley, UK). NaCl solutions (range 0.1- 2 mM) were used to obtain a standard curve for the $Cl^-$ ion concentration.

### 2.3.10. Sample preparation of plasma treated chromatography supports for Time of Flight Secondary Ion Mass Spectrometry (ToF SIMS) analysis

Prior to their usage in ToF SIMS, support samples were dried following an adapted protocol by (Johansson *et al.*, 2004).

For each sample, 50 µL of SBV beads were equilibrated three times in a 2 mL Eppendorf tube in 2 mL of MQW, centrifuged (2,000 g; 10 sec) and the supernatant was carefully pipetted out. The samples were suspended in 2 mL of 0.5 M NaCl (in MQW), centrifuged (2,000 g; 10 sec) and the supernatant was carefully pipetted out before suspending the pellet in 2 mL of MQW followed by centrifugation (2,000 g; 10 sec) and the supernatant was discarded. The supports were transferred to a HetoVac Speed vacuum system and gently dried overnight at 1 mbar.

The samples were sealed, shipped to and ToF-SIMS spectra for analysis of the chemical composition of adsorbent surfaces were recorded with the help of Dr Martina Modic (Jožef Stefan Institute, Ljubljana).

### 2.3.11. Imaging of chromatography media

For selection of chromatography media for nanoplex purification, several parameters such as stability (how often can the column be used before the media needs to be replaced?), rigidity (what cleaning in place (CIP) regiment can be applied without damaging the media?), pore size distribution (what is the exclusion limit of the media?), breakthrough capacity (how much can be loaded onto the column in a single chromatographic (batch) operation?) and level of cross-linking (what pressures/ flow velocities can be applied to a packed column?) are important factors to be considered.

Often secondary for the choice of media is its visual appearance; however, when aiming to modify the exterior of particles' surfaces, their structural integrity becomes relevant.

It was previously reported that plasma treatments of chromatography media to modify the chemical composition of the surface of hydrogel chromatography particles lead to severe visual alteration (Olszewski *et al.*, 2014). Several techniques, used in this study to monitor the visual integrity post plasma treatment (ESEM, light microscopy), to assess the spatial

distribution of protein and pDNA binding (CLSM) of the particles as well as their size distributions, were therefore employed.

#### 2.3.11.1. Environmental Scanning Electron Microscopy

Chromatography support samples were prepared by dehydration in ethanol followed by critical point drying. Imaging of samples was carried out on a Philips XL-30 FEG Environmental SEM (FEI Company, OR, USA).

ESEM visualization of chromatography supports was kindly assisted by Mr Paul Stanley, School of Metallurgy and Materials, University of Birmingham.

#### 2.3.11.2. Light microscopic analysis of chromatography media

80 μL of chromatography supports slurry in MQW were pipetted onto a microscope slide (VWR VistaVision Microscope Slides, VWR International, UK) and covered with a cover glass (VWR Micro Cover Glasses), carefully avoiding the formation of air bubble inclusions. The sample was then analysed in an Olympus BX50 light microscope using 4x, 10x, 20x or 40x magnification respectively. For images taken with a 100x magnification, a droplet of immersion oil (Sigma Aldrich) was used to bridge the gap between the lens and the cover slide. Images were taken with a Moticam 800x600 PIX, controlled by Motic Images plus 2.0 ML software. Further image analysis was conducted with (Fiji is just) ImageJ (Version 1.0 for Mac).

### 2.3.12. Exploring the binding topography of SEC-AEC media using confocal laser scanning microscopy (CLSM)

#### 2.3.12.1. Tagging of BSA with fluorescent dye Cy5

To get an insight into the spatial distribution of bound probes (BSA and pDNA) to chromatography media, CLSM was employed. The fluorescent probe Cy5 was attached to BSA according to the following protocol (due to light sensitivity of Cy5, all sample tubes were wrapped in aluminium foil and kept away from light):

5 mL of BSA solution (70 mg/mL) was prepared in TE buffer (10 mM Tris-HCl, 1 mM disodium EDTA, pH 8.0). The solution was incubated with 32.4 μL of Cy5 NHS Ester stock solution (1 mg/mL in DMSO) for 1 h on a Stuart Scientific SB1 rotor.

To acquire a molar ratio of 1: 100 Cy5: BSA (Hubbuch *et al.*, 2008) the required amounts were calculated using the following equations:

$$n(BSA) = \frac{c(BSA\ solution) * V(BSA\ solution)}{M(BSA)}$$

$$= \frac{0.07\ \frac{g}{mL} * 5\ mL}{66430\ \frac{g}{mol}} = 5.267 * 10^{-6}\ mol$$

$$n(CY5)\ = \frac{n(BSA)}{100} = 5.267 * 10^{-8}\ mol$$

$$m(CY5) = n(CY5) * M(CY5)$$

$$= 5.267 * 10^{-8}\ mol * 616.19 \frac{g}{mol} = 0.0324\ mg$$

$$V\left(CY5\ solution;\ 1\frac{mg}{mL}\right) = \frac{m(CY5)}{c(CY5)} = \frac{0.0324\ mg}{1\frac{mg}{mL}} = 0.0324\ mL = 32.4\ \mu L$$

The used dye: protein ratio was found to reduce re-adsorption of emitted light and allowed for efficient purification of labelled protein. Free, un-conjugated dye was separated from the bio-conjugated proteins using single-use PD-10 desalting columns packed with SE Sephadex G-25 media. The column was equilibrated in 25 mL of TE buffer (10 mM Tris-HCl, 1 mM disodium EDTA, pH 8.0) before 2.5 mL of the Cy5 tagged BSA solution was applied to the column in gravitational flow and subsequently eluted using 3.5 mL of TE buffer (10 mM Tris-HCl, 1 mM disodium EDTA, pH 8.0), yielding 3.5 mL of Cy5 tagged BSA solution (c= 50 mg/mL). The solution was stored away from light in the fridge until further usage.

2.3.12.2. Labelling of pDNA with green fluorescent stain Syto 9

To provide a quantitative correlation between signal intensity and pDNA binding capacity, the pDNA solution was pre- stained using the minor grove binding fluorescent dye Syto 9 according to the following protocol:

$$Vdye = mpDNA * \frac{\#bp\ per\ pDNA\ molecule}{tagging\ factor} * \frac{1}{MpDNA * cdye}$$

Purified pDNA stock solution (26.688 kbp; M = 16.49 * 10^6 g/mol (Bioinformatics, 2017) in TE buffer (10 mM Tris-HCl; 1 mM disodium EDTA; pH 8.0); see 2.3.3. ) was thawed overnight in the fridge and diluted with TE buffer (10 mM Tris-HCl; 1 mM disodium EDTA; pH 8.0) to a concentration of 15 $\mu g_{pDNA}$/mL. A sample of 4 µL Green fluorescent stain Syto 9 stock solution (c = 5mM in DMSO) was mixed with 96 µL of MQW to create a Syto9 working solution (c = 0.2

mM; due to the light sensitivity of the Syto9 dye all tubes were wrapped in aluminium foil and kept away from light).

pDNA solution was incubated with Syto9 working solution (ratio of 100 bases of nucleic acid to 1 dye molecule) on a Stuart Scientific SB1 rotor mixer for 1 h:

$$\frac{\text{Vsyto 9 working solution}}{\text{1 mL pDNA solution}} = 1.215\ \mu\text{L}$$

During the assay development, it was found that a separation step, ridding the solution of unconjugated dye was unnecessary for subsequent use in the CLSM analysis. This is the result of both the high binding affinity of the dye to ds DNA as well as its enhancement of fluorescence intensity upon binding (Stocks, 2004).

2.3.12.3. CLSM Analysis of chromatography supports

50 μL SBV of chromatography supports were equilibrated three times in TE buffer (10 mM Tris-HCl; 1 mM disodium EDTA; pH 8.0), centrifuged (2,000 g; 10 sec) and the supernatant carefully pipetted out. The beads were incubated with 1 mL Syto 9 tagged pDNA solution (c = 15 μg/mL) on a Stuart Scientific SB1 rotor mixer for 1 h. Then the samples were centrifuged (2,000 g; 10 s) and the supernatant was carefully pipetted out. The beads were washed three times with 1 mL of TE buffer (10 mM Tris-HCl; 1 mM disodium EDTA; pH 8.0) to avoid unspecific binding.

The samples were then incubated with 1 mL of Cy5 labelled BSA solution (c= 5 mg/mL) on a Stuart Scientific SB1 rotor mixer for 2 h, centrifuged (2,000 g; 10 s) and the supernatant carefully pipetted out. The beads were washed three times with 1 mL of TE buffer (10 mM Tris-HCl; 1 mM disodium EDTA; pH 8.0) to avoid unspecific binding and resuspended in 950 μL of TE buffer (1 mL total volume).

100 μL of the suspension was pipetted onto a microscope slide and covered with a cover glass. A droplet of immersion oil was used for the microscopic analysis.

All samples were analysed on a Leica TCS SPE 102A CLSM system equipped with krypton/ argon (λ = 488 nm and λ = 568 nm) and helium/ neon (λ = 633 nm) lasers, using a 40x/ 1.15 Oil ACS Objective. A light microscopic image was taken of the analysed beads (LCMOS 3M, Brunel Microscopes), focussing on the central meridian of each bead.

The beads were manually focussed and a z-stack image series was recorded for both excitation wavelengths; Cy5 tagged BSA ex/em: 635 nm/654- 715 nm; Syto9 tagged pDNA ex/em:

488 nm/492- 533 nm. Images were captured using the Leica Application Suite (LAS X) software (Version 1.9; Leica Microsystems, GmbH). Settings including laser intensity, signal gain, offset and emission detection range were optimised to suppress auto-fluorescence. Control tests ensured that the detected emitted light intensity was within detection range and blank tests confirmed the absence of auto-fluorescence of untagged protein, pDNA and chromatography resin (Close *et al.*, 2013). Emission detection ranges for the photomultiplier tube, gain, offset and thresholds were adjusted to enhance fluorescence detection.

ImageJ was used for data analysis and processing. GIMP 2.8.22 was used to remove artefacts from images.

### 2.3.13. Measurement of the particle size distribution of beaded chromatography media

Particle size distributions of various chromatography media were analysed using, a Mastersizer Hydro 2000 SM (Malvern Instruments; Malvern; UK).

The optic cell was drained and flushed three times with MQW. To remove air bubbles from the sample lines, the stirrer speed was set to 1,000 RPM for 10 s prior to sample addition.

Chromatography supports were washed three times in water (1 mL of supports (SBV) in 15 mL MQW) and gently centrifuged to assist sedimentation and clearance of fines (500 RPM; 2 min).

A background measurement was taken to ensure absence of artefacts and to calibrate the baseline of laser obscuration. Chromatography support samples in MQW were then pipetted into the chamber (laser obscuration between 10 and 20%- aim 13%).

For the SOP controlling the measurement, the refractive index of agarose was used (1.42 (Deane, 2013)). After the measurement was done, the support sample was drained from the chamber and flushed three times with MQW before the next measurement.

For post experimental data analysis; number, surface and volume weighted size distributions were calculated and the respective histograms plotted using MATLAB_R2017a.

# Chapter 3 Cold atmospheric pressure plasma etching and oxidation of AEC media for preparation of multifunctional bilayered supports

## Abstract

Means for the production of bilayered size exclusion/ ion exchange chromatography materials by modification of support exteriors via plasma etching and oxidation using cold atmospheric pressure plasmas was investigated. Four different anion exchange chromatography adsorbents (Q Sepharose Fast Flow, DEAE Sepharose Fast Flow, Q Hyper Z and EMD Fractogel DEAE) were treated using plasmas generated from He-$O_2$ admixed gasses in a Dielectric Barrier Discharge and a novel underwater fluidised bed reactor configuration. The degree of bilayering was assessed via static binding studies using BSA and pDNA as probes for retention of core and surface binding respectively.

In the DBD configuration, SI values were seen to have an inverse correlation with distance between the sample and upper electrode plate during treatment, with treatments at a distance of 4.5 mm producing SI values up to ~5 (85% loss of pDNA binding with <25% loss of BSA binding). In the fluidised bed configuration, treatment of supports with a He-$O_2$ plasma produced supports with SI values up to ~3, corresponding to 70% loss of pDNA binding in exchange for 8% loss of BSA binding.

A CLSM method was developed to visualise the binding topography of BSA and pDNA, adsorbed to chromatography supports, revealing limitations of the plasma etching and oxidation technique due to the presence of irregularities on the surface of single adsorbents.

## 3.1. Introduction

Preparative chromatography is considered a pivotal tool in DSP for the biopharmaceutical industry (Ghanem *et al.*, 2013; Abdulrahman *et al.*, 2018).

However, in comparison to advances made in upstream production of biopharmaceutical manufacturing, DSP has seen little innovation, especially in development of novel column chromatography approaches. Advances in the development of high-level expression systems for upstream processing have led to dramatic cost reductions as well as titre increases, and DSP is increasingly viewed as a bottleneck for the overall manufacturing costs associated with the production of biopharmaceuticals (Pinto *et al.*, 2015). New challenges, that column chromatography is facing include increased size and complexity of emerging bio-products, rising product titres, increasing costs of goods and waste disposal requirements as well as tougher competition from other DSP purification techniques. Confronted with such multifaceted challenges, it becomes increasingly unlikely that optimisation of existing mono-functional chromatography techniques will be able to hold up to fulfil all expectations posed on beaded chromatography as a purification technique. As opposed to the 'one column- one functionality' approach that has dominated the chromatographic research for decades, solutions for the outlined challenges can be achieved by reimagining chromatographic separation based on multifunctional adsorbents.

Among more complex geometries, the simplest multifunctional support design is a bilayered adsorbent featuring a ligand functionalised core surrounded by an inert, outer layer that restricts access of large molecular entities such as plasmid DNA, viruses, VLPs, immunoglobulin M (IgM) to the binding core via size cut off (Figure 3-1, B). Bilayered beads based on combining adsorptive chromatography with a SE shell have been successfully utilised in the purification of pDNA molecules (Gustavsson *et al.*, 2004; Kepka *et al.*, 2004), separation of organic acids (Dainiak *et al.*, 2002b; Viloria-Cols *et al.*, 2004) and in protein purification in the form of EBA media (Dainiak *et al.*, 2002b; Jahanshahi *et al.*, 2008). Since 2012, media with the outlined properties have been introduced to the market (GE Healthcare Bio-Science, 2012) and are commercially available for purification of viruses and other large biomolecules (Blom *et al.*, 2014; Weigel *et al.*, 2014; Lagoutte *et al.*, 2016; Somasundaram *et al.*, 2016).

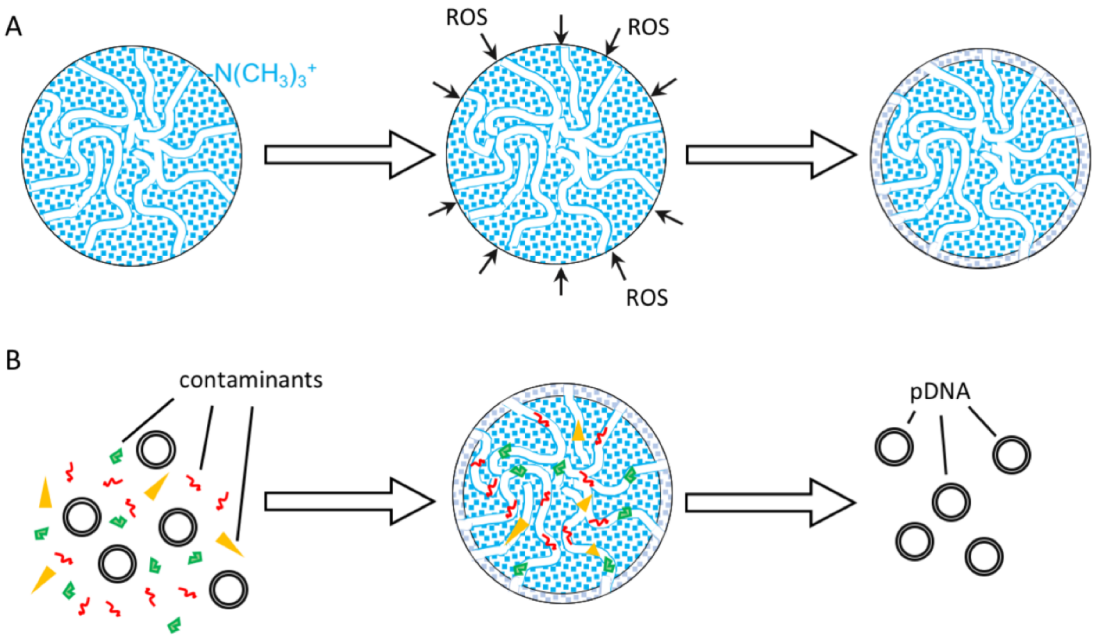


Figure 3-1 Working principle of plasma etching and oxidation to create SEC- AEC supports (A): the ROS react with the $N(CH_3)_3^+$ ligand groups etching them off the surface, leaving only the agarose base matrix behind. Small charged contaminants are able to penetrate through the outer SEC layer and bind to the functionalised interior of the bead whereas large pDNA molecules are too big to access the pores -the inert exterior prevents them from binding altogether, passing the column in the flow through (B)

Most chromatographic purification techniques available for the separation of bio-therapeutic entities were originally developed and optimised for the separation of protein based products. More complex bioproducts such as pDNA, viral vectors or vaccines of high molecular weight do however differ dramatically in size and properties to protein based products and as a result require different purification strategies (Lyddiatt *et al.*, 1998; Prazeres *et al.*, 1999; Ferreira *et al.*, 2000b; Theodossiou *et al.*, 2001). Current industrial purification techniques for pDNA products still rely heavily on packed bed chromatography with IEC being the most prevalent first capture step, followed by SEC to polish the elution fractions (Prazeres *et al.*, 1999; Ferreira *et al.*, 2000b; Freitas *et al.*, 2009a).

Bilayered SEC-IEC support media based on a charged core surrounded by a non-binding, size restricting shell have shown to improve performance of pDNA purification from smaller, chemically similar contaminants such as RNA, HCP and endotoxins (Gustavsson *et al.*, 2004; Kepka *et al.*, 2004).

The bilayered SEC-IEC design also shows benefits for EBA (Arpanaei *et al.*, 2010). Problems associated with collapsing beds, due to cross-linking of the surfaces of IEC particles by 'sticky' molecules in the feedstock, have resulted in a slow uptake of the technique in industry (Ameskamp *et al.*, 1999; Theodossiou *et al.*, 2001; Abdulrahman *et al.*, 2018). Attempts to resolve inter-particle linking of the adsorbents via chemical and mechanical conditioning of the feedstock have yielded limited success (Lin *et al.*, 2004; Hubbuch *et al.*, 2006; Sonnenfeld *et al.*, 2006). Ideally, the surfaces of EBA supports would hence be non-interactive, with bilayered media offering exactly that- small entities of the feedstock such as RNA and proteins are bound within the core, while larger molecules cannot link the adsorbents due to the non-interactive nature of the surrounding shell and pass through the system in the flow through. To compromise the least on mass transport and binding capacity, the particle exteriors need to be as thin as possible, while still preventing surface binding (Theodossiou *et al.*, 2002).

In order to provide such multifunctional media, new approaches must be developed, that are capable of modifying surfaces at the nano scale by either applying ultra-thin coatings to bury exposed ligands or removing them from the surface.

Plasma irradiation has been shown to be a useful technology for modifying material surfaces at the 'nano-scale'. Plasma hereby is defined as a wholly or partially ionised medium comprising of ions, electrons, as well as neutral species and photons (Fisher, 2002; Arpanaei *et al.*, 2010). Advantages of such plasma treatments include: (i) operation at low (room) temperatures; (ii) shallow modifications can be achieved, without altering the bulk properties of underlying media; (iii) suitable for modifying many different types and compositions of surfaces; and (iv) no generation of large amounts of toxic by-products (Schram *et al.*, 1987).

Surface modification by plasma is performed in a reactor supplied with a suitable gas (e.g. helium admixed with oxygen (Knake *et al.*, 2008; Park *et al.*, 2010)). An electrical or electromagnetic supply of energy is provided to ignite a plasma within the reactor. Collisions between the energetic plasma species and gas particles lead to the generation of highly reactive oxygen species suitable for carrying out surface modifying reactions, such as etching away functionalised groups off substrate surfaces and replacing them with polar oxygen containing functions (Figure 3-1, A) (Bruggeman *et al.*, 2016). Surface modifications of materials for bioseparations, induced by the application of plasma have been demonstrated

for numerous studies involving adsorbents for analytical chromatography (Sudo *et al.*, 1998) and membrane materials (Ulbricht *et al.*, 1995; Chen *et al.*, 1999; Pieracci *et al.*, 1999; Liu *et al.*, 2004).

Recent approaches have demonstrated the use of low temperature, low pressure plasma methods to remove anion exchange ligands from the surface of Pall's Q Hyper Z AEC media, leading to bilayered chromatography adsorbents with non-adsorptive exteriors (Arpanaei *et al.*, 2010). Under static binding conditions, these plasma etched beads showed a loss of ~53% of their DNA binding capacity at the expense of merely 9.3% loss of protein binding. Dynamic EBA studies showed that 10% breakthrough capacities of the beads with respect to DNA binding dropped significantly after plasma etching, while retaining their protein binding capacity of the untreated Q Hyper Z.

Given the rigid nature of its base matrix, transferring these low temperature low pressure plasma treatments to other beaded chromatographic support media is, however, hindered by the low pressure (~10 Pa) at which the plasma treatment was carried out. Many common chromatography adsorbents, based on stationary phases such as Sepharose and Sephacryl have soft hydrogel structures. Under aqueous conditions at atmospheric pressure, their stationary phases comprise of swollen agarose (or allyl dextran-N,N'-methylenebisacrylamide copolymer for Sephacryl) beaded structures, with water accounting for over 90% of the support volume, playing an important role to the structural integrity of the supports. Under low pressure conditions, water is easily evaporated from the pores of these hydrogels, due to the reduced vapor pressure of water, leading to loss of support structure and rendering low pressure plasma treatment unsuitable for etching of hydrogel materials.

Alternatively, low temperature plasma can be generated at atmospheric pressure using atmospheric pressure glow discharge approaches (Kanazawa *et al.*, 1988; Xiaogui *et al.*, 2012). Modification of polymeric surfaces using APGD treatment has been demonstrated in a number of studies (Temmerman *et al.*, 2005; Choi *et al.*, 2006; Pappas *et al.*, 2006; Walsh *et al.*, 2007), indicating that APGD may be a suitable alternative for plasma etching of soft hydrogel chromatography adsorbent surfaces.

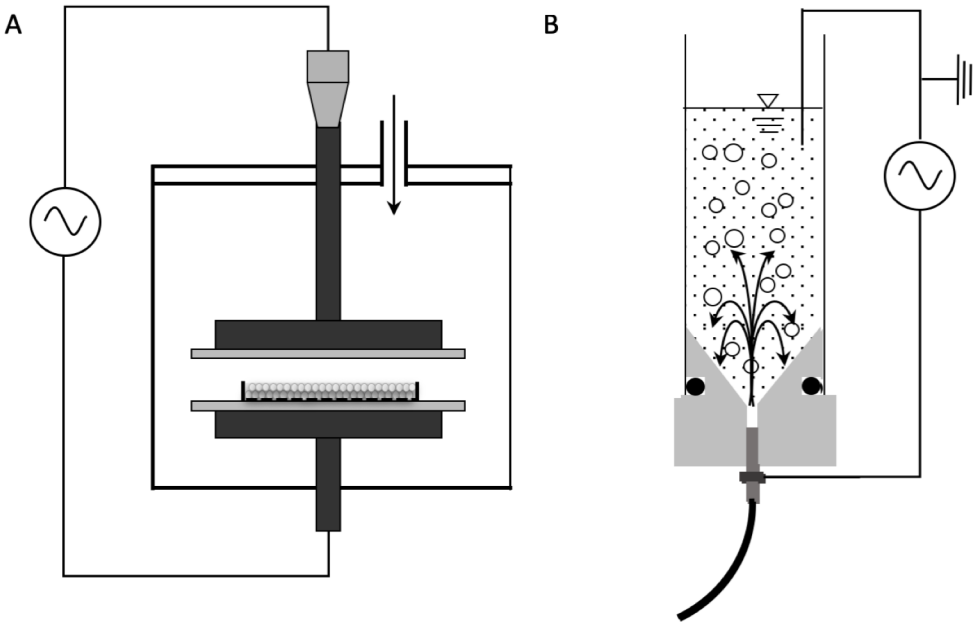


Figure 3-2 Parallel plate set-up (A); Fluidised bed reactor design for in situ treatment of chromatography media in aqueous suspension (B); arrows indicating inlet of carrier gas

In this chapter, the feasibility of creating bilayered chromatography support media based on hydrogel stationary phases by modifying the exteriors of AEC supports through plasma etching at atmospheric pressure was investigated.

Initial plasma etching treatments were conducted using a dielectric barrier discharge (DBD) parallel plate reactor set-up using helium as a carrier gas. The produced supports were analysed using static pDNA and BSA binding studies (combined in the SI, providing a parameter to judge the selectivity of surface vs core binding reduction), featuring a continuation of the early work conducted by Willet (unpublished) and (Arpanaei *et al.*, 2010) (Figure 3-2, A).

Results obtained in these parallel plate experiments have led to the design of a fluidised bed reactor system. The system allows for in situ treatment of fully hydrolysed chromatographic media; the ROS are transported to the supports by bubbling plasma gas through the reaction vessel, providing turbulent mixing of the suspension during treatment (Figure 3-2, B). Parameters controlling the performance of resulting multifunctional chromatography supports were screened by assessing the bulk binding properties of manufactured supports via static protein and pDNA binding studies. The samples were further analysed via ESEM and light microscopic techniques. Spatial distribution of protein and residual pDNA binding sites

post treatment to the exterior of the beads was made visible by implementing CLSM. The chemical composition of the surface of supports was assessed via ToF-SIMS analysis.

## 3.2. Materials and Methods

To avoid repetition of almost identical method descriptions across different chapters of this work, the methods as well as a conclusive list of materials (instrumentation) used for their practical implementation are presented in a separate 'general' Materials and Methods (M&M) section of this thesis (Chapter 2).

Some of the conducted experiments do however require more explanation in regard to specific parameters, complementing the content of Chapter 2. When further information is essential, it is given in the respective sections to aid readability and understanding of the processes.

### 3.2.1. Calculation of SI

The effectiveness of plasma etching of chromatography supports was assessed by static pDNA (surface restricted) and protein (diffusional access throughout adsorbent pores) binding studies of treated media in comparison to an untreated control sample.

The % reductions of static pDNA binding capacities in comparison to the untreated control samples were calculated using:

Reduction of pDNA binding capacity =

$$\frac{(pDNA\ capacity\ of\ control\ sample - pDNA\ capacity\ of\ plasma\ treated\ sample)}{pDNA\ capacity\ of\ control\ sample}\ X\ 100\%$$

The % reductions of static BSA binding capacities in comparison to untreated control samples were calculated using:

Reduction of BSA binding capacity =

$$\frac{(BSA\ capacity\ of\ control\ sample - BSA\ capacity\ of\ plasma\ treated\ sample)}{BSA\ capacity\ of\ control\ sample}\ X\ 100\%$$

When modifying IEC supports to create a bilayered SEC-IEC media it is desirable to reduce the outer shell binding capacity as much as possible, while maintaining a high core binding capacity. To assess the selectivity of shell vs core binding capacity, the Selectivity Index value, first described by Professor Thomas (Arpanaei *et al.*, 2010) was used:

$$Selectivity\ Index = \frac{100\% - reduction\ of\ BSA\ binding\ capacity}{100\% - reduction\ of\ pDNA\ binding\ capacity}$$

It describes the ratio between the residual BSA binding capacity and the residual pDNA binding capacity and consequently the core charge vs the elimination of functional binding ligands off the surface of the chromatography supports. It aids to assess the quality of the bilayering process by factoring in not only the absolute reduction levels but providing a tool to determine the thinness of the inert layer created via the bilayering method of choice.

### 3.2.2. Plasma etching of various chromatography media under atmospheric pressure gas in a dielectric-barrier discharge (DBD) configuration

Plasma etched chromatography resins, manufactured by using the DBD plasma reactor configuration used in this section were functionalised and kindly provided for further analysis by Dr Thomas C. Willett.

A range of anion exchange adsorbents (Q Sepharose FF, DEAE Sepharose FF, EMD Fractogel DEAE and Q Hyper Z) were treated under cold-atmospheric plasma etching conditions to produce bilayered SEC-AEC supports using a DBD set-up (Figure 3-3).

Voltage was applied between two circular powered electrodes measuring 30 x 0.8 mm each attached to an aluminium tile of 40x40 mm with a gap of 5 mm between the surfaces of the two tiles (Figure 3-3). The electrode unit was closed off to surrounding air, with a gas inlet supplying helium gas to the chamber.

Supports were equilibrated in MQW and allowed to settle. Support samples were pipetted from the settled bed onto a 30 mm diameter nylon net (10 µm) rings cut from XK 26 net rings (GE Healthcare, Buckinghamshire), forming a cake of 20 mm diameter, which was then allowed to dry in air (600 s). A pipette tip was used to form each cake into circular shape of

consistent height, air dried for 300 s before placing it on the base electrode in the chamber under helium and consecutively directly exposed to the plasma treatment.

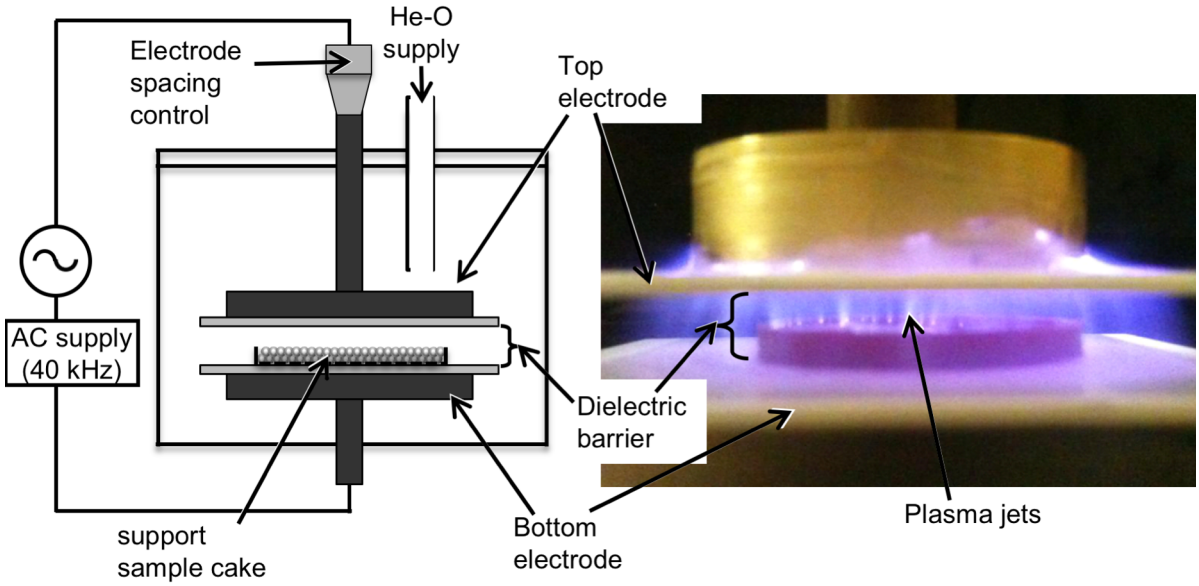


Figure 3-3 'Top down' fabrication of bilayered chromatography supports using atmospheric pressure gas plasma treatment in a DBD configuration
Left: Sketch of apparatus
Right: In situ treatment of chromatography supports under He plasma

Supports were treated under helium (4 SLM) in a parallel plate set-up under continuous and pulsed AC operation modes. A range of support cake volumes (0.16- 1.3 mL), sample distances between plate and sample (0.5- 4 mm), contact times (100- 600 s) and input powers (5- 7 W) were investigated.

Current and voltage waveforms were measured with a Pearson Current Monitor 2877 (Pearson, California) and a Tektronix P5100 High Voltage Probe (Tektronix, Oregon). Signals were recorded on a Tektronix DPO4104 Digital Phosphor Oscilloscope (Tektronix, Oregon).

### 3.2.3. Decomposition of azo dye solutions using cold atmospheric pressure plasma treatment to explore the parameters influencing the efficacy of the FBR

Plasma generated ROS are routinely used in wastewater facilities to reduce the amount of dye molecules in aqueous solutions (Tichonovas *et al.*, 2013). Plasma oxidation methods have proven to be a viable option for effective decomposition of complex structures such as Acid Orange 7 (Du *et al.*, 2008) or Methylene Orange (MO) (Jin *et al.*, 2014).

For scouting of parameters for the fluidised bed (FB) plasma reactor, a series of experiments was conducted decolouring aqueous dye solutions in the reactor. Although the mechanisms of ligand surface etching and decolourization are not directly transferable, they do yield insights into the efficacy of the ROS generated in the reactor in quantitatively easily assessable manner.

The dye molecules are subject to photobleaching when exposed to light (Guo *et al.*, 2011). To avoid interference via fading of dye molecules, all sample tubes were wrapped in aluminium foil and kept away from light whenever possible. The azo dyes MO and CR were dissolved in MQW and subsequently serially diluted to a final concentration of 20 μg/mL for MO (absorption maxima 270 nm and 465 nm (Al-Qaradawi *et al.*, 2002)) and 1.073e-5 mol/L (absorption maximum at 497 nm (Iwunze, 2010)) for CR respectively. A total of 8 mL dye solution was pipetted into the FBR supplied with 1 SLM upward gas flow to avoid backflow of the solution into the gas supply line. After equilibrating the solution with the feed gas for 1 minute, the solution was plasma treated as described in 2.3.5.After treatment time had finished, the solution was poured into a clean 15 mL Eppendorf tube and analysed for $OD_{460}$ using a Suprasil High Precision Quartz Cuvette (10 mm path length) at various time points post treatment. MQW was used as a blank.

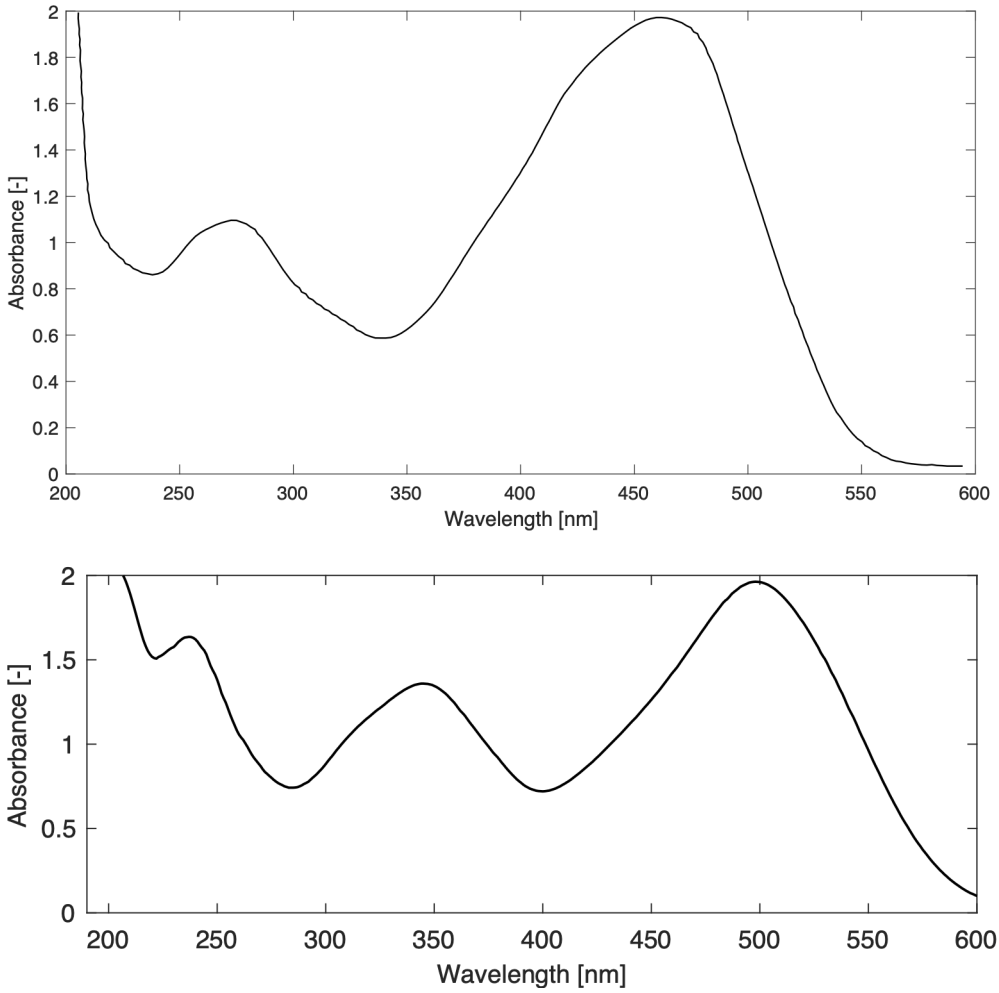


Figure 3-4 Top: UV- visible spectrum of MO in MQW, adapted from (Al-Qaradawi *et al.*, 2002)
Bottom: UV-visible spectrum of CR in MQW

## 3.3. Results and Discussion

### 3.3.1. Plasma etching and oxidation of chromatography supports in parallel plate Dielectric Barrier Discharge plasma reactor

A total of four AEC adsorbents (Q & DEAE Sepharose FF, Q Hyper Z, EMD Fractogel (M) DEAE) were plasma treated in a parallel plate DBD set-up, using helium as a carrier gas. The adsorbent samples were exposed to plasmas with input power levels reaching from 1 W up to 16.6 W for treatment times up to 600 s (2 mm sample cake; 650 $\mu L_{SBV}$; 3 mm sample-electrode distance). Reductions of pDNA (shell) and BSA (core) binding capacities cf. an untreated control were analysed using static binding studies as described in 2.3.6.2 and 2.3.6.3 respectively, and results are presented in Figure 3-5.

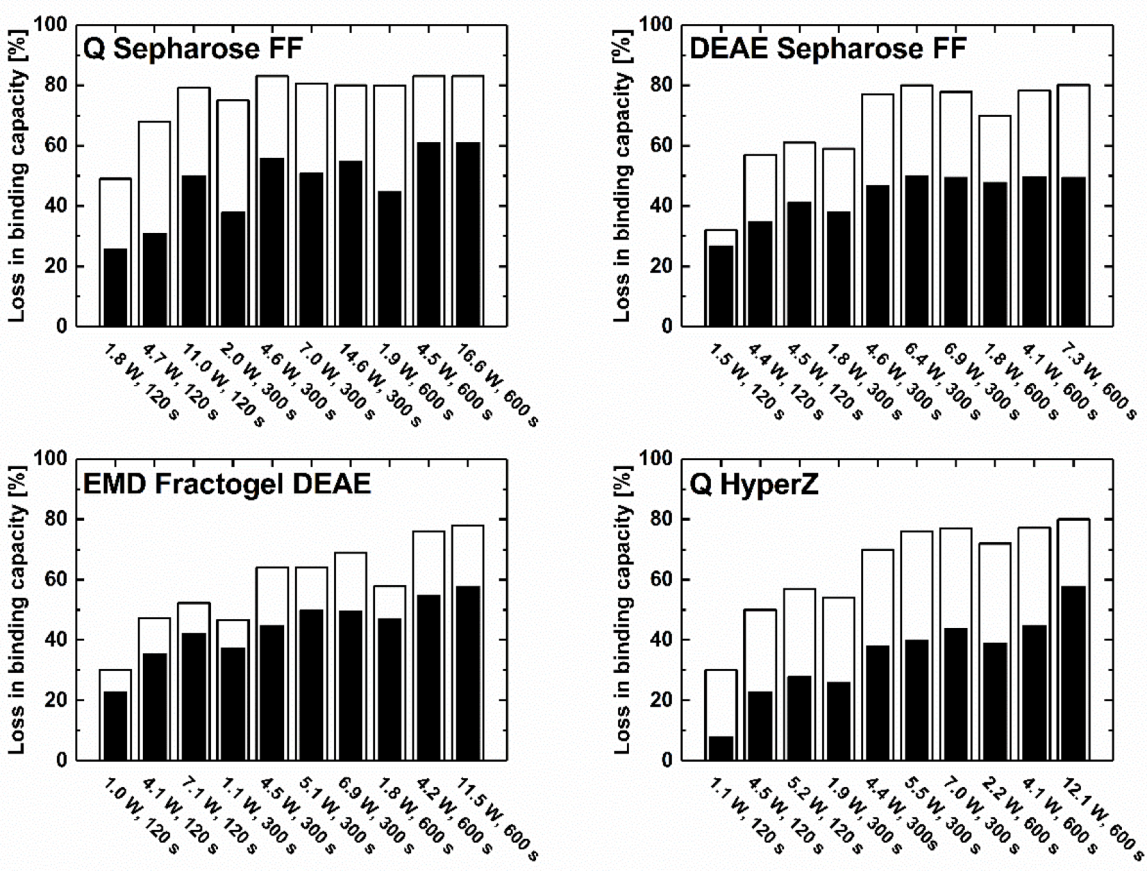


Figure 3-5 Bar charts illustrating loss of surface pDNA (white bars), core BSA (black bars) binding capacities of anion exchange adsorbents following exposure to helium plasmas in the parallel plate DBD set-up. Adsorbents (sample volume = 650 µL, sample depth = 2 mm, 'plate to sample' gap = 3 mm) were exposed to plasma of various electrical power plasmas for up to 600 s (all measurements performed in triplicates with errors <5%)

Plasma etching and oxidation of AEC in the DBD configuration led to reduction of surface pDNA binding capacities up to around 80% for all adsorbent types.

For Q Sepharose FF, necessary conditions for pDNA clearance above 70% involve either (i) high energetic plasma operations for short treatment times (11 W; 120 s). Reductions of pDNA binding capacity levelled out for (ii) longer treatments irrespective of power input at around 80% (i.e. 1.9 W for 600 s).

Whilst treatment at moderate conditions (120 s; 1-1.8 W) eliminated 20% of BSA binding in all support types, either longer treatment times or increase of power input resulted in more severe losses of BSA binding (up to >50%).

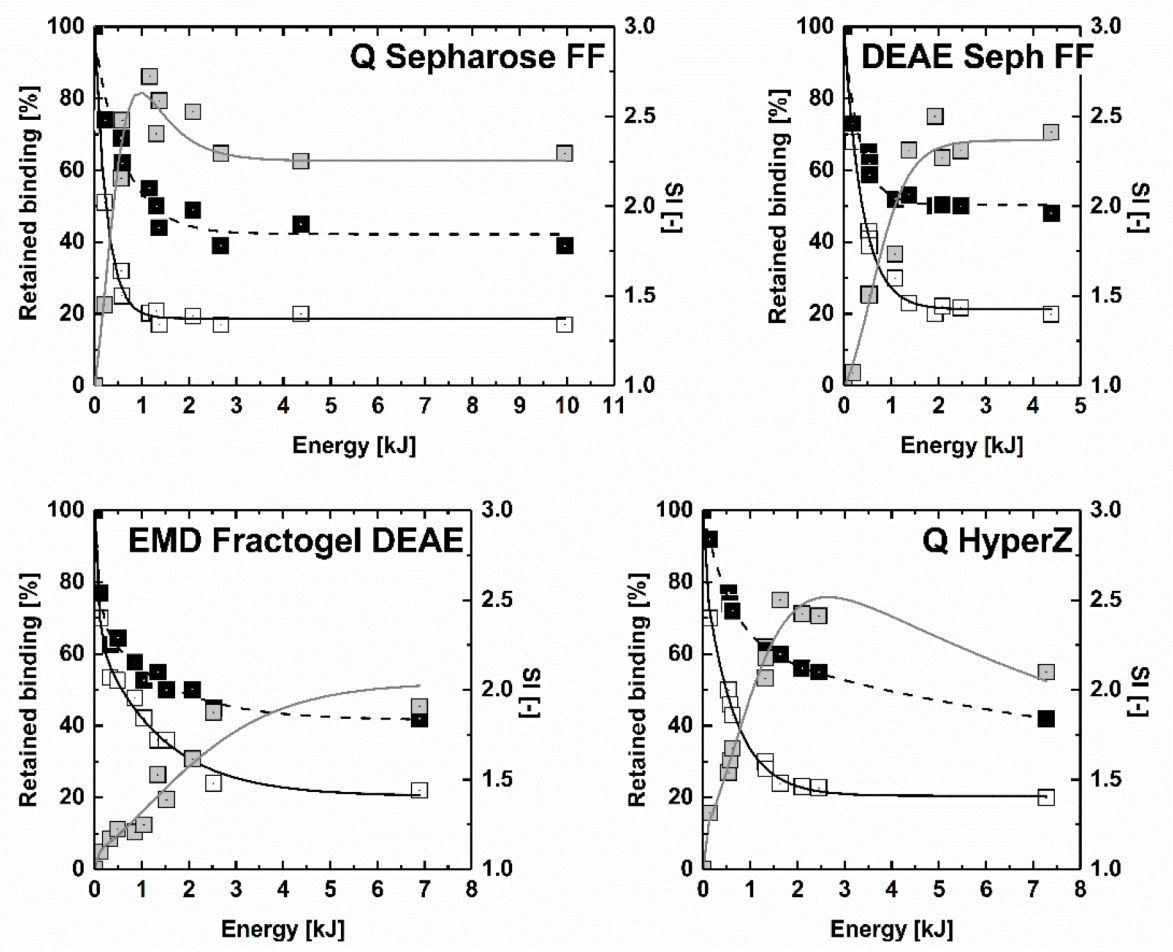


Figure 3-6 Retained surface pDNA binding capacity (□), core BSA binding capacity (■), and SI (■) of AEC adsorbents as functions of plasma energy for helium plasma treatment in the DBD configuration (sample volume = 650 µL; sample depth = 2 mm, 'plate to sample' gap = 3 mm). The lines through the pDNA (**—**) and BSA (---) binding data points are fitted second order exponential decay curves, whereas those through the SI (—) data were obtained by dividing the BSA binding decay curves by the corresponding pDNA binding decay curves (all measurements performed in triplicates with errors <5%)

To correlate the losses of pDNA binding and BSA binding, SI values for each adsorbent type were calculated and plotted alongside the binding retention levels of pDNA and BSA against the overall energy input (Figure 3-6).

As expected, increasing the total input plasma energy to which the supports were exposed resulted in greater loss of pDNA binding capacity for all support types (Figure 3-6). However, exposure to increased plasma energy also led to greater loss of BSA binding. The resulting relationship between total plasma energy used during treatment and SI shows that the softer Sepharose FF supports reached their optimum SI values at lower treatment energies (<2 kJ) in comparison to the harder EMD Fractogel (M) DEAE and Q Hyper Z supports.

Results indicated that optimum selectivity indices for EMD Fractogel (M) DEAE were achieved with longer treatment times, and that plasma treatments exceeding 600 s might be beneficial for achieving higher SI values, as neither BSA binding reduction, nor pDNA binding levelled out for total input energies up to 7 kJ. In contrast, optimum selectivity indices were obtained with treatment times of ~200 s for Q Sepharose FF, at a sample-electrode distance of 3 mm at energy inputs of 1.5 kJ, with an SI of 2.75 (80% loss of pDNA binding with 45% loss of BSA binding) and DEAE Sepharose FF at energies >2 kJ, with the SI levelling out at around 2.4. Surface binding of Q Hyper Z was mostly reduced at energy inputs of <2 kJ, with additional energy contributing only to enhanced loss of core binding.

Reducing the distance between the top of the sample cake and the top electrode of the plasma rig (increased thickness of the sample cake) from 4.5 mm to 1 mm resulted in a decrease of selectivity for all adsorbent types (Figure 3-6). The SI decreased from 4.8 to 1.1 for Q Sepharose FF, 4.7 to 1.2 for DEAE Sepharose FF, 4.1 to 1.0 for EMD Fractogel (M) DEAE and 4.9 to 1.2 for Q Hyper Z. These SI values correspond to additional losses of BSA binding seen when decreasing the sample-electrode distance from 4.5 mm (BSA binding reductions of ~20% for both Sepharose media) to 1 mm which yielded a BSA binding reduction of up to 56% for DEAE Sepharose FF and 49% for Q Sepharose FF.

With the sample cake being slightly conductive and the electrode gap remaining fixed at 5 mm, increased sample heights serve to reduce the gas gap. For treatments at a given power setting, a smaller gap is likely to result in a more concentrated, hotter plasma treatment, so thermal damage to the supports may play a pivotal role in the loss of BSA binding capacity.

Reducing the sample/ electrode gap and consequently increasing the process temperature of the supports also led to enhanced evaporation of (remaining) water during the treatment. After the “hotter” treatments had finished, the sample cake appeared to have dried a lot more in the process than was observed with larger gaps between sample and electrode.

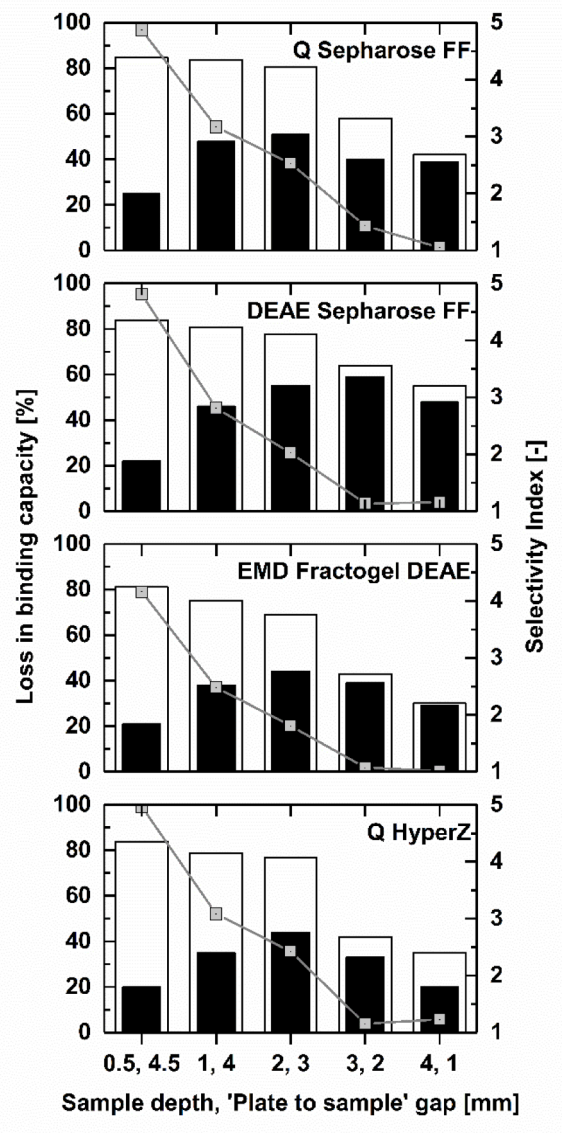


Figure 3-7 Impact of sample depth/ ’plate to sample’ gap on the loss of surface pDNA (white bars) and core BSA (black bars) binding capacities, and SI (grey symbols) of AEC adsorbents following exposure to helium plasmas in parallel plate DBD set-up. Adsorbent bed volumes of 160 µL to 1.3 mL, corresponding to sample depths of 0.5 to 4 mm and upper plate to sample gaps of 4.5 to 1 mm, were exposed to 7 W plasmas for 300 s (all measurements performed in triplicates with errors <5%)

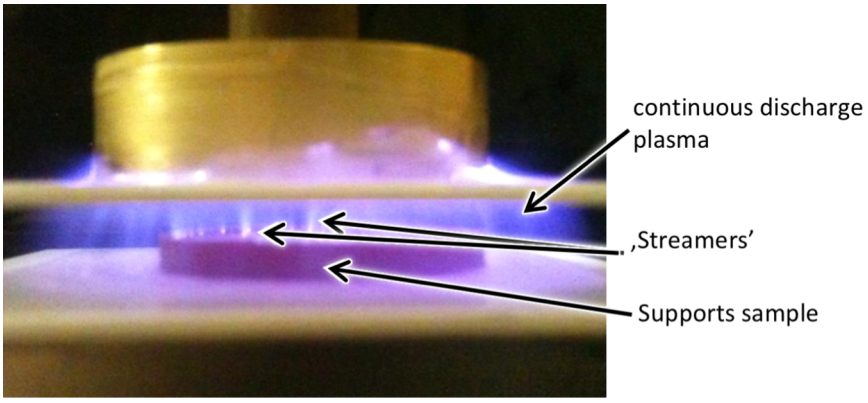


Figure 3-8 Treatment of chromatography supports in a DBD plasma operation; while the continuous blue/ purple glow plasma is filling up the chamber, the occurrence of 'streamers' penetrating the sample cake are clearly visible

A continuous problem, that the plasma treatment in the DBD configuration is facing, is the formation of streamers (Figure 3-8). Although operation at the scale used in this work produced some good selectivity indices, operation at larger scale would require a larger treatment area likely leading to localised hotspots, with lower uniformity of treatment and an overall hotter sample temperature.

All treatments with sample-electrode distances of 3 mm or more gave SI>1.5, indicating that the DBD configuration used for plasma etching under atmospheric pressure gas was suitable for creating a degree of bilayered SEC/ IEC structure on the AEC beads tested.

Previous studies into the effectiveness of treating Q Hyper Z materials using low temperature low pressure plasma etching (Arpanaei *et al.*, 2010) gave selectivity indices up to 2.0 (53% reduction in pDNA binding and 9% loss of protein binding) from static binding studies. By comparison, treatment of Q Hyper Z in the DBD configuration gave a maximum selectivity index of 5 (corresponding to 84% reduction of pDNA binding alongside 20% loss of BSA binding) for treatment of a sample at 4.5 mm sample-electrode distance for 300 s at 7 W, indicating that the cold atmospheric pressure plasma used in this work may be even more suitable for etching of hard chromatography support surfaces than the method described by Arpanaei et al. However, it should also be noted that all treatments which achieved SI of 2.0 or above in the DBD configuration also incurred at least 20% loss of BSA binding, this being true for all the support types tested. This indicates that the DBD configuration treatment described here is no more successful than that of Arpanaei et al. in making the outer layer 'ultrathin'.

Furthermore, although all of the selectivity indices described in this work relate to capacities measured by static binding studies, dynamic binding studies with the same materials might be expected to produce even better selectivity index values. This expectation arises from results obtained with low temperature low pressure plasma (Arpanaei *et al.*, 2010) in which the method used to produced Q Hyper Z beads with selectivity index of 2.0 in static binding studies gave a selectivity index of 2.7 when used in dynamic binding studies with BSA and pDNA feedstocks in a FastLine$^{TM}$ 10 EBA column (note: separate plasma treatments carried out on a 5 g batch for static binding studies and a 10.5 g batch for dynamic binding studies while using identical plasma parameters).

From this, it seems likely that adsorbents etched with cold atmospheric pressure plasma will display higher SI values in dynamic binding modes than those seen in static binding, due to the similarities with the low temperature low pressure etching method. The differences between the effective contact time of large pDNA molecules cf. smaller proteins in dynamic frontal loading chromatography environments, hereby result in slightly more favourable selectivities cf. static binding data. While BSA as a small molecule can easily diffuse and bind throughout the pores of the AEC supports, large pDNA molecules take longer contact times to fully saturate all available binding sites provided by the ligands lining the pores.

Due to foreseeable problems with scaling up, it was decided to focus subsequent investigations on treatment by plasma filled gas bubbles in a fluidised bed set-up which, in contrast to the DBD configuration, is expected to produce a relatively well distributed plasma and to achieve a more even treatment of supports.

Due to the colder nature of the process (water cooled), streamers and/ or hot spots are less likely to occur by design of the reactor and hence the thermal damage to the supports as observed in the DBD configuration is expected to have a lesser (if any) impact on the structural integrity of the adsorbents.

### 3.3.2. In situ plasma etching of hydrogel chromatography supports in the Fluidised Bed Reactor set-up

Although EBA supports (Q Hyper Z) showed promising levels of pDNA binding reduction in the parallel plate DBD plasma configuration, treating heavy support particle slurries in the FBR set-up was hampered by the density of the adsorbents. Mixing via gas bubbles traveling through the reactor proved insufficient for a functional plasma operation, with supports settling at the bottom of the reactor. Plasma treatment of soft hydrogel supports was hence focussed on Q Sepharose FF, DEAE Sepharose FF and EMD Fractogel (M) DEAE.

Initial parameter scouting was focussed on carrier gas composition (He-$O_2$ (99.5-0.5%); pure oxygen), amount of sample treated in reactor as part of the overall 8 mL sample volume (12.5%, 18.8% and 25% slurry concentration), input power (1.5 and 3.7 W) as well as treatment times (150, 300 and 600 s).

Reductions of pDNA and BSA binding were assessed in static binding studies as described in 2.3.6 and the loss of binding capacities was plotted in Figure 3-9.

Unlike the DBD plasma operation, treatment of hydrogel supports in aqueous solution with He-$O_2$ plasmas was found to be more moderate, with BSA binding reductions below 20% for all support types irrespective of plasma conditions, while short treatment times at low power only compromised core binding capacity by around 5%.

Surface etching and oxidation has eliminated over 50% of initial pDNA binding in all support types, with Q Sepharose FF showing the highest reduction levels (up to 70%).

While He-$O_2$ gas plasmas indicate promising reduction levels for both BSA and pDNA, supports treated with plasma generated from pure oxygen tell a different story. Plasmid DNA reductions are falling short of 40% while core binding ligands were attacked overproportionately. This indicated that ROS generated from pure oxygen gas penetrated further into the supports before reacting with core ligands, bypassing ligands situated on the very surface of the AEC adsorbent.

Alteration of slurry concentration yielded no significant difference between the samples.

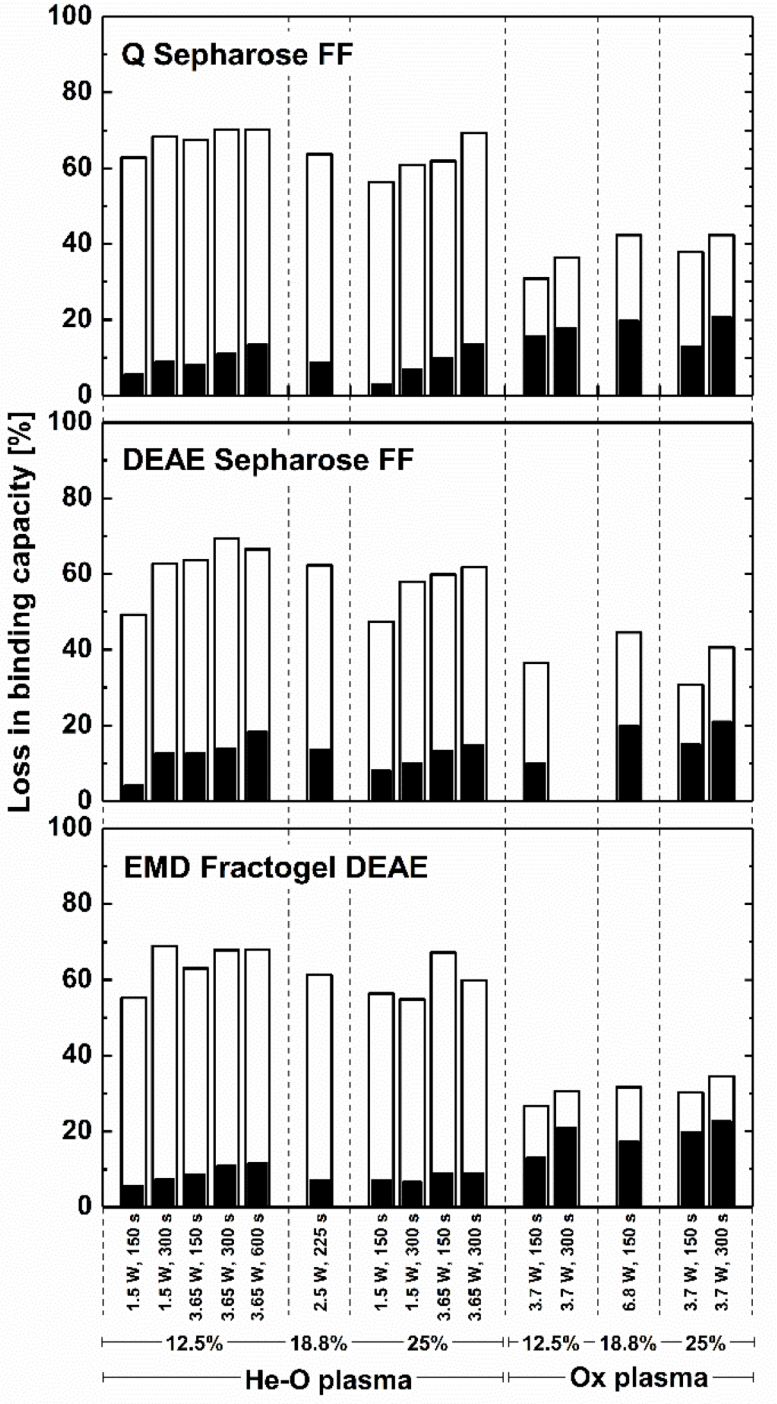


Figure 3-9 Bar charts illustrating loss of surface pDNA (white bars) and core BSA (black bars) binding capacities of packed bed anion exchange adsorbents following treatment with He-$O_2$ (99.5-0.5%) and pure oxygen (Ox) plasmas in the underwater FBR plasma generation system. Adsorbent slurries (12.5 – 25% v/v) were treated with different plasma powers (1.5 – 6.8 W) for various times (150 – 600 s)
all measurements performed in triplicates with errors <5%

To correlate losses of pDNA and BSA binding, SI values were calculated and plotted alongside the retention binding levels of pDNA and BSA against the overall energy input (Figure 3-10).

Throughout He-$O_2$ plasma treatments, reduction of pDNA binding was found to level out at 70%, 75% and 75% for Q Sepharose, DEAE Sepharose FF and EMD Fractogel DEAE respectively, after an energy input of around 0.5 kJ for all adsorbent types. Applying further energy into the system did, however, lead to continued decrease of BSA binding.

The highest surface binding reduction was recorded for Q Sepharose FF with 70% clearance at a loss of around 8% core binding, leading to an SI value of 3.0.

In accordance with observations outlined above, SI of samples treated with pure oxygen plasma fell short cf. their respective He-$O_2$ counterparts, yielding SI values <1.5 for all adsorbent types.

Neither the BSA, nor the pDNA binding retention curve level out after 0.5 kJ as observed in the He-$O_2$ samples, instead it appears that oxygen plasmas at higher energy inputs may reduce the surface binding capacity further. However, the selectivities do not indicate that higher energy inputs lead to a selective reduction of surface over core binding.

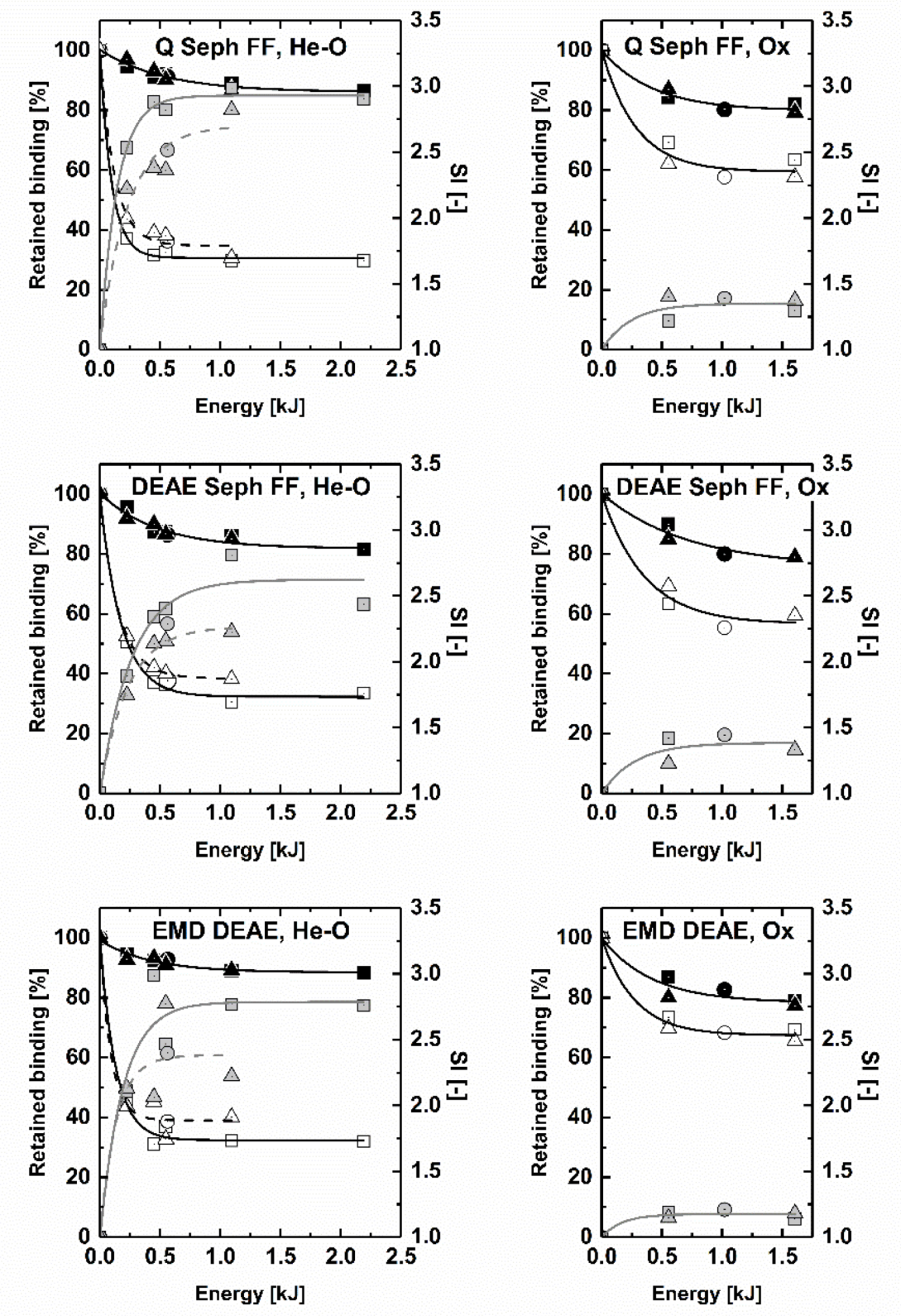


Figure 3-10 Retention of surface pDNA (white symbols) and core BSA (black symbols) binding capacities, and variation in SI (grey symbols) as functions of plasma energy for He-$O_2$ and pure oxygen (Ox) plasma treatments of packed bed AEC adsorbents in the underwater cold atmospheric plasma apparatus. Squares, circles and up triangle symbols indicate 12.5%, 18.75% and 25% (v/v) support slurry samples respectively. The lines through the BSA and pDNA data points are fitted first order exponential decay curves, whereas those through the SI (—**)** data were obtained by dividing the BSA binding decay curves by the corresponding pDNA binding decay curves (all measurements performed in triplicates with errors <5%)

3.3.2.1. Influence of leached substances created during plasma treatments of chromatography media on spectrophotometric measurements to quantify pDNA contents post static binding studies

The spectrophotometric measurement of pDNA concentration in liquid samples by UV absorbance ($OD_{260}$) relies on the absence of contaminants that absorb light of the respective wavelength (Reule, 1976).

During initial scouting experiments (decolouring dye solutions in the FBR), it was observed that plasma reactions, triggered in situ proceeded after treatment had finished (Appendix A-5).

While the buffer surrounding the chromatography media during the plasma treatment is exchanged post treatment, concern arose whether species leached off chromatography supports post buffer exchange (in storage tubes) could influence subsequent analysis (pDNA quantification). To ensure assay robustness and the absence of such contaminants (or their respective impact on the spectrophotometrical measurements of pDNA concentration), Q Sepharose FF media (1 mL SBV) was plasma treated as described in 2.3.5 (14.5 kHz; 7 W; 10 min; He-$O_2$ (99.5-0.5% v/v) admixed gas; gas flowrate 750 mL/min). The UV absorbance ($OD_{260}$) of the TE storage buffer of the supports was analysed over time (immediately after the treatment, 1, 24 and 48 h post buffer exchange) and compared to TE buffer (Figure 3-11; MQW used as blank).

| Sample | $OD_{260}$ |
|---|---|
| TE buffer | 0.016 |
| Immediately after contact | 0.011 |
| 1 h post treatment | 0.006 |
| 24 h post treatment | 0.014 |
| 48 h post treatment | 0.015 |

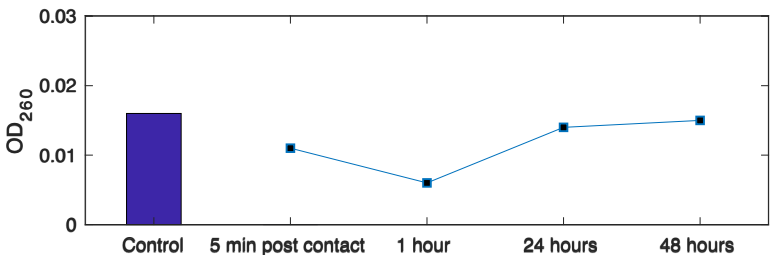


Figure 3-11 $OD_{260}$ of the supernatant (TE buffer) after different contact times with plasma treated Q Sepharose FF chromatography supports (14.5 kHz; 7 W; 10 min; He-$O_2$ (99.5-0.5% v/v) admixed gas; gas flowrate 750 mL/min) in comparison to control TE buffer

The maximum variance of the $OD_{260}$ measurements (after 1 h vs control) is 0.01 [-], correlating to 0.2 $\mu g_{pDNA}/mL_{SBV}$ in static pDNA binding studies. With typical Q Sepharose FF pDNA binding capacities of ~300 $\mu g_{pDNA}/mL_{SBV}$, the difference accounts for a statistically irrelevant error of 0.067%.

The results obtained confirm that either, the reaction does not continue leaching off substances of the beads post plasma treatment, or that the molecules leached off the supports do not compromise the assay by absorbing light in the UV-range.

The treatment of Q Sepharose FF supports with cold atmospheric pressure plasma does not impede subsequent static binding studies or following measurements of pDNA content in the supernatant via UV-spectrophotometric analysis.

3.3.2.2. Plasma parameter screening for FBR

Due to the high number of parameters associated with the treatment of chromatography supports in the FBR set-up, the amount of different support media was limited and the strong AEC media Q Sepharose FF was chosen throughout the experiments.

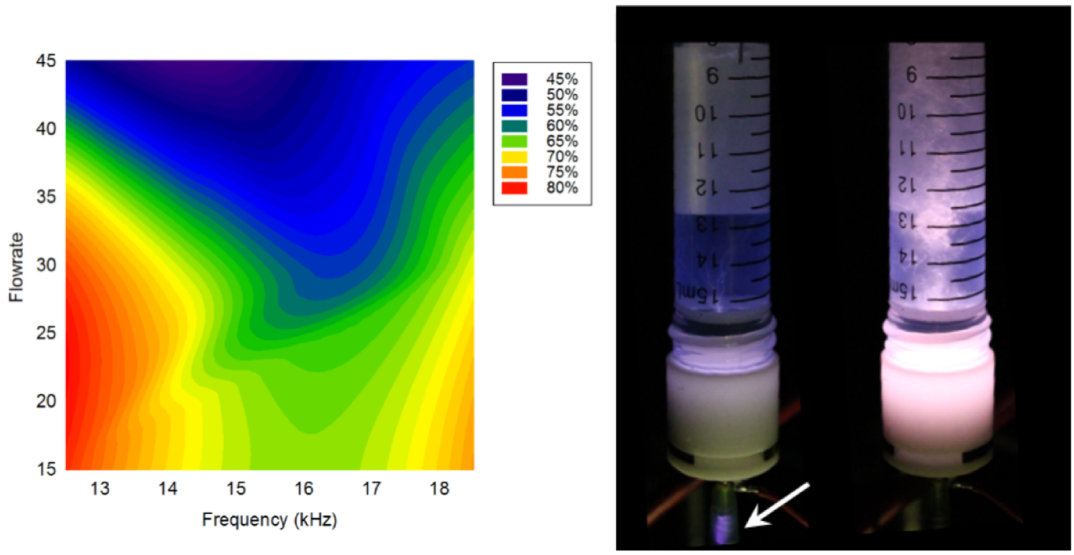


Figure 3-12 Contour plot of dissipated/ input power in FBR during plasma operation with MQW as a buffer system (left); backflow of plasma gas into the gas supply line at flow rates below 700 mL/min (right); flow rate prior to conversion into mL/min

In experiments without chromatography media in the FBR, measuring the conversion of energy being put into the system to the energy dissipated, suggests that operation of the FBR at low flow rates was beneficial (Figure 3-12, left). However, plasma stability becomes a concern when the flow rate is too low, with plasma sparks backlashing into the gas line (Figure 3-12, right). Furthermore, the system is reliant on a constant supply of carrier gas into the system, while avoiding spilling of supports. Balancing both effects, a flow rate of 750 mL/min was found appropriate to ensure mixing of the sample, avoiding plasma backlashes and spilling of reactor contents.

3.3.2.3. Variation of plasma input powers

In previous studies using plasma etching and oxidation to reduce the surface binding capacity of chromatography supports, the depth of the alteration induced by the plasma treatment in AEC supports, was strongly influenced by the power input (Arpanaei *et al.*, 2010); it stands to reason that investigating the effects different input powers have on the chromatographic performance of plasma treated AEC supports is of utmost importance.

1 mL SBV Q Sepharose FF media was treated with He-$O_2$ (99.5%-0.5% v/v) plasma with varying input powers (2-12 W), as described in 2.3.5.1 (14.5 kHz; 20 min treatment time).

Post treatment, each support sample was analysed in duplicate (results averaged) for BSA and pDNA static binding capacities, to assess the reduction of core and shell binding levels respectively as described in 2.3.6.

To check whether binding to plasma treated chromatography supports has an impact on pDNA stability, unbound pDNA supernatant was collected post static binding, concentrated using phenol chloroform extraction of NA and visualised by agarose gel electrophoresis (2.3.4.1; Figure 3-13).

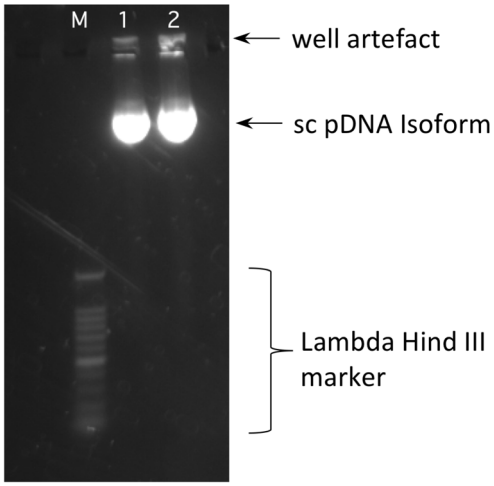


Figure 3-13 Agarose gel of unbound IT14: pPR322-p170 plasmid in the supernatant after binding to 1: Q Sepharose FF; 2: He- $O_2$ plasma treated Q Sepharose FF (7 W; 14.5 kHz; 20 min; He-$O_2$ (99.5%-0.5%) admixed gas plasma)

The gel image confirms the stability of the pDNA in the supernatant and the plasma treatment has no impact on the conformation of the unbound pDNA. The difference in brightness between the two gel lanes is due to the reduced surface binding capacity of He-$O_2$ plasma etched support samples which consequently yields a higher concentration of pDNA in the supernatant.

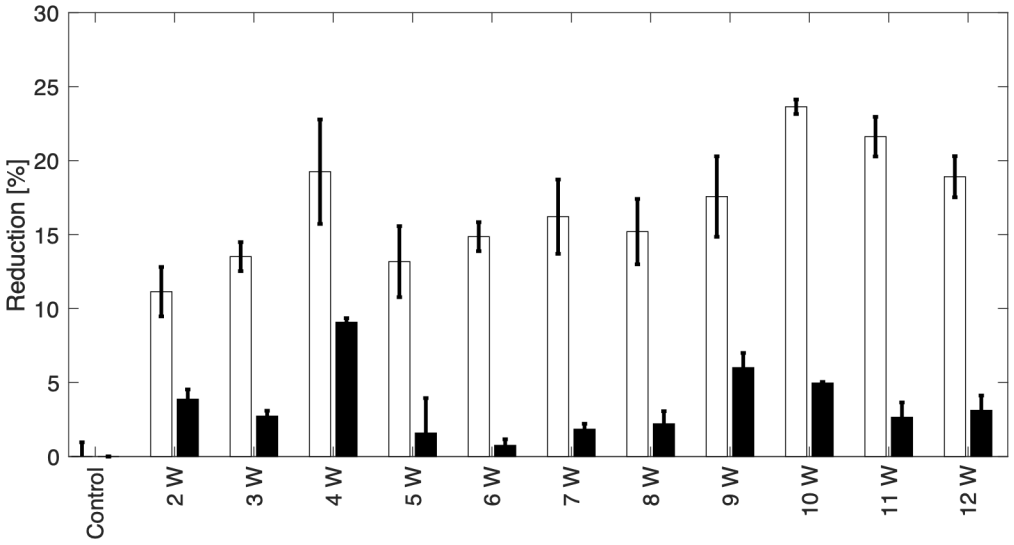


Figure 3-14 Static binding capacity reductions (pDNA and BSA) of Q Sepharose FF media after in situ plasma treatments with various input powers (14.5 kHz; helium-oxygen (99.5%- 0.5% v/v) admixed gas; 20 min) in comparison to an untreated control sample

The reductions of pDNA binding levels all range above 10%, with higher reduction levels occurring at higher input powers. While the plasma treatments do not etch away enough ligands off the particles' surfaces to reduce the BSA binding capacity significantly (less than 7% for all samples), higher input powers (9 W and above) do have a larger impact on the core binding capacity of the beads.

The 4 W sample falls slightly out of trend, both for BSA as well as pDNA binding capacity reductions. This is assumed to be a result of a variation in the amount of media (SBV) either treated (slightly less beads in reaction vessel) or analysed (scraping particles off the filter frit prior to their resuspension does inevitably leave a small portion of beads behind).

An increase in power input leads to higher reduction levels of pDNA binding capacity up to 10 W, after which the samples show a slight decline of surface binding reduction. This could be due to a number of different reasons; the surface of the beads gets disrupted by the voltage

or the ROS, generating binding sites for pDNA. These 'new' binding sites grant pDNA access to ligands previously inaccessible to pDNA due to the SEC structure of the base matrix. By etching away the outer matrix (or piercing holes into the agarose backbone) the pDNA can diffuse into the holes and bind to ligands that prior to the plasma treatment were part of the 'core ligands'. One of the factors that could lead to a permanent alteration of the support's backbone structure is temperature spikes in close proximity to plasma filled gas bubbles (similar to plasma streamers observed in DBD configuration). These (localised) high temperatures occurring at elevated input power levels, melt the agarose for a short period of time prior to immediate resolidification of the media as the beads travel to a colder region within the reactor (turbulent mixing in the reactor as a result of the gas flow jetting through the reaction vessel). Localised melting of the agarose base matrix and subsequent resolidification will alter the pore structure of the media, leading to a reduction of pore size or blockage to the core of the beads (the matrix has an agarose content of 6%, even a short overheating causes significant alteration to the pore walls by either 'sealing them off' or 'burying' ligand sites with agarose). This effect, as well as reduction of overall accessible (core) binding sites due to 'shrinking' of the media's accessible binding volume lead to a reduction of BSA binding capacity.

Overall, the treatment at 7 W input power achieved the highest reduction of surface binding (16.2%) while maintaining a very high BSA binding capacity (98.2%) yielding the best balance between the two effects outlined above.

3.3.2.4. Treatment time and temperature profile dependency

The plasma treatment to etch away functional ligands off the surface of chromatography beads is a gentle treatment without the generation of large amounts of toxic by-products (Schram, 1987). During the plasma operation, the support slurry in the reactor heats up over time due to the dissipation of energy in the system (Figure 3-15). Elevated temperatures can not only have a crucial effect on occurring plasma reactions but also on the formation of different ROS species (Fridman, 2008).

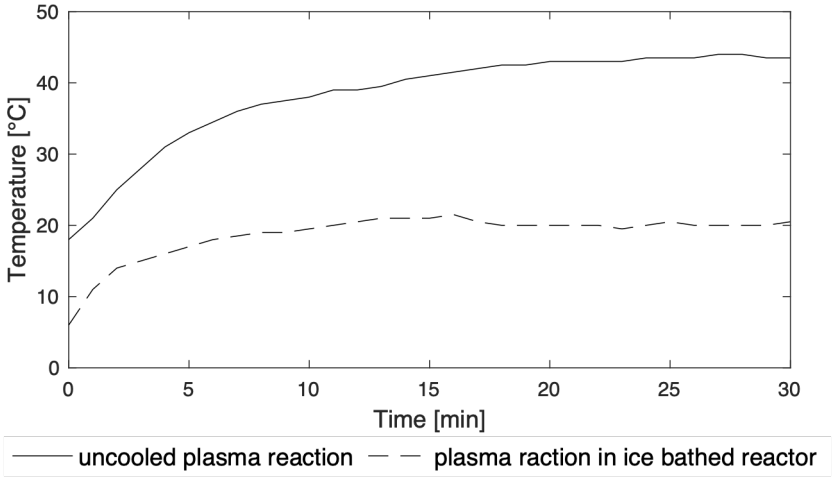


Figure 3-15 Temperature profiles of plasma treated MQW over time, both in the uncooled reactor (-) as well as during plasma operation in ice bath (--); 7 W, 14.5 kHz, helium-oxygen admixed gas (99.5- 0.5% v/v)

To investigate the impact, elevated temperatures have on plasma treatment of Q Sepharose FF media, two sets of samples were treated under identical electronic parameters using different temperature profiles in the reaction vessel. To avoid the occurrence of high average temperatures in the reactor (temperature spikes around the gas inlet are unavoidable given the geometry of the system), an ice-cooled water bath to maintain a lower working temperature of the reactor was used to modify the reactor as described in 2.5.3.2.

Both sets of Q Sepharose FF media (1 mL SBV; cooled and uncooled) were plasma treated as described in 2.3.5. The samples were treated for 5, 10, 20, 40 and 60 min respectively with 7 W input power, 14.5 kHz, 750 mL/min gas flow of He-$O_2$ (99.5%-0.5% (v/v) admixed gas).

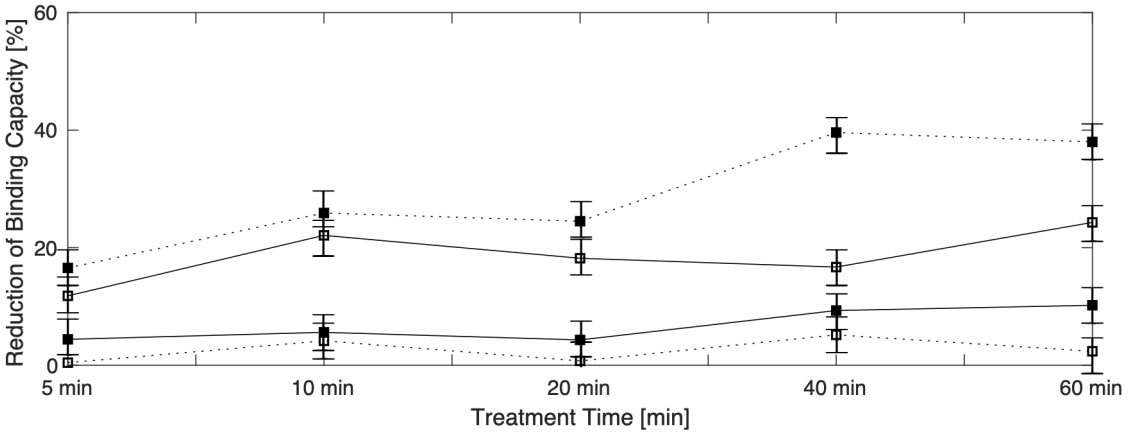


Figure 3-16 Reduction of static binding capacities to an untreated control sample of Q Sepharose FF media after plasma treatment for different times in both uncooled and cooled reaction vessel; electrical plasma parameters: 14.5kHz; 7 W; helium-oxygen admixed gas (99.5- 0.5% v/v)

The reductions of pDNA and BSA binding capacities compared to an untreated control sample are depicted in Figure 3-16. All samples showed very minor reductions of their core (BSA) binding capacities post plasma treatment in comparison to the untreated control sample (the uncooled 60 min treatment showing the highest reduction of BSA binding capacity (10.3%) with all other samples below 10%). While no severe BSA binding capacity reduction was observed in any of the samples, the reductions seen in the samples treated in the reactor submerged in the stirred ice bath consistently produced lower values, indicating that an increased process temperature of the chromatography slurry during the treatment aids the ROS to penetrate through the outer several micrometres of the beads and access (further) into the core of the particles.

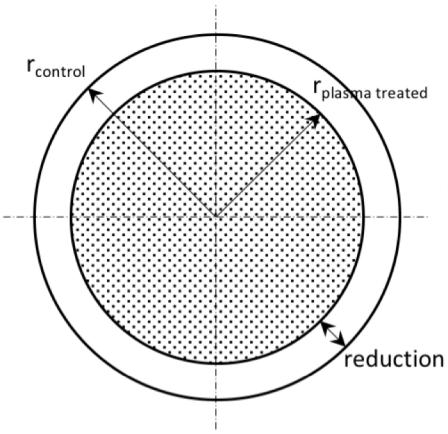


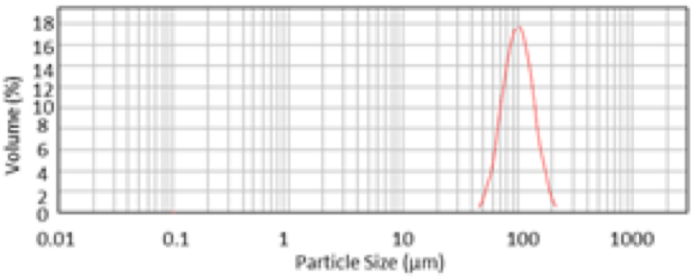


$$V_c = {}^4/_3\ \pi * r_c^3$$

$$V_{pt} = residual\ [\%] * V_c$$

$$r_{pt} = \sqrt[3]{residual\ [\%]} * r_c$$

$$\text{reduction} = r_c - r_{pt}$$

$$= (1 - \sqrt[3]{residual\ [\%]}\ ) * r_c$$

$$= \underline{1.72\ \mu m}^*$$

* Assuming spherical bead shape
Q ligand evenly distributed across $V_{control}$
BSA binding capacity ~ $V_{control}$

With:

$V_c = V_{control}$
$r_c = r_{control}$ = 50 µm
$V_{pt} = V_{plasma\ treated}$
$r_{pt} = r_{plasma\ treated}$
residual [%] = $residual_{pDNA\ binding\ capacity}$ [%]

Figure 3-17 Volume size distribution of Q Sepharose FF media, measured as described in 2.3.13 (Top right); Calculation of the size of the SE outer shell of plasma treated Q Sepharose FF chromatography supports (bottom left) under the assumptions that the Q ligand is evenly distributed across the spherical volume of the supports and a mean volume particle size of 100 µm

A BSA binding reduction of 10% of the original value corresponds to a thickness of 1.72 µm of the created uncharged SE layer surrounding the core (Figure 3-17). The assumption, that all particles are of identical size hereby implies, that a SE layer thickness of 1.72 µm corresponds to different reduction levels for individual beads- particles of 50 µm diameter lose 19.3% of their BSA binding capacity while particles of 150 µm lose only 6.8%. While the size distribution of chromatography media has a large impact on mass transfer kinetics when used in 'traditional' column chromatography (Kaczmarski *et al.*, 2003), it is evident that different sizes of individual particles add an additional burden when the supports are functionalised on a single bead basis.

The samples treated in the cooled reactor show reduction levels of max 5% of BSA binding capacity (corresponding to 0.85 µm thickness of the SE outer shell for 100 µm diameter bead size). Similar to the results in the DBD configuration, elevated temperatures aid the ROS to

penetrate further into the core of the particles etching off Q ligands from the backbone structure of the media further away from the surface.

For the uncooled set-up, the reductions of pDNA binding capacities showcase that treatment times of 5 min are not enough to achieve higher reduction values of shell binding than 17%. With longer overall treatment times the values rise up to and level out at around 40% reduction after 40 min, with longer treatment times (60 min) providing no additional loss. The temperature in the reactor reaches steady-state after 20+ min, indicating that with a further increase of temperature, pDNA binding reductions may still be going up.

The pDNA binding reduction values of the samples treated in the ice-bathed reactor level out after 10 min (22%) with minor differences for additional treatment time (18, 17, 24% for the 20, 40 and 60 min treatments, respectively) coinciding with reaching the steady state temperature of the reactor around 20°C.

As not all of the surface charges have been eliminated, the ROS must have diffused into the core of the particles further than the 1.7 μm (0.85 μm for the ice-bathed reactor set-up, respectively) to cause the 10% (5%) reduction of the BSA binding capacity, as ligands on the surface of the particles that have not been etched away by the plasma treatment will still bind BSA in static binding studies. This suggests that the zone affected by the ROS is not necessarily a sharp cut off zone, with some ROS travelling past the initial ligands presented on the very surface and reacting deeper in the bead with a respective partner.

Table 3-1 SI values dependent on treatment time for both the ice bathed and ambient temperature reactor

| Treatment time [min] | SI value (uncooled) | SI (ice bathed reactor) |
|---|---|---|
| **5** | 1.13 | 1.15 |
| **10** | 1.23 | 1.27 |
| **20** | 1.21 | 1.27 |
| **40** | 1.14 | 1.50 |
| **60** | 1.29 | 1.45 |

An overall lower temperature of the sample slurry leads to lower losses of core binding capacity however, this is at the expense of surface binding capacity reduction (Table 3-1).

From all SI values being higher for samples treated at elevated temperatures, it can be concluded that the 'savings' of core binding capacities seen with the ice-bathed reactor do not justify the loss of surface reduction compared to the uncooled reactor.

Overall it can be concluded that cooling the system reduces the overall efficacy of the treatment while enhancing selectivity of surface vs core binding reduction.

3.3.2.5. 'Interval cascade' treatment

Plasma etching in batch reactors inevitably leaves the etched species in the surrounding buffer solution. Whether or not the presence of these species has an impact (and if so to what extend) on the plasma etching and oxidation has not yet been investigated.

The maximum solubility of leached off species in solution could be a key parameter for the success of the plasma etching reaction- if the solubility is very low, the initial etched off species will prevent accumulation of further species in solution and the reaction chokes itself. The presence of these species could furthermore interact with the plasma reaction itself by 'poisoning' the reaction due to their high reactivity. Interaction between the plasma species and leached molecules could restrict their ability to target other ligands on the surface of chromatography supports.

By repeatedly changing the surrounding buffer during the reaction, both of these effects can be minimised.

During plasma treatments of chromatography supports in the FB reactor, the slurry containing the chromatography media heats up over time (Figure 3-18).

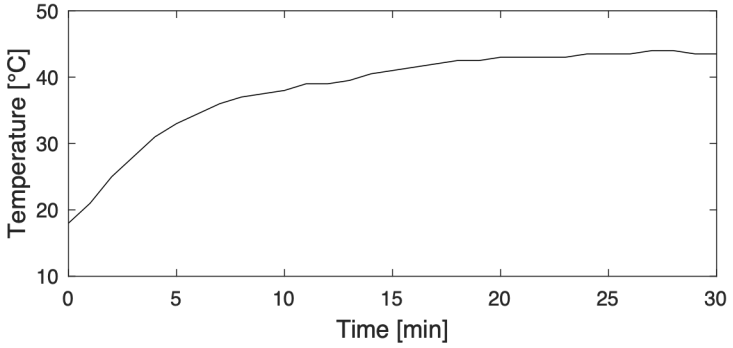


Figure 3-18 Temperature profile of chromatography media suspended in plasma reactor over time (He-$O_2$ admixed gas plasma (99.5%-0.5%); 7 W; 14.5 kHz)

To reduce the amount of time the media is exposed to elevated temperatures (yielding higher losses of core binding capacities), and to investigate whether changing the surrounding buffer of the chromatography media during the plasma treatment has a significant impact on the media's performance post treatment, the overall treatment time was split up into several shorter intervals with buffer exchange steps in between.

Rather than one long treatment a 'cascade' of intervals with overall constant treatment times was investigated: Four different treatment times (5 min, 10 min, 20 min, 40 min) were analysed with e.g. 40 min overall treatment time correlating to 4x 10 min, 2x 20 min and 1x 40 min.

Samples were treated using 99.5% helium and 0.5% oxygen gas plasma (premixed by BOC specialty gasses) with a pulse frequency of 14.5 kHz at an input power level of 7 W (manual voltage modulation to maintain constant power supply) and gas flow rate was kept constant at 750 mL/min (correlation chart of flow meter for pure helium- neglecting the 0.5% admixed Oxygen).

With one intention of the experiment being the investigation of the effect, constant heat exposure has on the Q Sepharose FF media, the reactor was not cooled during the reaction (ambient 21°C at the beginning of each treatment).

After every treatment, the sample slurry was poured onto a vacuum filter frit, suction dried and washed three times with 150 mL MQW. The dried media was then gently scraped off the filter frit and resuspended in MQW (8 mL total sample volume) before the next treatment. After the last treatment, samples were resuspended in TE buffer (10 mL total volume) in preparation for subsequent analysis (2.3.6). The results of the quantification of the static binding capacities are depicted in Figure 3-19.

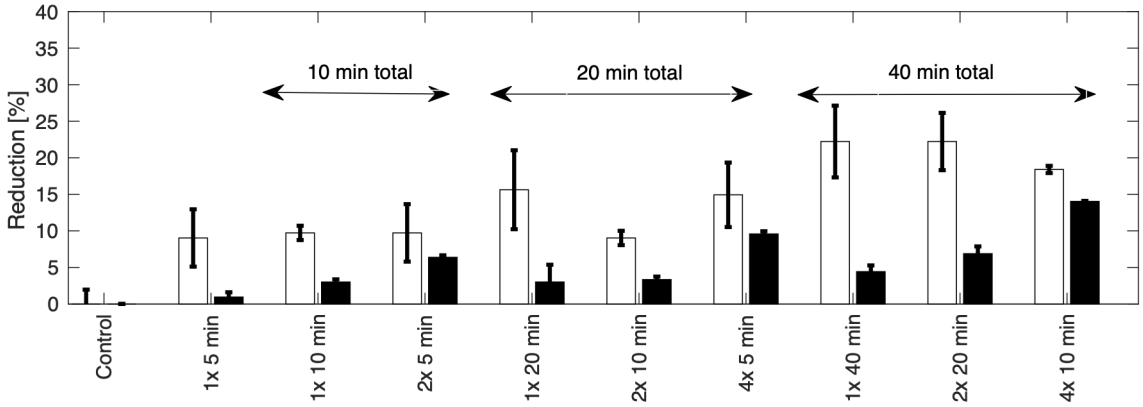


Figure 3-19 Reduction of surface (pDNA) and core (BSA) binding capacities of plasma treated Q Sepharose FF media in comparison to an untreated control sample assessed by static binding studies post cascade plasma treatments for various times and intervals (7 W; 14.5 kHz; He-$O_2$ (99.5%- 0.5%) gas plasma)

The (shortest) 5 min single treatment of the slurry led to a pDNA binding reduction of 9% with a loss of only 1% of the overall protein binding capacity.

With longer single treatment times pDNA binding capacity was reduced to 90%, 84% and 77% compared to the untreated control samples for 10 min, 20 min and 40 min treatments, respectively. Accompanying BSA binding reductions (3%; 3%; 4%) also show a trend towards higher loss of core binding, however, less so than compared to the reductions seen for pDNA binding capacities. All protein binding reductions are below 5% of their initial binding capacity, indicating that in a single plasma treatment, the majority of plasma species do not (or only at the start of the treatment) interact with the core of the chromatography particles.

However, when the treatment time is split up into several shorter intervals, the protein binding capacity is reduced further in comparison to the capacities observed in single treated samples. By splitting 10 min overall treatment time into 2 treatments of 5 min each, the BSA binding capacity was reduced twice as much (from 3% to 6%) while no change in the pDNA binding capacity was observed. A similar trend can be observed for the 20 min and 40 min overall treatment time samples; while the reduction of the pDNA binding capacities is almost identical across the samples with the same overall treatment times, the reductions of protein binding capacities are going up with an increased number of (shorter) plasma treatments; for the 40 min overall treatment time sample, reductions of BSA binding capacities were 5%, 7% and 14% for 1, 2, and 4 cycles respectively.

From this data, it can be concluded, that the plasma species are etching regions further inside the core of chromatography supports towards the beginning of each plasma cycle. Each of those plasma cycles contributes to further core damage without proportionally reducing the shell binding capacity of Q Sepharose FF media. Overall the data suggests that by increasing the number of cycles, mostly the core of the supports gets 'attacked'. Additional treatments do not contribute to the selectivity of shell over core binding capacity reduction and longer single treatments are beneficial over shorter repetitions.

Linking the results to the elevated temperatures occurring during longer treatment times suggests that the plasma species are actively reacting with the core of the particles at lower temperatures. Longer treatments in which the reaction vessel as well as the contained particle slurry heat up, do not contribute to additional core damage after an initial 'cold' phase of the reactor.

Overall, no poisoning of the reaction due to presence of ROS in the reactor over an extended period of time could be observed. Even if such an effect exists, it has no (negative) impact on media performance in static binding studies post plasma treatment.

3.3.2.6. Offline treatment

During cold atmospheric pressure plasma treatment of beaded chromatography media, the volatile plasma species adsorb onto the media and react with compounds on the outside of the media (Cardinaud, 2000). The created plasma species are of various solubilities in water especially with the formation of peroxides (ROOH) and peroxide radicals ($RO_2$) (Fridman, 2008). These and other highly reactive radicals, have various longevities in aqueous solutions. The FBR used in this study is effective to etch small batches of chromatography supports. However, scale up of a FBR that requires operational conditions (continuous gas flow) to maintain mixing of the supports is difficult. Other designs are imperative for larger scale manufacturing conditions.

One option to enhance the throughput of the reactor is to separate the plasma treatment from the actual etching of chromatography media. If reactive species are stable enough in solution, in conjuncture with a high solubility in aqueous solution, plasma treatments of MQW containing no chromatography media would offer several elegant solutions: Plasma treatment of MQW is much easier to scale up and could be engineered into a continuous reaction,

providing the plasma radicals offline for the subsequent etching reaction of chromatography media.

In order to explore whether ROS retain their efficacy to modify the binding behaviour of chromatography supports, MQW was treated 'offline' with no chromatography supports suspended in the slurry. Post treatment the solution was then mixed with Q Sepharose FF chromatography supports and their subsequent static binding performance was analysed.

1 mL SBV aliquots of Q Sepharose FF in MQW were scaled in 15 mL tubes and supernatants pipetted out. The MQW (7 mL; retaining SBV: MQW ratio of previous experiments) was treated in the FBR as described in 2.3.5 (14.5kHz; 7 W; 10 min; gas flow: 750 mL/min (flow chart of pure helium); He- $O_2$ (99.5- 0.5%) premixed by BOC specialty gasses) with the exception of lacking supports in slurry.

Due to the volatile nature of the experiment, two sets of 1 mL SBV Q Sepharose FF chromatography supports were mixed separately with plasma treated MQW immediately after the reactor was turned off by pouring the contents of the reactor straight into tubes containing 1 mL of Q Sepharose FF media. The tubes were mixed on a vortex mixer and incubated for 10 min on a blood tube rotator SB1. The beads were then rebuffered in TE buffer (10 mM Tris-HCl; 1 mM disodium EDTA; pH 8.0) afterwards.

Static binding studies for pDNA and protein binding were performed in duplicate (averaged), immediately after mixing, 1 h, 24 h and 6 days post incubation as described in 2.3.6.

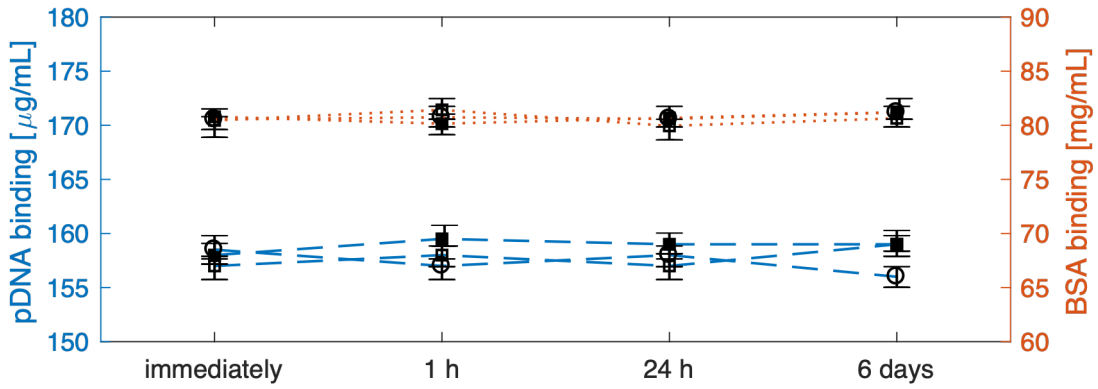


Figure 3-20 Static pDNA and BSA binding capacities of Q Sepharose FF media post mixing with cold atmospheric pressure plasma treated MQW for 10 min measured immediately after initial mixing, 1 h, 24 h and 6 days respectively

The pDNA binding capacities of both offline treated Q Sepharose FF samples are not different from adsorption capacities displayed by the control sample, for both pDNA and BSA adsorption. The reaction requires the plasma species to adsorb onto the chromatography supports in order to etch away and oxidise ligands on their surfaces. Even after allowing the reaction time to develop, no alteration of pDNA binding capacity can be observed. This indicates that, although some of the plasma species may have a longer lifespan, allowing them to not react off prior to contact with chromatography media, it is not sufficient to achieve a reduction of pDNA binding capacity. As one would expect, given that the outer shell logically would be affected before the core, the BSA binding capacities are matching the binding properties of the control sample. Over time, allowing the species to diffuse further into the core, binding properties still remain at their initial values (around 80 $mg_{BSA}/mL_{SBV}$).

It becomes evident that ROS with shorter lifespan are responsible for the plasma etching of the supports. The longer-lived ROS, present in the MQW plasma species solution, do not contribute to binding capacity reductions observed in previous experiments.

Although plasma is clearly altering the binding properties of AEC media in-situ, merely plasma treating aqueous solutions with the aim to create a 'ROS solution' to mix it with media offline does neither alter the binding behaviour of pDNA nor BSA.

3.3.2.7. Variation of the surrounding buffer

Throughout the plasma treatment experiments, MQW was used as a non-interactive buffer with low electric conductivity. However, etching away ligands off the surface of AEC beads leads to the generation of other charged groups (where ligands have been etched away and replaced by ROS).

Figure 3-21 follows the visual development of the plasma reaction containing 1 mL Sepharose CL-6B media in 20 mM NaCl over the first 12 seconds after voltage was applied.

The colour of a plasma is determined by emitted photons, when electrons recombine with ions and is dominantly determined by the carrier gas used (Xu, 2017). The photon energy and, hence, it's wavelength (colour) is dependent on the energy difference between the two energy levels.

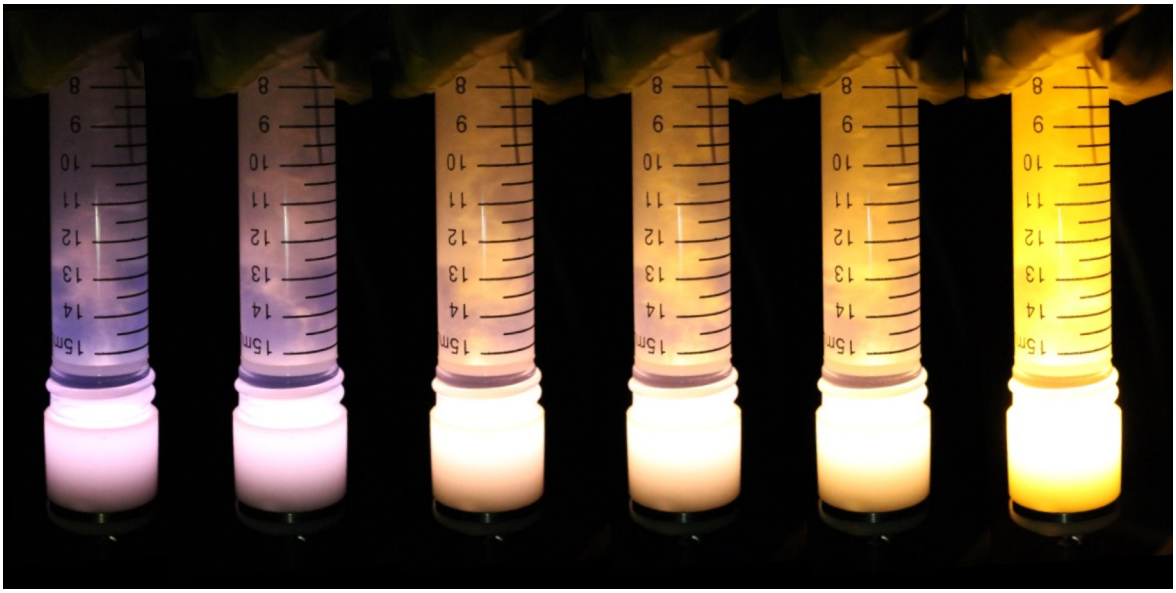

Figure 3-21 Photographic depiction of the first 12 seconds (left to right) of plasma treatment of Sepharose Cl-6B chromatography supports in 20 mM NaCl (1 mL SBV; 3.6 W; 14.5 kHz; He-$O_2$ (99.5%-0.5% v/v) gas; 750 mL/ min)

The characteristic blue-purple plasma (helium associated) dominates during the first seconds of plasma development, however quickly shifting its colour towards a bright yellow glow. This phenomenon has been attributed to the presence of sodium in solution (Bruggeman *et al.*, 2016).

However, with no chromatography supports suspended in the reactor, the glow retains its initial blue-pinkish colour (Figure 3-22), indicating that the sodium is not available with NaCl

alone in the chamber. Either the etched off species or the newly generated groups on the surface of the beads are reacting with the chloride ions allowing the sodium to influence the plasma colour.

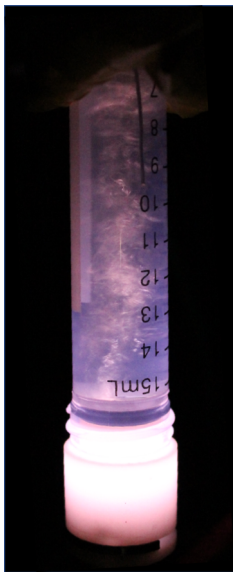


Figure 3-22 Steady state visual appearance of plasma treatment of 20 mM NaCl (no chromatography supports; 3.6 W; 14.5 kHz; He-$O_2$ (99.5%-0.5% v/v) gas; 750 mL/min)

This poses the question, whether quenching these groups in their higher energetic states with ions provided in the surrounding buffer is beneficial for the reduction of surface binding of the chromatography supports. Therefore, Q Sepharose FF media (1 mL SBV each) was equilibrated in different buffers (8 mL total sample volume; NaCl, $Na_2CO_3$, $CH_3CO_2K$ - all 100 mM) before plasma treating the suspensions (as described in 2.3.5; 7 W; 14.5 kHz; 10 min; He-$O_2$ (99.5%-0.5% v/v) gas; 750 mL/min).

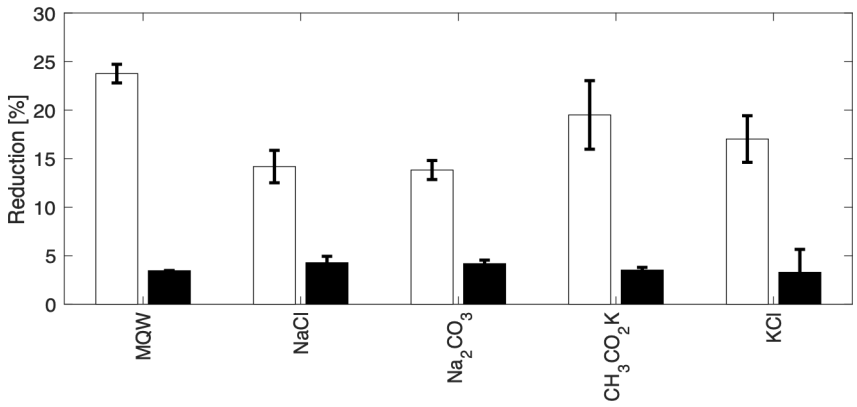


Figure 3-24 Reduction of Q Sepharose FF static binding capacities post plasma treatment (7 W; 10 min; 14.5 kHz; He-$O_2$ (99.5%-0.5% v/v); 750 mL/min) after equilibration in different salt buffers (100 mM)

As seen previously, reduction of BSA binding capacity of Q Sepharose FF media in MQW due to plasma etching is minimal (3.5%; Figure 3-24) and no significant damage was done to the core of the particles. Changing the surrounding buffer of the media neither enhances nor reduces the damage caused to the core of the particles. With all reductions of BSA binding capacities being below 5%, in comparison to an untreated control sample, the effect of the plasma treatment on the core of the particles is therefore independent of the surrounding buffer.

The plasma treatment reduced pDNA binding of the MWQ buffered sample by 24% (SI= 1.27). While pDNA binding capacity of the sample buffered in 100 mM potassium acetate is reduced by 20% (SI= 1.18), yielding a comparable result. However, none of the additional salt buffers get close to the reduction levels achieved when using pure MQW as surrounding buffer.

The addition of different 100 mM salts in the surrounding buffer (sodium chloride, sodium acetate, potassium acetate, potassium chloride) during cold atmospheric pressure plasma treatments of hydrogel AEC media, does not contribute to a higher loss of surface binding capacity in static binding studies. This may be due to reduced electric resistance and subsequently increased higher electric current, hindering the plasma development and its efficacy.

3.3.2.8. Visual Batch to Batch variations in Q Sepharose FF media

Upon acquisition of chromatography media and prior to their usage for pDNA purification, it is important to confirm their performance in chromatographical scouting experiments resembling their later field of application. Throughout the plasma etching experiments in the FBR, especially with Q Sepharose FF, irregularities in results led to light microscopic inspection of different batches of starting media.

All media performed similarly (and in accordance with manufacturer's protocols) with regards to protein binding capacities and pDNA isotherms; but despite these similarities, the media behaved differently before and after plasma treatments in static binding studies across batches.

To assess which batch of Q Sepharose FF is best suited for plasma surface etching, four different batches of media were equilibrated in MQW and light microscopic images of 10x and 40x magnification were taken as described in (2.3.11.2).

Table 3-2 Lot numbers of different analysed Q Sepharose FF media batches

| Media description (including supplier) | Batch | Lot # of the different batches |
|---|---|---|
| **Q Sepharose FF (directly from GE Healthcare)** | 1 | 10227073 |
| **Q Sepharose FF (directly from GE Healthcare)** | 2 | 10237687 |
| **Q Sepharose FF (from Sigma Aldrich)** | 3 | MKCB8745 |
| **Q Sepharose FF (directly from GE Healthcare)** | 4 | 10037837 |

At 10x magnification (Figure 3-24, top), different batches of Q Sepharose FF show similar size distributions and indicate the presence of small imperfections on the surfaces of the particles as will be discussed in detail later in the respective sections (SEM images (3.3.2.14. ) as well as quantitative analysis of said imperfections (0)). However, upon higher magnifications it becomes evident that supports of batch 2 and 3 show entirely different surface topologies than the other two. Both are punctuated by small holes in ways previously unobserved.

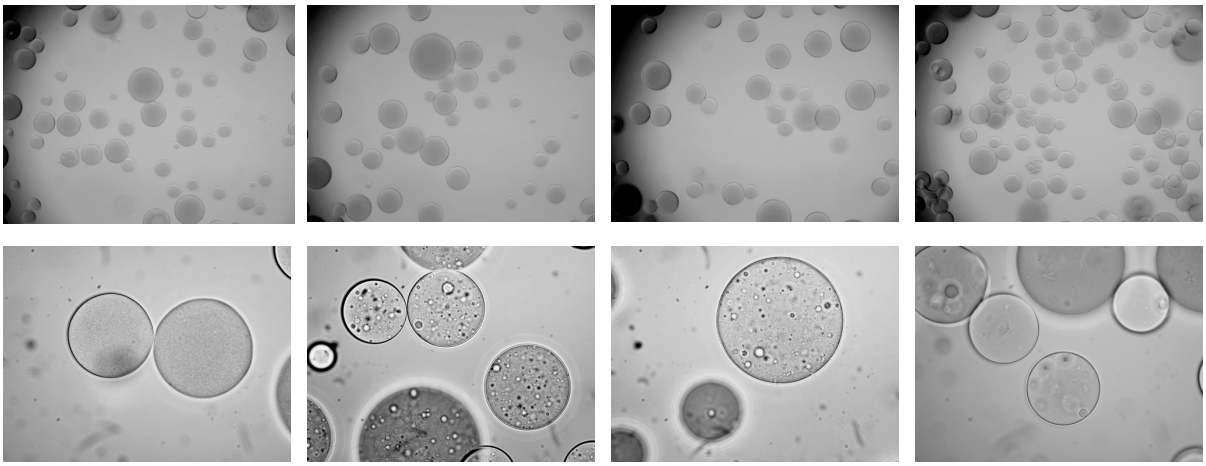

Figure 3-24 Light microscopic images of different Q Sepharose FF batches (see Table 3-2 for description); 10x magnification (top); 40x magnification (bottom); left to right Lot #: 10227073, 10237687, MKCB8745, 10037837

These small holes on the surfaces of the beads grant pDNA molecules access to the core of the beads, adsorbing to the ligands lining the pores, even if the remaining surface was totally inert to pDNA binding.

None of the media are ideal for plasma etching and oxidising ligands off the surfaces of the beads, however batch 2 and 3 would even after a sorting process (eliminating the non-spherical/ imperfect beads) remain unsuitable due to the amount of small entry holes to regions inaccessible to etching ROS.

When selecting AEC media for cold atmospheric pressure plasma experiments with the aim of eliminating surface charges, it is crucial to inspect the beads on a batch to batch basis not only for their chromatographic performances in the 'native' state without surface modifications, but also visually as batch-to-batch variances of the same media have a severe impact on the efficacy of subsequent plasma etching operations. Even for the same brand of beads (Q Sepharose FF) differences across batches make some of the media unsuitable, based on their optical properties alone.

3.3.2.9. How far does pDNA penetrate into the core of AEC beads (Q Sepharose FF)?

It was previously reported that the vast majority of the interior of agarose based AEC matrices is inaccessible to pDNA binding due to size limitations (Prazeres *et al.*, 1998; Ljunglof *et al.*, 1999).

The base matrix of Q Sepharose FF is a highly cross-linked 6% agarose media (GE Healthcare Bio-Science, 2014) with a pore size limit of around 29 nm (Hagel *et al.*, 1996b). pDNA molecules are hence expected to be unable to access the inner core of the particle and binding is limited to the surface of the media.

In order to quantify the penetration depth of pDNA binding into the interior of Q Sepharose FF adsorbents, CLSM images of single chromatography particles were recorded as described in 2.3.12.

Stack images with a magnification of 63x were recorded for various support diameters.

The thickness of each adsorptive layer was measured as the radial length in μm of peak areas with intensity values >20 counts. The numerical average of 6 peaks around the perimeter of each bead was calculated (omitting values originating from peaks with a large discrepancy to the average peak height to avoid the impact of discordant values). The intensity traces' LUTs were adjusted to visualise the fluorescent binding 'halo' of the adsorptive layer.

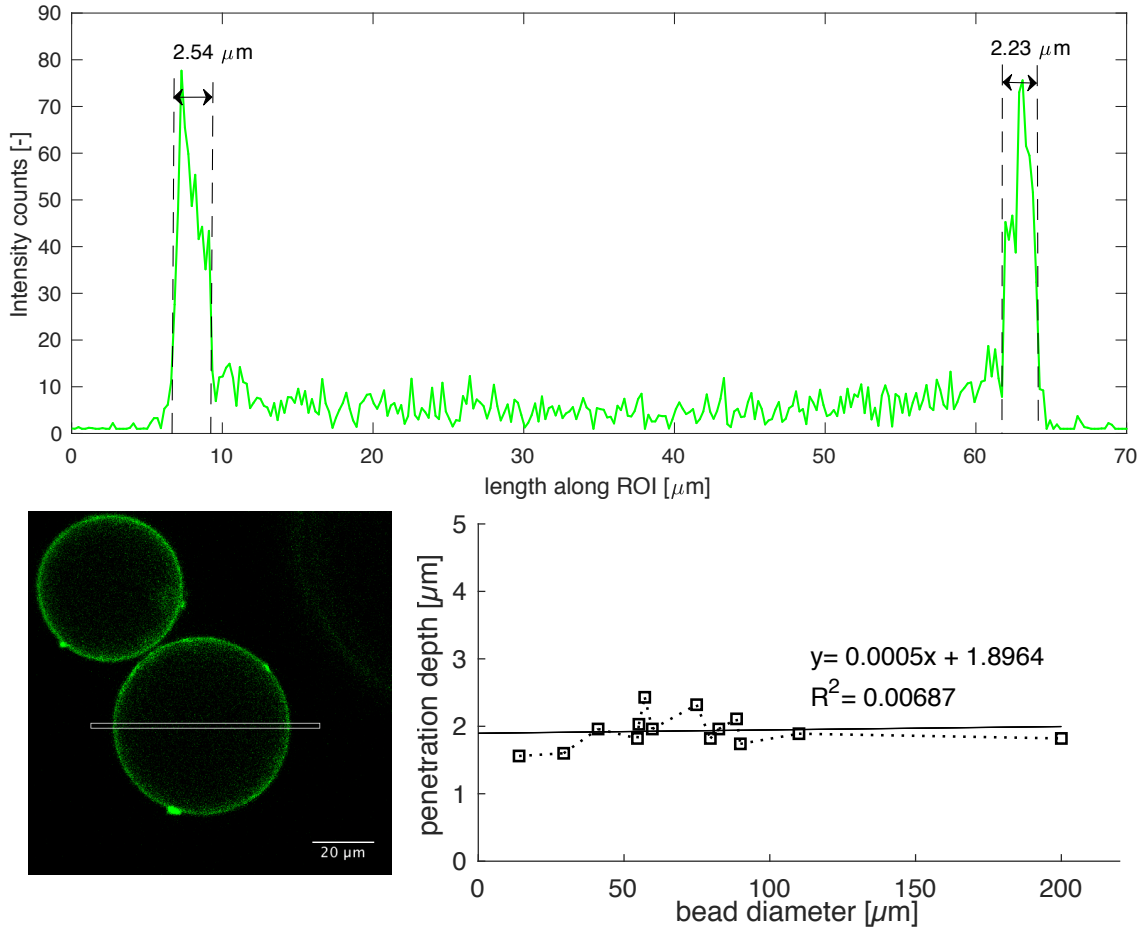


Figure 3-25 Top: Example fluorescence intensity profile of Syto 9 tagged pDNA along the radial position along the ROI of the bottom left CLSM image
Bottom left: CLSM image of Q Sepharose FF with one (of 3 per image) ROI (73x 5 μm) for the determination of penetration depth of pDNA into the shell of the media
Bottom right: Average of penetration depths for different bead diameters of 6 different pDNA peaks (intensity counts >20) each around the bead per image; linear fit of data over all measured diameters

An example of an intensity profile of one analysed bead diameter is depicted in Figure 3-25. The consolidation of the obtained data (Figure 3-25, bottom right) shows that the thickness of the adsorptive layer is largely independent of the particle diameter (neglecting the miniscule slope of the linear fit through the data points). The extend of pDNA binding into the core was calculated at an average of 1.9 μm with all data points spreading between 1.5-2.5 μm.

However, small particle diameters still result in higher pDNA binding capacities per volume of media due to the larger surface binding area to volume ratio per bead. If a process designed to eliminate all ligands on the surface of chromatography particles, to create bilayered SEC-

AEC supports, cannot entirely etch away/ cover the ligands on the surface, AEC media with larger diameters as starting materials would be beneficial.

Whether or not the depth of the binding layer of pDNA depends upon the binding region of a bead is of great interest when considering that some beads within a batch of chromatography media show non-spherical shapes. These non-uniform beads are of particular interest with regard to binding of pDNA to surface regions that are less accessible to convection from the surrounding media. To assess the extent of pDNA binding depth to these 'unconventional' surfaces, CLSM images of supports bearing 'beads inside bead' shapes were recorded, and binding penetration measured in the same way as for the outer shell of the particles (Figure 3-26).

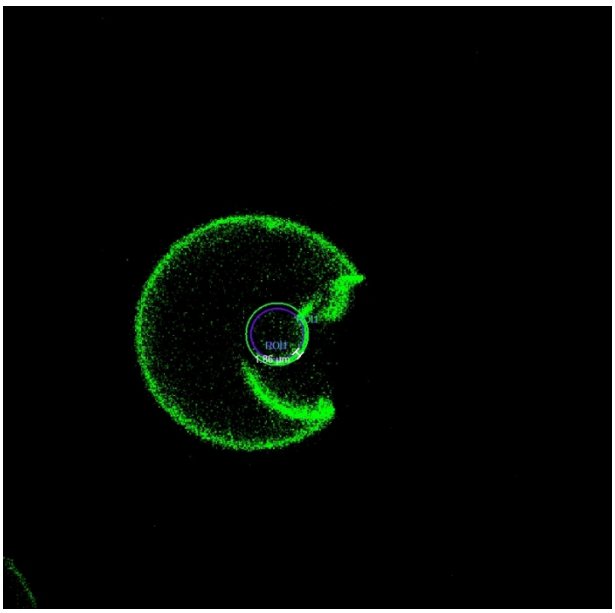

Figure 3-26 CLSM image of a Q Sepharose FF chromatography particle incubated with Syto 9 tagged pDNA; the chosen stack of analysis focusses on the centre of the small bead, not the main bead, nor the 'cut out'

The size of the pDNA binding layer in the small bead inside the 'main' particle was 1.8 μm showing no differences to the 'main' bead. Several other CLSM images of similar particles confirm this trend and it can be concluded that the extend of pDNA binding to Q Sepharose FF supports is independent of bead diameter as well as location of the binding sites on its surface, given enough incubation time.

3.3.2.10. CLSM analysis of the binding topography of plasma etched hydrogel AEC support media

CLSM is a powerful visualisation tool used in biochemical applications to investigate spatial distributions of fluorescent molecules embedded in three-dimensional scaffolds (Carlsson *et al.*, 1987; Ljunglof *et al.*, 1999; Pawley, 2006). It allows tracing positions of different moieties within a matrix such as beaded chromatography supports (Kim *et al.*, 1996; Close *et al.*, 2013). Fluorophores with enhanced fluorescence upon binding to target molecules (tagging) are used to create clear images and help to avoid interference caused by autofluorescence of the scaffold by allowing a reduction of excitation. Due to the use of fluorescent labels without overlapping excitation/ emission spectra, several different compounds can be visualised simultaneously within the same environment.

To visualise the binding properties of different chromatography media and to localise regions where binding of different species occur, beaded supports were incubated with both, fluorescently tagged BSA (CY-5) and the 26.88 kbp plasmid IT14: pPR322-p170 (tagged with Syto-9).

Prior to applying the technique to plasma functionalised supports, (untreated) Q Sepharose FF was analysed as described in 2.3.12, focussing on single supports of the strong AEC media. Image size for all images is given at 512x512 pixels with a pixel size of 0.42 μm. To allow visual inspection of the particles, light microscopic images of supports were recorded, respectively. The distribution of bound fluorescent molecules (Cy5 tagged BSA and SYTO9 tagged pDNA) through the adsorbent particles was obtained by translation of the confocal images into fluorescence intensity profiles after manually selecting equator stacks (largest diameter among z-stacks) of each bead. (FIJI is just) ImageJ (Version 1.0 for Mac) was used for data processing; a region of interest (ROI) (150 μm x 5 μm) was drawn through the centre of each bead and the intensity profile depicts fluorescence in arbitrary units as a function of radial position along ROI.

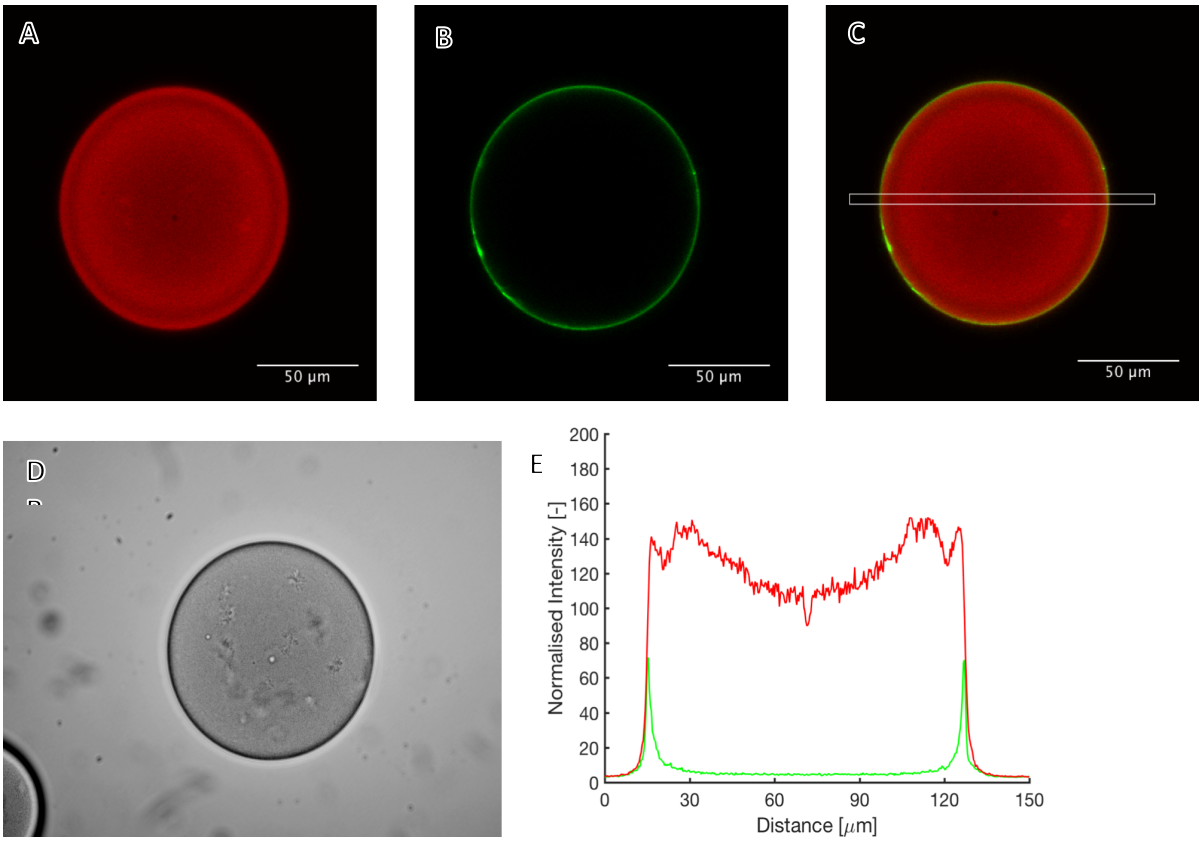


Figure 3-27 CLSM analysis of a Q Sepharose FF (untreated control) chromatography support
A: Cy5 tagged BSA fluorescence emission (ex/em: 635 nm/654- 715 nm)
B: Syto 9 tagged pDNA fluorescence emission (ex/em: 488 nm/492- 533 nm
C: Overlay of both fluorescence channels, ROI for intensity distribution analysis (150 µm x 5 µm)
D: Light microscopic image of the scanned bead
E: Fluorescence intensity profile after image analysis: x-axis shows distance along the meridian of the particle (as depicted in C), y-axis average fluorescence intensity over 5 µm above the x-coordinate (in arbitrary units)

Ljunglof et al. reported a 6.3 kbp plasmid to be too large to enter the pores of Q Sepharose FF (Ljunglof *et al.*, 1999), so binding of 26.88 kbp plasmid IT14: pPR322-p170 is limited to the ligands on the surface of the adsorbent particle (Figure 3-27, B).

The much smaller BSA molecules (66.43 kDa (Hirayama *et al.*, 1990); stokes radius: 3.48 nm (Axelsson, 1978)) have steric access to diffuse through the porous stationary phase and adsorb to ligands lining the internal pores throughout the support (A).

To ensure the observed fluorescence is solely attributed to fluorescence enhancement of SYTO-9 and CY5 binding to pDNA and BSA respectively, a control experiment in absence of either fluorophore was conducted. Figure 3-28 confirms the absence of autofluorescence of pDNA, BSA and the stationary phase at 488 and 635 nm.

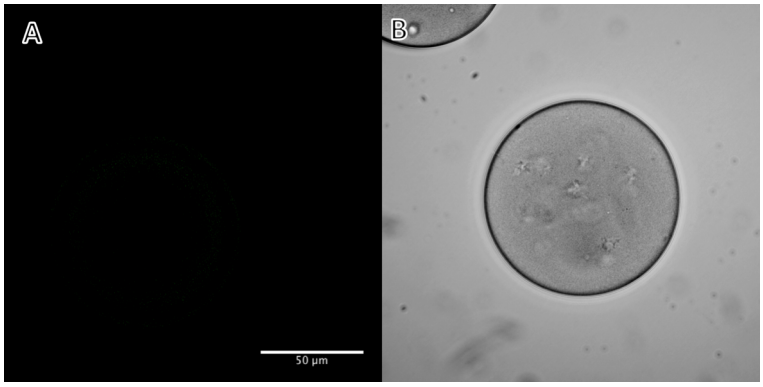


Figure 3-28 CLSM analysis of Q Sepharose FF chromatography support in the absence of fluorophores confirming the absence of autofluorescence of BSA, pDNA and the support matrix at both 488 nm and 635 nm
A: Overlay of fluorescence channels at emission ranges of 492-533 nm and 654-715 nm
B: Respective light micrograph

3.3.2.11. CSLM analysis of He-$O_2$ plasma treated Q Sepharose FF chromatography supports

Cold atmospheric pressure helium plasma (admixed with 0.5 % (v/v) oxygen) was used to functionalise chromatography supports by modifying the exteriors of Q Sepharose FF, DEAE Sepharose FF and EMD Fractogel (M) DEAE via plasma etching and oxidation as described in 2.3.5, with exception that voltage was held constant rather than power input. Results of medias performance post plasma treatment was analysed and discussed in ((Olszewski *et al.*, 2013); a summary of the results is depicted in Table 3-3.

For each media, two different treatment times (150 s; 300 s) at different voltages (10 V; 20 V) were investigated. Static protein and pDNA binding studies were preformed to assess reduction of core and surface binding capacities respectively as described in 2.3.6;

CSLM image analysis of plasma etched Q Sepharose FF supports shows a qualitative reduction of pDNA binding capacity cf. the untreated control for all analysed samples (Figure 3-29). The pDNA 'halo', surrounding the bead, fluoresces more brightly in the untreated control sample as opposed to the plasma treated samples.

Quantitatively, pDNA peak intensities get reduced further with increased treatment time of the samples in the reactor (12.5% reduction after 150 s as opposed to 39.1% reduction after 300 s); a similar effect can be observed with an increase in voltage/ power input (12.5% reduction at 10 V; 26.2% reduction at 20 V).

Table 3-3 Reduction of BSA and pDNA binding capacities of He-$O_2$ plasma treated chromatography supports in comparison to their untreated control samples assessed with static binding studies (adapted from (Olszewski et al., 2013))

| Base Matrix | Applied voltage [V] | Treatment time [s] | Reduction of surface binding (pDNA) capacity [%] | Reduction of core binding (BSA) capacity [%] |
|---|---|---|---|---|
| **Q Sepharose FF** | 10 | 150 | 61.5 | 4.8 |
| **Q Sepharose FF** | 20 | 150 | 66.3 | (-1.3) |
| **Q Sepharose FF** | 10 | 300 | 67.3 | 17.3 |
| **DEAE Sepharose FF** | 10 | 150 | 47.5 | 6.4 |
| **DEAE Sepharose FF** | 20 | 150 | 62.4 | 18.8 |
| **DEAE Sepharose FF** | 10 | 300 | 61.3 | 26.1 |
| **EMD Fractogel DEAE** | 10 | 150 | 55.8 | 2.9 |
| **EMD Fractogel DEAE** | 20 | 150 | 74.1 | 17.9 |
| **EMD Fractogel DEAE** | 10 | 300 | 69 | 16.4 |

Correlating pDNA binding capacity to peak fluorescence intensities can be slightly misleading due to the binding nature of pDNA to AEC supports; however, when comparing the integral values of areas under the pDNA fluorescence signals (sum of all intensity values, corrected by the baseline fluorescence assuming no core binding of pDNA to Q Sepharose FF), the trends of power input and treatment time remain the same as for the reductions of the peak intensity values.

Plasma etching of Q Sepharose FF yielded significant reduction of shell binding capacity in static pDNA binding studies of up to 67% for the 300 s, 10 V sample (Table 3-3).

When comparing the data to reduction of pDNA fluorescence intensity within the same sample (both peak intensity and average peak area), pDNA binding capacity is reduced less (39.1% and 32.5%, respectively). So, although the trends of the plasma parameters for the reduction of shell binding capacity with increased voltage and treatment time remain the same, quantitatively the results are not directly comparable.

Comparing the fluorescence intensity profiles of plasma treated beads to untreated controls, no significant alteration of average BSA fluorescence intensities can be observed. Unlike the BSA static binding studies, there is no indication that the plasma treatment has an effect on the core binding capacity of the supports.

Reasons for this discrepancy may be aging of the media, differences in the assay implementation or data analysis.

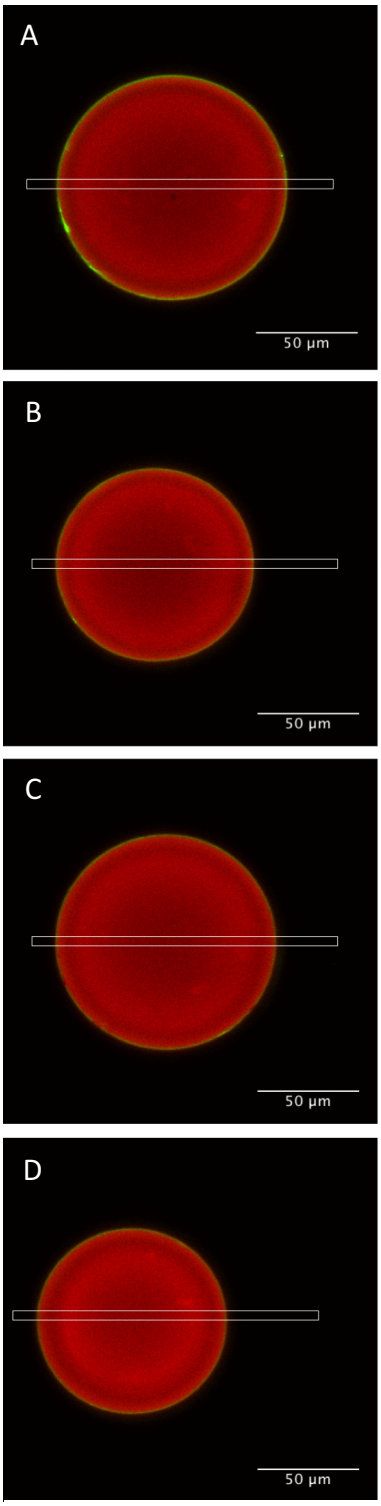


**Untreated Q Sepharose FF control treated Q Sepharose FF**
Average pDNA intensity: 7.4
Peak pDNA intensity: 71.6
Peak intensity/average: 9.7
Average BSA intensity: 118.8
(for intensities >10)

**10 V; 150 s; helium oxygen plasma treated Q Sepharose FF**
Average pDNA intensity: 6.5
Peak pDNA intensity: 62.6
Peak intensity/average: 9.6
Average BSA intensity: 122.5
(for intensities >10)
Loss in peak intensity: 12.7 %
(against control)
Loss in peak area: 18.9 %
(against control)

**20 V; 150 s; helium oxygen plasma treated Q Sepharose FF**
Average pDNA intensity: 6.0
Peak pDNA intensity: 52.9
Peak intensity/average: 9.6
Average BSA intensity: 130.3
(for intensities >10)
Loss in peak intensity: 26.2 %
(against control)
Loss in peak area: 28.5 %
(against control)

**10 V; 300 s; helium oxygen plasma treated Q Sepharose FF**
Average pDNA intensity: 5.8
Peak pDNA intensity: 43.6
Peak intensity/average: 7.5
Average BSA intensity: 139.5
(for intensities >10)
Loss in peak intensity: 39.1 %
(against control)
Loss in peak area: 32.5 %
(against control)

Figure 3-29 CLSM analysis of plasma treated Q Sepharose FF;
left: overlay of Cy5 and Syto9 fluorescence channels with ROI;
centre: intensity profiles of Cy5 and Syto 9 along ROI;
right: calculated parameters of binding reduction to control and others; loss in peak area was calculated using the integral intensities adjusted by the baseline intensity

3.3.2.12. CSLM analysis of He-$O_2$ plasma treated DEAE Sepharose FF chromatography supports

CSLM image analysis of plasma etched DEAE Sepharose FF beads shows a qualitative reduction of pDNA binding capacity in comparison to untreated control for all analysed samples. The fluorescent pDNA bound to the outer shell of the supports is a lot brighter in the untreated control sample cf. all plasma treated samples irrespective of plasma parameters (Figure 3-30). Quantitative comparison of fluorescence signals of the tagged pDNA yielded peak intensity losses of up to 46% (10 V, 150 s) with a reduction of BSA binding of 12% (SI= 1.6).

Unlike the plasma treatment results seen with Q Sepharose FF, the plasma treated DEAE Sepharose FF samples do not show the same tendencies with an increase power input (similar reductions seen for the 10 V and 20 V samples) and treatment time (doubling the treatment time did not lead to a further reduction of pDNA peak height, nor peak area).

Longer treatment times did however, reduce the average BSA fluorescence of the samples. The sample treated for 150 s (10 V) lost 7.8% of its BSA fluorescence (SI= 1.7), while the sample treated for 300 s (10 V) in the reactor shows a reduction of 19% (SI= 1.47).

A loss in BSA fluorescence cannot be observed in the 150 s (20 V) sample, yielding an SI of 1.8 (assuming no loss in BSA binding capacity).

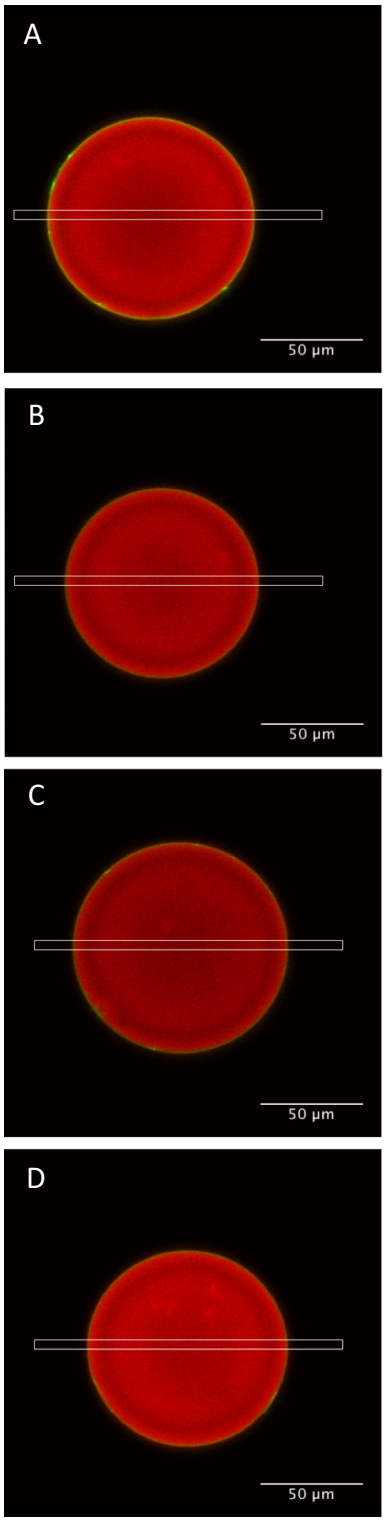


**Untreated DEAE Sepharose FF control**
Average pDNA intensity: 7.4
Peak pDNA intensity:79.4
Peak intensity/average:10.7
Average BSA intensity: 153.2
(for intensities >10)

**10 V; 150 s; helium oxygen plasma treated DEAE Sepharose FF**
Average pDNA intensity: 5.3
Peak pDNA intensity: 42.7
Peak intensity/average: 8.1
Average BSA intensity: 141.0
(for intensities >10)
Loss in peak intensity: 46.2 %
(against control)
Loss in peak area: 41.1 %
(against control)

**20 V; 150 s; helium oxygen plasma treated DEAE Sepharose FF**
Average pDNA intensity: 5.3
Peak pDNA intensity: 44.1
Peak intensity/average: 8.3
Average BSA intensity: 123.7
(for intensities >10)
Loss in peak intensity: 44.5 %
(against control)
Loss in peak area: 41.4 %
(against control)

**10 V; 300 s; helium oxygen plasma treated DEAE Sepharose FF**
Average pDNA intensity: 5.3
Peak pDNA intensity: 46.7
Peak intensity/average: 8.8
Average BSA intensity: 160.4
(for intensities >10)
Loss in peak intensity: 44.5 %
(against control)
Loss in peak area: 41.8 %
(against control)

Figure 3-30 CLSM analysis of plasma treated DEAE Sepharose FF;
left: overlay of Cy5 and Syto9 fluorescence channels with ROI;
centre: intensity profiles of Cy5 and Syto 9 along ROI;
right: calculated parameters of binding reduction to control and others; loss in peak area was calculated using the integral intensities adjusted by the baseline intensity

### 3.3.2.13. CSLM analysis of He-$O_2$ plasma treated EMD Fractogel DEAE chromatography supports

The pDNA fluorescence signal of the control EMD Fractogel DEAE shows a distribution of pDNA binding throughout the support. The binding of pDNA on the surface is higher than in the core of the beads, however, the results clearly show that pDNA binding occurs throughout the centre of the support as well as on the surface- pDNA diffuses through the stationary phase and binds to the ligands lining its pores. With a pore size of 800 Å (Millipore, 2016), the size cut-off of the Fractogel is significantly higher than for the Sepharose media with a pore size of around 29 nm (Hagel *et al.*, 1996a; Yao *et al.*, 2004). It has been reported that pDNA molecules can pass through much smaller pores than expected based on their molecular weight and calculated hydrodynamic radius (Arkhangelsky *et al.*, 2011).

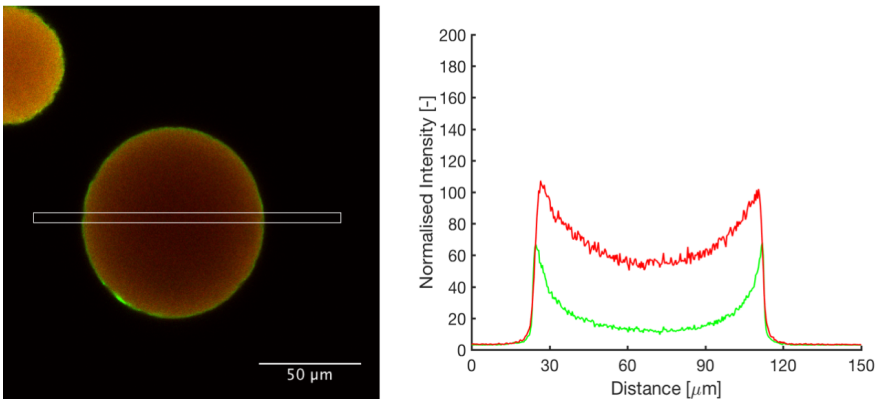


Figure 3-31 CLSM analysis of EMD Fractogel (M) DEAE;
left: overlay of Cy5 (red) and Syto9 (green) fluorescence channels with ROI;
right: intensity profiles of Cy5 and Syto 9 along ROI

The shape of the pDNA distribution curve showcases a behaviour similar to the protein adsorbance; diffusing through the pores, saturating binding sites from the outside to the inside with no hint to a size restriction attributed to either of the molecules.

Nonetheless, static binding studies yielded reductions of pDNA binding capacities >50% for plasma treated Fractogel media. These reductions can be explained by a reduced number of ligands on the surface of the supports in conjuncture to shorter incubation times, not allowing the pDNA to diffuse and bind throughout the core. However, lacking ligands on the surface of the supports does not significantly alter the equilibrium binding capacity.

The idea to create multifunctional supports by etching away the ligands off the surface of AEC media is relying on the stationary phase blocking access of large molecules to the internal porous structure of the beads. Both media based on Sepharose 6 FF show these properties, while the Fractogel does not.

Due to the ability of pDNA to diffuse and bind throughout the entire internal volume of the supports, given enough time to do so, the Fractogel base matrix is unsuitable to be used for plasma etching techniques to create a bilayered support media for pDNA purification.

3.3.2.14. ESEM analysis of cold atmospheric pressure plasma treated chromatography supports

Following up on the light micrographs of plasma treated chromatography supports taken alongside CLSM images, to evaluate the impact the plasma treatment has on the visual appearance of the structural integrity of Q Sepharose FF adsorbent material, ESEM images were taken as described in 2.3.11.

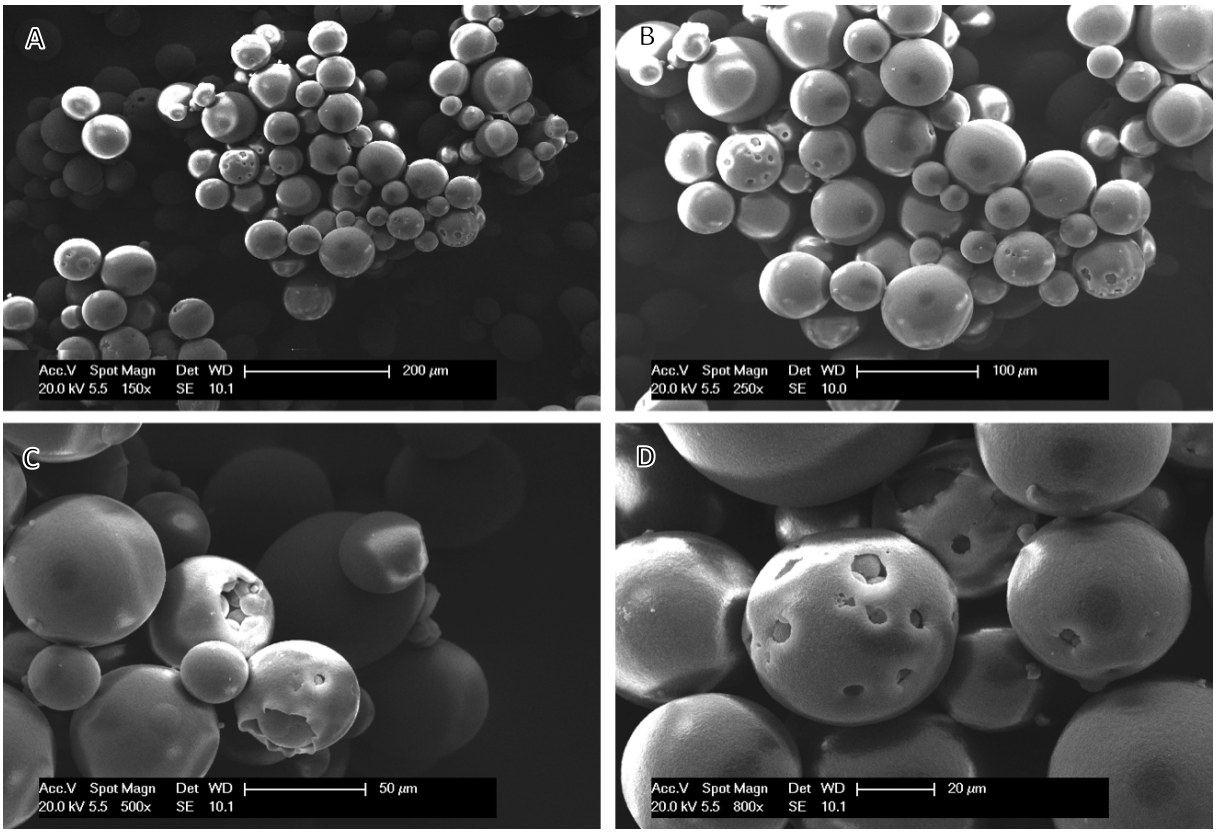


Figure 3-32 ESEM images of Q Sepharose FF at different magnifications

As mentioned previously, some Q Sepharose FF beads show 'imperfections' both on their surface as well as inside the internal core structure of the beads (Figure 3-32). Imperfections in this regard were defined as particles without a smooth surface and/ or spherical shape. These imperfections range from minor dents and cracks on the surface (Figure 3-32, B) to major disfigurations; 'beads inside bead', split open (outer) shell of particles (Figure 3-32, C), punctured surfaces granting non-diffusive access to buffer solutions to the core of the media (Figure 3-32, D).

When comparing the images of Q Sepharose FF to the images of beads following different plasma treatments (Figure 3-33), the same patterns of imperfections occur. Both He-$O_2$

(99.5%- 0.5%) plasma treated samples (3.6 W; 7 W, both 5 min) show macro pores granting open access to the core structure of the support, as well as 'bead-inside-bead' structures similar to those observed in untreated Q Sepharose FF.

The observation that He-$O_2$ (99.5%- 0.5%) plasma has no visual impact on the structural integrity of agarose based chromatographic media is in accordance with previously published work (Olszewski *et al.*, 2013), which concluded that cold atmospheric pressure helium/ oxygen plasma treatment was gentle enough (cold enough) to not cause any damage to the supports. However, comparing the images of Q Sepharose FF control and oxygen plasma treated supports depicted in Figure 3-33 (C & D) indicate that damage that was previously associated with thermal alteration as a result of contacting intensely hot plasma filaments was in fact not caused by the plasma treatment itself, but is an inherent flaw of the media as a result of its manufacturing process.

The similarity of images does not lend itself to the interpretation that the plasma treatment in the FBR set-up (both pure oxygen plasma and helium/ oxygen admixed plasma) has inflicted any alteration in the visual appearance of the chromatography resins. All imperfections also qualitatively appear in particles 'straight from the manufacturer'.

Agarose based chromatography media have been studied extensively over recent decades, however, to the authors knowledge, little work on visual depiction of chromatography particles has been published in the literature with regards to 'naturally' occurring surface imperfections (Caramelo-Nunes *et al.*, 2013; Santos *et al.*, 2017).

Although supports such as the ones observed in this study do appear in other publications, none of them mention their presence nor are concerned about an impact, misshaped supports may have on the purification performance of respective media (Figure 3-34).

The problem of structural imperfections in agarose based media is known amongst manufacturers of chromatography adsorbents. The complexity of controlling the associated parameters during the manufacturing process is tricky and generally not paid much attention. However, media with better surface integrity could be custom made to order (Gilbert, 2018).

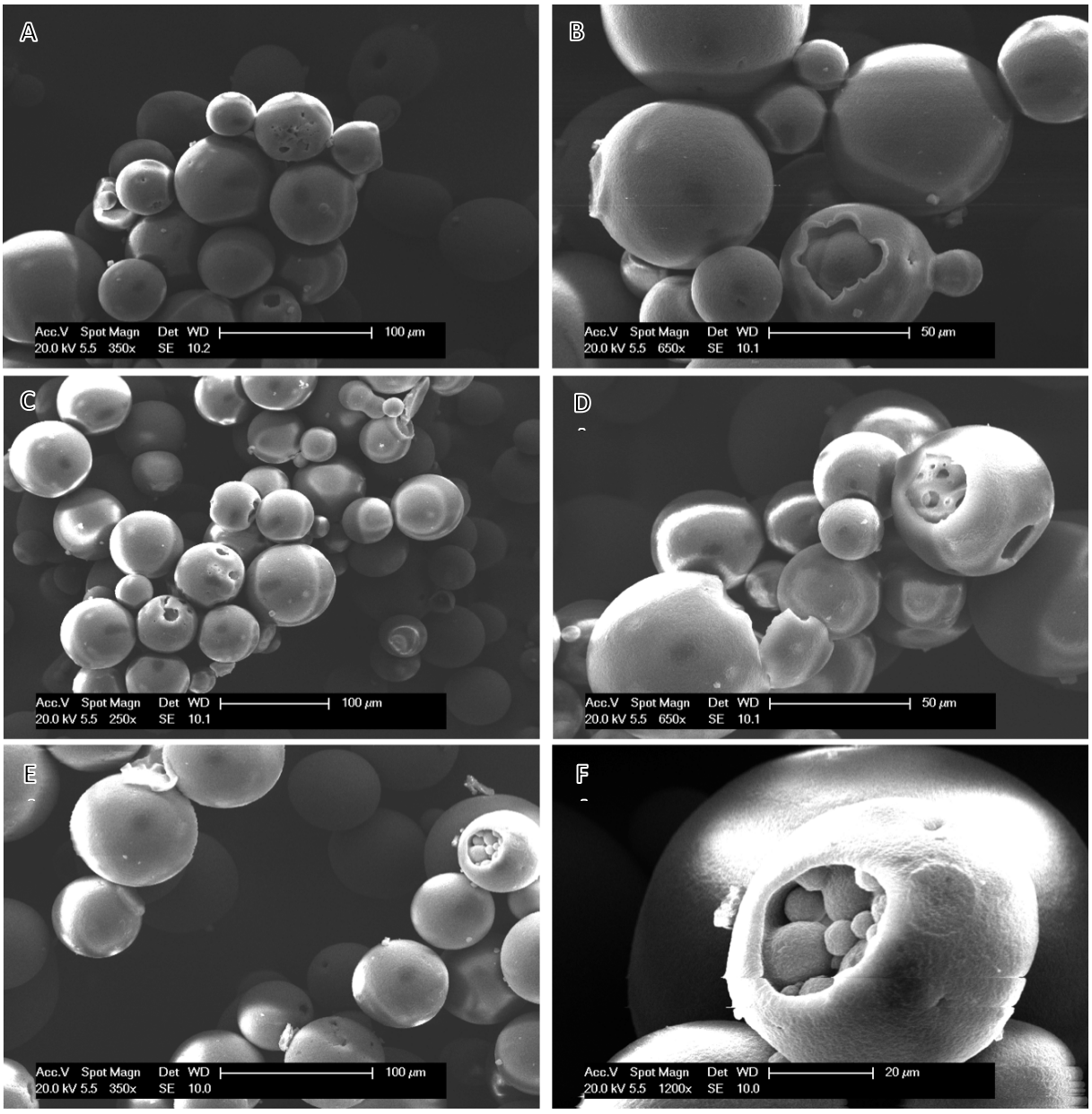


Figure 3-33 ESEM images of Q Sepharose FF at different magnifications after treatment with cold atmospheric pressure plasmas
A, B: He-$O_2$ (99.5%- 0.5%) plasma; 3.6 W; 5 min
C, D: He-$O_2$ (99.5%- 0.5%) plasma; 7 W; 5 min
E, F: Oxygen plasma; 10 W; 5 min

SEC is based (with regards to nanoplexes) on the principle that large molecules cannot access the pores of the media but only travel through the column in the inter-particle volume. Due to this reduced access of column space, larger molecules will elute earlier than smaller molecules, which are kept longer in the column due to their longer diffusive pathways through the porous stationary phase.

Even in such a classic chromatography environment the presence of these imperfections may impact the purification performance of the media.

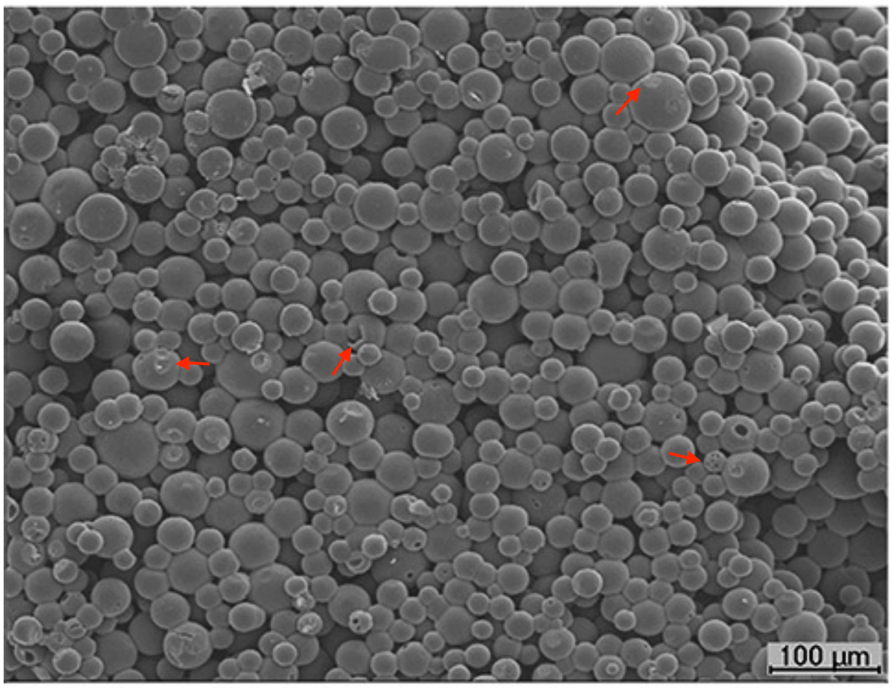


Figure 3-34 SEM image of Sepharose beads at 150x magnification, red arrows highlighting 'disfigured' beads, with access to the core of the beads, rendering them problematic to use in a SEC column operation (image taken from: (Caramelo-Nunes *et al.*, 2013))

Especially when SEC columns are used to approximate the molecular weight of a compound, well defined structural properties of the chromatography supports are of key importance. If a compound has access to complex structures (such as the observed 'bead-inside-bead') and is not limited to the columns void volume, the overall retention time of the compound changes, ultimately resulting in peak broadening/ tailing (Rouessac *et al.*, 2000; Ninfa *et al.*, 2010). Another problem in flow through chromatography operations is column fouling. The use of non-spherical chromatography supports with holes and imperfections enhances these problems as compounds get more easily 'trapped' in the crevices created by imperfections. The need to clean/ strip the column becomes more frequent and CIP protocols need to be adjusted in order to deal with larger concentrations of compounds expected from spherical particles with smooth surfaces.

The high reactivity of plasma species makes it less likely that the species will get close enough to the 'beads-inside-a-bead' and other hidden ligands to etch away the functional groups in these imperfections. The radicals only diffuse very short distances out of the gas plasma

bubbles and will react with the first surface they encounter, leading to overtreatment of the more easily accessible surfaces, leaving functional groups in hard to access regions of the particles untouched.

However, in frontal loading chromatography applications, pDNA will diffuse into these crevices and imperfections and bind to the ligands that have not been etched away by plasma radicals. These remaining binding sites will get supersaturated with pDNA due to their strong negative charges, distributed evenly all over the molecule. When granted enough time to equilibrate, the more desirable sc conformation of pDNA is likely to change its spatial orientation in order to fit in more molecules on these remaining binding sites.

3.3.2.15. Quantification of the 'natural' occurrence of imperfections in different chromatography media

SEM image analysis qualitatively showed the presence of imperfect beads and raised the question to what quantitative scope they are part of support populations. To get an overview of the magnitude of imperfections in large populations of different chromatography media, light micrographs were recorded and analysed by visual inspection. Each support entirely within an image was graded and associated to one of the following three categories (Figure 3-35):

Green- spherical particles with a smooth surface

Yellow- minor indentations and cracks on the surface

Red- majorly disrupted surfaces granting access to the core of the support; complex structures without easily accessible functional groups exposed to the surface

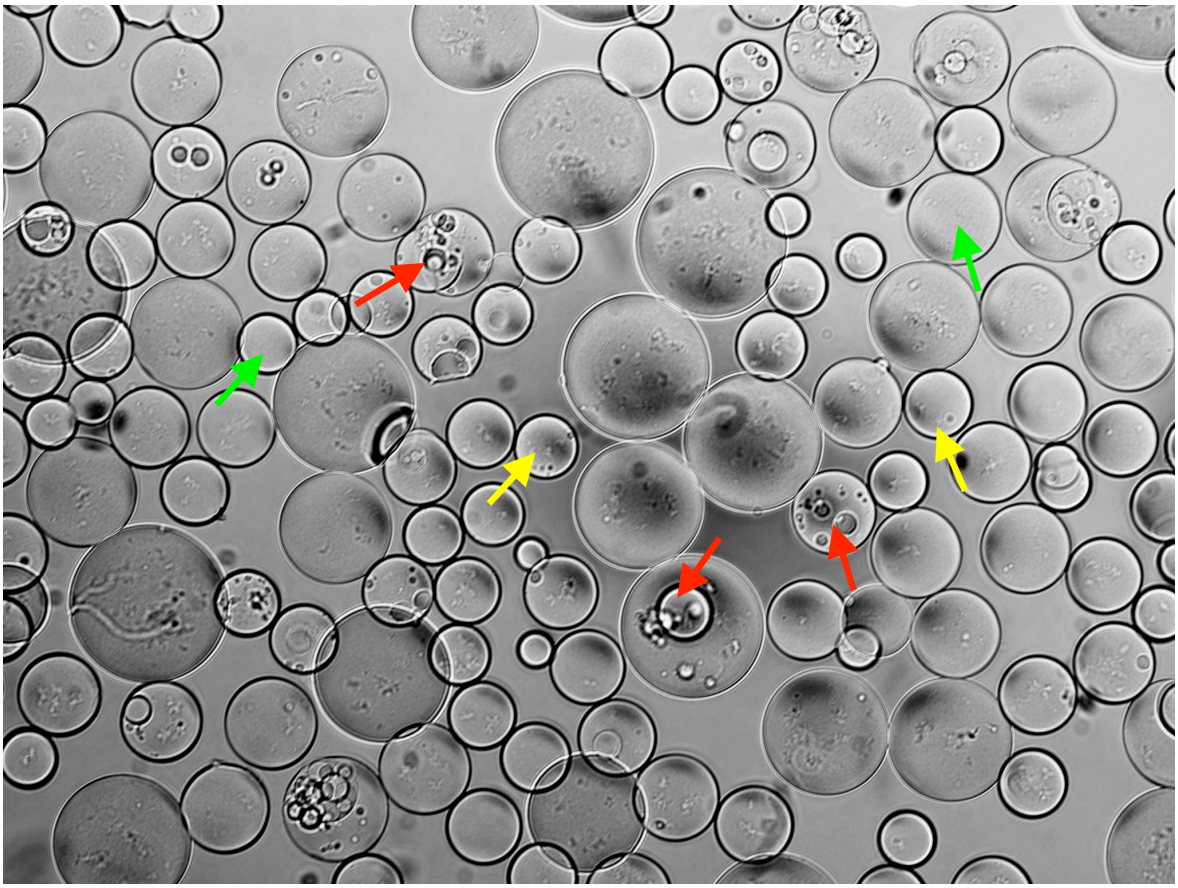

Figure 3-35 Light microscopic image analysis of Sepharose FF supports (10x magnification) to quantify the number of imperfect beads (in % of total population); arrows showcase examples of visual grading; green: spherical particles with a smooth surface; yellow: minor imperfections (indentations, cracks); red: heavily misshaped particles, 'bead inside bead' structures

The extend of imperfections was quantified for the following chromatography media:

- Q Sepharose FF
- Oxygen plasma treated Q Sepharose FF supports (15 V; 150 s; 18.5% SBV in a total of 8 mL MQW)
- He-$O_2$ admixed (99.5%- 0.5%) plasma treated Q Sepharose FF supports (10 V; 150 s; 25% SBV in a total of 8 mL MQW)
- DEAE Sepharose FF
- Capto Core 700
- Q Hyper Z
- EMD Fractogel

Due to the opacity of Q Hyper Z, a quantitative analysis of the visual integrity of the beads was not possible (Figure 3-36).

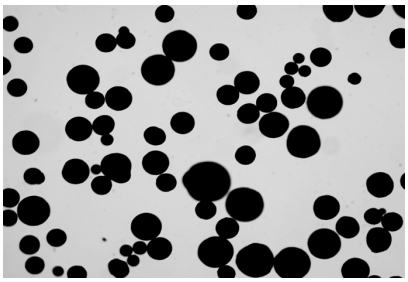

Figure 3-36 Light microscopic image of Q Hyper Z supports

Table 3-4 Quantification of visual integrity of different chromatography media, analysed by light microscopic imaging

| Media | particles analysed | 'green' graded particles [#/ %] | 'yellow graded particles [#/ %] | 'red' graded particles [#/ %] | Conf. interval |
|---|---|---|---|---|---|
| **Q Sepharose FF** | 664 | 109<br>16.4% | 419<br>63.1% | 136<br>20.5% | 3.8 |
| **He- $O_2$ plasma treated (15 V; 150 s; 18.5% SBV)** | 770 | 171<br>22.2% | 438<br>56.9% | 161<br>20.9% | 3.53 |
| **He- $O_2$ plasma treated (10 V; 150 s; 25% SBV)** | 786 | 202<br>25.7% | 445<br>56.60% | 139<br>17.70% | 3.49 |
| **EMD Fractogel (M) DEAE** | 664 | 444<br>66.9% | 172<br>25.9% | 48<br>7.2% | 3.8 |
| **Capto Core 700** | 726 | 509<br>70.1% | 198<br>27.3% | 19<br>2.6% | 3.63 |
| **DEAE Sepharose FF** | 917 | 205<br>22.4% | 556<br>60.6% | 156<br>17.0% | 3.24 |

For all other media, population sizes were selected to grant a minimum confidence level of 95% with confidence intervals of max 4% (Table 3-4). However, light microscopic imaging only analyses half of each particle; the 'actual' percentage of especially yellow classed particles is likely to be slightly higher when analysed with optical sorting instruments.

Unsurprisingly, both chromatography resins based on Sepharose FF base matrix (functional groups DEAE and Q) show similar distributions of imperfections, both for major impairments as well as minor flaws. The ligand on the surface has no impact on the visual appearance of the particles, leading to the assumption that imperfections occur during the manufacturing process of the base matrix. Overall, the majority of supports are spherical and without (major) imperfections (79.5% Q Sepharose FF; 83% DEAE Sepharose FF); however, the distribution of imperfections does not match the size distribution of the particles as the occurrence of major imperfections is almost exclusively limited to larger particles.

For plasma treated support samples, two samples were selected and analysed:

(i) The helium/ oxygen plasma treated sample with highest loss of surface binding capacity in static binding studies (around 70%).

(ii) The oxygen plasma treated sample that showed highest loss of core binding capacity in static binding studies (around 30%).

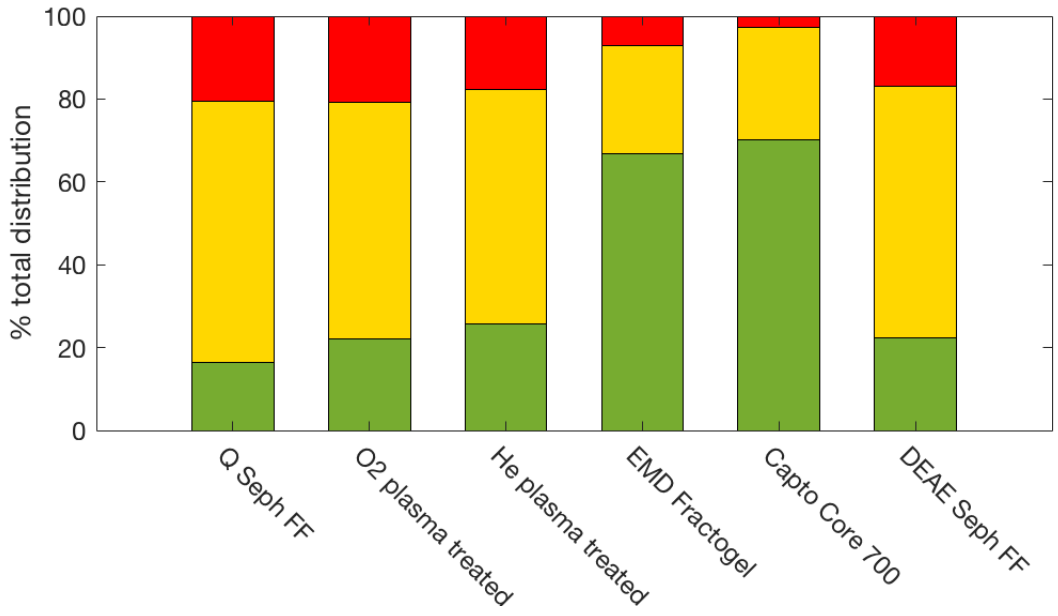


Figure 3-37 Quantitative distribution of visual imperfections in different chromatography media: Q Sepharose FF, oxygen plasma treated (15 V; 150 s; 18.5% SBV in 8 mL MQW) Q Sepharose FF, He-$O_2$ plasma treated (10 V; 150 s; 25% SBV in 8 mL MQW) Q Sepharose FF, EMD Fractogel (M) DEAE, Capto Core 700, DEAE Sepharose FF

Red: heavily disfigured; yellow: minor imperfections; green spherical particles with a smooth surface

Comparing the visual integrity of plasma treated supports to untreated control beads, no difference can be observed with confidence intervals of the distributions overlapping.

Previously it was suggested that the high loss of core binding capacity in oxygen plasma treated support samples could be due to plasma puncturing holes into the surface of the beads, reducing the overall core binding volume (Olszewski *et al.*, 2013). It must be concluded, that previously recorded SEM images were not representative of the phenomena but singularities that occur in all Sepharose FF based media.

Capto Core 700 stands out from other Sepharose based media with only 2.6% of beads showing major imperfections. Being a highly specialised media (and at a retail price of more than three times as much as Q Sepharose FF (GE Healthcare, 2018d; GE Healthcare Bio-Science, 2018)) it is likely that the media is either produced differently or that it went through a more vigorous sieving protocol in the production process.

Similar to Capto media, EMD Fractogel (M) DEAE media has an even size distribution and a low amount of 'red classed' particles, making it similarly suitable for plasma etching based on the visual appearance of the particles (however, the media is still unsuitable based on the presence of diffusive pores, granting pDNA binding throughout the media.

3.3.2.16. CLSM analysis of 'imperfect' supports

SEM images as well as quantitative light microscopic analysis of different chromatography support media have shown that large portions of the populations have visual imperfections on their surfaces. These imperfections range from minor visual impairments (dents, cracks on the surface) to major 'disfigurements'. Comparing images of plasma treated supports to respective images of untreated control samples yielded that these imperfections are not, as previously assumed a result of the plasma treatment process but find their origin in the manufacturing process of the media.

The static binding capacities of the media was assessed, but static binding capacities of a media as a whole does not explain whether the presence of imperfections has an impact on the chromatographic performance/ binding capacity of the media on a single bead level.

Although plasma treatment clearly reduces surface binding of chromatography supports, none of the samples showed a total elimination of surface charge in static binding studies.

As seen in the light microscopic analyses of chromatography media, up to 8% of beads show (at least minor) imperfections. If the residual binding capacity is mainly accounted for by imperfections, the overall outcome of the plasma treatment of chromatography media could be significantly enhanced by using 'more perfect' media.

To assess how and to what extend the presence of imperfections affects the performance of the media as a whole and to visualise the distribution of (pDNA) binding sites in plasma treated media, CLSM stack images of said imperfect beads were recorded as described in 2.3.12 focussing on imperfect single beads.

Static binding studies as well as CLSM analysis of chromatography supports treated with He- $O_2$ gas plasma (99.5%- 0.5%) showed a significant reduction of pDNA binding capacity on the surface of the supports for both DEAE Sepharose FF as well as Q Sepharose FF.

CLSM analysis of imperfect DEAE Sepharose FF beads for two sets of plasma parameters are depicted in Figure 3-38 and Figure 3-39 respectively.

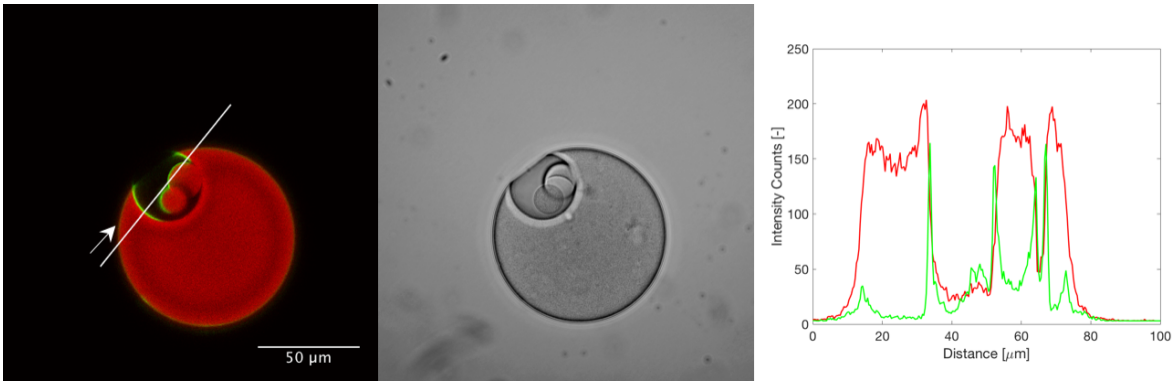


Figure 3-38 CLSM analysis of a helium-oxygen plasma treated DEAE Sepharose FF chromatography support (10 V; 150 s)
Left: Overlay of fluorescence channels (Cy5 tagged BSA, ex/em: 635 nm/654- 715 nm; Syto 9 tagged pDNA, ex/em: 488 nm/492-533 nm), ROI for intensity distribution analysis (150 µm x 5 µm)
Middle: Light microscopic image of the scanned bead
Right: Fluorescence intensity profile after image analysis: x-axis shows distance along meridian of the particle, y-axis average fluorescence intensity over 5 µm above the x-coordinate (in arbitrary units)

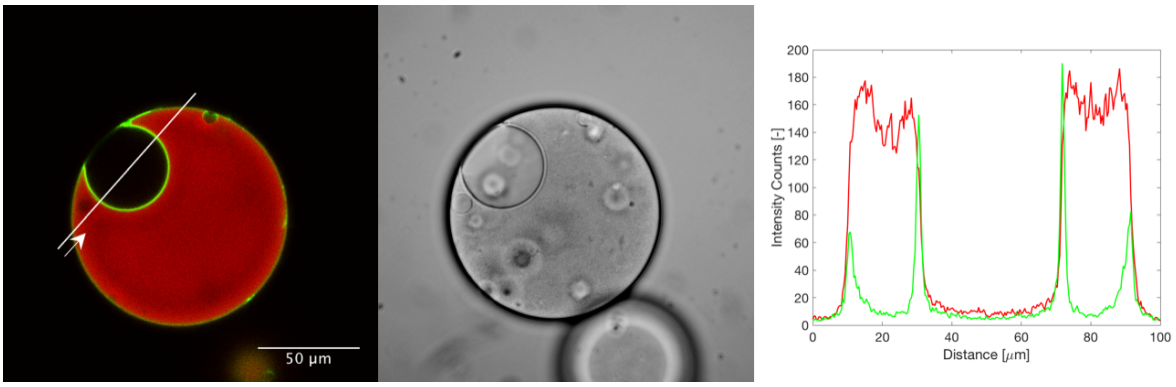


Figure 3-39 CSLM analysis of a helium-oxygen plasma treated DEAE Sepharose FF chromatography support (20 V; 150 s)
Left: Overlay of fluorescence channels (Cy5 tagged BSA, ex/em: 635 nm/654- 715 nm; Syto 9 tagged pDNA, ex/em: 488 nm/492-533 nm), ROI for intensity distribution analysis (150 µm x 5 µm)
Middle: Light microscopic image of the scanned bead
Right: Fluorescence intensity profile after image analysis: x-axis shows distance along meridian of the particle, y-axis average fluorescence intensity over 5 µm above the x-coordinate (in arbitrary units)

The respective intensity profiles show that significantly more pDNA is adsorbed within the imperfections than on the smooth (outer) surface of the media.

The plasma treatment of chromatography supports is an efficient way to modify the functionality of the beads on the surface of the media, however the modification can, by design of the reactor, only take place when ROS get into contact with the ligands on the surface.

The very short lifespan of the species, especially when diffused out of the plasma gas bubble makes it crucial for the targeted surface to be in close proximity to the host gas bubble of the radicals. Making the surfaces less accessible to the reactive plasma species hinders them in reacting with the ligands, reducing the treatment efficiency of lesser accessible areas of the beads.

Imperfections in chromatography adsorbents have different impacts on their binding capacities depending on the location they occur.

Holes or 'beads-inside-beads' structures found inside a bead (no connection of the hole to the surface of the particle; Figure 3-40, A) will affect only the core binding capacity by decreasing the overall binding volume (and subsequently capacity) of the particle due to a lack of binding ligands in the area:

$$V_b = \frac{4}{3}\pi\,({r_b}^3 - {r_i}^3)$$

Where; $V_b$ is core binding volume of the bead

$r_b$ is the radius of the bead

$r_i$ is the radius of a (spherical) imperfection

Although a reduction of overall core binding capacity is not desirable in a chromatography operation, using bilayered chromatographic media intended for pDNA purification in negative mode chromatography, the core binding capacity is less important than other defining factors of the media, all related to the shape and functionality of the media's surface.

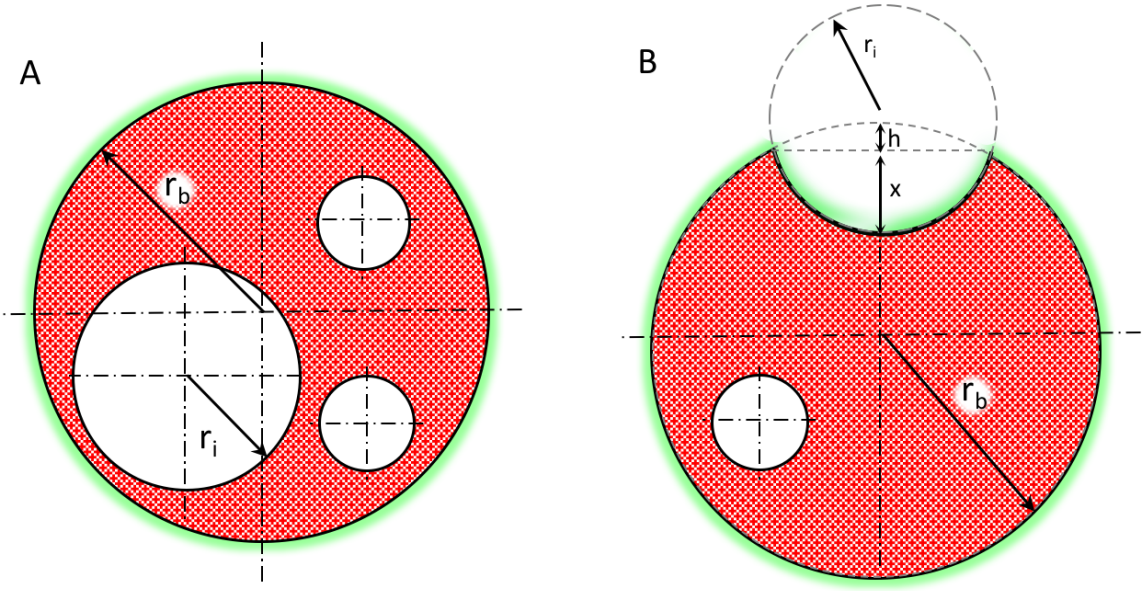


Figure 3-40 Impact of imperfections of chromatography media on (A) the volumetric binding capacity of a chromatography adsorbent due to reduction of the overall available backbone structure of the support (holes not connected to the surface of the media) and (B) the shell binding capacity due to the increase of surface binding area with imperfections connected to the surface of the particle

Unlike imperfections occurring within the beads, a connection of holes to the surface of the media, will not only reduce the core binding capacity, the shell binding is also altered in comparison to a spherical particle (Figure 3-40; B):

$$A_b = 4\pi\, {r_b}^2 - 2\pi\, r_b h + 2\pi\, r_i x$$

With: $A_b$ is the binding surface of the bead

$r_b$ is the radius of the bead

$r_i$ is the radius of a (spherical) imperfection

h height of the missing cap of the bead

x height of the imperfection

This increase of overall accessible surface area is directly linked to the surface binding capacity of the media in comparison to spherical particles with smooth surfaces, making a spherical bead preferable due to the its surface to volume ratio.

CLSM images of imperfect cold atmospheric pressure helium-oxygen gas plasma treated chromatography supports (Figure 3-38 to Figure 3-42) show that the plasma is unable to significantly modify the surfaces occurring within the imperfections (both Q and DEAE Sepharose FF). The reactive plasma species cannot access the crevices created by imperfections, nor are they able to diffuse far enough from the gas bubbles to reach the concave interiors of the 'beads-inside-a-bead' to etch away the binding ligands.

The intensities of pDNA adsorbed onto the smaller particles inside the (main) chromatography bead (imperfections) are around three to four times higher than the intensity values observed on the outside shell of the (main) bead of plasma treated DEAE Sepharose FF (Figure 3-38). Following the intensities across the bead, a slight increase can be observed on the shell of the bead, similar to the binding intensities observed in the respective spherical beads of the same sample (Figure 3-30).

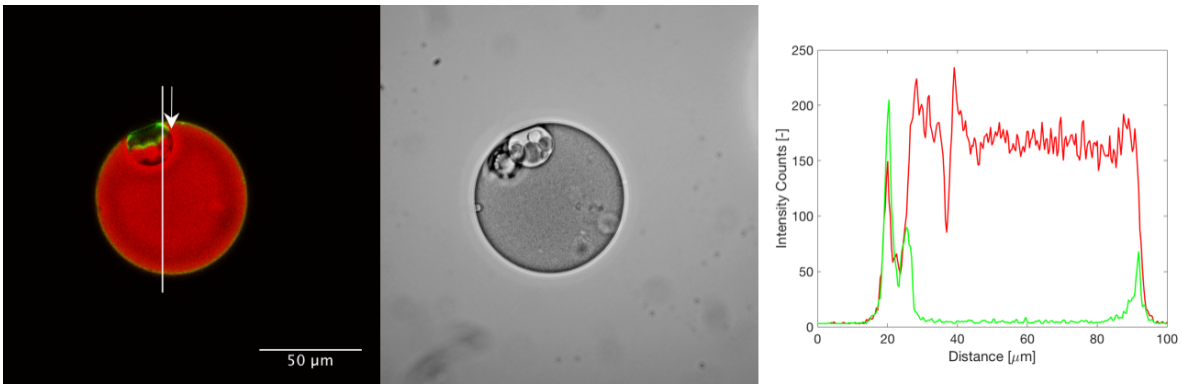


Figure 3-41 CSLM analysis of a helium-oxygen plasma treated Q Sepharose FF chromatography support (20 V; 150 s)
Left: Overlay of fluorescence channels (Cy5 tagged BSA, ex/em: 635 nm/654- 715 nm; Syto 9 tagged pDNA, ex/em: 488 nm/492-533 nm), ROI for intensity distribution analysis (150 µm x 5 µm)
Middle: Light microscopic image of the scanned bead
Right: Fluorescence intensity profile after image analysis: x-axis shows distance along meridian of the particle, y-axis average fluorescence intensity over 5 µm above the x-coordinate (in arbitrary units)

The BSA intensities remain similar throughout the bead with the exception that in close proximity to the imperfection, BSA fluorescence is higher than in the centre of the bead.

As stated previously, the fluorescence intensity on the surface of a sample will always be (slightly) higher than on the bottom or the bulk of a sample as the photons need to pass through media of different refractive indices.

However, the BSA intensity underneath the surface of the main bead is still lower when compared to the intensity observed in close proximity to the imperfect cut-out, suggesting that the ligand density is higher around the imperfections than the normal bead.

The agarose concentration (and consequently the Sepharose backbone structure) around the imperfections seems to be slightly higher than the 6% (GE Healthcare Bio-Science, 2014) found in the bulk of the media. As a result, one would expect a change of refractive index in these areas, which can be observed in the light microscopic images taken of the particles (Figure 3-38 & Figure 3-39).

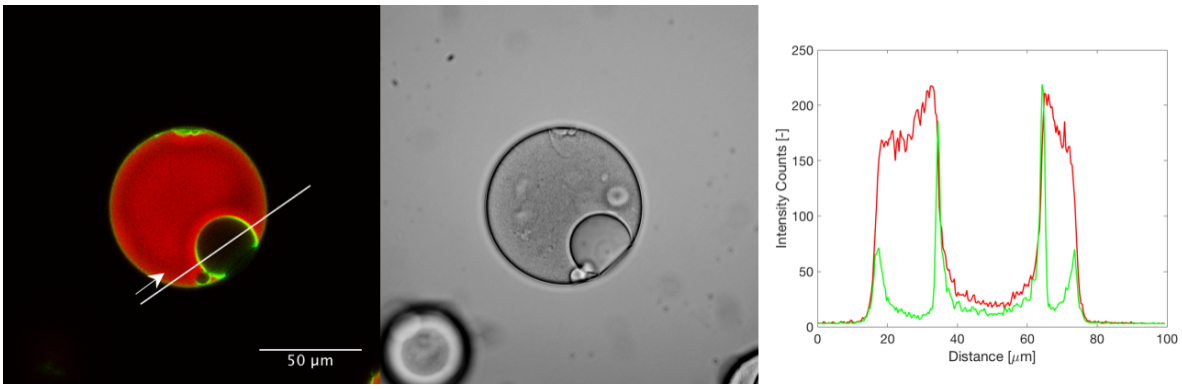


Figure 3-42 CSLM analysis of a He-$O_2$ plasma treated Q Sepharose FF chromatography support (10 V; 300 s)
Left: Overlay of fluorescence channels (Cy5 tagged BSA, ex/em: 635 nm/654- 715 nm; Syto 9 tagged pDNA, ex/em: 488 nm/492-533 nm), ROI for intensity distribution analysis (150 µm x 5 µm)
Middle: Light microscopic image of the scanned bead
Right: Fluorescence intensity profile after image analysis: x-axis shows distance along meridian of the particle, y-axis average fluorescence intensity over 5 µm above the x-coordinate (in arbitrary units)

During the manufacturing process of Sepharose based chromatography media, molten agarose droplets are being cooled down to induce agarose gelling. During this process, the surface tension of the droplets influences the agarose content, leading to a slightly different agarose content of the smaller 'beads-inside-a-bead' imperfections in comparison to the larger (main) particle. The parameters controlling the cooling of the media are difficult to control and so it is likely that batch to batch variations of a final product can lead to different agarose contents within the same bead.

In addition to the inability to etch binding ligands off the surfaces of the beads, a higher amount of pDNA binds within the grooves of the surfaces due to supersaturation of the remaining accessible binding sites as well as trapping molecules inside eddies of caverns (molecules get transported to the openings of the grooves via convection, diffuse into macropores but cannot leave again due to weak interactions and missing convective flows).

Comparing the fluorescence intensities observed in the imperfections to the intensities on the surface of untreated Sepharose FF media, a 2 to 2.5-fold increase for both DEAE Sepharose FF and Q Sepharose FF was observed. This is either due to the outlined supersaturation of the remaining accessible binding sites or due to higher pDNA adsorption as a result of locally increased ligand density.

Overall, the presence of imperfections in chromatography media hinder the efficacy of the plasma treatment by creating surface area available for plasmid binding that is inaccessible

for ROS eliminating ligands on the surface. They are one of the main contributors for residual binding of pDNA in plasma treated media. The imperfections, leading to several complications, make it imperative that for further research being conducted, the media to be treated is of a (more) homogenous distribution.

Little compromise can be made to the sphericity of the particles, leading to several options to ensure spherical particles as starting media.

Sieving of existent base media is not only hard to implement but also lacks the scope of scalability. Swapping Sepharose FF media for a starting media providing better optical properties could lead to great improvements of media performance. Capto media, for example, has shown to be superior over Sepharose FF in terms of level of imperfect supports. Conversations with media manufacturers concerning sphericity and surface integrity of chromatography supports suggest that 'more perfect' media could be made to order (Gilbert, 2018). For future work being conducted in this area, collaborations with media manufacturers are hence strongly encouraged.

3.3.2.17. Chemical characterisation of plasma etched chromatography supports by Time-of-Flight Secondary Ion Mass Spectrometry (ToF-SIMS)

In chromatographic applications tailored for pDNA purification, binding interactions between the nanoplex molecules and chromatography ligands take place in the outer few micrometres of the beads surfaces (Ljunglof *et al.*, 1999). It is therefore of great interest to investigate the chemical structure of the outside of chromatography supports targeted for nanoplex purification.

ToF-SIMS has proven to be useful as a surface analysis technique for the chemical characterization of polymer surfaces (Vickerman *et al.*, 2001). In order to assess modifications to the surface, happening during plasma etching of chromatography supports, the technique was used for the qualitative and semi-quantitative analysis of surface compositions of Q Sepharose FF media prior and post cold atmospheric pressure plasma treatment (both pure oxygen as well as helium-oxygen admixed (99.5%- 0.5%) gas plasma samples).

The resulting mass spectra contain a large number of peaks corresponding to various compounds, which by evaluating the masses associated to the signals, can lead to their identification from the molecular ion of the sample or its fragments (Belu *et al.*, 2003).

Chromatography support samples were dried as described in 2.3.10. All samples were mounted on carbon tape before using a ToF-SIMS 5 (IonToF Münster Germany) equipped with a Bi(3+) source for the sample analysis.

For each sample, duplicate spectra, both negative and positive (area of analysis 20x20 μm (Figure 3-43) were recorded. Due to the volume of data recorded for each sample, Matlab (R2017A) was used for data processing as well as graphical depiction of results.

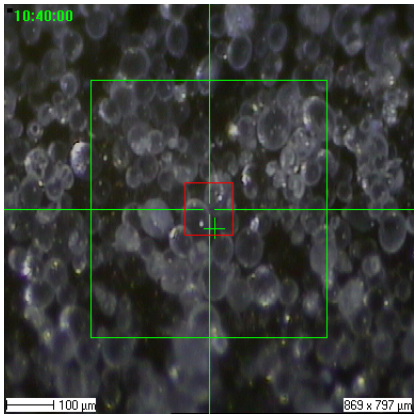

Figure 3-43 ToF-SIMS area of analysis (20 x 20 μm)

All analysed media are based on Sepharose 6 FF with the functional Q ligands covalently attached to the agarose backbone of the supports with no spacers used (Pezzini *et al.*, 2009). It was furthermore previously reported that the molecular surface structure of Sepharose 6 FF resembles that of agarose (Johansson *et al.*, 2004).

After eliminating machine artefacts, intensity values recorded by ToF-SIMS were normalised to respective maximum peak values of each sample. All recorded spectra were compared to the spectrum of the reference carbon tape (without any sample media) to avoid false peak associations. No overlaps between carbon tape peaks and sample peaks were detected (see Appendix A-4 for the positive ToF-SIMS spectrum of the background carbon tape).

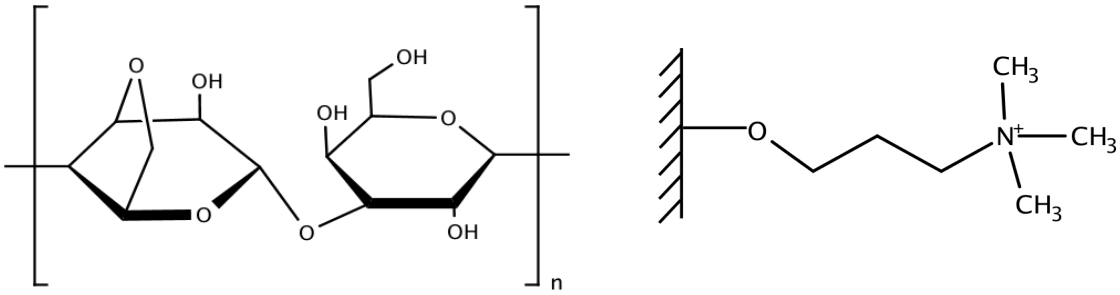


Figure 3-44 Left: Chemical structure of agarose (Sepharose), the polymer of the repeating unit of the disaccharide D-galactose and 3,6-anhydro-L-galactopyranose (PubChem-Substance-Database, 2016)
right: Tentative chemical structure of the strong anion exchange ligand Q Sepharose FF (GE Healthcare Bio-Science, 2016)

The positive ToF-SIMS spectrum of Sepharose 6 FF contains a large number of peaks that have been identified as $C_xH_yO_z$ and $C_xH_y$ molecules (Figure 3-45 ; Table 3-5). It was shown previously that anion exchange ligands coupled on to the surface of Sepharose 6 FF strongly influence the positive ToF-SIMS spectra of the media (Johansson *et al.*, 2004).

Table 3-5 Major positive ions found in Sepharose 6 FF and Q Sepharose FF in their respective TOF-SIMS spectra

| **Prominent positive ion peaks (m/z)** | **Structural assignment** | **Mainly base matrix/ Q ligand associated** | **Prominent positive ion peaks (m/z)** | **Structural assignment** | **Mainly base matrix/ Q ligand associated** |
|---|---|---|---|---|---|
| **15.02** | $CH_3$ | Sepharose | **60.09** | $C_3H_{10}N$ | Ligand |
| **27.02** | $C_2H_3$ | Sepharose | **69.03** | $C_4H_5O$ | Sepharose |
| **29** | CHO | Sepharose | **71.01** | $C_3H_3O_2$ | Sepharose |
| **29.04** | $C_2H_5$ | Sepharose | **73.03** | $C_3H_5O_2$ | Sepharose |
| **31.02** | $CH_3O$ | Sepharose | **81.04** | $C_5H_5O$ | Sepharose |
| **39.02** | $C_3H_3$ | Sepharose | **85.03** | $C_4H_5O_2$ | Sepharose |
| **41.04** | $C_3H_5$ | Sepharose | **97.03** | $C_5H_5O_2$ | Sepharose |
| **42.03** | $C_2H_4N$ | Ligand | **100.12** | $C_6H_{14}N$ | Ligand |
| **43.02** | $C_2H_3O$ | Sepharose | **102.09** | $C_5H_{12}NO$ | Ligand |
| **43.06** | $C_3H_7$ | Sepharose | **116.11** | $C_6H_{14}NO$ | Ligand |
| **45.03** | $C_2H_5O$ | Sepharose | **132.1** | $C_6H_{14}NO_2$ | Ligand |
| **53.04** | $C_4H_5$ | Sepharose | **174.15** | $C_9H_{20}NO_2$ | Ligand |
| **55.02** | $C_3H_3O$ | Sepharose | **176.13** | $C_8H_{18}NO_3$ | Ligand |
| **55.06** | $C_4H_7$ | Sepharose | **190.15** | $C_9H_{20}NO_3$ | Ligand |
| **57.04** | $C_3H_5O$ | Sepharose | **206.14** | $C_9H_{20}NO_4$ | Ligand |
| **58.07** | $C_3H_8N$ | Ligand | **234.17** | $C1_1H_{24}NO_4$ | Ligand |
| **59.07** | $C_3H_9N$ | Ligand | | | |

The fingerprint pattern of the positive ion spectrum of Q Sepharose FF is hence expected to be similar to its backbone matrix structure Sepharose 6 FF, with additional ligand specific peaks characterizing the spectrum. Most of the peaks associated with the Q ligand ($CH_2N(CH_3)_2$) occur due to their size at higher m/z values (Table 3-5). All ligand associated peaks bear nitrogen atoms, although it is evident that $CH_2$ and $CH_3$ fragments of the ligand also contribute to the spectra, which are unfortunately overlapping with peaks recorded for the Sepharose backbone.

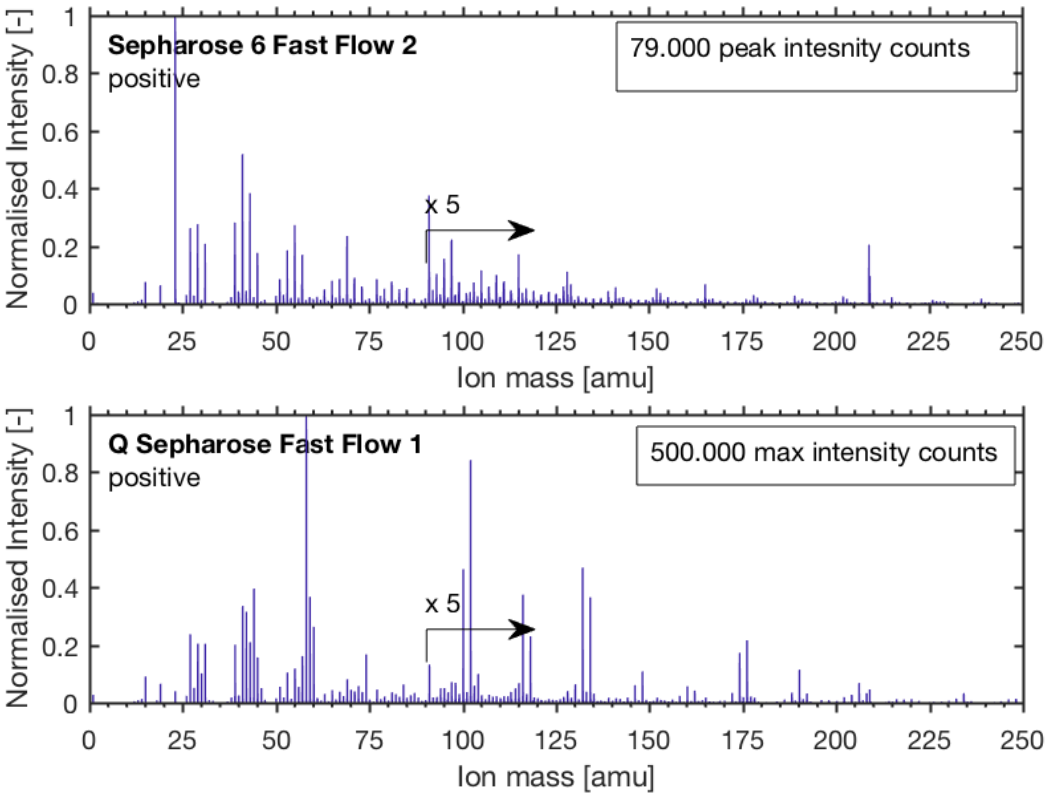


Figure 3-45 Positive ion spectra of Sepharose 6 FF (top) and Q Sepharose FF (bottom)

The ToF-SIMS spectrum of Q Sepharose FF is dominated by peaks associated to the Q ligand, although the ligand density is reported to only be around 0.21 mmol/mL medium ((GE Healthcare Bio-Science, 2014); Figure 3-45 ). Two different explanations could be responsible for this effect- the ligand density is higher on the surface than on the inside of the bulk media, the other is that ligand specific groups break more easily under the influence of the ion beam than the cross-linked Sepharose backbone.

Confocal microscopic images recorded of Q Sepharose FF (Figure 3-36), as well as previous studies however confirm that the ligand is homogenously distributed across the beads (Johansson *et al.*, 2004).

The highest peak of the spectrum is the first ligand associated fragment at 58.07 m/z ($C_3H_8N$). It dominates the spectrum with the following second peak being 40% of the height of the ligand molecule. This being the quaternary amine fragment suggests that the C-C bonds are harder to break than the C-N bonds by the beam, which is expected given the stability of the resulting fragments.

Both Sepharose 6 FF and Q Sepharose FF have very characteristic 'fingerprint spectra' of respective ToF-SIMS peaks (Figure 3-45 ) with the Sepharose 6 FF 'fingerprint' depicting a surface of a media exclusively made of agarose, while the Q Sepharose FF 'fingerprint' illustrates the impact of the presence of Q ligands has on the spectrum. To evaluate the effect of cold atmospheric pressure plasma treatments on the external (chemical) surface composition of Q Sepharose FF chromatography supports, their recorded positive ToF-SIMS spectra (Figure 3-37) were compared to fingerprint spectra of untreated control media (Figure 3-38).

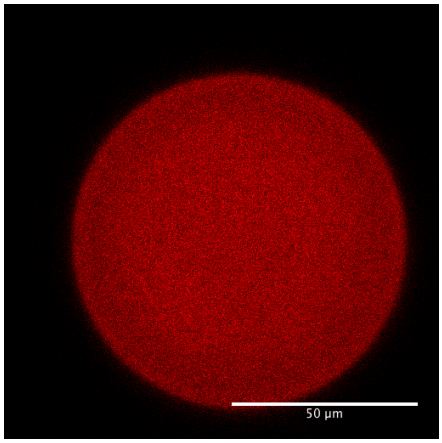


Figure 3-36 CLSM image of Q Sepharose FF with Cy5 tagged BSA

To assess the impact, plasma treatments have on the ToF-SIMS spectra of Q Sepharose FF supports, two different conditions- He- $O_2$ admixed (99.5%- 0.5%) gas plasma (20 V; 150 s; 12.5% SBV) and pure oxygen gas plasma treated (15 V; 150 s; 18.75% SBV) samples were analysed.

Both samples showed reductions of surface (66.3% and 44.2% reduction of pDNA binding capacity, respectively) as well as core binding capacity (0% and 24% loss of BSA binding capacity, respectively) in static binding studies (Olszewski *et al.*, 2013).

Comparing the first recorded spectrum of helium plasma treated supports to the fingerprint spectrum of the untreated Q Sepharose FF, it is apparent that different peaks dominate the spectrum.

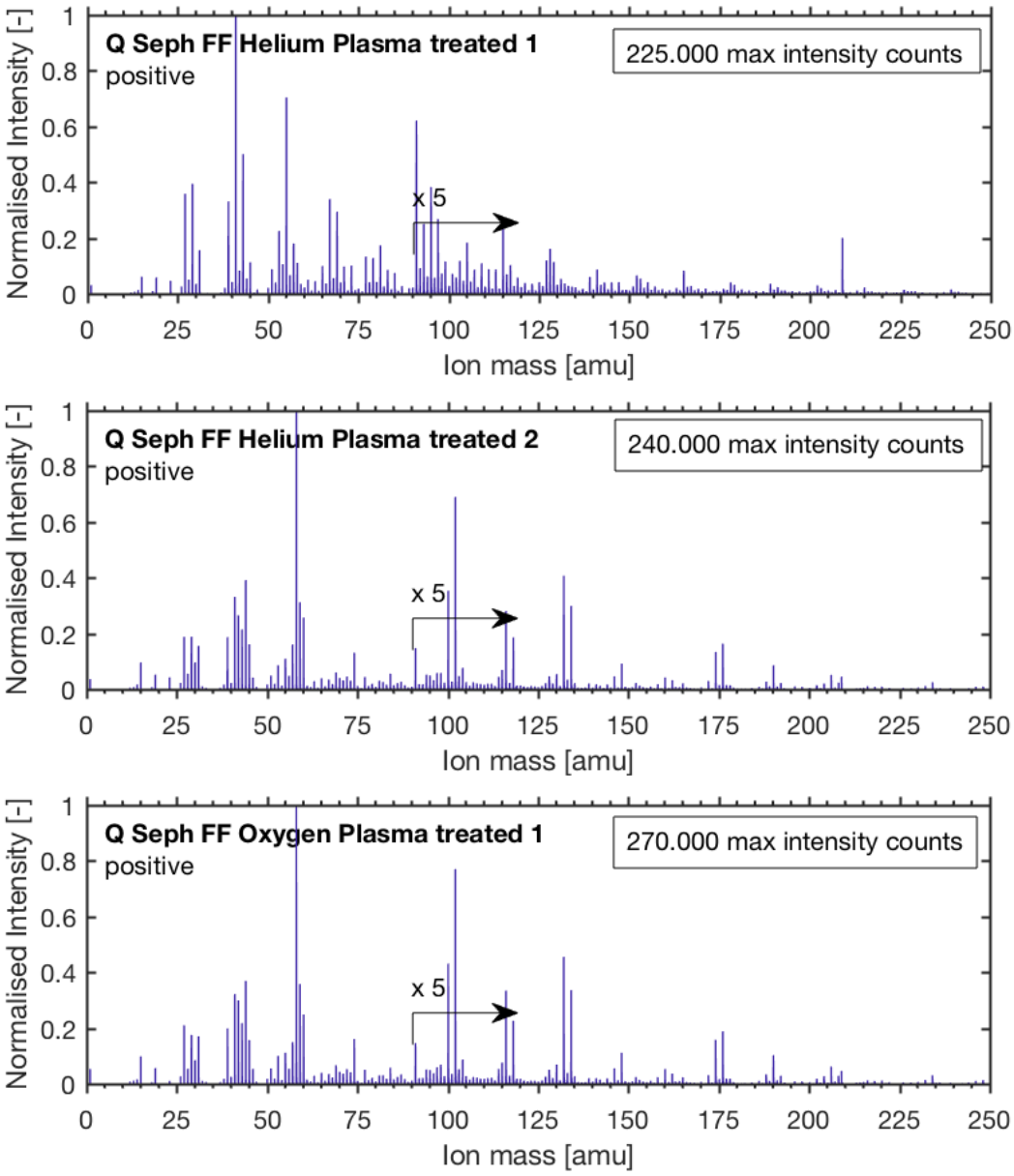


Figure 3-37 Positive ion spectrum of Q Sepharose FF supports treated with helium-oxygen gas (99.5- 0.5%) plasma (20 V; 150 s; 12.5% SBV; top and centre) and pure oxygen gas plasma (15 V; 150 s; 18.75% SBV; bottom)

The main ligand associated peak at 58.07 ($C_3H_8N^+$) is still visible in the spectrum, but a lot smaller in comparison to the untreated equivalent. Although ToF-SIMS intensity counts are not directly transferable across samples, comparing the absolute intensity counts reveals that the peak height has been reduced by 95% (from 500k counts to only 25k counts).

All Q ligand associated peaks have been significantly reduced and none of them exceed 10% of the maximum peak intensity of the spectrum.

In contrast to the reduction of Q ligands on the surface, the peaks have shifted to Sepharose backbone associated peaks now dominating the spectrum. Post helium plasma treatment, the ToF-SIMS spectrum is very similar to Sepharose 6 FF with only a residual presence of Q ligands (Figure 3-38).

The helium-oxygen plasma treatment of the supports has not only etched away a significant portion of the surface of the chromatography matrix but it has done so in a selective way; ToF-SIMS as a method of analysis cannot predict whether the agarose backbone structure of the media has been interacted with by the plasma, but it is evident that the reaction is heavily selective, etching away the Q ligands off the surface over the backbone agarose structure.

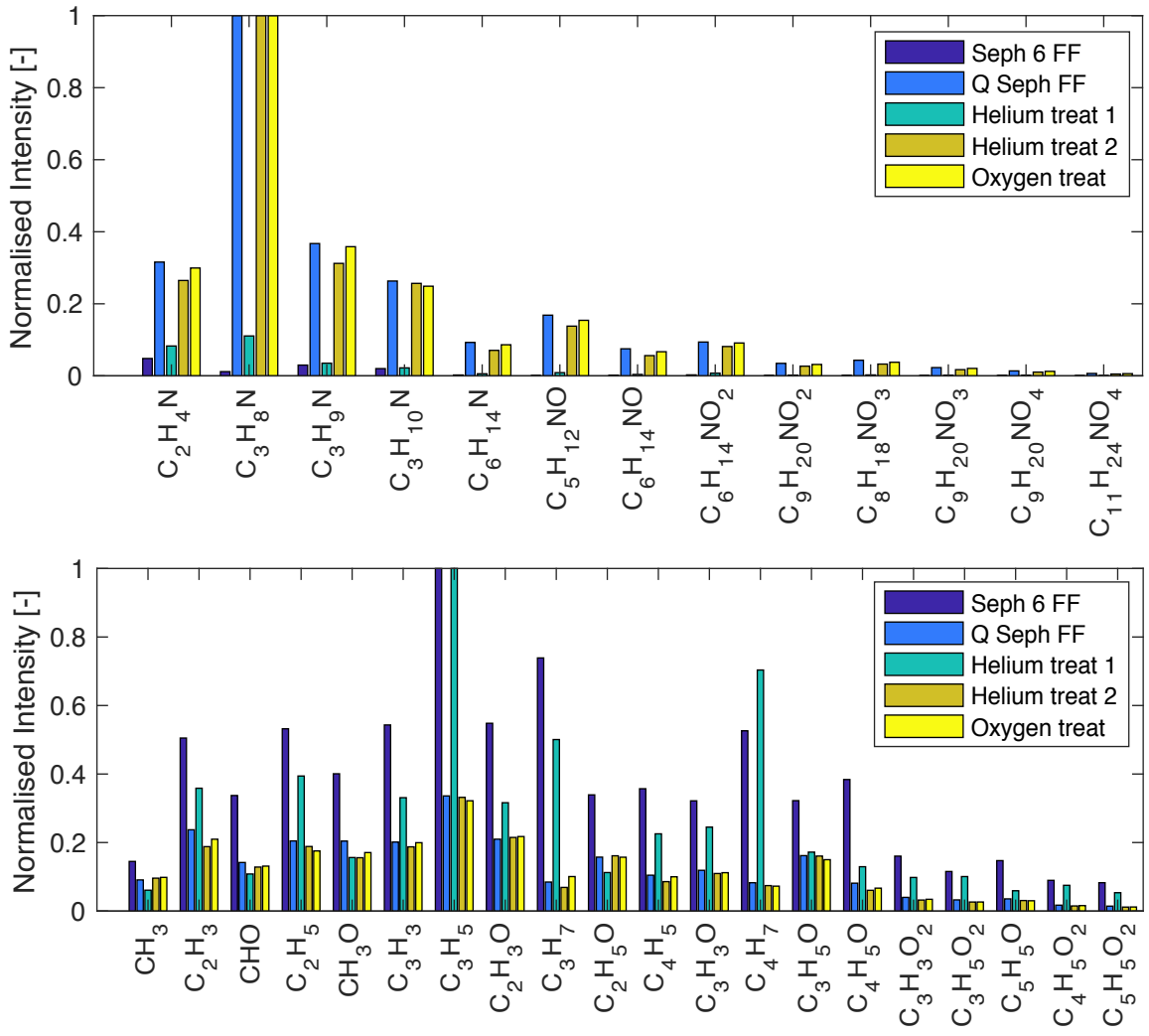


Figure 3-38 Top: Q-ligand associated positive ToF-SIMS peaks for different analysed media normalised to their respective maximum peak
Bottom: Sepharose backbone associated positive ToF-SIMS peaks for different analysed media normalised to their respective maximum peak

The duplicate of the helium plasma treated sample spectrum shows a reduction of the main ligand peak of 52% (from 500k counts to 240k counts), however, without adopting the fingerprint pattern of Sepharose 6 FF, suggesting that although the majority of Q ligands have been etched away during the plasma treatment, the residual few still have an impact on the ToF-SIMS spectrum (ligand concentration 0.21 mmol/mL).

It is evident that some areas have been almost entirely cleared of ligands, with others, despite the overall effectiveness of the plasma in eliminating surface charges, some 'binding islands' remain. These islands (although minor) may have an impact on the ToF-SIMS analysis due to the small area of analysis (lateral resolution/ probe size ~0.2 μm; 20x20 μm analysis area)- if the window of analysis hits one of these islands, lesser etched areas will bear a strong resemblance to the Q Sepharose FF spectra, rather than Sepharose 6 FF.

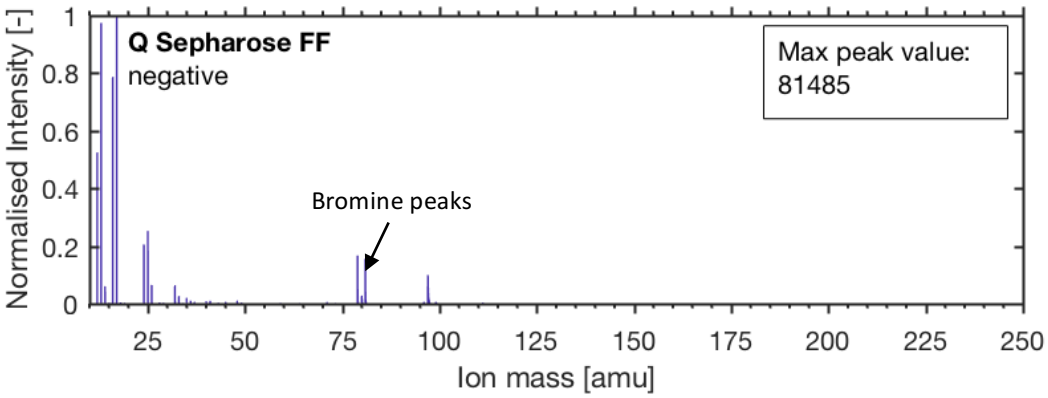


Figure 3-39 Negative ion spectrum of Q Sepharose FF, normalised to its maximum peak

Spectrum of oxygen gas plasma treated sample resembles the 'fingerprint' pattern of Q Sepharose FF. Similarly, to the second helium gas plasma spectrum, all ligand associated peaks have been reduced in comparison to the untreated control sample, while maintaining its characteristic peaks. As static binding studies suggest, the core damage inflicted by oxygen gas plasma is more severe than observed in the helium gas plasma samples (illustrated by the BSA binding capacity reduction). As etching takes place in the subsurface region (damage to the core) it is not surprising that the ToF-SIMS spectrum is less affected by the treatment than its helium gas plasma equivalent, given the small penetration depth of the technique.

To avoid false positives, derived from a single spectrum, the helium plasma treated sample was reanalysed focussing on different particles of the same batch. Due to the occurrence of

small ‘undertreated’ regions observed at 20x20 µm, the spectra were recorded focussing on larger analysis areas (50 x 50 µm and 100 x 100 µm respectively).

Positive ToF-SIMS spectra can be found in Appendix A-4; with summaries of agarose and Q ligand associated peaks depicted in Figure 3-50 and Figure 3-51 respectively.

As observed previously in the 20 x 20 µm analysis area, the base matrix associated peaks dominate the spectra of both plasma treated samples with the ligand associated peaks still being present but having been diminished significantly in comparison to the untreated control sample.

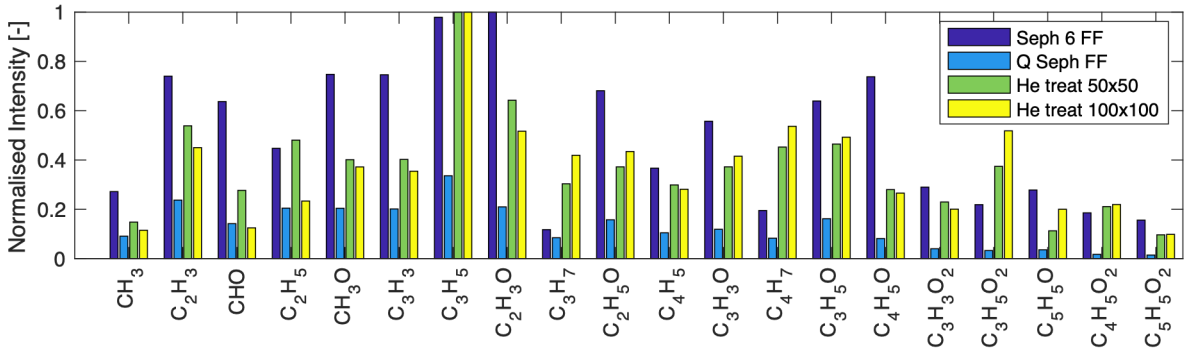


Figure 3-50 Agarose associated positive ToF-SIMS peaks of helium plasma treated Q Sepharose FF chromatography supports with analysis areas of 50 x 50 µm and 100 x 100 µm, as well as Sepharose 6 FF and (untreated) Q Sepharose FF all normalised to their respective maximum peak

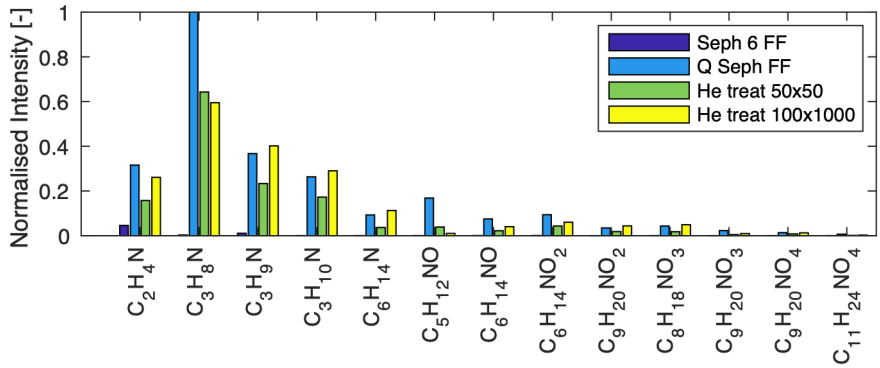


Figure 3-51 Q ligand associated positive ToF-SIMS peaks of helium plasma treated Q Sepharose FF chromatography supports with analysis areas of 50 x 50 µm and 100 x 100 µm, as well as Sepharose 6 FF and (untreated) Q Sepharose FF all normalised to their respective maximum peak

The negative ion spectra for all analysed media contain far fewer characteristic peaks due to the AEC nature of the Q ligand. One decisive difference in the analysed spectra of Q Sepharose FF (as well as its plasma treated samples) in comparison to the underivatised Sepharose 6 FF was the presence of two bromine associated peaks $^{79}Br^-$ and $^{81}Br^-$ around 80 m/z. The remaining presence of Bromine atoms on the surface of the supports are thought to be 'left-overs' from the coupling process with which the ligands are coupled onto the agarose matrix via bromination of allyl groups.

In general, the negative ion spectra are expected to provide more information for cation exchange supports and have hence not been investigated further in this study. The respective spectra of the plasma treated samples, Sepharose 6 FF as well as the carbon tape can be found in Appendix A-4.

## 3.4. Conclusions and suggested future work

The work presented in this study has shown that cold atmospheric pressure plasma can be employed to selectively modify the exteriors of chromatography supports, generating bilayered SEC-IEC materials with reduced surface pDNA binding. Although plasma technologies are normally known to act at the nanoscale, the presented results suggest that the effective penetration depth can run to several microns when applied to porous chromatography materials.

Cold atmospheric pressure plasma treatment under helium gas in a DBD configuration yielded selectivity indices of up to 3.0, corresponding to 75% loss of pDNA binding capacity with just 25% loss of BSA binding. Selectivity indices (up to 2.5) seen for Q Hyper Z in the DBD configuration compare favourably to results seen in previous studies with low temperature low pressure plasma treatments (Arpanaei *et al.*, 2010) (selectivity indices up to 2.0). The formation of plasma streamers, observed during DBD operation, could lead to issues from inconsistent treatment and localised support damage when operating at larger scale, a problem that can be avoided by the use of fluidised bed plasma treatment using He-$O_2$ bubbles.

Fluidised bed plasma treatment was shown to be suitable for treating soft hydrogel materials such as Q Sepharose FF and DEAE Sepharose FF to produce SEC-IEC supports with high selectivity indices (up to 3.0, corresponding to 66% loss of pDNA binding in exchange for 0% loss of BSA binding). These results compare well with methods used for 'bottom-up' synthesis of SEC-IEC materials based on Sepharose CL-6B seen in the literature (Bergstrom, 1997; Gustavsson *et al.*, 2004). 'Bottom-up' methods have been shown to produce slightly superior selectivity indices (up to 3.5) (Karnchanasri, 2012). The used technique does, however, require a far more costly multi-step synthesis contrasting with the simplicity and efficiency of cold atmospheric pressure plasma treatments used in this work.

ESEM images of plasma treated supports yielded that, unlike previously reported (Olszewski *et al.*, 2013), cold atmospheric plasma treatment is a gentle method, that does not alter the visual appearance of chromatographic supports during treatment.

A CLSM method has been developed to simultaneously visualise the binding topography of chromatography media in regard to pDNA and protein binding. Application of the method to

plasma etched supports revealed imperfect chromatography beads within the total sample population in agarose based media. The unsmooth fissures/ crevices on particle surfaces hinder the elimination of ligands within said imperfections, due to the short-lived nature of ROS. Quantitative light microscopic analysis of various batches of agarose based chromatography media suggest that imperfect supports account for the majority of residual binding.

ToF-SIMS analysis of plasma treated Q Sepharose FF media confirmed that the presence of residual pDNA binding is limited to binding islands with residual Q ligands. The chemical composition on the smooth surface of supports resembles the one of pure agarose, confirming that the plasma reaction selectively etches the ligands over the stationary backbone structure.

Underwater plasma treatment offers real promise for converting mono-functional chromatography supports into multifunctional varieties, such as the bilayered SEC-IEC materials described in this chapter. The recorded selectivity indices of 3.0 are: (i) higher than those delivered previously by low temperature low pressure plasma modification and RDB. Additional advantages of creating bilayers by cold plasma modification, rather than by RDB or lamination (Jahanshahi *et al.*, 2008) approaches, include its comparative simplicity, meagre energy requirements and potential use as a generic 'add on' treatment. The supplementation of established manufacturing processes for beaded chromatography materials with a cold atmospheric pressure plasma modification stage, could allow these materials to be converted into layered varieties through addition of a single cost-effective step.

The success of cold atmospheric plasma treatment for creating SEC-IEC chromatography supports indicates a need for further research in this area. It is also likely that larger-scale plasma treatment using an adapted fluidised bed set-up would allow estimates of costs of fluidised bed plasma operation at an industrial scale. Finally, in order to establish the competitiveness of these cold atmospheric plasma treatments, the performance of the media in static and dynamic binding studies needs to be compared to those of commercially available materials to identify the relative strengths and weaknesses of plasma treatment.

# Chapter 4 SEC-AEC bilayered chromatography media manufactured via Viscosity Enhanced Reaction Diffusion Balancing- analysis and limitations

## Abstract

Bilayered chromatography supports were manufactured in a bottom-up approach via AGE activation-partial bromination of Sepharose CL-6B. Viscosity enhanced, reaction diffusion balancing through sucrose addition to control viscosity was applied to control thickness and homogeneity of the ligand free size-exclusion layer.

A CLSM method was developed to screen the binding topography of prepared supports by investigating simultaneous binding of fluorescently tagged pDNA and BSA.

CLSM and light microscopy was applied to confirm the integrity of the manufactured media, while addressing the limitations of the technique with regards to the reduction of pDNA binding capacity in comparison to unmodified control media. It was found that the quality of the final product is strongly dependent on the starting SEC chromatography media, with flawed support beads binding pDNA after modification. These imperfections at the surface of the supports act as diffusion barriers during the partial bromination step, preventing the formation of a ligand-free zone within crevices/ grooves and account for the majority of pDNA binding to the supports after bilayer creation.

## 4.1. Introduction

Interest in DNA vaccines has led to an explosive increase of related patents from less than 20 p.a. in 1996 to close to 100 in the 2010s (Ghanem *et al.*, 2013). DNA vaccination uses DNA molecules of pathogens to induce immunity against specific diseases by providing genes that encode for target proteins and invoke both a cellular immune as well as a humoral (antibody mediated immunity) response (Wolff *et al.*, 1990). Plasmid DNA vaccine production offers quick development and manufacturing, as the production process does not rely on time-/ labour consuming means such as chicken eggs or cell cultures, but can easily be fermented in bacteria (Ghanem *et al.*, 2013). Furthermore, the stability of pDNA vaccine formulations eases transport and storage restrictions, encountered in traditional vaccines (Manoj *et al.*, 2004). Gene therapy uses genes as treatment for genetic defects and acquired diseases such as cancer and viral diseases (Abdulrahman *et al.*, 2018).

Many clinical trials involving gene therapy and DNA vaccination are showing promising efficacies, however safety concerns mainly regarding their delivery systems have hampered approval of therapeutic products for human applications (Sousa *et al.*, 2010b).

These safety concerns led to the rediscovery and focus of research on non-viral vector designs such as naked pDNA. Other means of application such as viral vectors exist and are still commonly used in clinical trials but pDNA is considered safer and expected to be easier produced on a large scale at reasonable cost (Ginn *et al.*, 2013). However, low transfection efficiencies of plasmid-based vectors do make large dosages mandatory (Ferreira *et al.*, 2000b), raising the need for large quantities of highly pure pDNA formulations and subsequently production facilities to meet the demand for cost-effective production and purification.

Among the different forms of pDNA, the sc isoform is the most desirable for pharmaceutical applications due to its antigenicity and stability (Sousa *et al.*, 2012).

Of the several available downstream processing techniques, beaded liquid chromatography is still the go-to method for nanoplex purification (Xenopoulos *et al.*, 2014). On a laboratory scale, purification of pDNA is generally viewed as a simple procedure, especially considering that such production strategies aim for small quantities of pDNA at high quality. Typical upstream processes of pDNA production under such non-optimised conditions yield very low

volumetric titres of 5-40 mg/L (Prather *et al.*, 2003). However, these purification methods do not aim for economic viability and scaling them to industrial production levels leads to very poor yield.

An industrial process, designed for large scale production of pharmaceutical grade pDNA formulations, typically includes several consecutive steps (Figure 4-1).

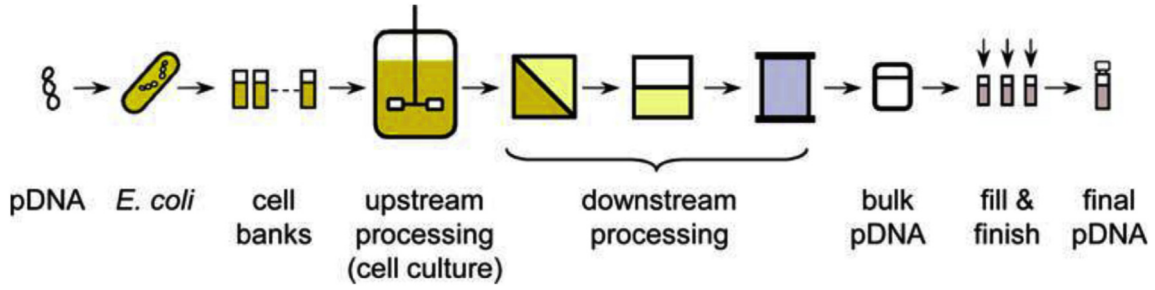


Figure 4-1 Flow chart of an industrial pDNA production process (Prazeres, 2011)

Many burdens are being put on purification steps of pDNA after cell lysis due to similarities of physicochemical properties of the target product and many of its main contaminants such as molecular weight, charge and hydrophobicity (Stadler *et al.*, 2004).

Among the plethora of DSP purification techniques, SEC and IEC are widely applied methods used for pDNA purification (Gustavsson *et al.*, 2004; Xenopoulos *et al.*, 2014).

AEC utilises positively charged ligands mounted onto a stationary phase, taking advantage of negatively charged phosphate backbone groups of DNA. While contaminants may be similar in overall net-charge and molecular weight, the pDNA isoform influences the density of its charge distribution on the surface (Ghanem *et al.*, 2013). These negative charges interact locally with ligands on stationary phases and are consecutively eluted by applying a salt gradient. The charge density is closely related to chain length due to the amount of phosphate groups in the molecule and consequently the sc isoform interacts more strongly with AEC ligands than the oc isoform, eluting at lower salt molarity (Quaak *et al.*, 2009).

Commercial IE chromatographic separation media have been optimised for protein purification, rather than for pDNA applications (Prather *et al.*, 2003). With common pore sizes of beaded supports being smaller than twice the radius of gyration of common sized pDNA molecules (Ellegren *et al.*, 1989), pDNA binding is restricted to the outer surface of support

particles due to steric hindrance (Ljunglof *et al.*, 1999). This inability of pDNA molecules to diffuse into the porous core, and consequent inability to interact with ligands lining the pore walls, leads to low binding capacities. While commercial AEC media bind proteins in the range from 10 to 100 g/$L_{medium}$ and in some cases up to 200 mg/m$L_{medium}$ (Shamlou, 2003), the same columns achieve pDNA binding capacities of merely 0.2 to 2 g/$L_{resin}$ (Prather *et al.*, 2003).

Several research attempts have been undertaken to circumvent these drawbacks by enhancing the low binding. Reducing the radius of gyration of pDNA molecules via addition of compaction agents shrinks pDNA molecules and allows for deeper pore penetration, enhancing pDNA binding capacity by up to 40% (Murphy, 2003).

The use of perfusive media allows pDNA molecules to enter supports via larger perfusion pores, binding to ligands lining the pore walls. Superporous beads increase the available binding area of conventional AEC media by crafting supports containing flow through pores (2-30 μm diameter). These pores allow pDNA to enter the beads via convective flow, with additional binding sites being provided on the pore walls, while at the same time allowing for increased flow velocities due to reduced back pressure (Deshmukh *et al.*, 2005; Tiainen *et al.*, 2007c). Monoliths use a rigid porous stationary phase with convective flow pores lined with adsorptive ligands (Zöchling *et al.*, 2004; Urthaler *et al.*, 2005c; Sousa *et al.*, 2011).

Extension of the externally available surface area was achieved by crafting polymers on the surfaces of adsorbents. In conjuncture with reduction of particle size for EBA applications, these supports were found to enhance pDNA binding capacity 25 to 70 fold. (Theodossiou *et al.*, 2001).

Enhanced binding capacity via size reduction of supports yields to the low capacities of classical supports, accepting the restriction of pDNA binding to the supports surfaces alone. These small beads have however, a larger overall surface area. Issues associated with increased back pressure are partially circumvented by choosing a non-porous stationary phase (Tiainen *et al.*, 2007d). However, enhanced flow velocities cause concern for pDNA degradation as a result of higher shear stresses (Carlson *et al.*, 1995; Levy *et al.*, 1999).

Purity demands of pDNA formulations to be used in pharmaceutical applications raise the need for other purification techniques to be applied such as SEC (Bellot *et al.*, 1993; Ferreira *et al.*, 1999).

SEC aims to separate moieties in solution via size difference (molecular weight) between the target molecule and its contaminants. Due to the nature of the technique, higher column loads lead to reduced resolution as well as a diluted sample. This could be circumvented by larger column diameters, however packing of such columns is challenging and generally avoided.

Each applied unit operation in the purification process does have its own yield and consequently a margin of product loss. With pDNA single step recovery rates beyond 85% being considered economically viable (Abdulrahman *et al.*, 2018), the appeal of combining two unit operations in a single column is a very interesting consideration. Operating the column in negative mode chromatography allows for the product not to bind to the column and elute in the flow through. A technique that allows pDNA to not interact with the stationary phase furthermore reduces product losses caused by irreversible binding and conformational changes due to binding/ elution cycles.

An alternative to classical IEC media, is a multifunctional support type with a non-interactive surface, with the easiest architecture imaginable being a SEC-AEC bilayered support, retaining positive charge properties on the inside of the support, while an inert exterior prevents binding of pDNA to the surface of the beads.

The principle of bilayered separation media with a core-shell design conveys numerous advantages in HPLC applications, like processing speed and resolution (de Faria *et al.*, 2017).

With commercial media of this type becoming more readily available for large scale purification of VLPs, this design also offers attractive possibilities for challenging separations of emerging bionanoparticulate products (plasmids, IgMs, etc.). However, fabrication methods employed for core-shell HPLC packings do not readily lend themselves to soft gels, such as agarose, required for separation of large biological entities.

Gustavsson et al. (2004) created bilayered core-shell adsorbents using the well-known, fast reaction of limited amounts of bromine (reactant) with double bonds, homogeneously distributed throughout the support (Bergstrom, 1997; Berg, 2003; Larsson *et al.*, 2003; Gustavsson *et al.*, 2004). This new 'lid bead' technology has been used in an integrated process for pDNA purification from crude cell lysates as a final polishing step (Kepka *et al.*, 2004). A single process step plasmid yield of 88% suggests however, that not all of the surface was cleared of ligands, especially as remaining pDNA was eluted via salt gradient. The success of

the approach requires balancing of the reaction rate (bromine with AGE) against depth and speed of diffusion into the pores of the supports. Reaction-diffusion balancing is affected by three obvious parameters; temperature, reactant size and viscosity of the bulk phase.

Challenges for the manufacturing of bilayered chromatography media for pDNA purification via the AGE-activation partial bromination route reside in controlling the layer thickness of the applied method in order to accommodate both the elimination of all surface ligands, whilst also keeping the shell as thin as possible to compromise as little as possible on overall binding capacity (30% loss of core binding capacity cf. fully Q functionalized supports in Gustavsson's initial study). Controlling the partial bromination step is hence key to achieve a homogenous, thin shell.

During partial bromination the high reactivity of bromine is of particular importance; low viscosity in the surrounding buffer leads to a 'directional', inhomogeneous bilayer development, as bromine is not given the chance to fully engulf the support (diffusion rate into core > mass transfer 'around' the bead).

However, if the transport of reactant to the surface is delayed too much, bromine is lost prior to reaction with AGE groups due to hydrolysis in water. Bromine reacting with sucrose may play a minor part, but overall the reaction rate with sucrose is slower cf. hydrolysis of bromine.

This chapter aims to study AEC-SEC bilayered chromatography supports, manufactured via the outlined AGE activation-partial bromination VE-RDB approach. In this 'bottom-up' technique, commercially available Sepharose CL-6B SEC media was utilised as a starting material and chemical functionality was built up in the supports via an adapted 5-step protocol (Gustavsson *et al.*, 2004). The impact of different parameters such as viscosity of surrounding buffer solution during partial bromination, degree of bromination and repetitive bromination cycles on the performance of the media in static binding studies with pDNA (surface binding) as well as BSA (core binding) was assessed.

CLSM is a very powerful visualisation/ quantification tool and finds widespread application in chromatographic research (Hubbuch *et al.*, 2008). A CLSM method was developed to screen the binding topography of bilayered supports, allowing simultaneous visualisation of pDNA as well as protein binding to the supports. Applying CLSM yielded insights into the location of residual pDNA binding sites on the beads' surfaces and helped in understanding the limitations of the technique due to single irregular shaped supports, preventing the formation of a distinct demarcation zone.

## 4.2. Materials and Methods

Due to similar methodologies throughout different chapters of this work, several methods are presented in a separate section of this thesis (Chapter 2).

Some of the conducted experiments do however require more explanation in regard to specific parameters, as Chapter 2 only describes their implementation. When further information is essential, it is given in the respective sections to aid readability and understanding of their processes.

Methods describing experiments that are exclusive to this chapter are listed below.

To avoid repetition, a comprehensive list covering all materials and equipment used to perform experiments during the practical implementation of the project is described in Chapter 2.

### 4.2.1. Preparation of SEC-AEC supports via AGE-activation- partial bromination, VE-RDB

AEC-SEC media used in this chapter were manufactured and kindly provided for further analysis by Dr Karnchanasri following an adapted protocol by (Gustavsson *et al.*, 2004).

The five-step process is depicted in Figure 4-2 followed by a more detailed description below.

#### 4.2.1.1. AGE activation

60 mL of Sepharose CL-6B media were washed in MQW, suction dried on a vacuum filter frit and incubated with 24 mL of 50% (wt/v) NaOH containing 0.25 g sodium borohydride and 6.7 g sodium sulphate at 50°C for 1 h (gently stirred). The supports were suction dried to remove excess NaOH from solution and incubated overnight (16 h) with 41 mL AGE in a stirred water bath (40°C; 170 RPM).

To remove chemical residues, supports were washed with MQW, 70% ethanol (ETOH) and MQW prior to storage in 20% ETOH (4°C).

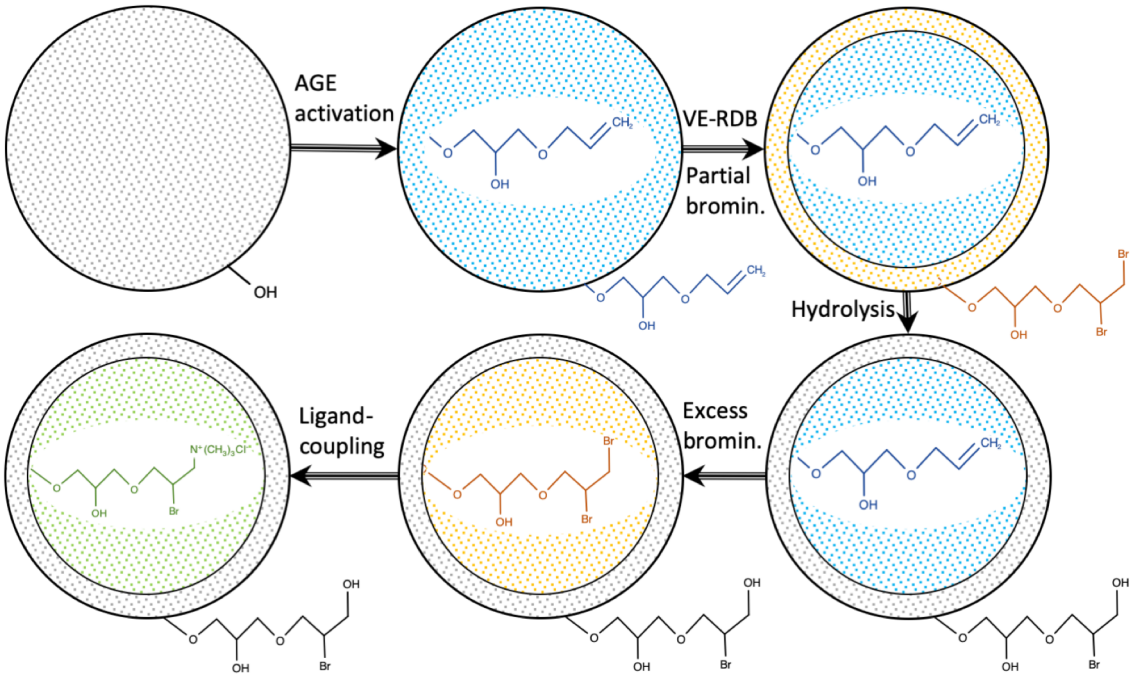


Figure 4-2 Flow chart of the manufacturing process for bilayered AEC-SEC supports applying VE-RDB/ partial bromination prior to ligand coupling; as the reaction of allyl groups with bromine is carried out in aqueous solution the brominated reaction product is likely a mixture of bromoalcohol (bromohydrin) and di-bromo adducts, the precise balance of these is dependent both on the rate of addition and the additives present (Zabicky *et al.*, 1986)

#### 4.2.1.2. Partial bromination/ viscosity measurement of sucrose solutions

Several different concentrations of sucrose in MQW were used as viscosity enhancement reagent (wt/v). After equilibrating 15 mL of supports three times in the respective solution, the media was suction dried and suspended in 12 mL of the respective sucrose solution.

An amount of 1% (v/v) bromine solution in MQW was added based on the aim of targeted AGE elimination levels (10%; 20%; 10%+ 10% of total allyl content). The reaction tube was shaken until the reaction had finished (discoloration of solution) and supports repeatedly washed in MQW.

Prior to suspending support beads in sucrose solutions, the rheological behaviour of the solutions was assessed. An Advanced Rheometer AR1000 (TA Instruments; New Castle; Delaware; USA) equipped with a 2° angle, 40 mm stainless steel cone shaped geometry was used for viscosity measurements. Temperature dependencies of viscosity were measured while applying a temperature ramp of 4° K/min from 2°C to 90°C (shear rate 10 $s^{-1}$).

4.2.1.3. Hydrolysis

1.12 mL of 50% (wt/v) NaOH and 0.04 g $NaBH_4$ were added to a tube containing 10 mL (SBV; suction dried) partially brominated supports in 10 mL MQW and incubated at room temperature overnight on an orbital shaker incubator.

The supports were subsequently suction dried and repeatedly washed in MQW to remove chemical residues.

4.2.1.4. Full bromination and ligand coupling

8 mL (SBV) of supports were rehydrated in 3.48 mL MQW and 0.39 g sodium acetate was dissolved in the slurry. Bromine solution (1% v/v) was added to the suspension until a permanent yellow/orange colour was obtained. The supports were drained and repeatedly washed with MQW before resuspending them in 3.48 mL of MQW. 2.61 mL of 50% NaOH (wt/v) followed by 35 mg $NaBH_4$ were added and mixed before adding 5.07 mL of 65% (wt/v) trimethylamine chloride (Q-ligand). The sample was mixed overnight on a blood tube rotator (21°C). The bilayered AEC-SEC supports were washed with MQW, 1 M NaCl and MQW prior to storage at 4°C in 20% ETOH.

Fully Q-coupled control media was manufactured by skipping the partial bromination and hydrolysis steps, fully brominating the supports immediately after AGE activation.

### 4.2.2. Light microscopic analysis of AEC-SEC supports dyed with Congo red to highlight the SE layer

For visualisation of the SE layer of AEC-SEC supports, 1 mL of supports (SBV) was washed three times in MQW and incubated for 1 h with a saturated aqueous CR solution. Due to their negative charge, CR dye molecules bind to AEC ligands while not interacting with the base matrix of the supports (Figure 4-3).

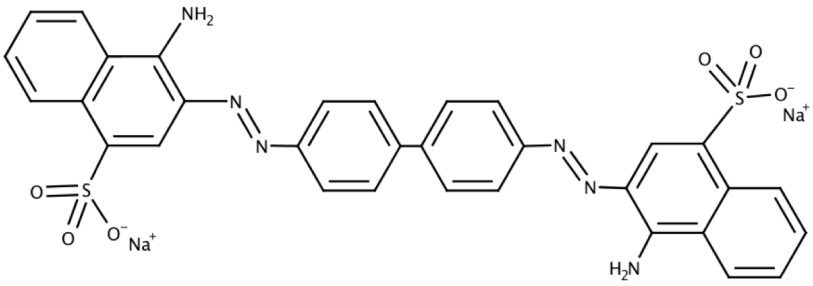


Figure 4-3 Chemical structure of the azo dye CR (skeletal formula)

The supports were centrifuged to assist sedimentation (2,000 g; 10 s), supernatant pipetted out and beads washed three times in MQW to remove unbound CR.

80 µL of chromatography supports slurry in MQW were pipetted onto a microscope slide (VWR VistaVision Microscope Slides, VWR International, UK) and covered with a cover slip (VWR Micro Cover Glasses), carefully avoiding the formation of air bubble inclusions. The sample was then analysed in an Olympus BX50 Light microscope using 4x, 10x, 20x or 40x magnification respectively. For images taken with a 100x magnification, a droplet of immersion oil (Sigma Aldrich) was used to bridge the gap between lens and cover slide.

Images were taken with a Moticam 800x600 PIX, controlled by Motic Images plus 2.0 ML software.

### 4.2.3. Light microscopic analysis and visual grading of chromatography media

Light microscopic analysis of supports was conducted as described in 4.2.2. but without the aforementioned addition of CR (thus the bilayered structures were not highlighted).
Further image analysis was conducted with (Fiji is just) ImageJ (Version 1.0 for Mac).
To grade the visual integrity of chromatography beads, light microscopic images at 10x and 20x magnification were analysed, respectively. With a confidence level of 95%, a confidence interval of 5 and assuming an infinitely large population, a minimum of 384 single beads need to be graded for statistical analysis (Amemiya, 1994):

$$ss = \frac{Z^2 * 0.25}{c^2}$$

With:

ss = sample size

Z = Z-value (1.96 for a confidence interval of 95%)

c = confidence interval in [%]

For each sample, several images were taken to acquire a total particle count of at least 400 supports.
Only whole particles were graded (no supports on the edge of images) and three categories of beads were distinguished:
Particles with no visual imperfections were rated green. Beads with small imperfections on the surfaces (dents, crevices, etc. of approximate depth up to 5 μm), that are shallow enough to be fully integrated into the SE layer after the partial bromination step were rated yellow. Particles with major imperfections that grant core access to larger nanoplexes after creation of the SE layer were rated red.

## 4.3. Results and Discussion

### 4.3.1. Static binding reductions of VE-RDB media

Crafting bilayered SEC-AEC supports following the bottom up approach described by Gustavsson involves a total of five working steps (Gustavsson *et al.*, 2004); (i) introduction of allyl groups throughout the stationary phase of Sepharose CL-6B by reacting AGE with hydroxyl groups on the backbone of the agarose based media; (ii) partial bromination of a targeted amount of allyl groups at the support surface; (iii) hydrolysis of the brominated surface groups to generate an inert outer layer; (iv) excess bromination of residual allyl groups throughout the support (v) coupling trimethylamine (Q) to the core of the media (Figure 4-2). While steps (i) and (iii)-(v) are reactions with surplus reactants aiming for reaction equilibrium, partial bromination involves several non-equilibrium transport phenomena, which have crucial impact on the shape and size of the inert shell.

Dispersion of bromine into the reaction vessel, aiming for immediate mixing; transport of bromine from slurry to bead surface, aiming for swift engulfing to avoid directionality of layer creation prior to; diffusion of bromine into the bead from the surface; reaction of bromine with allyl groups (almost instantaneous).

Meanwhile, further reactions occur simultaneously; hydrolysis of bromine in aqueous solution (Liebhafsky, 1939) and loss of bromine to oxidation of sucrose (Andersson *et al.*, 1980).

Addition of viscosity enhancing reagents (such as sucrose) offers control over the partial bromination by balancing reaction and diffusion rates.

Among other parameters influencing the partial bromination step (reaction temperature, addition of adjuvants, etc.), this study focusses on the degree of partial bromination all at different viscosities adjusted via sucrose addition (0- 80%).

Three sets of bilayered support samples were manufactured, featuring single 10% and 20% of the total allyl content, as well as double 10% partial bromination. Double 10% partial bromination was achieved by following an initial 10% partial bromination with a washing step prior to applying another 10% partial bromination followed by hydrolysis.

Crafted media were analysed for static pDNA and BSA binding capacities, degree of allylation and ionic capacity. SI values were calculated for all three ‘core parameters’ against fully derivatised AEC control media; results are depicted in Figure 4-4.

Both single brominations without sucrose addition, targeting 10 and 20% of allyl groups lead to reductions of all 'core parameters' (ionic capacity, protein adsorption, allyl content) of ~10 and 20% respectively.

While selectivity is very poor at low viscosities (<1.5), with pDNA binding reductions of ~20 and 45% respectively, addition of 50 and 64% sucrose led to targeted reduction of surface binding up to 80%. Sucrose contents exceeding 64% however, led to a decline in pDNA binding reduction in both single 10 and 20% partial bromination.

The results suggest that the viscosity is too high, preventing effective transport of bromine to the surface of the beads. Respectively low reductions of core parameters with increasing sucrose contents, furthermore suggest that, the longer bromine molecules take to get to allyl groups, the longer it is exposed to loss prior to reaction due to bromine hydrolysis/ oxidation of sucrose (Trombotto *et al.*, 2004).

While it is beneficial to allow bromine solution to engulf supports before diffusing into the shell/ reacting with allyl groups to avoid directionality of layer creation, enhancing buffer viscosity too much reduces the amount of bromine available for reaction (Figure 4-5).

Without addition of sucrose to the supports slurry, reduction of 'core parameters' indicate that double partial bromination of 10% led to reductions of ~30% of allyl groups. Higher reduction levels than the targeted 10+10% were associated to difficulties in pipetting very small sample volumes and immediate mixing of bromine. The resulting preparation can however be taken as a 30% partial bromination via repetitive incremental reaction.

Consistently high pDNA binding reductions >70% were found for all VE-RDB double 10% bromination samples, with a decline in reduction of core binding capacity at increasing viscosities, similar to the trends observed in single bromination samples.

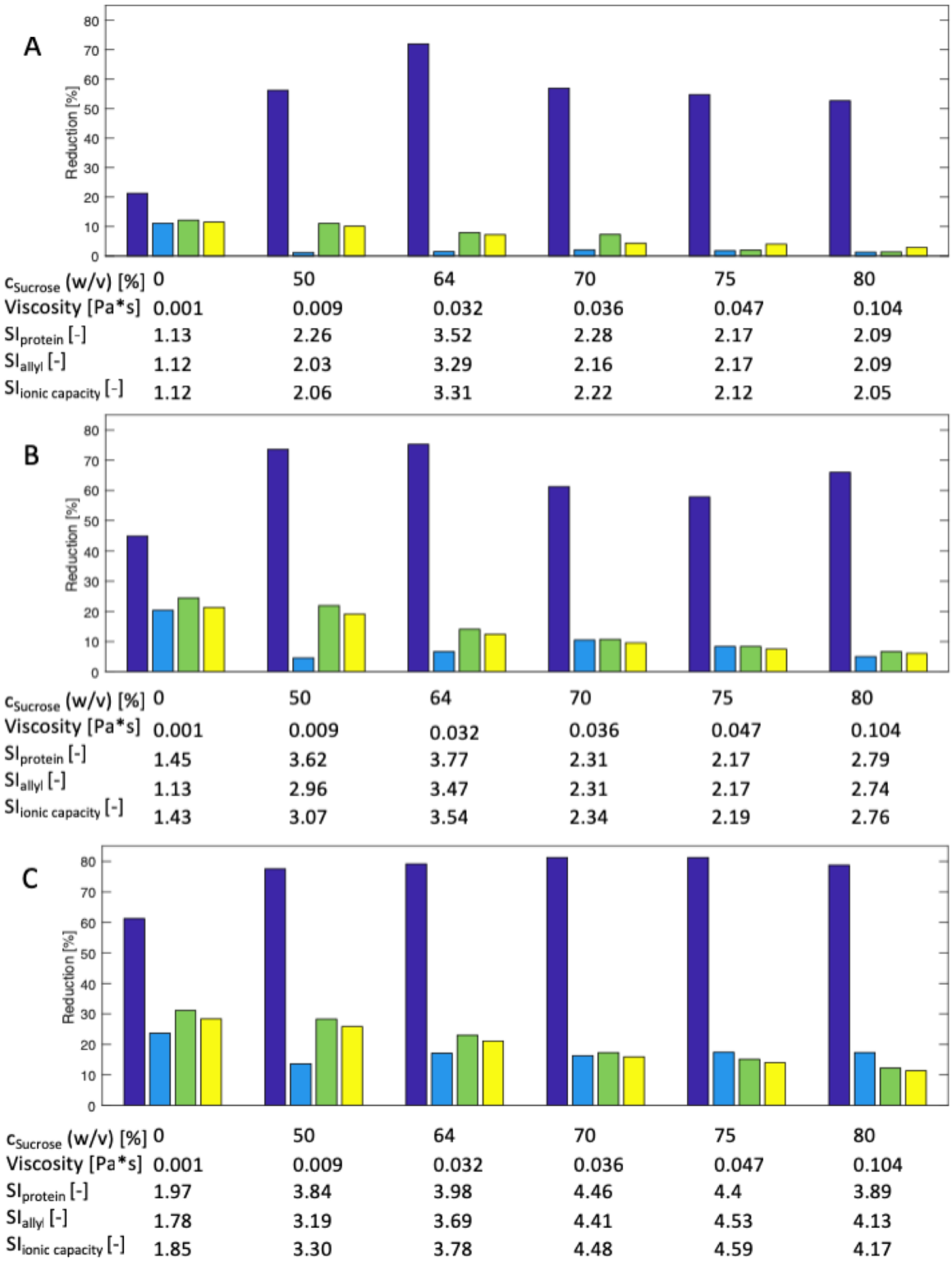


Figure 4-4 Characteristics of SEC/ IEC supports produced via; A) single 10%, B) single 20% and C) double 10+10% partial bromination/ hydrolysis cycle at room temperature (21°C) without further additives; reductions of static pDNA- (purple)/ protein binding capacity (blue), allyl content (green) and ionic capacity (yellow) to fully derivatised AEC control media

The highest SI values (>4) were recorded for double 10% bromination with sucrose contents of 64% and above. However, these are subject to bromine loss in solution as no additional pDNA binding reduction occurs while reduced core reduction levels elevate the SI.

Irrespective of the sucrose content or degree of partial bromination, no preparation was able to eliminate pDNA binding entirely. It appears that a base level of residual pDNA binding of around 20%, unaffected by the bilayer creation at the surface cannot be overcome by additional bromination and is independent of viscosity enhancing reagents. This effect cannot be explained by means of static binding capacity reductions alone.

To evaluate the effect of residual pDNA binding (on the surface?), the supports were investigated further using visualization techniques (light microscopy and CLSM respectively).

Avoiding samples with enhanced bromine loss due to hydrolysis/ sucrose oxidation, while providing significant selectivity, the three configurations featuring 64% sucrose addition were selected for investigation.

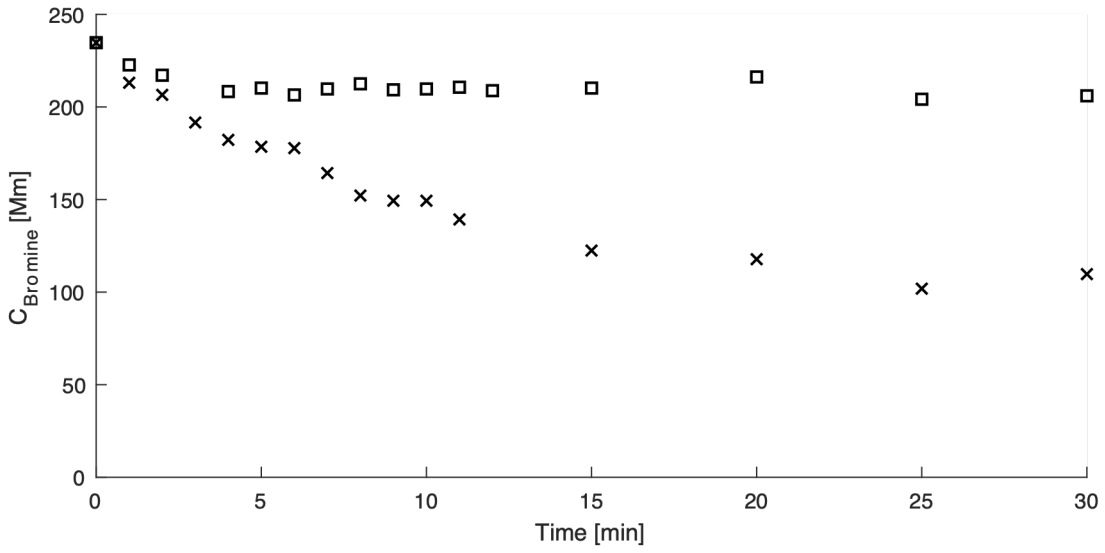


Figure 4-5 Bromine stability in aqueous solutions at room temperature; in water (x); 80% sucrose (w/v; □)

### 4.3.2. Light microscopic visualisation of restricted access media's architecture manufactured via VE-RDB during partial bromination

Restricted access media as manufactured and previously described by (Karnchanasri, 2012) call for validation through visualisation of the supports' architecture. Figure 4-6 (top) shows a micrograph of Sepharose CL-6B supports provided with a SE layer manufactured via 10% bromination (64% (wt/v) sucrose; 0.032 Pa·s). The supports' positively charged core was stained with negatively charged dye, CR, and imaged as described in 4.2.2. .

While the dye bound to the core of the supports, staining it in a strong orange/ red colour, the non-charged outer layer of the supports appears entirely uncoloured. This demarcation zone between the outer layer and the core of the supports is very distinct with a sharp interface. Fully Q-coupled Sepharose CL-6B (Figure 4-6 , bottom) did, as expected, not show a demarcation zone, with the dye's orange colour being homogenously spread across the entire bead. This leads to the conclusion that ligands are evenly distributed across the base matrix.

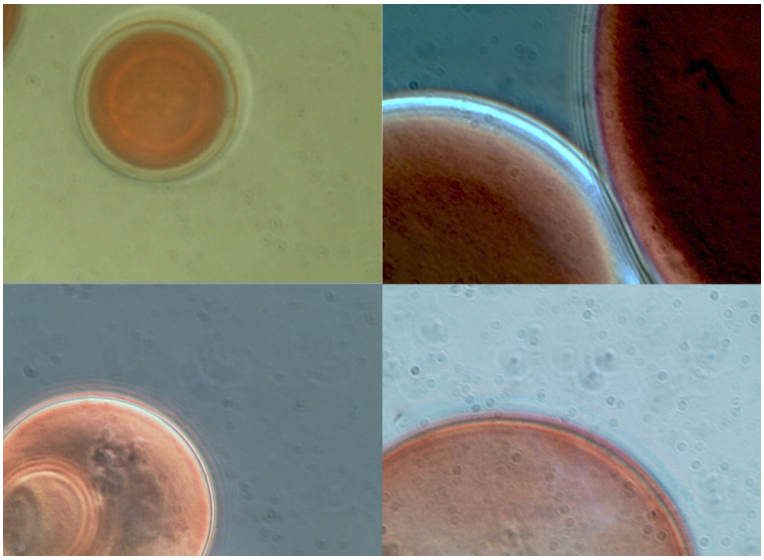

Figure 4-6 Light micrographs of Sepharose CL-6B based restricted access media (dyed with CR), with a distinct demarcation zone (top) and homogenous supports (bottom) both at 40x (left) and 100x magnification (right) respectively; difference in (background) colouring due to diffraction effect

Although visually compelling, light microscopic imaging does not possess the resolution to pick up on minor traces of 'left over' ligands that may have withstood the partial bromination step. Furthermore, due to the nature of this technique, light micrographs are unable to provide 3D insights of structures and are limited to a projective examination.

CLSM has proven to be a suitable tool addressing both of these limitations, providing 3D stack analyses as well as picking up charge traces in chromatography media (Hubbuch *et al.*, 2002). It was however reported that small remnants of ligand in the shell would not lead to significant pDNA adsorption (Gustavsson *et al.*, 2004).

### 4.3.3. CLSM analysis of VE-RDB manufactured AEC-SEC supports

Light micrographs of AEC-SEC supports showed a non-adsorptive layer surrounding a charged core after incubating supports with CR.

CLSM has been employed as a tool for visualisation, to get a more refined insight in the charge distribution within bilayered supports. To assess the location of residual pDNA binding sites, support samples were incubated with fluorescently tagged pDNA solution. To simultaneously also get access to core binding data, the supports were subsequently incubated with tagged BSA solution (binding throughout all binding sites of the bead) before analysing the samples as described in 2.3.12.

As control without a non-adsorptive exterior, Sepharose CL-6B SEC media was conjugated with the strong anion-exchange ligand Q via AGE-activation, directly followed by excess bromination and ligand coupling.

CLSM images of control supports show a bright green halo (SYTO-9 fluorescently tagged pDNA) surrounding a red core (Cy5 labelled BSA). The pDNA is too large (26.88 kbp) to penetrate through the outer micrometres of the porous bead and bind to ligands, lining internal pores of the supports. Binding is hence limited to the surface of the supports. BSA is small enough (66.5 kDa) to diffuse into the interior and bind throughout the particle (Figure 4-7).

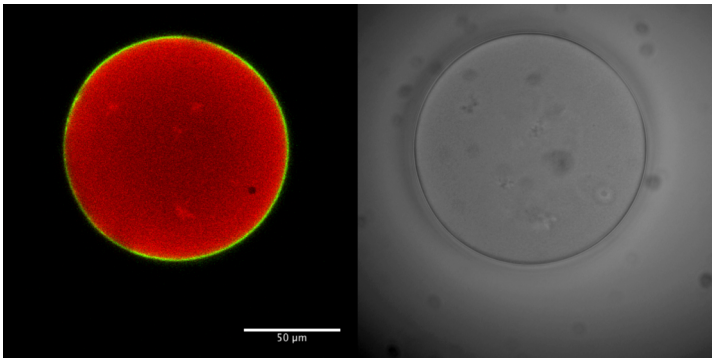


Figure 4-7 Left: Overlay of CLSM channels (red- fluorescently tagged BSA; green- pDNA) analysing IEC support manufactured via AGE activation, full bromination/ trimethylamine chloride (Q) coupling (control sample without SE layer)
Right: Respective light microscopic image

In order to compromise the least on overall binding capacity, the ligand free layer of AEC-SEC media would ideally be as thin as possible, while still preventing binding to the surface of the supports. CLSM coupled with light microscopic imaging was employed to investigate the architecture of bilayered supports manufactured via 10% partial bromination. After incubating support samples with both fluorescently labelled BSA (exemplifying core binding; depicted in red) and SYTO-9 tagged pDNA solutions (binding to residual ligands on the supports surfaces; green), the sample was analysed focussing on meridians of single support particles.

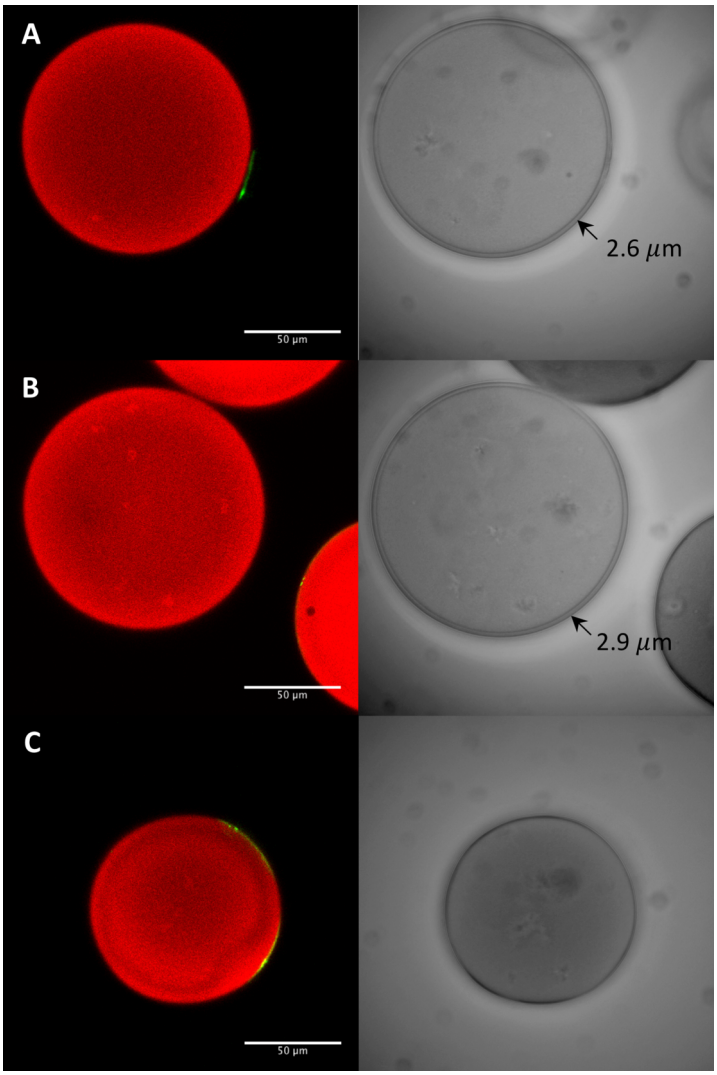


Figure 4-8 Left: Overlay of CLSM channels (red- fluorescently tagged BSA; green- pDNA) analysing SEC/ IEC supports manufactured via single 10% partial bromination/ hydrolysis cycle at room temperature (21°C); sucrose content of 64% w/v (0.032 Pa·s)
Right: respective light microscopic images with shell thicknesses of SE layer in μm

Figure 4-8 confirms a very thin ligand-free layer of around 2.5-3 μm (15.4% predicted loss of binding capacity- based on volume weighted mean D[4.3]= 110.81 μm (Figure 4-9)). The demarcation zone surrounding the core is of homogenous thickness.

Sucrose slows down the diffusion of bromine into the core and hence condenses the charge elimination to a small area. This leads to a sharp cut-off between the non-interactive stationary phase cleared of ligands and the charged core.

While providing a desirable distinct shell, sucrose also slows down the overall mass transport of bromine to the reaction sites at the supports. Delaying the reaction of bromine with AGE groups of the supports allows more time for bromine hydrolysis in the surrounding buffer. Whilst addition of sucrose reduces the rate of bromine hydrolysis in aqueous solutions (Joseph, 2018- in preparation), the effect is outweighed by a slower rate of bromine mass transfer from the bulk solution to the supports. This reduces the overall amount of bromine being accessible for reaction, explaining why less allyl groups are removed than expected. Assessing the amount of allylation after a targeted 10% bromination yielded reductions of only 8% of the allyl groups (Figure 4-4).

While support B is totally inert to pDNA binding on its surface, the 10% partial bromination was insufficient to clear all ligands on the surface of supports A and C. The cleared zone surrounding the core of bead C appears too thin, allowing pDNA binding to occur, raising the demand for an overall thicker SE layer to avoid under treatment of single supports.

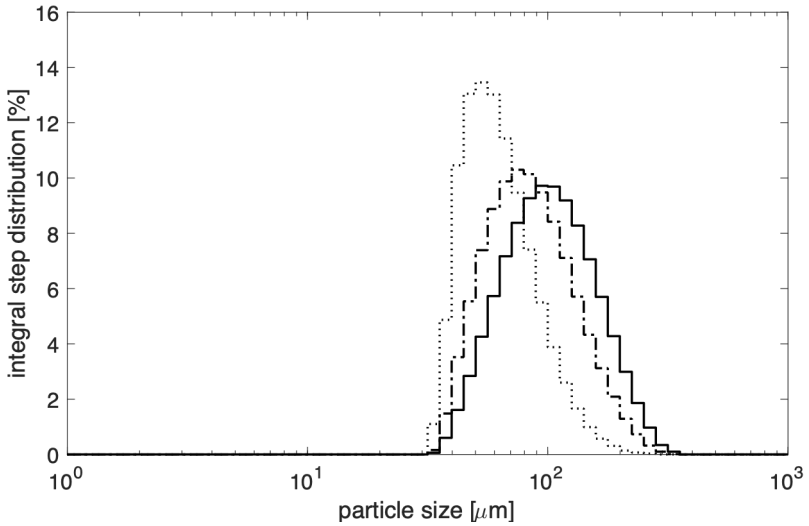


Figure 4-9 Particle size distributions of Sepharose CL-6B based AEC-SEC supports modified by 10% partial bromination at room temperature in 64% (w/v) sucrose (0.032 Pa·s viscosity); solid line- volumetric; dash-dotted line- surface weighted; dotted line- number weighted distribution

Increasing the level of partial bromination to 20% should thwart the occurrence of residual binding isles.

As expected, the increase in the amount of bromine led to a formation of a thicker non-adsorptive layer. Figure 4-10 illustrates, that with increased layer thickness, the likelihood of residual surface charge is indeed diminished. Only the third support (C) shows a small island of residual pDNA binding, whereas the others are entirely devoid of surface binding.

The layer preventing pDNA adsorption is however, not as homogenous as observed in the 10% single bromination media. The direction of the flux- pathway of bromination is clearly visible.

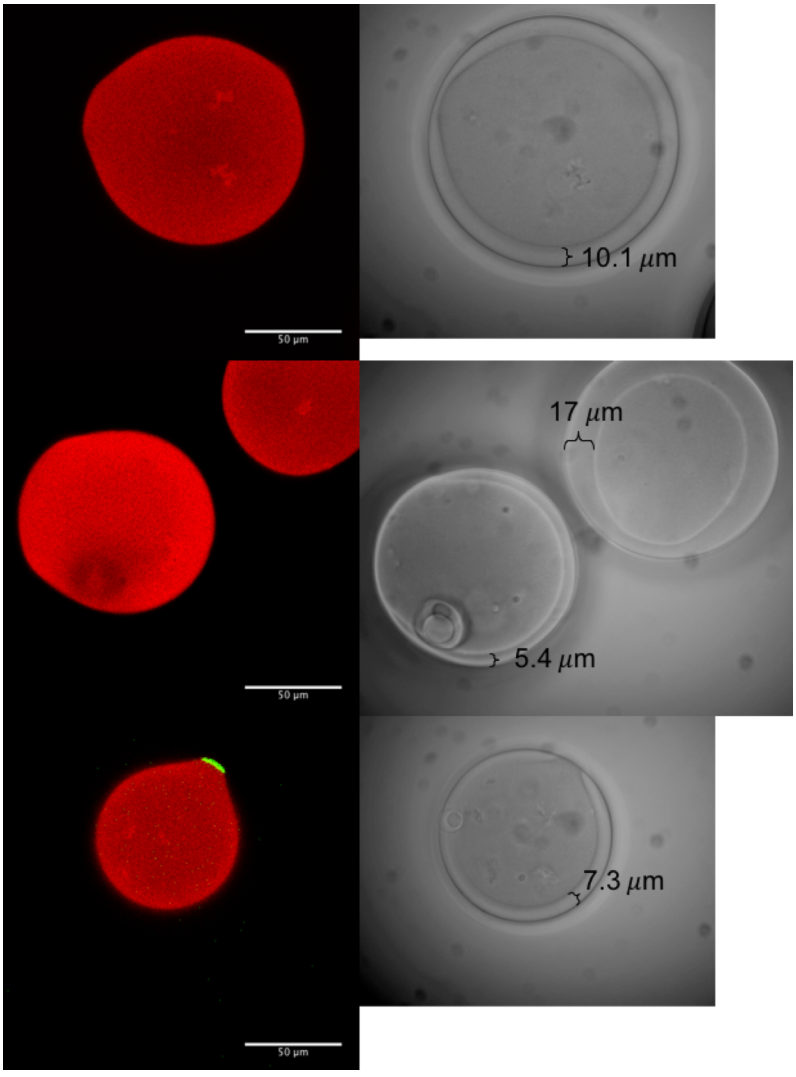


Figure 4-10 Left: Overlay of CLSM channels (red- fluorescently tagged BSA; green- pDNA) analysing SEC/ IEC supports manufactured via single 20% partial bromination/ hydrolysis cycle at room temperature (21°C); with a sucrose content of 64% w/v (0.032 Pa·s)
Right: Respective light microscopic image with shell thickness of SE layer in µm

While the SE layer on one side of the supports being slightly thicker than on its flanks, the demarcation zone on the opposing side is very thin.

The shape of the SE layer depends on mass transfer of bromine to the brink of the bead, the diffusion rate through the stationary phase into the core of the particle as well as the reaction rate with AGE, all while bromine gets slowly hydrolysed. The shape of the supports hints that a single 20% partial bromination step results in fast mass transfer into the bead without granting the bromine enough time to first enshroud the support as a whole even at higher sucrose concentrations. Such an inconsistent thickness of the SE layer (6.5- 17 μm), sacrifices (too) much core binding capacity as only the shortest distance is of importance to the overall media performance when aiming to fully eliminate surface binding (characteristic length).

In an attempt to avoid directional layering, as observed in 20% partially brominated supports, while providing a slightly thicker overall layer than 10% partially brominated beads, supports were treated repeatedly. Two thin layers statistically avoid both thin spots in the SE layer as well as under-/ overtreatment due to diffusion barriers.

10% partially brominated supports were exposed to a second 10% partial bromination step following the same protocol, prior to hydrolysis (10%+ 10%).

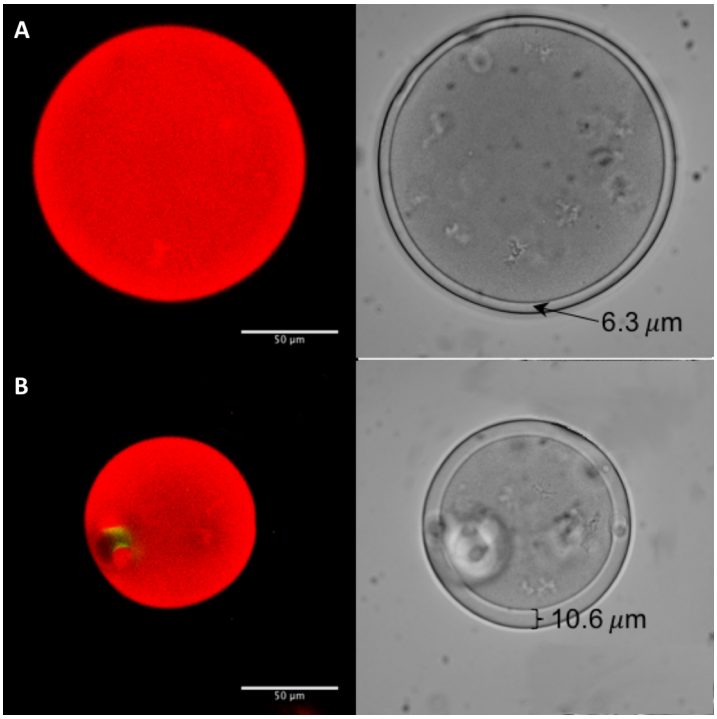


Figure 4-11 Left: Overlay of CLSM channels (red- fluorescently tagged BSA; green- pDNA) analysing SEC/ IEC supports manufactured via double 10+10% partial bromination/ hydrolysis cycle at room temperature (21°C); with a sucrose content of 64% w/v (0.032 Pa·s)
Right: Respective light microscopic image with shell thickness of SE layer in µm

Light micrographs of prepared supports show, as expected a homogeneous layer devoid of pDNA binding with no connection of the core to the surface (Figure 4-11).

The thickness of the surrounding layer was, as expected, thicker than observed in the 10% partial bromination supports, with the additional bromination eliminating the spots of residual binding caused by the directionality of applying bromine in a single step as seen in the 20% partial bromination supports.

However, these minor flaws in shape and thickness of the SE layer of manufactured AEC-SEC bilayered media, cannot account for retentions of 22.5, 24.1 and 32.5% static pDNA binding capacity in comparison to AEC control supports (10%; 20% and 10%+10% partially brominated respectively).

It is apparent that a different effect has to be responsible for residual pDNA binding to media en gros.

### 4.3.4. Imperfect beads with flawed surfaces

Upon analysing AEC-SEC media (CLSM, light microscopy), a number of non-spherical, damaged and/ or misshaped chromatography particles stood out from the bulk of the population. Several different patterns of imperfections were observed, affecting the crafting of bilayered support structures in their own ways.

Hollow spots within the internal structure of particles were observed (Figure 4-12, A). These hollow spots are not beneficial from an overall (core) binding capacity point of view, as they create additional internal void volume in a column. However, they do not influence the crafting of a SE layer onto AEC supports via the AGE activation- partial bromination route as long as they are fully inside the support without connection to the surface.

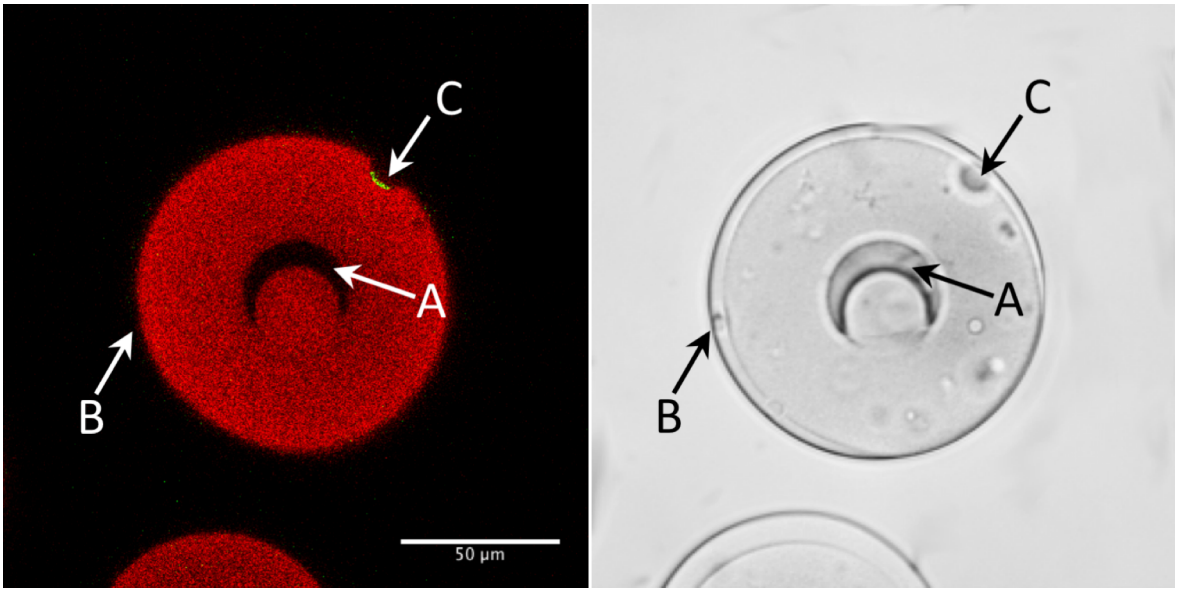


Figure 4-12 AEC-SEC support containing internal hollow areas (A), small impairments that can be ignored due to the layer thickness (B); dents causing pDNA binding (C); bead crafted via 20% single step bromination, 50% sucrose addition
Left: Overlay of CLSM channels (red- fluorescently tagged BSA; green- pDNA)
Right: Respective light microscopic image

Small crevices/ dents on the surface of supports are 'swallowed' by the SE layer (Figure 4-12, B). As a result, the layer thickness is locally slightly thinner in these creviced surface regions. However, the crafted layer does still prevent pDNA adsorption and the impact of small impairments on the surface can be discarded for the manufacturing process, as long as their depth is less than the thickness of the surrounding shell.

Only when dents on the surface are too deep or too inaccessible, pDNA can be found to bind to the support (Figure 4-12, C).

However, among such minor imperfections, more severe impactions to the particles' shapes arose concern as to whether the applied bromine would reach within these imperfections. Unless the bromine diffuses into the crevices lining the surfaces of these craters, it cannot cut the double bond of AGE molecules and as a result, Q ligands will subsequently be coupled onto the pores exposed to hidden away surfaces. Not eliminating AGE double bonds will hence ultimately lead to pDNA adsorption to the support media.

Light micrographs revealed 'bead-inside-a-bead' structures, where small particles are partially submerged into the surface of larger particles. CLSM analysis of such a support clearly shows how imperfect areas on the surface of the beads bind pDNA to the support.

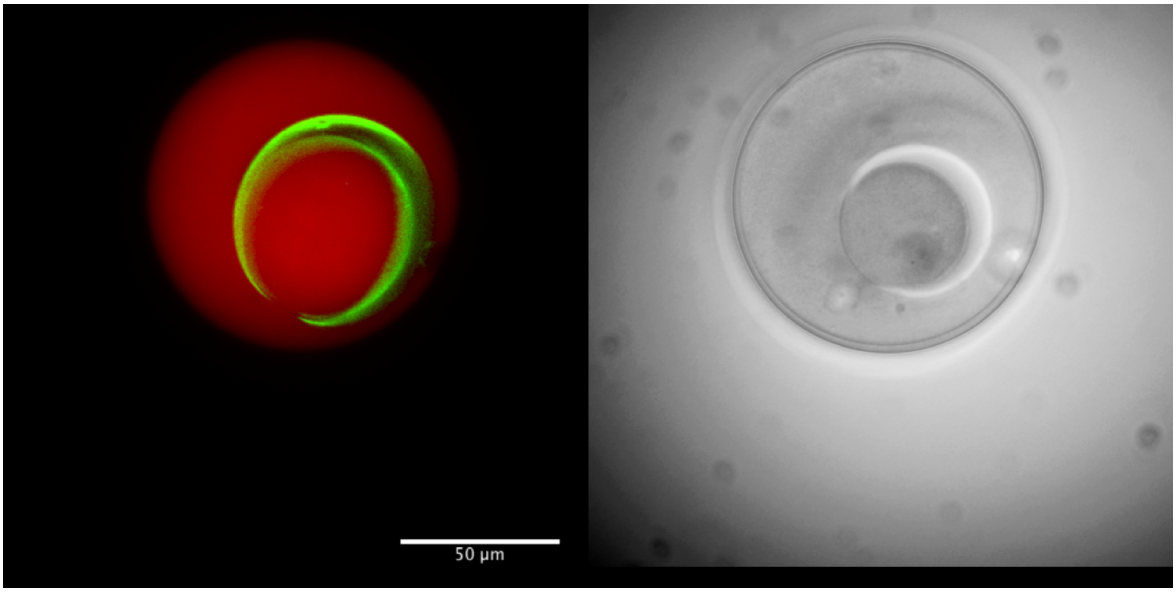


Figure 4-13 Z-stack projection of overlaid CLSM fluorescent intensities (averaged) orthogonal to the visual plane (51 stacks; 1.5 µm slice thickness; left); respective top view light micrograph of 10% partially brominated support (right)

Figure 4-13 (left) shows a 3D z-stack projection, of 51 cross-sectional stacks being compiled into one image, with the respective light micrograph given on the right. The smooth surface of the support shows no pDNA binding, as the ligand free layer prevents adsorption. However, pDNA was found to bind to the surface of the 'bead-inside-a-bead' structure. The bromine was evidently unable to react with AGE groups tucked away from the easily accessible surface, allowing ligand coupling at the creviced surface of imperfections. Plasmid DNA in static binding experiments (CLSM) was subsequently able to diffuse in between the surfaces and bind to exposed ligands deep within the grooves, yielding retentions of at least 22.5% static pDNA binding capacity in comparison to fully Q-coupled control media.

Similar effects were observed in other supports with smaller 'beads-inside-the-bead' imperfections (Figure 4-14).

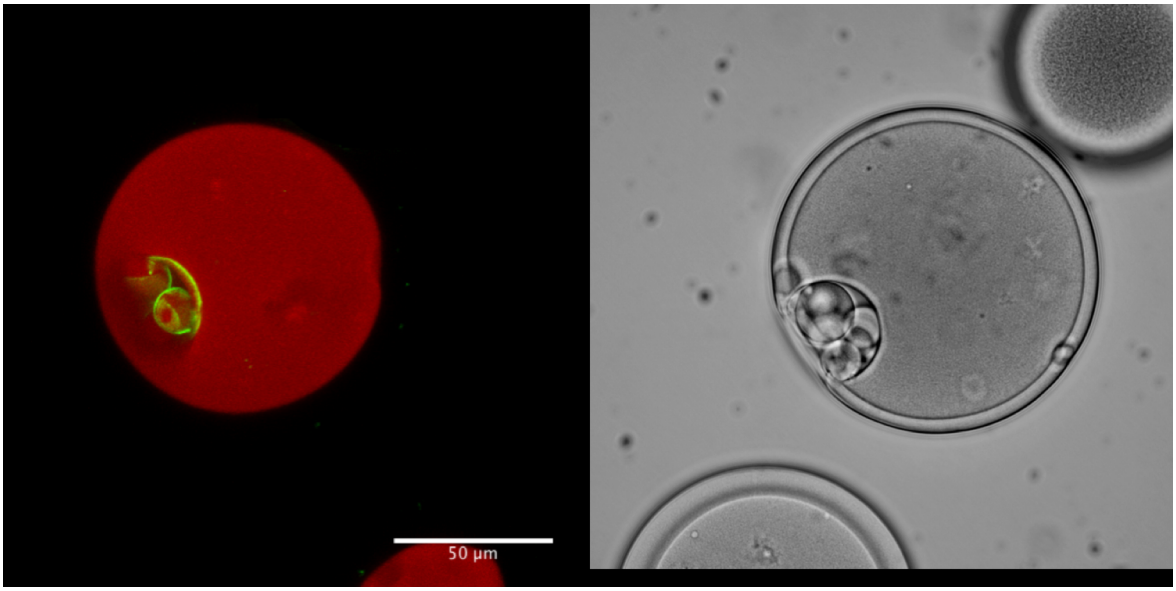


Figure 4-14 Rotated view of 3D projection of z-stack CLSM images (36 stacks; 1.5 µm slice thickness; left); respective top view light micrograph of 10% partially brominated support (right)

Furthermore, it appears that some hollow areas described earlier do indeed have channels to the surface of the beads. These channels connect the surrounding buffer with the ligands of the core and allow pDNA to diffuse from the buffer solution through these 'entrances' to ligands situated in the core of the particle (Figure 4-15). The 3D projection of such a support confirms that, while the SE layer prevents pDNA adsorption to the surface of the bead, a small opening on the left side has granted access to pDNA to bind to the ligands lining the hollow areas inside.

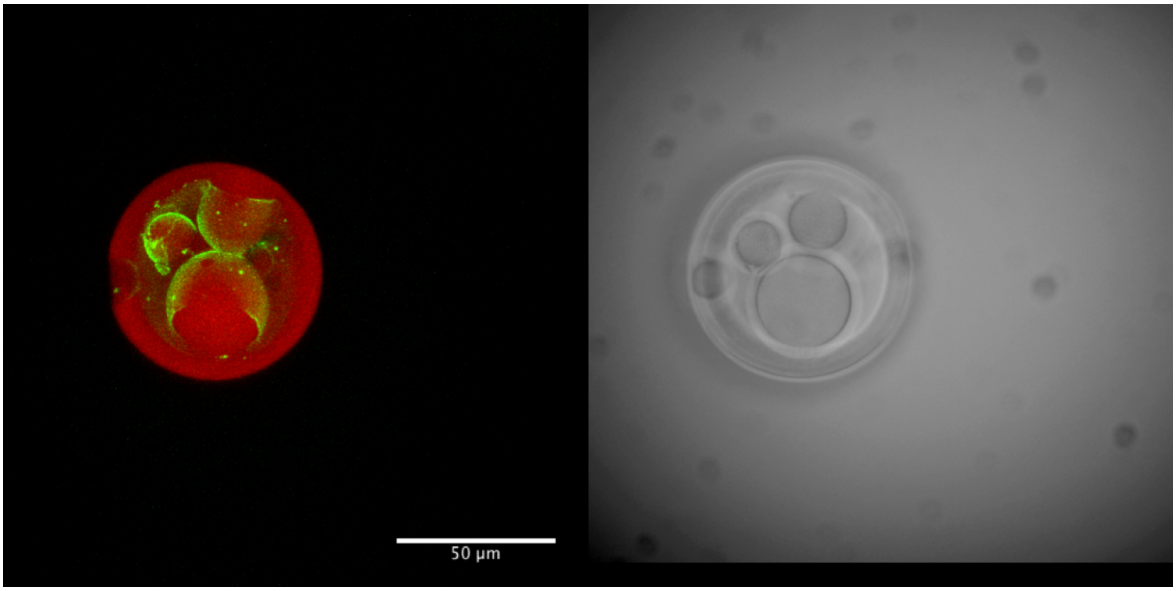


Figure 4-15 Top view of 3D projection of z-stack CLSM images (36 stacks; 1.5 µm slice thickness; left); respective top view light micrograph of 10% partially brominated support (right)

Overlaying CLSM channels with their respective light micrographs confirms that bromination eliminates all surface charges that are easily accessible to the bromine, while pDNA binding is limited to the inside of surface imperfections (Figure 4-16 ).

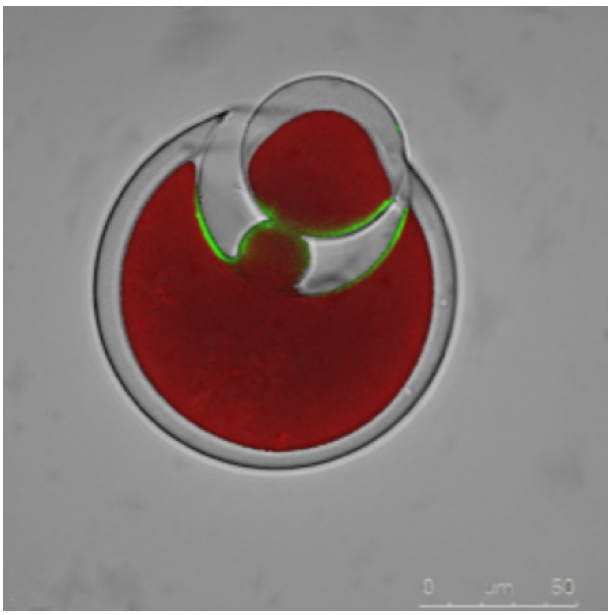

Figure 4-16 Overlay of centre stack meridian CLSM fluorescence channels with light micrograph of bilayered chromatography support after double 10+10% partial bromination

### 4.3.5. Quantification of misshaped bead population

CLSM investigation of imperfect supports within the bulk of chromatographic media shows that some of the retention of pDNA binding capacity, after the application of partial bromination- AGE activation- ligand coupling steps can be attributed to imperfect supports in the SEC base matrix.

This raises concern about the quantitative extent of which these imperfect beads are part of the overall population and subsequently are responsible for residual pDNA binding post treatment. To assess the degree to which the presence of misshaped supports within a sample population contribute to remaining pDNA binding of restricted access media, light micrographs of a large population of supports have been collected and evaluated. For each analysed SEC media (fully derivatised media based on Sepharose CL-6B used as control media for static binding studies and CLSM; a different batch of the same media; 10% partially brominated supports (64% sucrose addition); Superose 6; Superose 12 and Sepharose 6 FF) a statistically relevant sample size of particles was imaged and grading of visual integrity of each bead was performed as described in 4.2.3. Flawless supports were rated green, minor imperfections (dents/ crevices on the surface) were rated yellow, while supports assumed to grant pDNA binding post SE layer application were rated red (Figure 4-17 features example supports of all three categories).

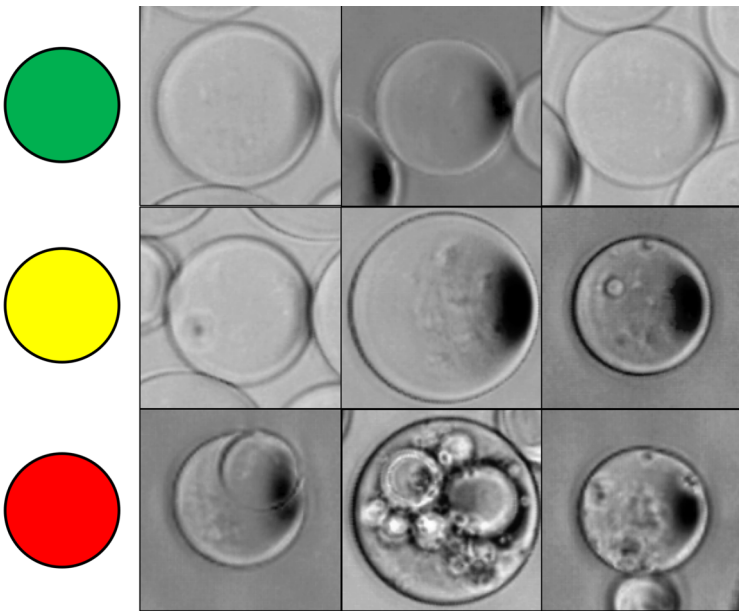

Figure 4-17 Grading categories of chromatography supports for their use in VE-RDB experiments

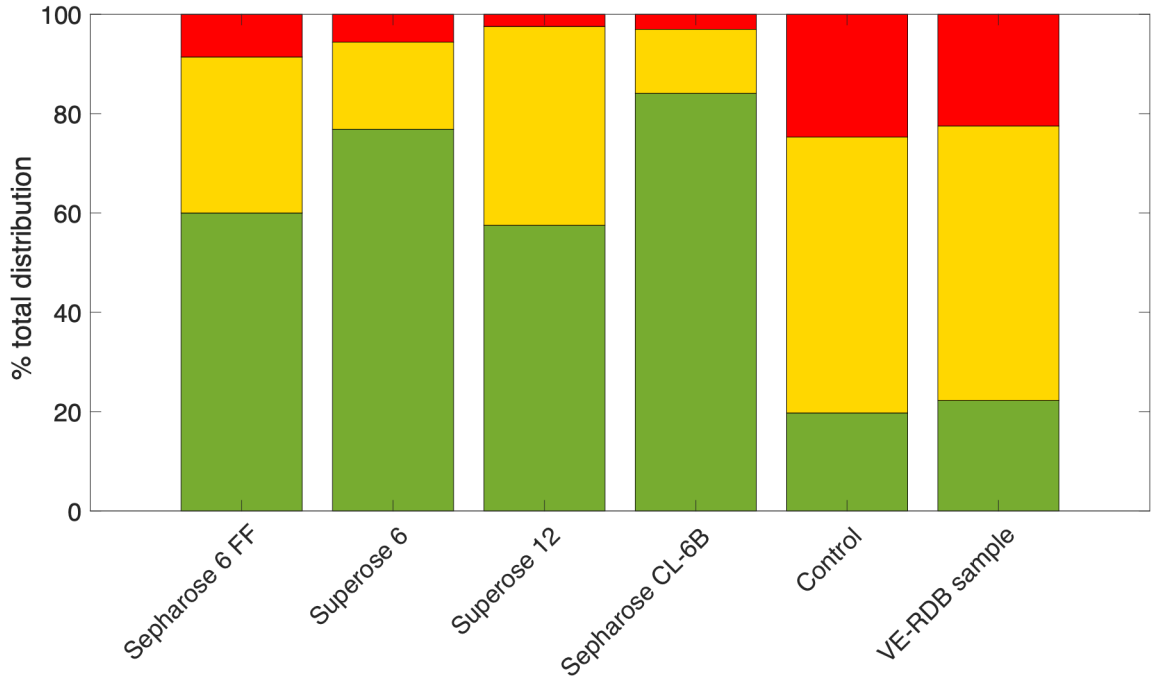


Figure 4-18 Grading of visual integrity of different chromatography media as part of the bulk population; red: supports with major surface imperfections granting pDNA binding post SE layer application; yellow: minor impairments on the surface that can be covered up via the SE layer creation; green: spherical supports without any flaws on the surface

Figure 4-18 summarises the quantitative analysis of light microscopic images taken from random sample populations of various chromatography media.

The shell thickness of successful VE-RDB media are in a range from 2.5-10 μm as confirmed by CLSM studies. The yellow graded beads show small imperfections on their surfaces, that are expected to be fully integrated into the SE layer when exposed to partial bromination, controlled by VE-RDB. To determine whether a SEC media is suitable for VE-RDB treatment, the yellow and green populations can hence be combined into one category with regards to expected pDNA binding post bilayered chromatography media creation.

The red graded population is considered to be responsible for residual pDNA binding and the limiting factor of a base matrix.

The control group of fully functionalised supports and the partial bromination VE-RDB sample (10% bromination; 64% sucrose addition) showed 25 and 23% of their respective populations to have major surface imperfections. These imperfect beads would bind pDNA, if used in a chromatographic operation. Given that both media are based on the same batch of

Sepharose CL-6B, it is not surprising that the ratings of the visual integrity of both media are very similar.

The amount of red graded particles used for VE-RDB controlled partial bromination studies is however high in comparison to other commercial SEC media such as Sepharose 6 FF, Superose 6 and Superose 12 with 9%, 6% and 2%, respectively. Purely based on the visual appearance of the supports, all three media are expected to yield better SI when crafted into RAM following a similar protocol.

The population of 'red' supports in the second Sepharose CL-6B batch, was with 3%, a lot smaller than the batch used for crafting bilayered media. This highlights the importance of batch-to-batch variations. The main function of the media is targeted for gel filtration of proteins, peptides, polynucleotides and other biomolecules on a micro-preparative scale (GE Healthcare, 2013). Within their field of application, the media may be performing according to expectations and the presence of imperfect supports, as well as the outlined batch-to-batch variance, does not change their chromatographic performance.

It is therefore imperative to assess the quality of each batch prior to its use as base matrix in a bottom up manufacturing technique for the creation of restricted access AEC-SEC support media.

## 4.4. Conclusion/ suggested future work

Bilayered AEC-SEC supports manufactured via partial bromination VE-RDB pathway comprise of a thin, inert homogeneous SE layer, surrounding a positively charged core.

A novel CLSM method was developed, allowing for direct and simultaneous visualisation of the binding topography of both protein and pDNA binding to chromatography matrices.

Applying the method to investigate bilayered media, manufactured via AGE activation- partial bromination pathway yielded that spherical RAM supports with smooth surfaces are totally inert to pDNA binding due to steric limitations (core), as well as a lack of available binding sites on the surface due to the inert shell surrounding the inner charged core.

Respective micrographs of RAM media revealed that structurally imperfect beads with irregular surface properties occur within total support populations. Minor structural flaws on the surface of starting media do not contribute to the residual pDNA binding of the media as they are overcome by the creation of the ligand-free zone.

However, large surface imperfections including macropores, deep fissures, 'bead-inside-a-bead' structures as well as deep craters, create areas on support surfaces that cannot be accessed by bromine during the partial bromination step of manufacturing.

This leads to the creation of ligands on the surface being exposed to the surrounding feed. Plasmid DNA is unable to bind to ligands inside the core, however it still adsorbs to surface exposed ligands. This effect overall accounts for residual surface binding capacities of at least 22.5% in comparison to a fully derivatised media.

Quantifying the populations of these flawed beads in several different chromatography media revealed that the majority of residual static pDNA binding capacity can be attributed to the presence of such imperfect chromatography supports. The amount of flawed supports is hereby strongly dependant on the respective batch and type of SEC starting media used.

While on a laboratory scale, a visual inspection/ sieving of imperfect beads would be conceivable, it is not a serious consideration for industrial production scale. This emphasises the importance of starting media selection, as well as a visual batch-to-batch analysis of support surface integrity.

Quantitative analysis of CLSM fluorescence intensity traces indicate that pDNA binding to remaining binding sites within the groves of imperfections are elevated in comparison to

smooth surfaces of control media. In static binding studies, the 10% partially brominated media (64% sucrose addition) showed a reduction of 77.5% pDNA binding capacity in comparison to the fully derivatised control sample, with 23% of the supports binding pDNA due to major surface imperfections.

Matching of numbers may be coincidental, but given the strong pDNA fluorescence within the imperfections and that no binding was observed in CLSM images of 'perfect', spherical supports, the data suggests that the main residual pDNA binding can be attributed to hidden areas on the surface or within the internal structure of supports, both caused by the presence of surface imperfections in the starting media.

Having yielded a better understanding of the limitations, underlying the processes involved in the manufacturing of RAM via the AGE-activation, partial bromination route, a couple of improvements are to be considered when applying the technique for future work.

To avoid mismatching values between targeted bromination and actual reduction of allyl contents, it is suggested to base calculations for bromine addition on the amount consumed within the support sample (accounting for bromine loss due to hydralisation), rather than on the total amount of AGE groups in the starting sample.

While single 10% bromination left some particles undertreated, increasing the concentration to 20% in a single bromination step led to directionality of layer expression. Repeated 10% partial bromination helped reduce directionality of layer expression on the expense of core binding capacity, so it stands to expect that a repeated 5% plus 5% bromination would yield better results, avoiding the creation of residual binding sites on support surfaces while at the same time compromising very little on overall (core) binding capacity and homogeneity of the non-adsorptive layer.

The dependence of the final product on the visual integrity of the starting media calls for application of the technique to use 'better' SEC resins. These could either be crafted to purpose by changing the existing production protocols in a collaboration with a manufacturer for chromatography resins, or, as a starting point, use commercial resins such as Superose 6/ 12, that have fewer beads inducing pDNA binding post treatment due to flawed or imperfect supports.

Some of the outlined suggestions have already been incorporated to create AEC-SEC bilayered media, however these further experiments exceed the scope of this project.

By using the 'better' base matrix Superose 6 over the 'more flawed' Sepharose CL-6B, SI indices of up to 370 could be achieved, confirming the conclusions presented in this study, that sphericity and lack of imperfections on the surface of agarose media are crucial parameters for the production of bilayered SEC-AEC media via the VE-RDB approach (Joseph, 2018- in preparation).

# Chapter 5 Characterization of the commercial bilayered chromatography resin Capto Core 700

## Abstract

Since its introduction to the commercial market in 2012, Capto Core 700 has been used for the intermediate purification of large nanoplex biomolecules, such as VLPs. Although the manufacturer suggests reducing nucleic acid concentrations in the feed prior to loading it onto a column, its SEC-MMC bilayered architecture suggests that it could be ideal for negative adsorptive chromatographic purification of pDNA from crude *E. coli* lysates.

Several characterization tools have been applied to investigate pDNA purification properties of the media from crude lysates, yielding encouraging results for the medias performance in dynamic chromatography studies, where RNA and HCP were retained in the core, allowing larger (26.88 kbp) pDNA molecules to flow through the column unretained.

However, in static binding studies, pDNA was found to bind to remaining octylamine ligands on the 'inert' surface of adsorbents, especially after longer (>2 h) incubation times.

These observations were confirmed by CLSM analysis of the binding topography of single supports, using Syto 9 and Cy5 as fluorescent markers for pDNA and BSA, respectively.

Applying a gentle cold atmospheric pressure, helium plasma etching treatment (9 W; 14.5 kHz; 10 min treatment time) in a FBR set-up to Capto Core 700 was able to reduce the pDNA binding capacity of the media by up to 7.7% in static binding studies, providing a simple add-on treatment to (further) reduce residual surface binding ligands of the media.

## 5.1. Introduction

Capto Core 700 (CC700) was the first multifunctional chromatography resin for the intermediate purification and polishing of viruses, and other larger biomolecules, for process scale chromatography, to be introduced to the commercial market in 2012 (GE Healthcare, 2012).

The media is based on a highly cross-linked spherical agarose stationary phase (d~ 85 µm) functionalised by the 'core bead technology'. The core of the particles is activated with the MMC ligand octylamine, surrounded by a 5 µm layer devoid of ligands. The outer layer prevents large target molecules from binding to ligands, while smaller contaminants can enter freely into the beads, where they are being retained via strong multimodal interaction with the stationary phase. The size cut off of the agarose shell is 700 kDa, any molecule larger than that will pass through the column in flow through mode (Figure 5-1).

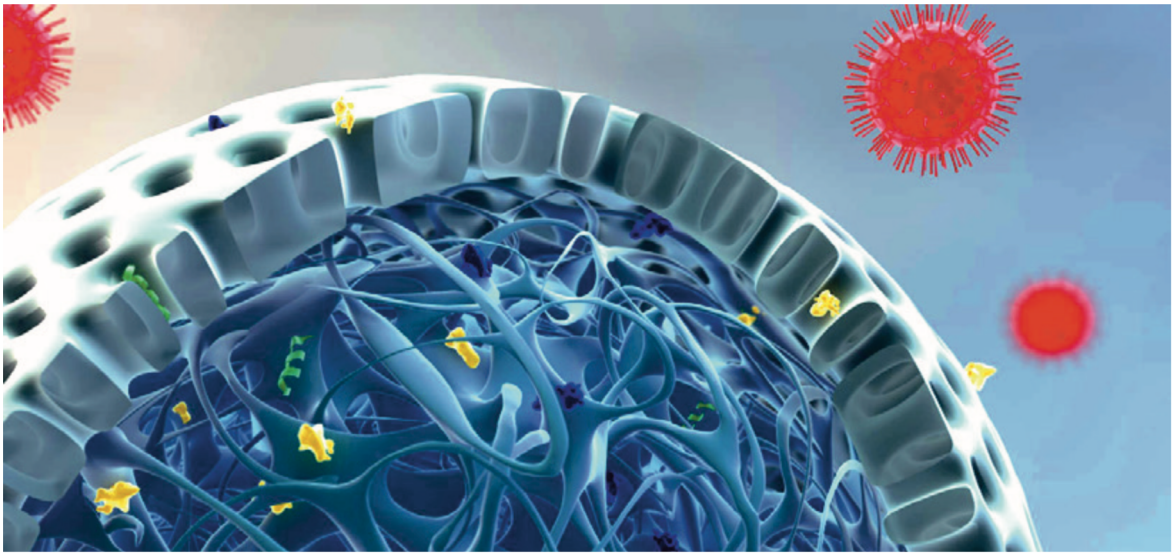

Figure 5-1 Schematic representation of the principle for CC700. Large targets are excluded from the beads, whereas smaller impurities can enter into the core where they are being captured by MMC ligands (GE Healthcare Bio-Science, 2012; Ge Healthcare, 2018a)

The media is available in different packing formats (GE Healthcare, 2018b): prepacked as HiScreen columns optimised for method and process development, HiTrap columns for manual or automated purification at the laboratory scale and ReadyToProcess as beaded media in various packaging sizes.

Table 5-1 Product specifications of Capto Core 700 and Capto Core 400 as published by the manufacturer (Ge Healthcare, 2018a, GE Healthcare, 2018b)

| Parameter | Capto Core 700 | Capto Core 400 |
|---|---|---|
| **Ligand** | Octylamine | Octylamine |
| **Particle size, $d_{50v}$** | ~90 μm | 90 μm |
| **Matrix** | Highly cross-linked agarose | Highly cross-linked agarose |
| **Binding capacity/mL chromatography medium** | ~13 mg ovalbumin | 22 mg ovalbumin |
| **pH stability (operational)** | 3-13 | 3-13 |
| **pH stability (CIP)** | 2-14 | 3-14 |
| **Flow velocity** | <500 cm/h | 700 cm/h |
| **Molecular weight cut-off** | ~700 kDa | 400 kDa |

In 2018, Capto Core 400 was introduced to the market. The media has a smaller size cut-off of 400 kDa and resembles CC700 in most other specifications (Table 5-1).

Mixed mode chromatography is based on a stationary phase that interacts with solutes via more than one mode of interaction (Yang *et al.*, 2011). Octylamine interacts with small contaminants (HCP, Endotoxins, etc.) based on two methods; positive groups in conjuncture with a hydrophobic nature (Cunha *et al.*, 2016). The recommended application of CC700 as a negative chromatography resin to capture only impurities, renders the structural integrity of contaminants unimportant. This is crucial given the vigorous elution conditions that are necessary to reverse the ligands strong interactions post loading.

Since its release, CC700 media has been successfully used in various DSP strategies for the production of VLPs (Nestola *et al.*, 2015; Zhao *et al.*, 2015; Lagoutte *et al.*, 2016; Somasundaram *et al.*, 2016), nanoparticles (He *et al.*, 2016), virus purification (Weigel *et al.*, 2014; James *et al.*, 2016; Lee *et al.*, 2016; Mundle *et al.*, 2016; Shen *et al.*, 2016; Tseng *et al.*, 2018), capsular polysaccharides (Ji *et al.*, 2014), extracellular vesicles (Corso *et al.*, 2017) and secretory immunoglobulins (Matlschweiger *et al.*, 2017). Furthermore, it is part of patented endotoxin removal strategies (Adielsson *et al.*, 2018) and von-Willebrand-Factor purification (Schroeder, 2016).

The route of manufacturing of CC700 is proprietary, however several patents suggest a manufacturing process based on chemical build-up of functionality within porous soft hydrogel beads ('bottom-up' approach) involving AGE-activation partial bromination, similar

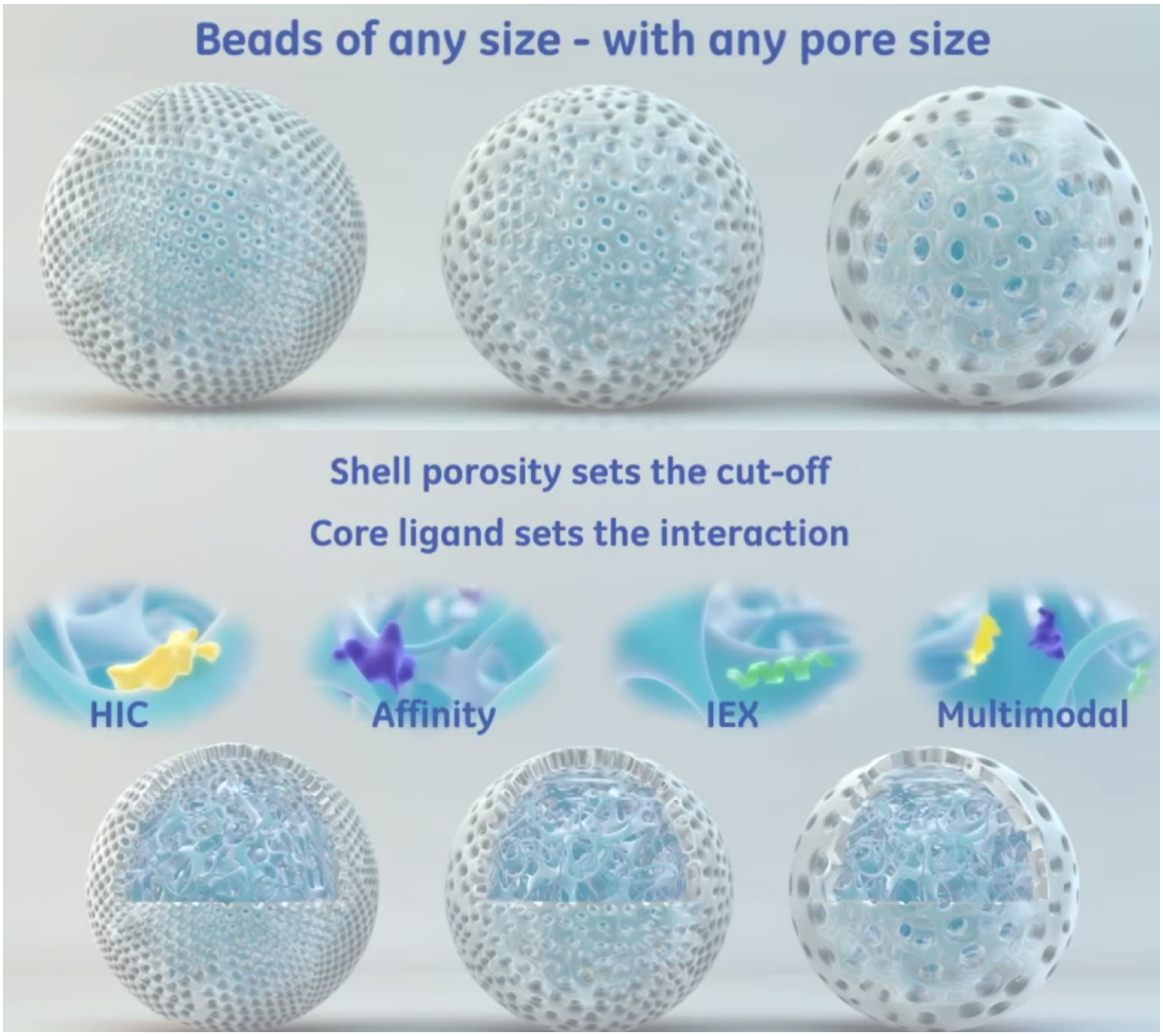


Figure 5-2 Different designs of bilayered chromatography resins, featuring different size cut-offs as well as ligands tailored for specific modes of interaction (image source: (GE Healthcare Life Sciences, 2012))

to the process described in Chapter 4 (Bergstrom, 1997; Berg, 2003; Gustavsson *et al.*, 2004; Maloisel *et al.*, 2016; Hall *et al.*, 2018). Although the manufacturer advertises further bilayered chromatography media with different pore sizes/ particle size distribution (PSD), as well as tailoring ligands to specific binding properties to satisfy operational demands can be achieved (Figure 5-2), only the two aforementioned multifunctional bilayered chromatography resins have been released to date (Glaser, 2013; Maloisel *et al.*, 2016; GE Healthcare, 2018c).

In this chapter, options for the purification of pDNA from crude *E. coli* feedstocks utilizing CC700 have been explored. Several visualisation techniques have been employed to analyse the bilayered media and its limitations for pDNA applications.

Cold atmospheric pressure plasma treatment in a FBR, for the functionalisation of beaded hydrogel chromatography media has been explored to provide an add-on treatment, attempting to enhance plasmid yield.

## 5.2. Materials and Methods

Several experimental methods applied in this chapter have been utilised in different sections of this work. To avoid describing methods that found application in more than one chapter of this thesis, a collection of 'general' M&M as well as a conclusive list of materials used for their implementation can be found in the respective sections of this thesis (Chapter 2).
Methods related to experiments that are exclusive to this chapter are presented below. Experiments that deviate from the outlined methods are provided in the respective sections or where additional information is required for better understanding.

### 5.2.1. Column packing and frontal loading column chromatography for purification of pDNA from crude *E. coli* lysates

All column chromatography was performed at room temperature on an Äkta Explorer 100 system controlled by UNICORN Software (version 4.11; GE Healthcare, Uppsala, Sweden).
Capto Core 700 was packed into a Tricorn 5/50 column to a final bed height of 5 cm (1 mL SBV total; settling beads at 0.1 mL/min for 60 min; column compacted at 1 mL/min for 10 min using MQW).
The column was then washed and equilibrated (0.1 mL/min) with 5 CV of Buffer A. Buffer A was prepared as follows; 36 mL of 10 mM Tris-HCl; pH 8 containing 61 mM glucose and 50 mM EDTA were mixed with 78 mL of 0.2 M NaOH containing 1% SDS; the solution was mixed with 59 mL of 3 M potassium acetate (4°C); pH 5.5 and the final solution was sterile filtered with a Millex syringe filter unit (Millipore, Sigma) and adjusted to a conductivity of 33 mS/cm, mimicking the composition of clarified, neutralized alkaline *E. coli* lysate.
The lysate obtained in 2.3.3 was diluted with MQW to a conductivity of 33 mS/cm before it was loaded onto the column using a P-960 sample pump (flow rate 0.1 mL/min; 80 mL total loading volume). After the loading of the column, it was washed with 4 CV Buffer A before elution of bound species using a gradient salt elution of 20 CV (2 M NaCl; 1 mM EDTA; 25 mM Tris–HCl; pH 8). The system was stripped with 25 CV of stripping buffer (0.2 M NaOH; 2 M NaCl

solution). Throughout chromatography runs, $UV_{260}$, $UV_{280}$ absorbance as well as pH and conductivity were monitored, and 5 mL fractions were collected for subsequent NA quantification via DPA and Orcinol assay as well as gel electrophoresis.

### 5.2.2. Static RNA binding studies for optimisation of elution conditions

CC700 media was washed twice in MQW and equilibrated in a buffer resembling the loading buffer of frontal chromatographic experiments. The beaded supports (75 μl SBV) were incubated with 1.5 mL of 0.5 mg/mL baker's yeast RNA (*S. cerevisiae*) for 30 min on a blood tube rotator. The suspension was subsequently centrifuged (2,000 g; 10 s) and the supernatant carefully pipetted out. The samples were then incubated with 1.5 mL of various elution buffers for 30 min, centrifuged and the supernatant and the supports were analysed separately for their RNA contents via Orcinol assay.

## 5.3. Results and Discussion

### 5.3.1. Frontal loading chromatography for purification of a 26.88 kbp plasmid from cleared *E. coli* feedstock

CC700 aims at the intermediate purification of viruses and other large biomolecules. The manufacturer suggests to reduce the amount of NA in the feedstock as “high levels of DNA and RNA can, in some cases impair the performance of CC700” (GE Healthcare, 2012).

The shell of the beaded media is, according to the manufacturer, devoid of ligands on the outside of the particles and is permeable only by moieties <700 kDa, such as RNA or HCP (GE Healthcare, 2018b). These properties should make the media ideal for capturing pDNA from crude *E. coli* feedstocks, if the plasmid is large enough to not enter and bind to the core alongside contaminants in the lysate, such as RNA and HCP.

The size of plasmid IT14: pPR322-p170 is 26.88 kbp (16.49 MDa (GSL Biotech LLC, 2004; Bioinformatics, 2017)). NA and protein weights are not directly comparable and hydrodynamic radii of pDNA molecules and proteins of equal MW will be slightly different due to differences in density and conformation.

However, the plasmid is more than 20 times larger than the size cut-off of the media and the inert SEC shell should prevent pDNA molecules from penetrating through the shell and elute in the flow through fraction of a chromatographic operation. With a size cut-off of 700 kDa, it is unclear what the manufacturers concerns about high NA concentrations in feedstocks may be.

The high copy number plasmid IT14 was introduced into potent *E. coli* DH5α cells and fermented as described in 2.3.1 and 2.3.2. Cells were subsequently disrupted via alkaline cell lysis and genomic DNA and cell debris were removed by centrifugation (2.3.3). The resulting cell lysate was adjusted to 33 mS/cm and loaded onto a 1 mL SBV CC700 column (5.2.1). After loading 80 mL of lysate onto the column, a salt gradient was used to elute bound moieties from the core of the supports (1 M NaCl; 25 mM Tris-HCl; 1 mM EDTA).

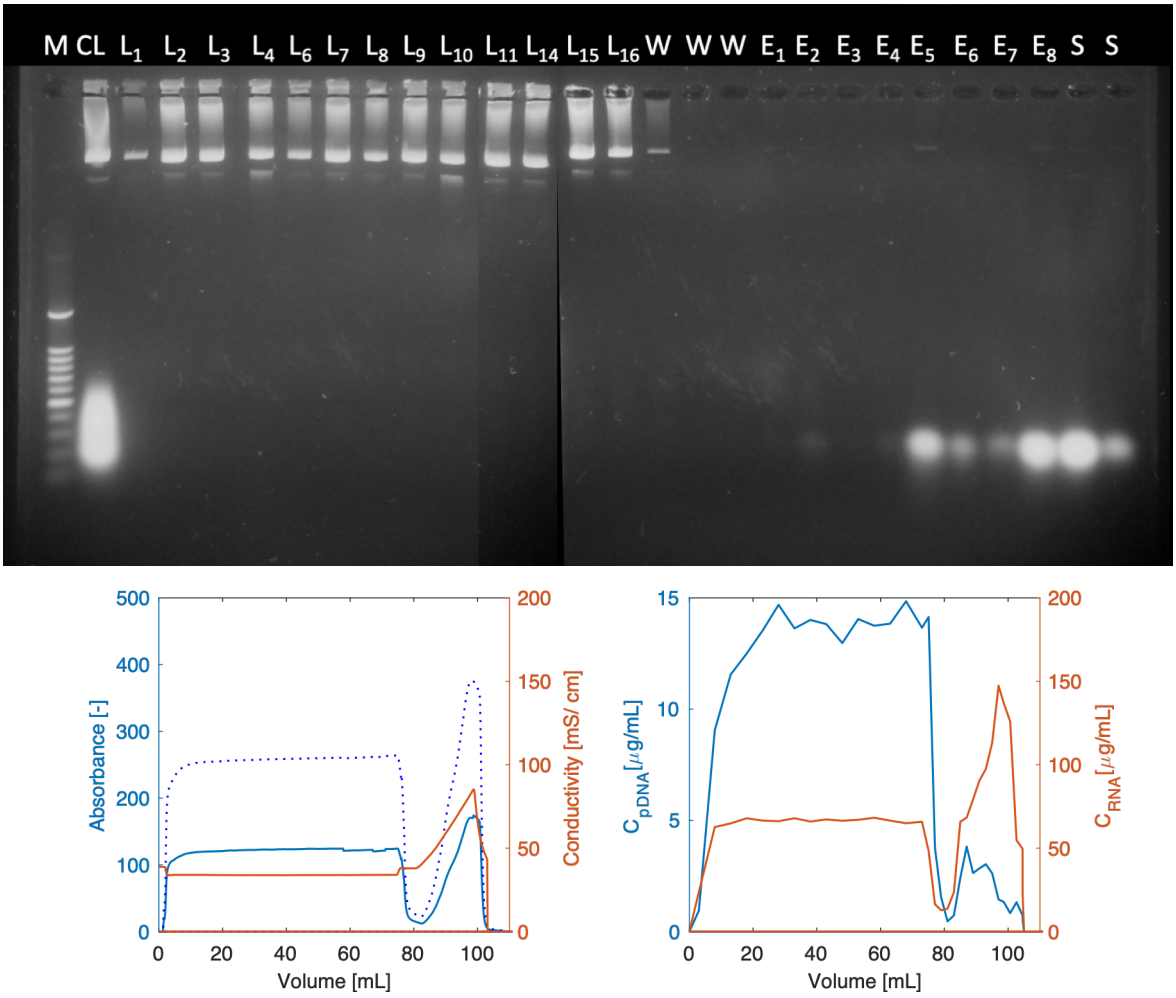


Figure 5-3 Top: Agarose gel electrophoresis of obtained chromatographic fractions; M: Lambda- HinDIII marker; CL: cleared lysate (control); $L_1$-$L_{16}$: cleared lysate led through the column; W: wash; $E_1$-$E_8$: elution fractions; S: strip; Fraction size 5 CV; conductivity 33 mS/cm; linear flow rate 6 mL/h
Bottom: Chromatograms of loading cleared *E. Coli* lysate onto 1 mL SBV CC700, dashed line: $A_{280}$, solid line: $A_{260}$ (left); respective chemical quantification of NA contents in the elution fractions (right)

Looking at the gel electrophoresis image of the chromatographic fractions, several points stand out; the absence of RNA molecules in loading fractions indicate that breakthrough capacity of the core is not reached after loading 80 mL of cleared lysate on to the column (Figure 5-3, top). Furthermore, pDNA did elute in the flow through during the loading phase without interacting with the media, with fractions L2-L16 resembling the pDNA contents of the cleared lysate (CL). However, small amounts of pDNA show up in the elution/ stripping fractions. These small amounts of pDNA correlate with the first loading fraction (L1), showing a reduced amount of pDNA, suggesting that small amounts of pDNA can in fact interact with

the media during initial stages, until binding areas have been quenched and subsequent pDNA flows through the column without interacting with the media.

Residual binding of NA to the media after elution suggests that NA, bound to octylamine ligands, cannot be eluted by enhancing the ionic strength alone, as is customary for AEC operations (Prazeres *et al.*, 1998; Ferreira *et al.*, 2000a; Pitarresi *et al.*, 2004). The mass balance for pDNA and RNA furthermore suggests that even after stripping the column with 2 M NaCl and 0.5 M NaOH, some NA moieties are still tightly bound to the core of the media. Overall, CC700 is suitable as an initial purification step for capturing pDNA in negative chromatography mode from typical contaminants. A small compromise of yield was observed as a result of initial interactions of small amounts of pDNA with the media. However, elution conditions as well as applied CIP regimes are in need of optimisation to regenerate the column for a sustainable process.

5.3.1.1. Optimisation of elution conditions for clearing bound nucleic acids from Capto Core 700

Elution of bound NA post stripping of a 1 mL SBV column of CC700 after loading cleared *E. coli* lysate containing a 26.88 kbp plasmid, via an applied salt gradient leaves residual NA still bound to the media. Enhancing the salt concentration from 1 M to 2 M was insufficient to clear out and sanitise the media for future applications, although small amounts of pDNA could be eluted using 2 M NaCl (Figure 5-4).

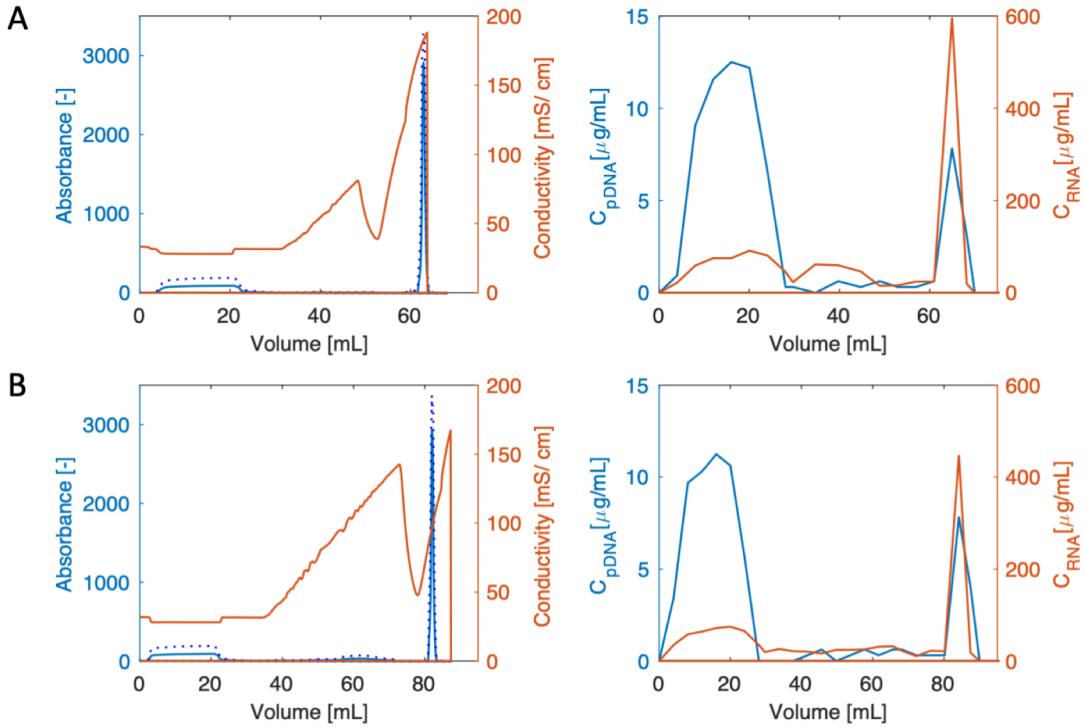


Figure 5-4 Chromatograms of loading cleared *E. Coli* lysate onto 1 mL SBV CC700, dashed line: $A_{280}$, solid line: $A_{260}$ (left); respective chemical quantification of NA contents in the elution fractions (right)
A: 1 m NaCl elution buffer
B: 2 M NaCl elution buffer

Isopropanol has been described as a suitable eluent in HIC by weakening hydrophobic interactions (Tseng *et al.*, 2005; Shukla *et al.*, 2007). However, applying a 10% isopropanol gradient elution did not weaken the binding interactions of RNA to CC700 enough to clear the core of the beads (Figure 5-5 , A). The multimodal octylamine ligand combines properties of both traditional AEC and HIC. Preparation of an elution buffer combining both isopropanol and salt was shown to be effective in stripping bound molecules from Quiagen AEC columns and showed promising results for application with CC700, by eluting a large peak of RNA from

the column (Figure 5-5 , B; (Budelier *et al.*, 1998)). The chaotropic agent guanidine hydrochloride is routinely used as an additive to elution buffer preparations for the removal of lipids and proteins from chromatography resins. The moieties disrupt the hydrogen bonds, responsible for stabilising bound molecules by weakening the hydrophobic effect and as a consequence enhance solubility of hydrophobic molecules. At higher concentrations however, protein structures are fully denatured and consequently reduce the dynamic binding capacity of AEC columns (Ng *et al.*, 2007; Ge Healthcare Bio-Science, 2013). Application of 1 M guanidine hydrochloride (GuHCl) in conjuncture with 1 M NaCl for removal of bound NA to CC700 however, did not yield any RNA elution from the column (Figure 5-5 , C).

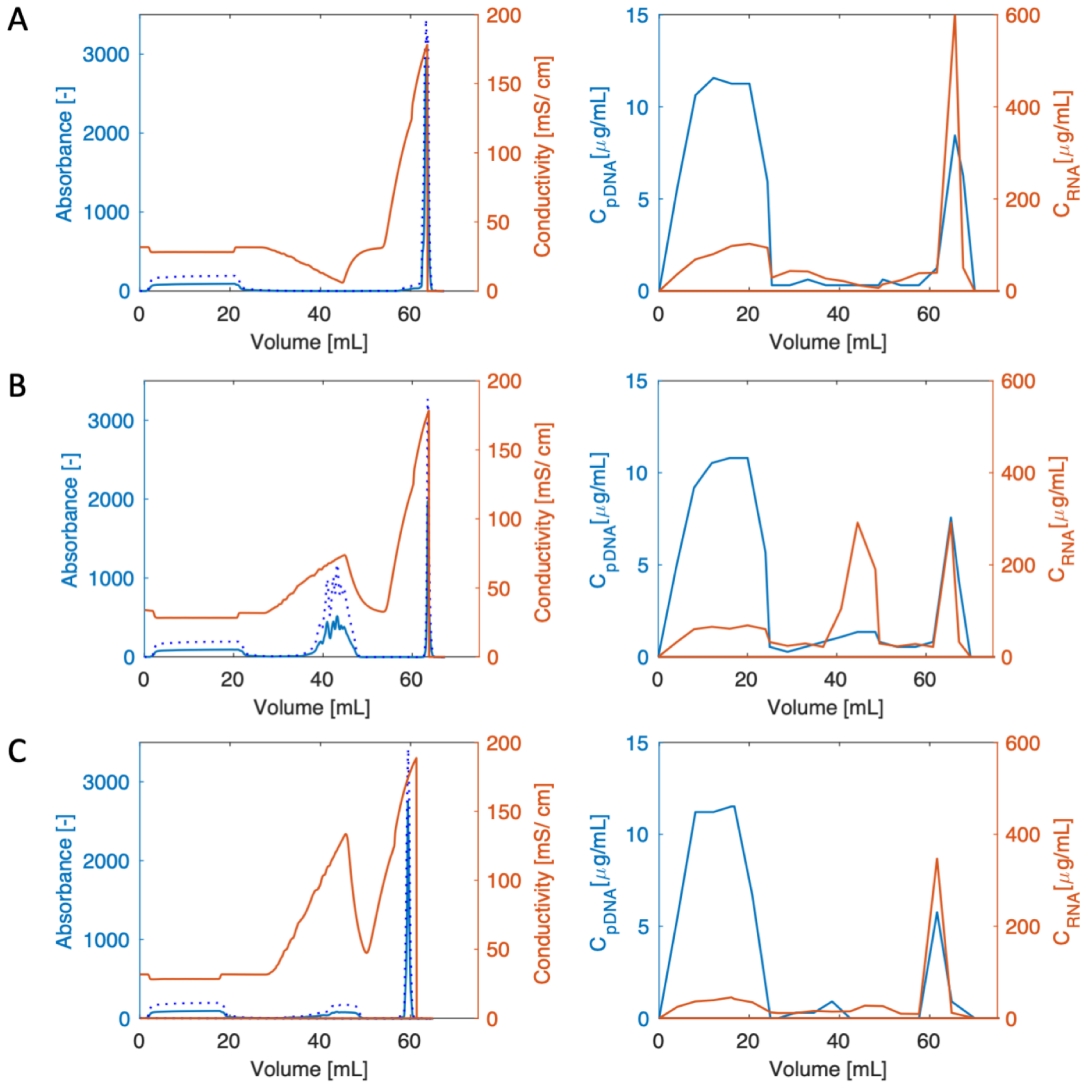


Figure 5-5 Chromatograms of loading cleared *E. Coli* lysate onto 1 mL SBV CC700, dashed line: $A_{280}$, solid line: $A_{260}$ (left); respective chemical quantification of NA contents in the elution fractions (right); A: 10% Isopropanol as elution buffer; B 15% Isopropanol with 1.25 M NaCl elution buffer C: 1 M Guanidine HCl with 1 M NaCl elution buffer

Further elution buffer conditions were investigated by loading CC700 media with baker's yeast RNA in static binding studies as described in 5.2.2.

Three different groups of elution buffers were analysed, (i) focussing on different concentrations of NaOH and isopropanol (Biosciences, 2001; Blom *et al.*, 2014), (ii) combinations of NaCl and Isopropanol, and (iii) stripping buffer (2 M NaCl; 0.5 M NaOH).

All buffer preparations from the first group performed very similarly, eluting around 80% of bound RNA (incubation time 30 min). Formulations containing high concentrations of isopropanol (30%) in conjuncture with 1.25 M NaCl as well as the high salt (2 M) buffer with 15% isopropanol proved the most suitable, eluting all RNA from the core.

Given the high elution values for all buffer preparations in comparison to the frontal loading experiments, this suggests that incubation time of the media with elution buffer plays a pivotal role when attempting to clear out bound moieties adsorbed to CC700, which is in accordance with the manufacturers suggestions (GE Healthcare Bio-Science, 2012).

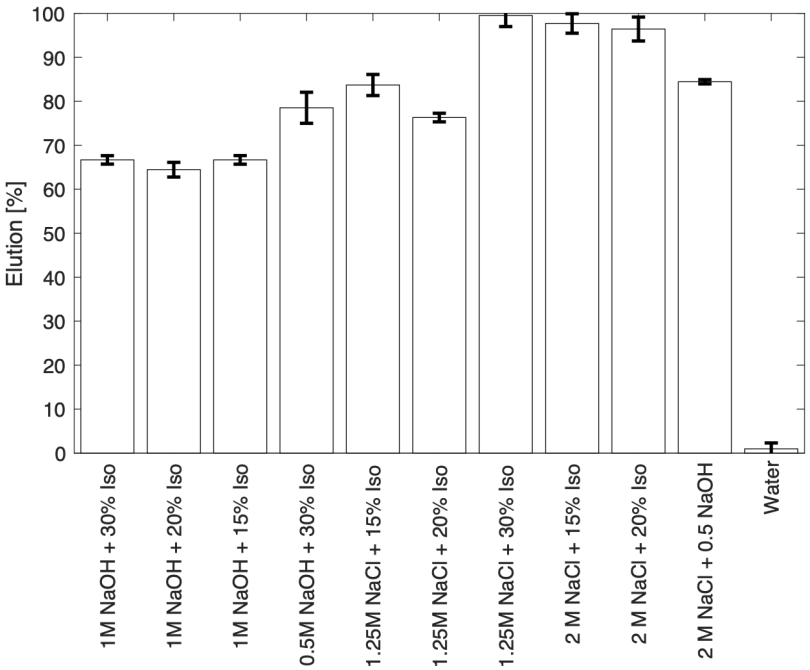


Figure 5-6 Elution of baker's yeast RNA from CC700 obtained from supernatants in static binding studies with different elution buffers; %Eluted RNA based on loading RNA

Difficulties to clean the media after chromatographic operations could be the reason why a reduction of NA concentrations prior to the application of cleared lysate to CC700 was recommended.

Attempts to determine the residual RNA contents still bound to CC700 after elution, via Orcinol assay proved unsuitable, as chemical reactions with the base matrix during sample incubation caused sample discoloration, preventing spectrophotometric analysis of the supernatants (Figure 5-7).

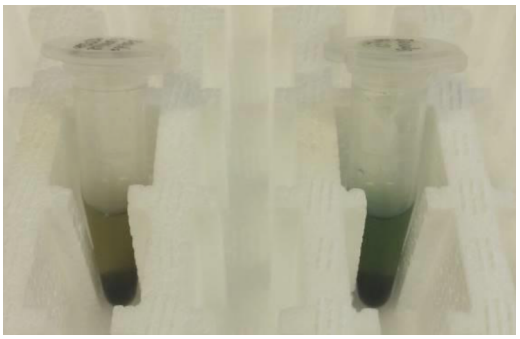

Figure 5-7 Discoloration of Orcinol sample after resuspension of 20 μL SBV CC700 in 200 μL of MQW, followed by incubation with working reagent at 95°C for 20 min and centrifuged at 14,000 rpm; elution buffer: 1.25 M NaCl, 30% isopropanol (left) and MQW (right)

## 5.3.2. Visualization and characterization of bilayered architecture

### 5.3.2.1. Environmental Scanning Electron Microscopic analysis and particle size distribution of Capto Core 700

To analyse the visual integrity of CC700, ESEM images of the media were recorded as described in 2.3.11.1. As sample preparation for ESEM via freeze drying was reported to cause bead disruption to the visual integrity of chromatography resins, the sample supports were dehydrated in ethanol followed by critical point drying (Nweke *et al.*, 2016).

Particle size distribution data was recorded on a Mastersizer 2000 as described in 2.3.13. The refractive index of the media was estimated at 1.43 resembling the value of pure agarose (following manufacturers suggestions).

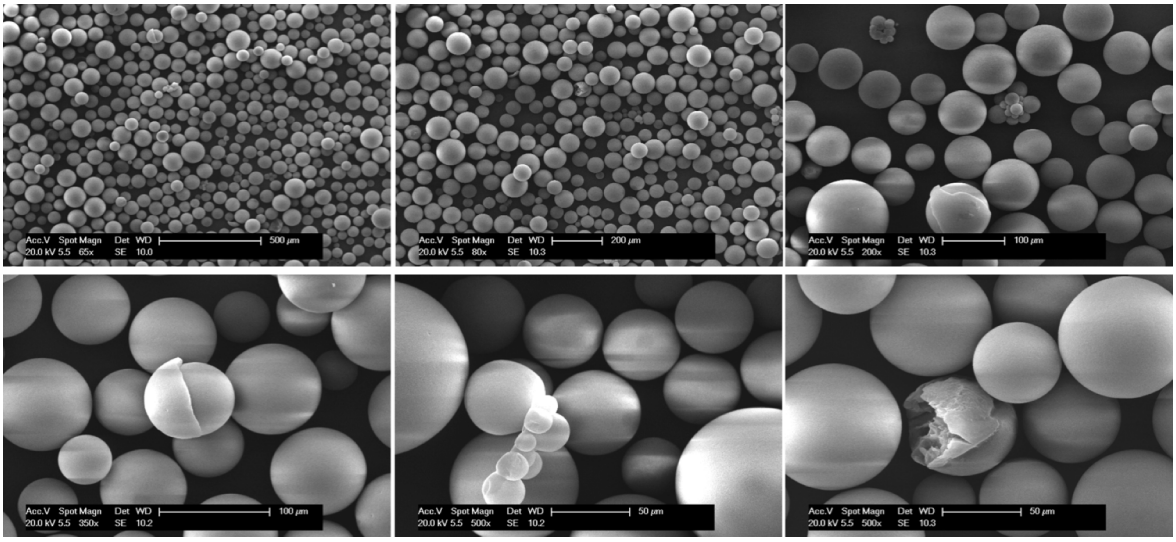

Figure 5-8 Scanning electron micrographs of Capto Core 700 media at different magnifications

Unlike other beaded chromatography media (see Chapter 3 for ESEM illustrations of Q Sepharose FF), the surfaces of the supports are very smooth without macropores leading into the internal structure of the beads (Figure 5-8). Furthermore, the vast majority of beads are spherical with very few 'misshaped' beads in the population suggesting that a lot of care was taken during the manufacturing process of the Capto base matrix. The split shell, that can be observed in some particles (Figure 5-8, bottom left & right), reveal the core structure of the media. The patterns give the impression to be due to mechanical disruption of support surfaces rather than originating from the production process of the agarose base matrix.

Overview images (Figure 5-8, top left/ middle) show that support particles are of very similar size, which was confirmed by PSD analysis (Figure 5-9). The population has a volumetric span of 0.792, corresponding to a very narrow and homogenous PSD (compared to other beaded chromatographic media: $span_{Q\ Sepharose\ FF}$= 0.995; $span_{Sepharose\ 6\ FF}$= 1.032; $span_{Sepharose\ CL\ 6B}$= 1.054).

$$span = \frac{d(v,0.9) - d(v,0.1)}{d(v,0.5)}$$

With a volume weighted mean of $D_{[4,3]}$ = 86.95 μm, the results confirm the manufacturers specification of the media (cumulative volumetric mean $d_{[50V]}$ = 83.3 μm vs '~90 μm' (GE Healthcare, 2012) or '~85 μm' (GE Healthcare, 2018c)).

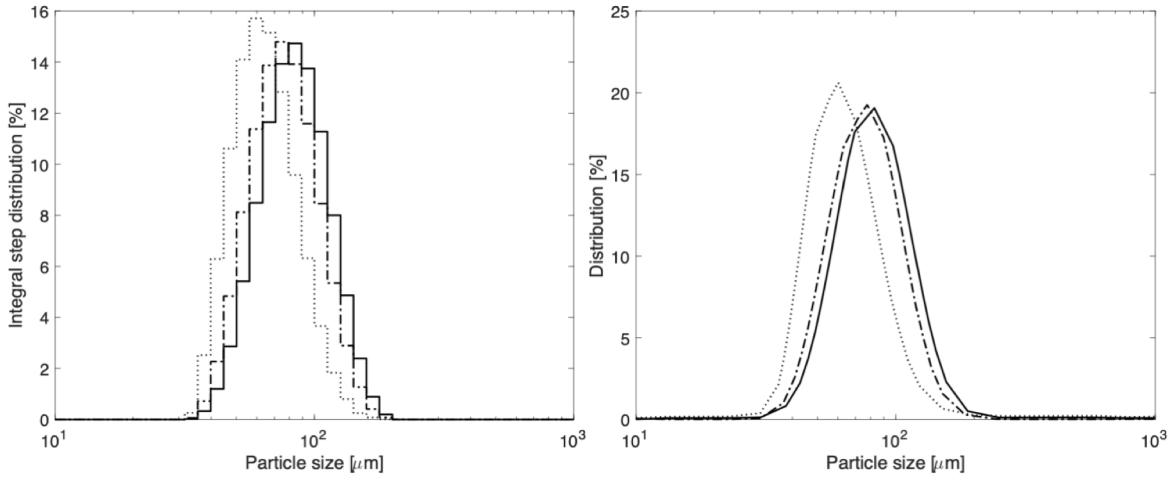


Figure 5-9 Particle size distribution functions of Capto Core 700; left: integral step distribution; right: size distribution; solid line- volumetric; dash-dotted line- surface weighted; dotted line- number weighted distribution

5.3.2.2. Light microscopic analysis

Illustrations of the working principle of the 'core bead technology' depict the shell of a different composition than the core. However, light microscopic images (Figure 5-10, A) suggest that the supports are of homogenous composition as no change in refractive index at the interface between core and shell can be observed. However, the applied optical tools may not be able to showcase a solid-solid interface with refractive indices being very similar (typical agarose concentrations of agarose supports range from 4-6%, with refractive indices of 1.3325 and 1.42 for water and agarose respectively (Hale *et al.*, 1973; Deane, 2013)).

Due to the multimodal nature of the octylamine ligand, dye molecules willingly bind to the core of CC700, highlighting the demarked zone devoid of ligands in the shell (Figure 5-10, B & C). The shell thickness of supports is between 5-10 μm. A thin shell is preferable for bilayered chromatography media to compromise as little as possible on core binding capacity. The manufacturer states static protein (ovalbumin) binding capacities of around 20 mg/mL SBV (GE Healthcare, 2012), which is low compared to AEC media with binding capacities more than two-three times higher (static BSA binding capacity was slightly higher with around 30 mg/mL; see Appendix A-6 for BSA binding isotherm of CC700).

As already observed in the ESEM images, a small fraction of the support population present deviations in their visual appearance, compared to the bulk of the media.

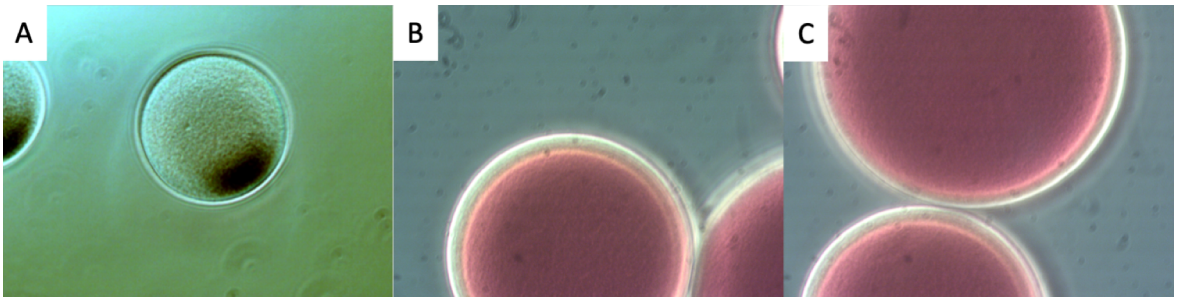


Figure 5-10 Light micrograph of single CC700 supports; A: in MQW; B&C: core stained with CR

Visual grading of CC700 media and quantification of disfigured supports as part of a larger population was conducted as described in 4.2.3. Figure 5-11 depicts the prevalence of misshaped supports in CC700. Overall the media has outstanding sphericity with only 2.6% of the supports showing major imperfections on their surfaces and very little binding of pDNA to surface exposed ligands is to be expected, which is in accordance with the chromatographic data (5.3.1. ).

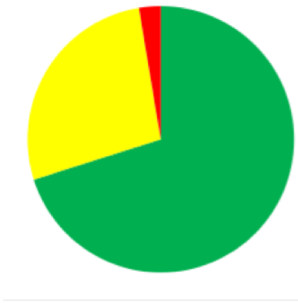

| | Green | Yellow | Red |
|---|---|---|---|
| Example support | 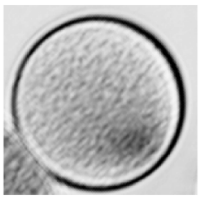 | 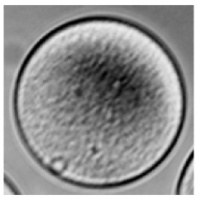 | 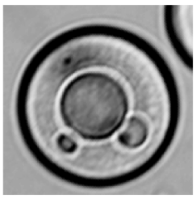 |
| % of total | 70.1 | 27.3 | 2.6 |

Figure 5-11 Visual grading and quantification of CC700 media as part of total population; red: supports with major surface imperfections (presumably) granting pDNA binding; yellow: minor surface impairments; green: spherical supports without any flaws on the surface; total number of beads analysed: 729

5.3.2.3. CSLM analysis of CC700 beads

BSA is, at 66.5 kDa small enough to pass through the pores in the shell of CC700. To visualise the binding behaviour and spatial distribution of protein binding in CC700, BSA was fluorescently tagged with CY-5 as described in 2.3.12, and loaded onto CC700 followed by CLSM analysis.

The fluorescence signals in Figure 5-12 confirm that BSA binding is limited to the core, while the ligand-free shell surrounding the charged core being visible in the respective light micrographs.

The thickness of the shell structure varies slightly across supports ranging from around 5 µm up to 15 µm. The ligands are evenly distributed inside the support, forming structures, with slightly different degrees of sphericity inside the supports.

ESEM analysis of CC700 media suggested, that misshaped beads may be able to bind pDNA by circumventing the size cut-off of the shell via direct exposure of ligands within the core to the surrounding buffer.

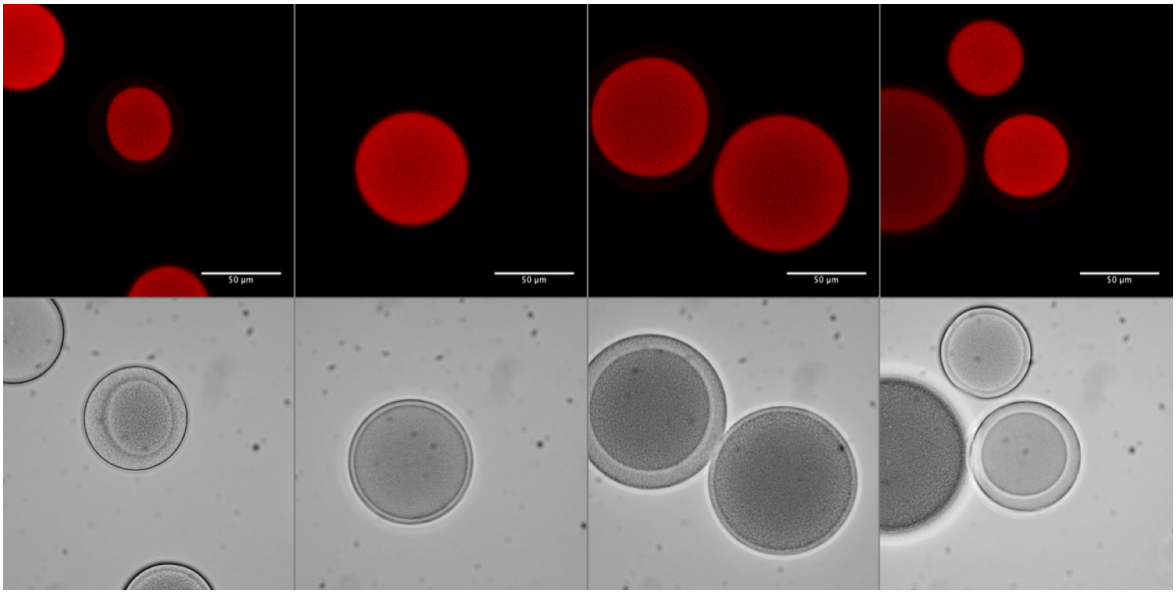

Figure 5-12 CLSM analysis of CC700 media incubated with CY-5 tagged BSA (top); respective light micrographs of single supports (bottom)

Analysing whether pDNA could potentially bind to irregularly shaped supports, CLSM was employed to trace both tagged BSA and pDNA in a single support (Figure 5-14). Against expectations, the entire support was surrounded by a thin green halo correlating to the fluorescence signal of tagged pDNA molecules. Although the size cut-off has prevented pDNA to penetrate through the pores on the surface, pDNA evidently was able to bind to the surface of the media.

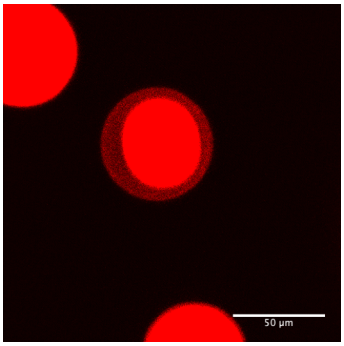

Figure 5-13 LUT/ threshold adjusted CLSM image of CC700, suggesting ligand presence in the demarked shell zone

Lowering the fluorescence threshold/ adjusting the look up table (LUT) of images from Figure 5-12 does suggest miniscule binding of tagged BSA within the 'ligand-free' zone surrounding the core (Figure 5-13). This faint glow may result from unspecific binding or indicate the presence of very low amounts of ligands in the shell. The strong negative charge of the sugar phosphate backbone of NA could, in conjuncture with minor amounts of octylamine ligand on bead surfaces, explain the presence of pDNA on the surface of CC700 supports (no penetration of pDNA into the shell due to pore size restrictions).

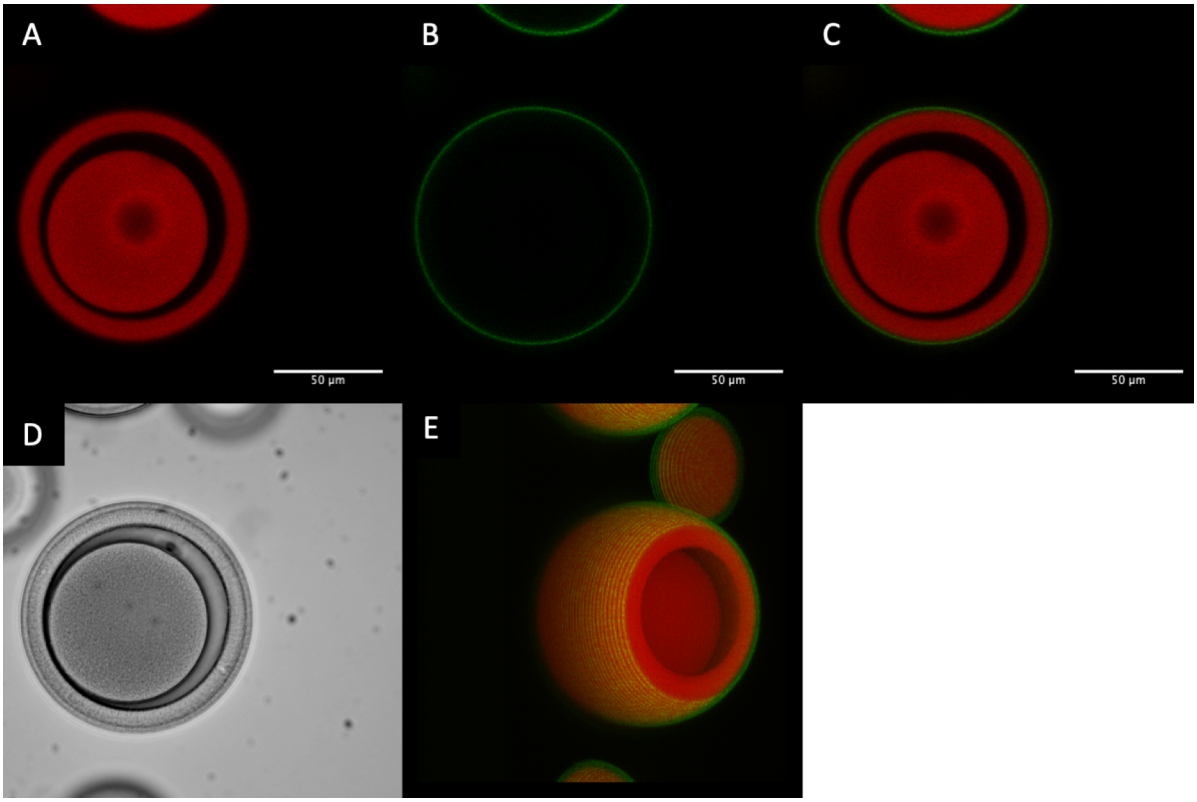


Figure 5-14 CLSM analysis of CC700 media post incubation with tagged CY-5 tagged BSA and Syto9 tagged pDNA; BSA fluorescence channel (A); pDNA Fluorescence channel (B); overlay of both channels (C); respective light micrograph (D); 3D stack projection of fluorescence signals (E)

The 3D projection in Figure 5-14, E showcases the structure of CC700, the pDNA highlights the brim of the support, while (separated by the shell) the BSA reveals the underlying stationary matrix lined with ligands.

To investigate the 'binding' of pDNA to the surface of CC700 supports, the media was incubated with Syto9 tagged pDNA solution for various lengths of time.

### 5.3.3. CLSM analysis of pDNA creeping into the shell of Capto Core 700 over time

Feeding cleared *E. coli* lysate onto a CC700 column in frontal loading chromatography experiments have suggested that the architecture of CC700 is not truly inert to pDNA binding. Furthermore, CLSM images of CC700 supports incubated with fluorescently tagged pDNA revealed that pDNA was able to bind to the surface of the supports when given enough contact time.

To investigate this 'creeping' over time, CC700 media was incubated with Syto 9 tagged pDNA solution, followed by incubation with CY 5 tagged BSA to visualise the shell region of the supports.

With a size cut-off of 700 kDa, IT14: pPR322-p170 (26.88 kbp) should not be able to diffuse through the inactive shell of CC700 due to size limitations (Ljunglof *et al.*, 1999; Gustavsson *et al.*, 2004; GE Healthcare Bio-Science, 2012).

The green pDNA 'binding halo', surrounding the supports in Figure 5-15 does however confirm that despite their large size, pDNA molecules do bind at surface of the supports. This suggests either (i) the presence of a small amount of octylamine ligands within the inactive shell of the media, or (ii) the presence of macropores with sizes >700 Da.

The molecular weight of proteins is dependent on their amino acid composition, as well as other factors. The size cut off of 700 kDa for the outer shell of CC700 correlates to proteins of around 5850 amino acid residues (120 g/mol) and a hydrodynamic radius of around 8-12 nm (Tyn *et al.*, 1990; CalcTool, 2008).

Several attempts have been made to explain pDNA permeation through nanopores in membranes via expanded plasmid elasticity (Ager *et al.*, 2009; Latulippe *et al.*, 2009; Arkhangelsky *et al.*, 2011). Although the reasons for transport are still not entirely explained, it was found that plasmids of 380 nm diameter can penetrate through pores as narrow as 10 nm under hydrodynamic pressure (Arkhangelsky *et al.*, 2008).

To confirm that the observed effect is due to pDNA binding and not a result of artefacts, caused by Syto-9, bound to pDNA molecules; CC700 media was incubated overnight with pDNA solution (50 μL SBV with 1 mL of 15 μg/mL pDNA solution). After washing the supports three times in MQW and buffering in TE buffer, the suspension was mixed with 5 μL of 5 μM Syto-9 solution (serially diluted from DMSO stock in MQW; same dye/bp ratio as CLSM) and CLSM images were taken as described in 2.3.12.

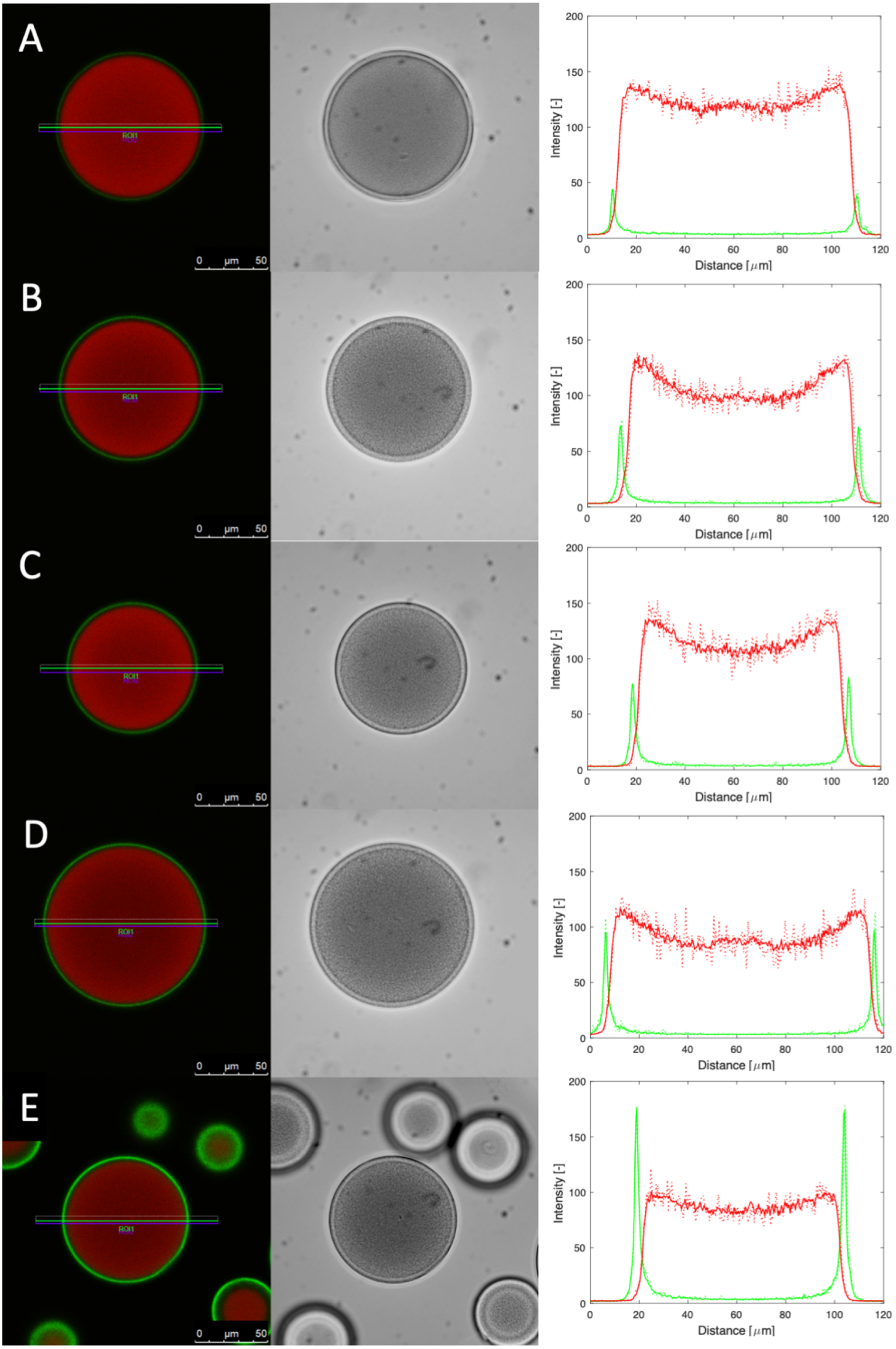


Figure 5-15 pDNA diffusion into the shell of CC 700 over time; left: overlay of CLSM channels for tagged BSA (red) and pDNA binding (green); middle: respective light micrograph of the support; right: plotted intensity traces along an 125x 1 µm ROI (dotted line) and 125x 5 µm ROI (solid line); After 10 min (A), 30 min (B), 60 min (C), 120 min (D) and overnight incubation (E)

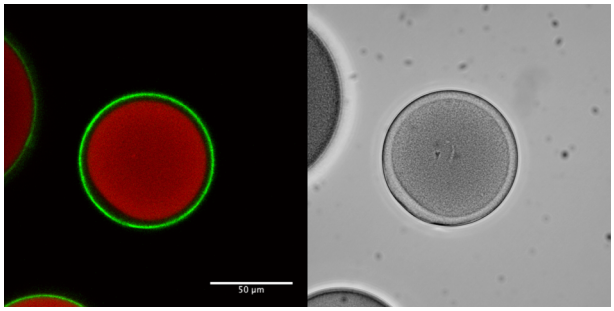


Figure 5-16 Penetration of pDNA into the shell of CC700 in the absence of fluorophore during incubation (addition of Syto-9 post incubation of supports with pDNA).
Left: CLSM emission image of the meridian stack of a CC700 support excited at 488 nm (Syto 9 tagged pDNA)
Right: respective light micrograph of the support

The green halo surrounding the support in Figure 5-16 confirms that pDNA binding to the shell of CC700 is independent of fluorophores tagged onto pDNA prior to static binding studies.

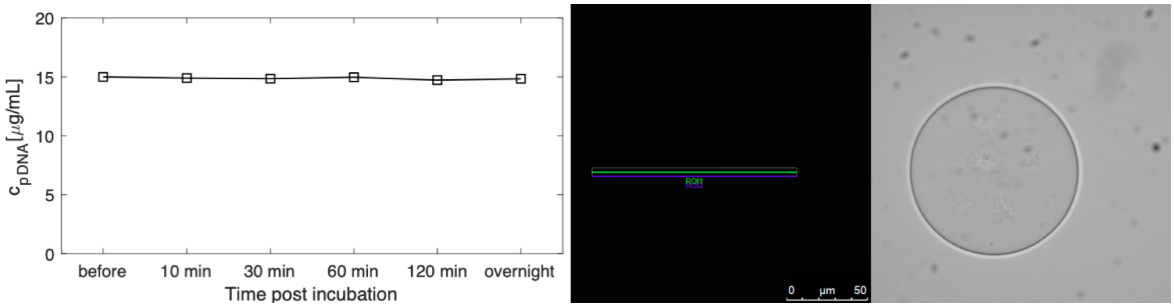


Figure 5-17 Plasmid concentration in supernatant of Sepharose 6 FF/ pDNA suspension over time; 50 µL of supports incubated with 1mL of pDNA solution (15 µg/mL), $OD_{260}$ measured over time (left)
Middle: CLSM image of Sepharose 6 FF after overnight incubation with tagged pDNA (no pDNA binding detected)
Right: Respective light micrograph of support

Incubating the SEC media Sepharose 6 FF with pDNA solution in the same way revealed that the concentration of pDNA in the supernatant did not diminish over time (Figure 5-17, left). Unlike the penetration of pDNA into the shell of CC700, CLSM confirms that no pDNA diffuses into the outer regions of Sepharose 6 FF supports (Figure 5-17, middle/ right).

After incubating CC700 supports with BSA prior to pDNA, in order to allow smaller protein molecules to quench residual octylamine ligands within the shell of the supports, the pDNA binding halo can still be observed, suggesting that stronger interactions of pDNA with the ligands compete with and supplant the BSA molecules.

### 5.3.4. Cold atmospheric pressure plasma treatment of Capto Core 700 to eliminate remaining surface binding sites

The SEC-AEC/ HIC architecture of Capto Core 700 has proven to be 'almost perfect', i.e. the outer layer of the supports is inert, surrounding an AIC/ HIC core.

However, when incubated with pDNA (especially for longer incubation periods) the media does bind low amounts of pDNA (Figure 5-14).

Light microscopy image analysis of chromatography media indicated that chromatography supports based on Capto base matrix were in terms of sphericity, lacking in imperfections and monodispersity the best base matrix for cold atmospheric pressure plasma treatment to eliminate surface binding of AEC media.

To investigate whether the remaining pDNA binding sites of CC 700 can be eliminated/ reduced, CC700 support samples were treated in the FBR as described in 2.3.5 using the parameters listed in Table 5-2.

Table 5-2 Plasma parameters for Capto Core 700 plasma treatment

| Power input [W] | SBV of supports [mL] | Treatment time [min] | Frequency [kHz] | Gas composition | Gas flow Rate [L/min] |
|---|---|---|---|---|---|
| **7** | 0.5 | 10 | 12.5 | helium CP grade | 0.75 |
| **9** | 0.5 | 10 | 12.5 | helium CP grade | 0.75 |

In previous experiments, it was observed that the incubation time of CC700 for static binding studies had an impact on the amount of pDNA bound to supports; static binding studies post plasma treatment were conducted for 30 min and 120 min incubation time with pDNA solution (1 mL; 15 μg/mL).

Incubation of CC700 with pDNA solutions in static binding studies for 30 min (binding 4.15 $\mu g_{pDNA}/mL_{SBV}$) yielded a binding capacity of around half cf. incubation for 120 min (8.4 $\mu g_{pDNA}/mL_{SBV}$), confirming the role of incubation time.

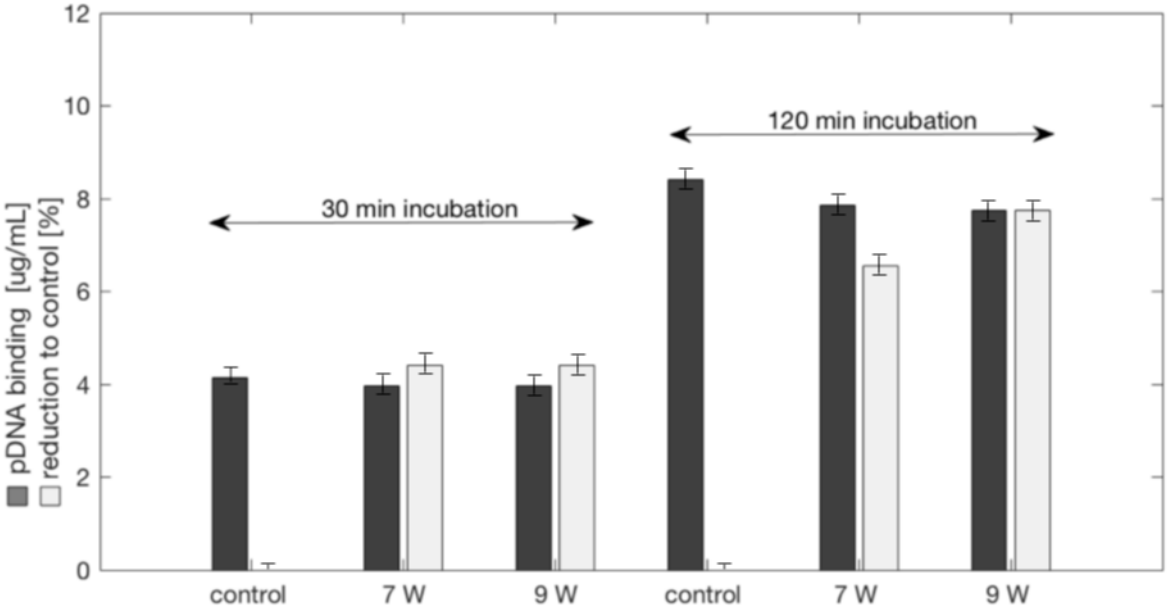


Figure 5-18 Reduction of static pDNA binding capacity of Capto Core 700 plasma treated chromatography supports (0.5 mL SBV; 10 min; 750 mL/min helium CP grade; 12.5 kHz)

Cold atmospheric pressure plasma treatment of CC700 supports was able to reduce pDNA binding capacities of supports in static binding studies (Figure 5-18). For the samples treated at 7 W, binding was reduced by 4% and 6.5% for 30 min and 120 min incubation, respectively. For higher power treatment (9 W) a similar reduction was observed with 4% reduction for 30 min incubation and 7.7% reduction for 120 min.

Although plasma etching and oxidation reduced the binding capacity of CC700 in all samples, the overall reductions are lower than seen previously with other base matrices/ligands. The reason for these low reduction levels may be that the high reactivity of ROS limits their efficacy when treating supports with very few (remaining) binding sites on the surface of the beads (maximum binding capacity of untreated control CC700 was 8.4 $\mu g_{pDNA}/mL_{SBV}$ in comparison to Q Seph FF with ~300 $\mu g_{pDNA}/mL_{SBV}$). Treatment of support samples with high ligand density on the surface requires plasma species to get to the proximity of a bead in order to find a reaction partner, while treating support particles with few remaining scattered ligands on the surface are statistically less likely to be 'found' by the plasma radicals within their short lifetime. So, although specific, the reaction is sterically hindered by the availability of suitable reaction partners.

For both power levels, samples incubated for 120 min show higher losses of pDNA binding than the 30 min samples. Longer incubation times lead to reorientation of pDNA on the surface (Diogo *et al.*, 2005), accommodating further molecules to adsorb to a binding region on the surface of a support. This effect was reduced by plasma etching suggesting that the limited binding sites have been etched, so longer incubation times do not lend themselves to higher pDNA binding (anymore).

CC700 has shown to have very few binding sites for pDNA to adsorb on its surface. However, the few remaining ligands lead to losses when using the media for pDNA purification.

Cold atmospheric pressure plasma etching and oxidation treatment of CC700 supports has been demonstrated to reduce the (limited) pDNA binding further by up to 7.7%. Depending upon the scale of operation, a plasma treatment of the media prior to its use in DSP may reduce the overall costs associated to the unit operation, where loosing less product due to undesired binding to the supports is only one of the advantages; CIP regimes need to be applied less often as column fouling becomes less of an issue, reducing 'dead time' in purification facilities during cleaning procedures.

## 5.4. Conclusion and suggested future work

The structure and working method of CC700 make the media ideal for purification of large pDNA molecules directly from crude cell lysates via negative adsorption chromatography.

Loading 80 mL of cleared lysate, containing the 26.88 kbp plasmid IT14: pPR322-p170 onto a 1 mL chromatography column packed with the SEC-MMC bilayered chromatography resin yielded no breakthrough of RNA/ HCP in the flow through fractions, despite the overall low binding capacity of the media (around 30 $mg_{BSA}/mL_{SBV}$). With minor amounts of pDNA co-eluted/ stripped from the column alongside captured impurities, the media performed well as a first capture step for pDNA from crude *E. coli* feedstocks in frontal loading chromatographic operations.

Light micrographs of beaded supports stained with negatively charged dye CR illustrate the bilayered topology of CC700, where the stained core is surrounded by a clearly defined shell of 5-15 μm and its narrow PSD suggests a careful crafting of the agarose beads, followed by several sieving regimes.

Plasmid DNA was found to bind to the 'inert' surface in static binding studies, especially after long contact times with the resin (>2 h). CLSM analysis of the binding topography of single supports, using labelled pDNA and BSA confirmed the presence of pDNA on the surface of the media. Monitoring pDNA accumulation over time yielded significant adsorption, with 160 $\mu g_{pDNA}/mL_{SBV}$ after overnight incubation of CC700 with a load of 300 $\mu g_{pDNA}/mL_{SBV}$ in static binding studies.

Applying a gentle cold atmospheric pressure helium plasma treatment (9 W; 14.5 kHz; 10 min treatment time) in a FBR was able to reduce the pDNA binding capacity of CC700 by up to 7.7% in static binding studies. The use of plasma etching and oxidation technology for altering the surface properties of chromatography resins, could provide a simple add-on treatment to reduce (remaining) surface binding ligands.

Overall, pDNA binding is very minimal for short contact times in frontal loading chromatography, making the use of CC700 a considerable option for capturing pDNA products directly from crude cell lysates, when operating at higher flow rates.

# Chapter 6 Concluding remarks and future work

Attempts to improve and control human life have fascinated medical scientists through the ages. To date, only a limited number of gene therapies have been approved by authorities for the treatment of human diseases.

Recent advances in gene therapy, however, have opened a door that could not only permanently influence the way we think, but ultimately who we as humans are. We may have already entered the age where human genetic augmentation is reality and even if it still may be a young field of scientific interest, the opportunities as well as potential consequences develop at a very quick pace.

Facing ethical questions associated to gene therapy, especially in non-somatic cells, which would allow genetic alterations to be passed on to future generations will become crucially important. Scientific interest deserves moral guidance provided by authorities and should not be left to companies or individuals to drive the speed of innovation.

Technical questions associated to the production of pDNA products to satisfy future market needs requiring large scale production facilities can, however, already be addressed today.

While new purification strategies are being developed, the use of packed bed chromatography is still the method of choice to face separation challenges.

Most chromatographic media for the purification of biotherapuetic products have, however, been designed for protein based products. Due to the porous structure of classical AEC adsorbents, pDNA binding is restricted to the supports' surface, resulting in poor column binding capacities.

Combining two DSP unit operations in size exclusion and anion exchange chromatography in a single chromatographic operation, using bilayered supports with a non-adsorptive, size selective shell, surrounding a charged core, has been shown to provide significant advantages for chromatographic separation of pDNA from chemically similar, but smaller contaminants from crude lysates.

The feasibility to prepare multifunctional bilayered SEC-AEC materials from commercially available AEC media in a 'top-down' approach by applying plasma etching and oxidation treatments to soft hydrogel support surfaces was investigated.

The oxidative potential of cold atmospheric pressure plasmas was used to selectively etch away binding ligands off the surface of commercial AEC adsorbents. Plasma treatments in a parallel plate DBD set-up with helium as carrier gas, have led to reductions of up to 85% pDNA binding capacity with SI values of up to 5.

Cold atmospheric pressure plasma treatment of AEC supports in a FBR set-up have shown to reduce surface over core binding capacity, with SI values up to 3.

ESEM images of plasma treated supports yielded that, unlike previously reported, cold atmospheric pressure plasma treatment is a gentle method, that does not alter the visual appearance of chromatographic supports during treatment.

Although plasma technologies are known to act at the nanoscale, the presented results suggest that effective penetration depths can run to several microns when applied to porous chromatography materials.

Applying CLSM analysis to simultaneously visualise the binding topography of BSA and pDNA, adsorbed to chromatography adsorbents, revealed limitations of the plasma etching and oxidation technique due to the presence of irregularities on the surface of single adsorbents.

Preparations of bilayered supports produced via 'bottom-up' approach of AGE activation-partial bromination, controlled by viscosity enhanced reaction-diffusion balancing, led to the creation of 'nice' supports in previous studies.

However, independent of associated parameters, all support preparations resulted in supports with a minimum 20% residual pDNA binding capacity, which could not be explained.

Investigation of the binding topography of pDNA and BSA to bilayered supports in CLSM, revealed that imperfections, as part of the overall sample population offer binding sites at particles' surfaces.

Quantification of the phenomena via analysis of light micrographs, revealed a heavy reliance on structural integrity of the starting media. Minor structural surface flaws were found to not contribute to residual pDNA binding of the media as they can be overcome by the creation of

the ligand-free zone, deep fissures and other disfigurations resulting from the manufacturing process account for residual pDNA binding.
Implementing the findings by selecting a more suitable base matrix consequently yielded SI values >300, corresponding to a 99% clearance of pDNA binding at the expense of only 4.3% loss of BSA binding capacity.

The commercial bilayered media Capto Core 700 was successfully implemented as a first capture step for purifying a 26.88 kbp plasmid from cleared *E. coli* lysate, with column binding capacity >80 $mL/mL_{SBV}$ before breakthrough.
Although the media performed well in frontal loading chromatography operations, static binding studies revealed that pDNA to bind to remaining octylamine ligands on the 'inert' surface of adsorbents, especially after longer incubation times.
These observations were confirmed by CLSM analysis of the binding topography of single supports, using Syto 9 and Cy5 as fluorescent markers for pDNA and BSA, respectively.
By applying a gentle cold atmospheric pressure plasma treatment using $He\text{-}O_2$ as a carrier gas in a FBR set-up, the pDNA binding to Capto Core 700 was reduced further by up 7.7%, providing a simple and inexpensive add-on treatment to reduce residual surface binding ligands of the media.

For future continuation of work in the field outlined in this thesis, the following points are suggested for consideration:

While exploring the main parameters, associated with cold atmospheric pressure plasma treatments for the selective alteration of surface properties of beaded chromatography support samples yielded valuable insights as to how the ROS interact with ligand structures on the surfaces of soft hydrogel chromatography supports, further parameters need to be investigated. By further optimising the parameters of cold atmospheric pressure plasma treatments to selectively reduce surface over core binding capacity, a boost in efficacy of the treatments is to be expected.

In the dye decolourization studies, the use of pure (cp grade) helium as a carrier gas has shown even more promising reduction levels than the recommended admixture found in the literature.

With surface imperfections creating difficult to reach areas for ROS hampering the etching and oxidation of surface ligands, more care should be taken when choosing the AEC starting media. Light microscopic image analysis has proven to be a suitable tool for evaluating batches prior to cold atmospheric pressure plasma treatment.

As nanoplex of choice throughout this study, pDNA was used. Due to its structural properties, having a high charge density, small residual 'binding-islands' are enough to retain the large molecules, especially when granting enough time for reorientation (like i.e. in static binding studies). By investigating further nanoplexes with lower charge densities, bilayered media produced following the outlined process, may be more suited cf. its pDNA counterpart.

With new bilayered media entering the commercial market, potential residual pDNA binding needs to be investigated prior to application of the media for pDNA purification. The use of Capto Core 700 as an initial capture step for purification of pDNA indicated pDNA binding to the commercial SEC-AEC supports. Although at this stage it seems unlikely that a full elimination of surface binding can be achieved by means of plasma etching and oxidation alone, the technique holds great promise as an add-on treatment targeting residual surface ligands on bilayered beads manufactured via different approaches.

The use of more suitable starting media for the manufacturing of bilayered supports following the VE-RDB approach has shown to provide significant selectivities of surface over core binding reduction. Without the necessity to 'cover up' imperfections on supports surfaces, the thickness of the cleared layer should be considered. An estimated layer thickness of 5 μm is expected to compromise very little on core binding capacity, while the non-adsorptive layer is thick enough to prevent binding of large nanoplex products.

In order to reduce the loss of core binding capacity even further, the use of big bead SEC starting media, available from various suppliers should be considered, as layers of several micrometres devoid of ligands have less of an impact on core binding due to the beneficial surface to volume ratio in spheres with larger diameters.

In addition to the points outlined above, a piece of advice related to handling small quantities of beaded chromatography media (i.e. for static binding studies); when pipetting small volumes of SBV supports it is highly advised to prepare 10x suspensions using large pipettes. Around the nozzle of the pipette, liquid drag on the particles can lead to over-/under pipetting, so in order to grant equal sample sizes, slow liquid ejection is crucial while preventing bead settling within the pipette tip.

# Appendix

## A 1. Bacterial growth curve of *E. coli* (DH5α) containing plasmid IT14: pPR322-p170

The production of plasmid containing cells was conducted as described in 2.3.2. The fermentation was terminated after the cells had reached the late exponential stage (final $OD_{600}$ 8.55).

The overall yield was 65 g wet cell paste or 16.25 g/$L_{medium}$.

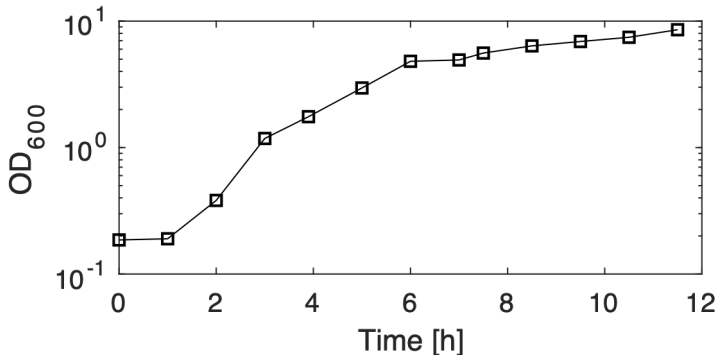


Figure A-1 Growth curve of DH5α *E. coli* containing plasmid IT14: pPR322-p170 batch fermentation for the production of pDNA solution for binding studies as well as frontal loading chromatography experiments

## A 2. Calibration standard curve for fluorometric pDNA quantification

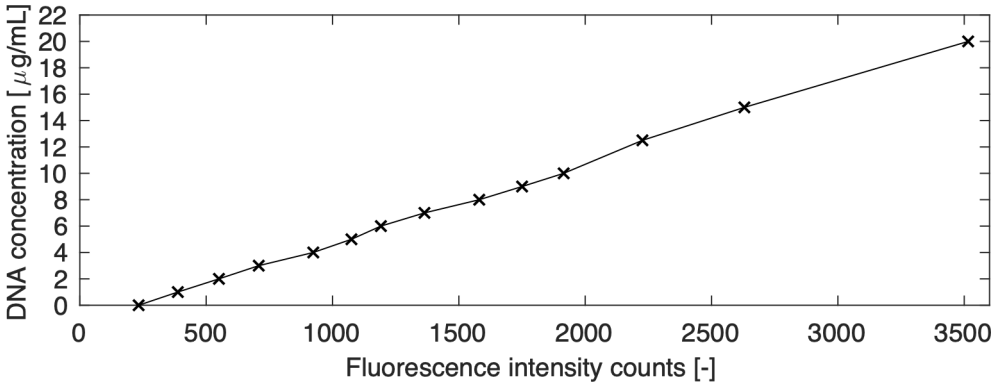


Figure A-2 Standard curve of ct DNA tagged with Hoechst dye 33258 and analysed as described in 2.3.8.2

## A 3. Plasmid map of pBR322-P170

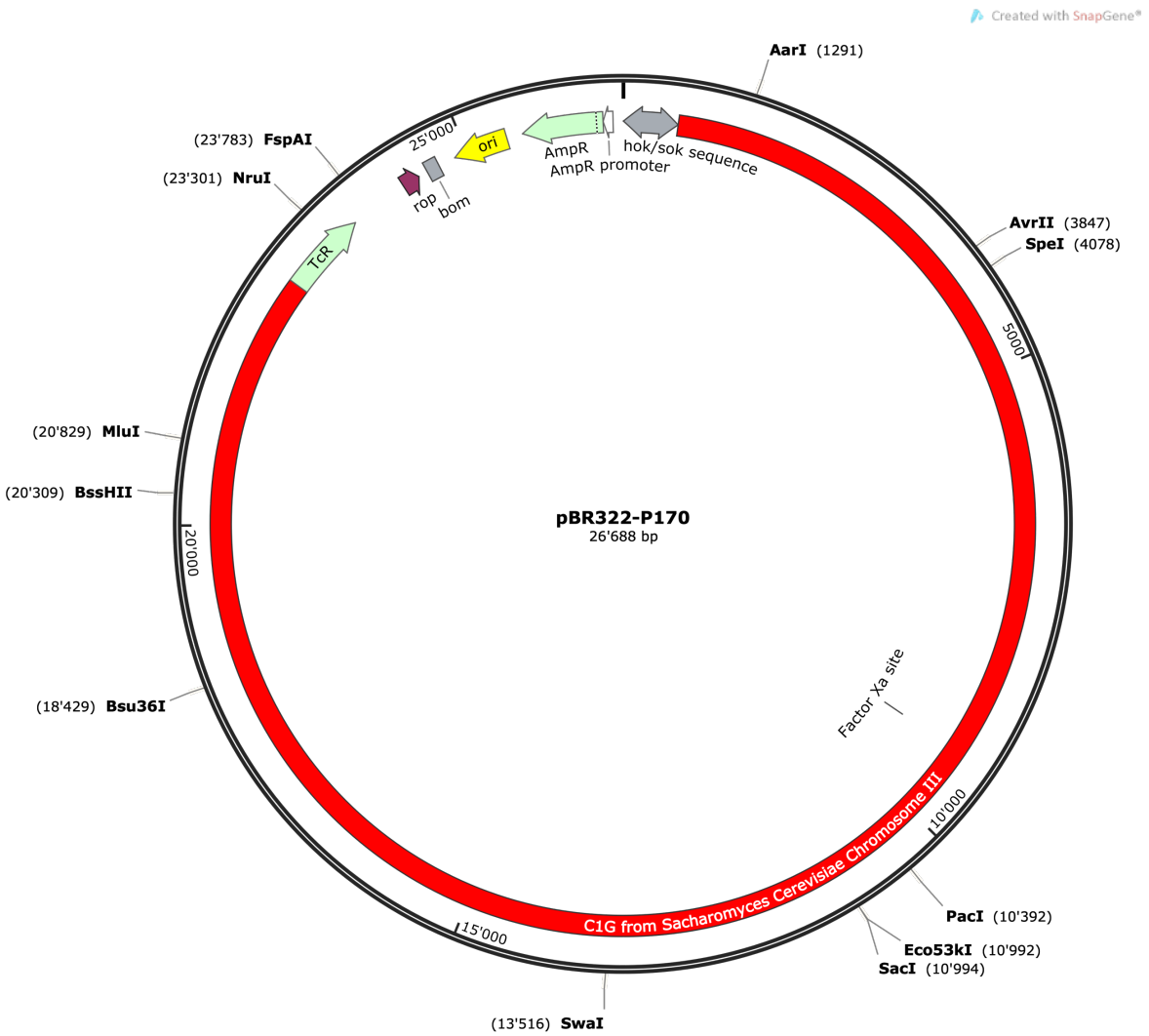


Figure A-3: Plasmid Map of pBR322-P170 containing a hok/sok sequence (579bp), a tetracycline efflux protein conferring Tetracycline resistance (900 bp), a rop sequence encoding for the rop protein, which maintains the plasmid at low copy numbers (192 bp), a pBR322 basis of mobility region (bom, 141 bp), a high-copy-number ColE1/ pMB1/ pBR322/ pUC origin of replication (ori, 589 bp), and an Ampicillin resistance cassette consisting of the β-Lactamase gene (AmpR, 861 bp) under control of the AmpR-promoter (105 bp). The C1G-insert comprises a BamH1 inserted 22118 bp stretch from the Saccharomyces Cerevisiae chromosome III

## A 4. Supplementary data of TOF-SIMS experiments

Figures A-4 to A-6 comprise of supplementary data collected during TOF-SIMS analysis of plasma treated Q Sepharose FF. All figures are referenced in their respective sections in 3.3.2.17.

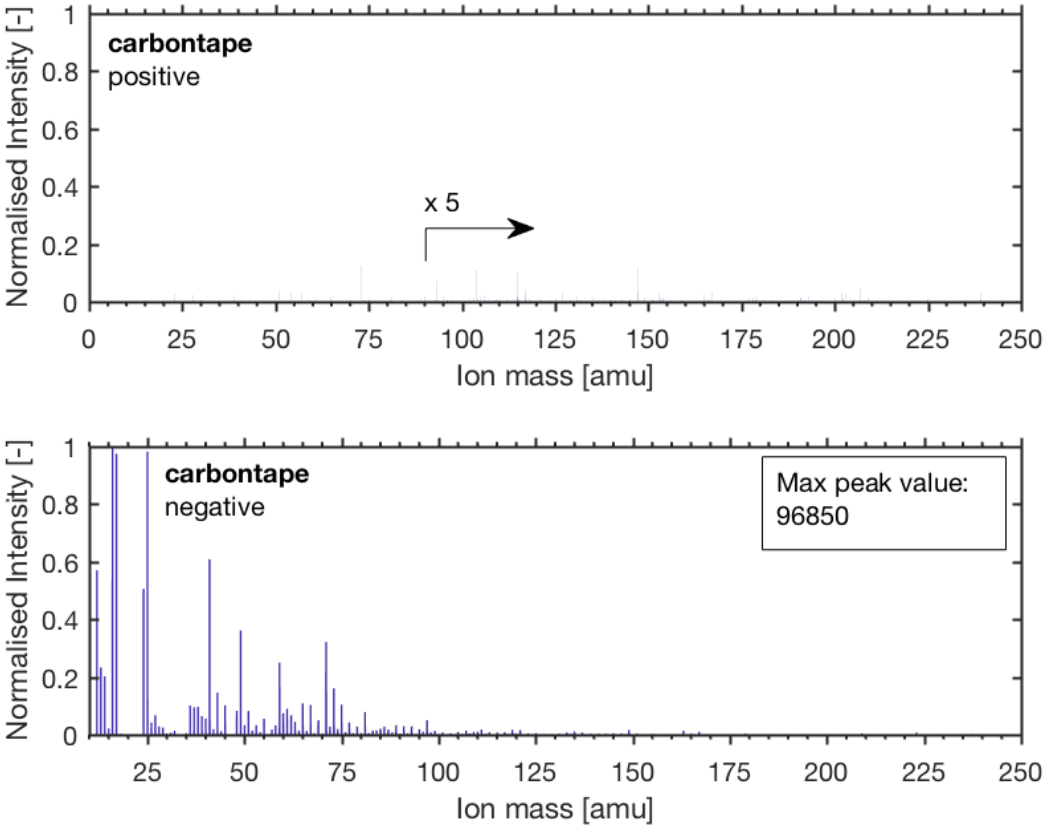


Figure A-4: Positive (top) and negative (bottom) TOF-SIMS spectra of carbontape background

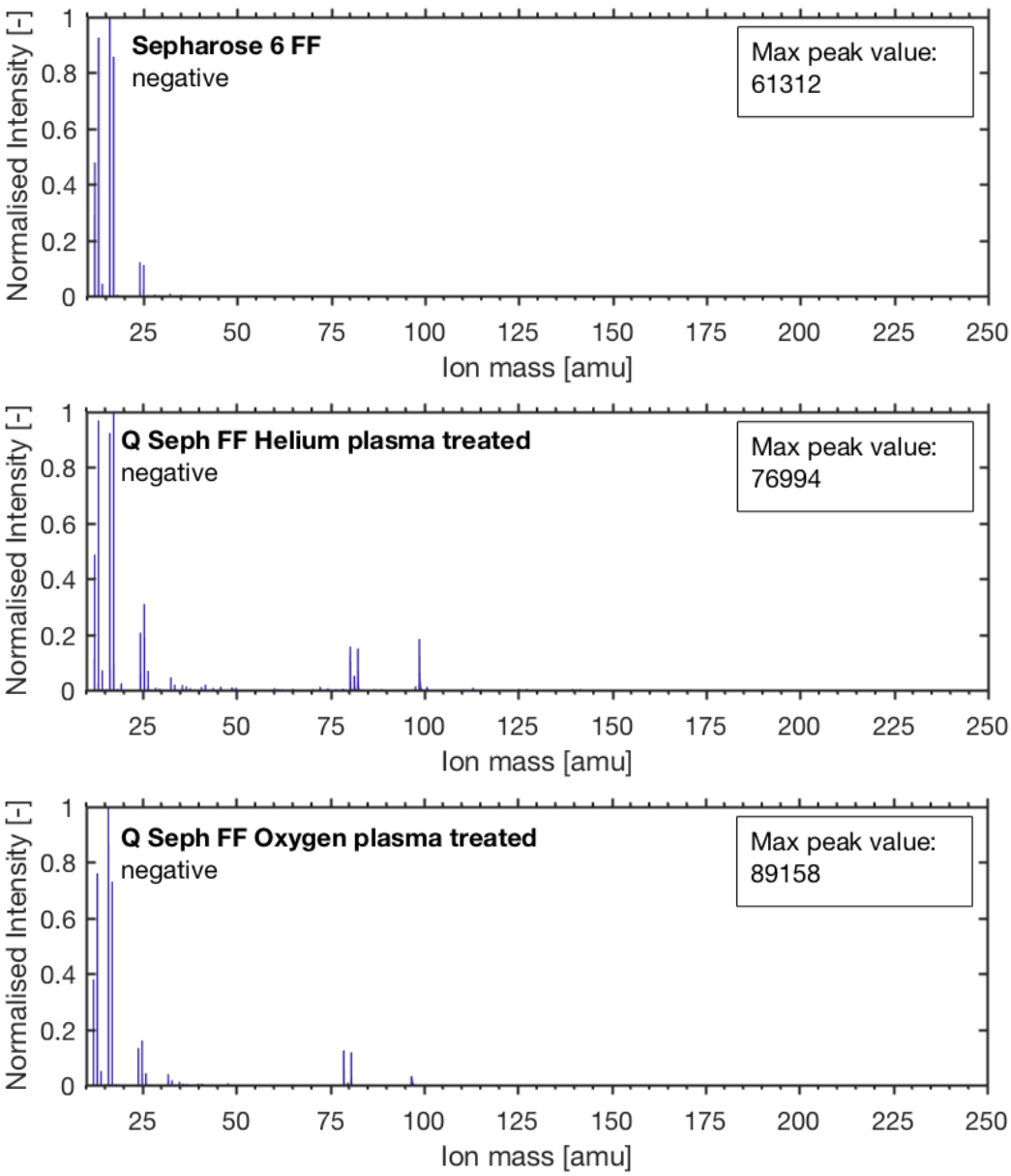


Figure A-5: Negative TOF-SIMS spectra of Sepharose 6 FF (top), Q Sepharose FF plasma etched with He-$O_2$ (99.5-0.5% v/v) (middle) and pure Oxygen (bottom) plasma (see 3.3.2.17. for details)

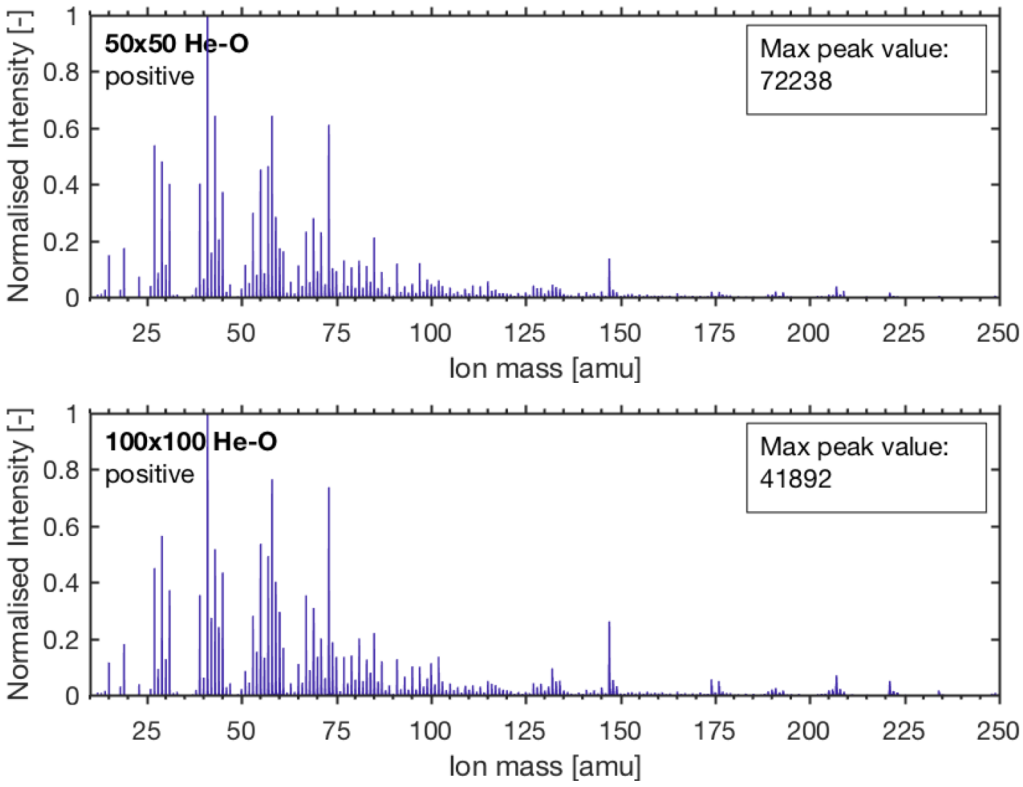


Figure A-6: Positive TOF-SIMS spectra of Q Sepharose FF treated with He- $O_2$ gas (99.5%- 0.5%) plasma (20 V; 150 s; 12.5% SBV); analysis area of 50 x 50 μm (top) and 100 x 100 μm (bottom)

## A 5. Decomposition of azo dye solutions in FBR

Initial scouting experiments for parameters of the FBR were conducted by plasma treating aqueous azo-dye solutions (MO and CR). Although not directly transferable to the etching and oxidation of soft gel chromatography supports, it yielded valuable insights into the efficacy of the generated ROS.

Figure A-7 depicts the native spectra of CR and MO in aqueous solution. The spectra are stable over time, with no alteration detectable after 10 days.

Plasma treating MQW (followed by immediate mixing of the 'ROS solution' with MO solution) was not able to generate a 'ROS solution' able to alter the absorbance spectrum of MO (Figure A-8).

Applying cold atmospheric pressure plasma generated from pure helium gas to MO solutions (20 μg/mL) revealed that longer treatment times lead ultimately to the largest peak reductions over time (Figure A-9). A treatment time of 10 min let to full decolourisation of the solution after 5 days.

Applying He-$O_2$ admixed gas plasmas (99.5%-0.5%) led to similar trends with overall slightly reduced decolourisation efficacies in comparison to the samples treated with plasma using pure helium as a carrier gas (Figure A-10).

Even after 5 days incubation post plasma treatment using pure oxygen gas plasmas, none of the MO absorbance spectra showed any effect, concluding that plasmas generated from pure oxygen gas are unable to provide ROS necessary for decolouring MO (Figure A-11).

Figures A-12 to A-14 depict the changes cold atmospheric pressure plasmas have on CR solutions using the same parameters and experimental set-up as for MO solutions. All trends observed with the MO spectra repeat itself in the CR solutions.

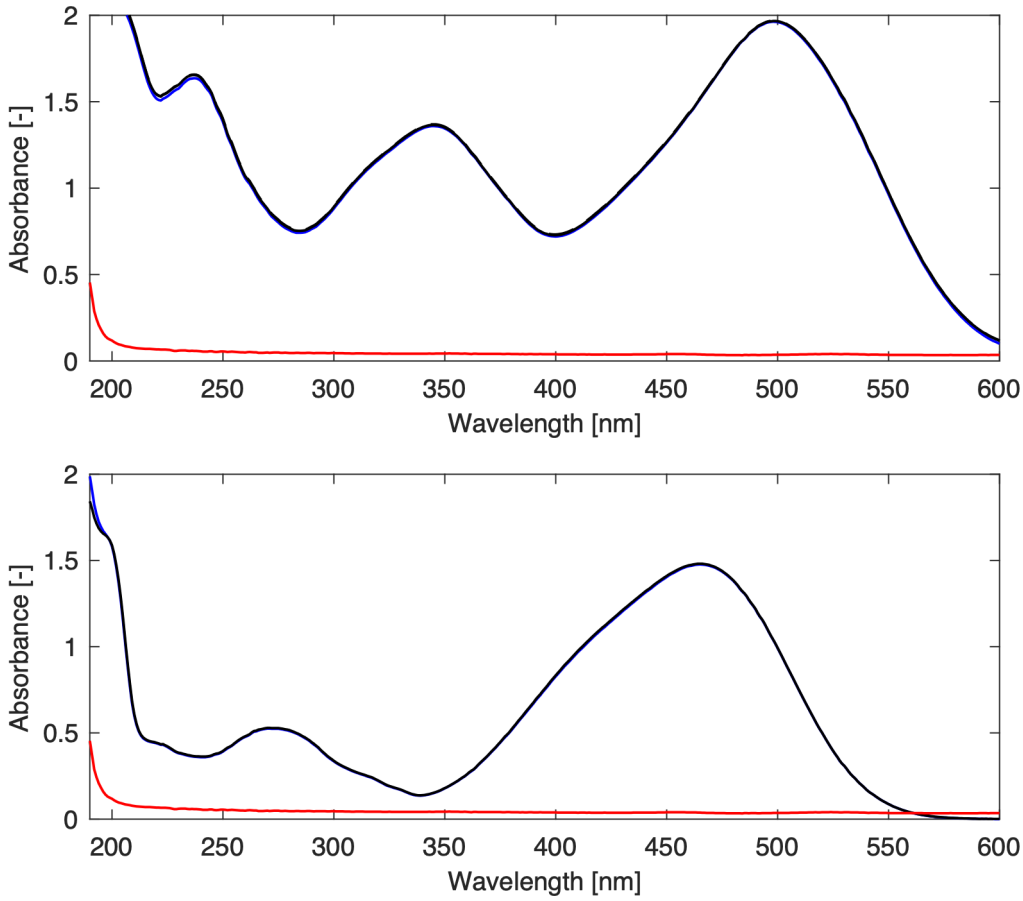


Figure A-7: Absorbance spectra of azo dye solutions of CR (top) and MO (bottom), initial (blue line) and after 10 days (black line); absorbance corrected by background spectra of MQW in quartz cuvette (red line)

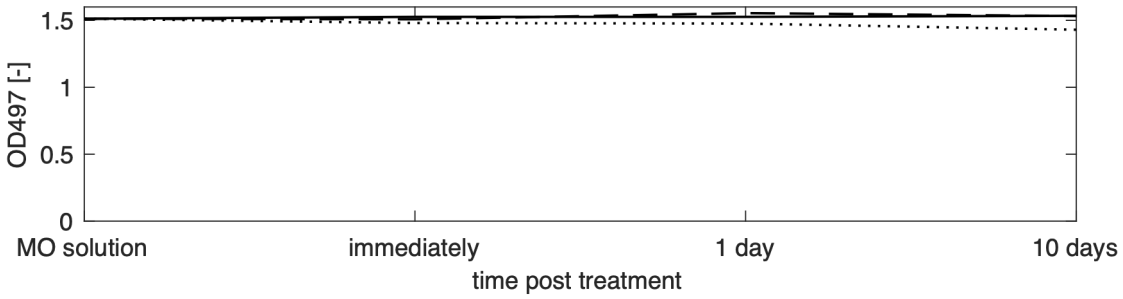


Figure A-8: Peak absorbance of MO solution after contact with pure gas plasma treated MQW (5 min treatment time); oxygen 7 W (solid line), 10 W (dashed line); 7 W Helium (dotted line)

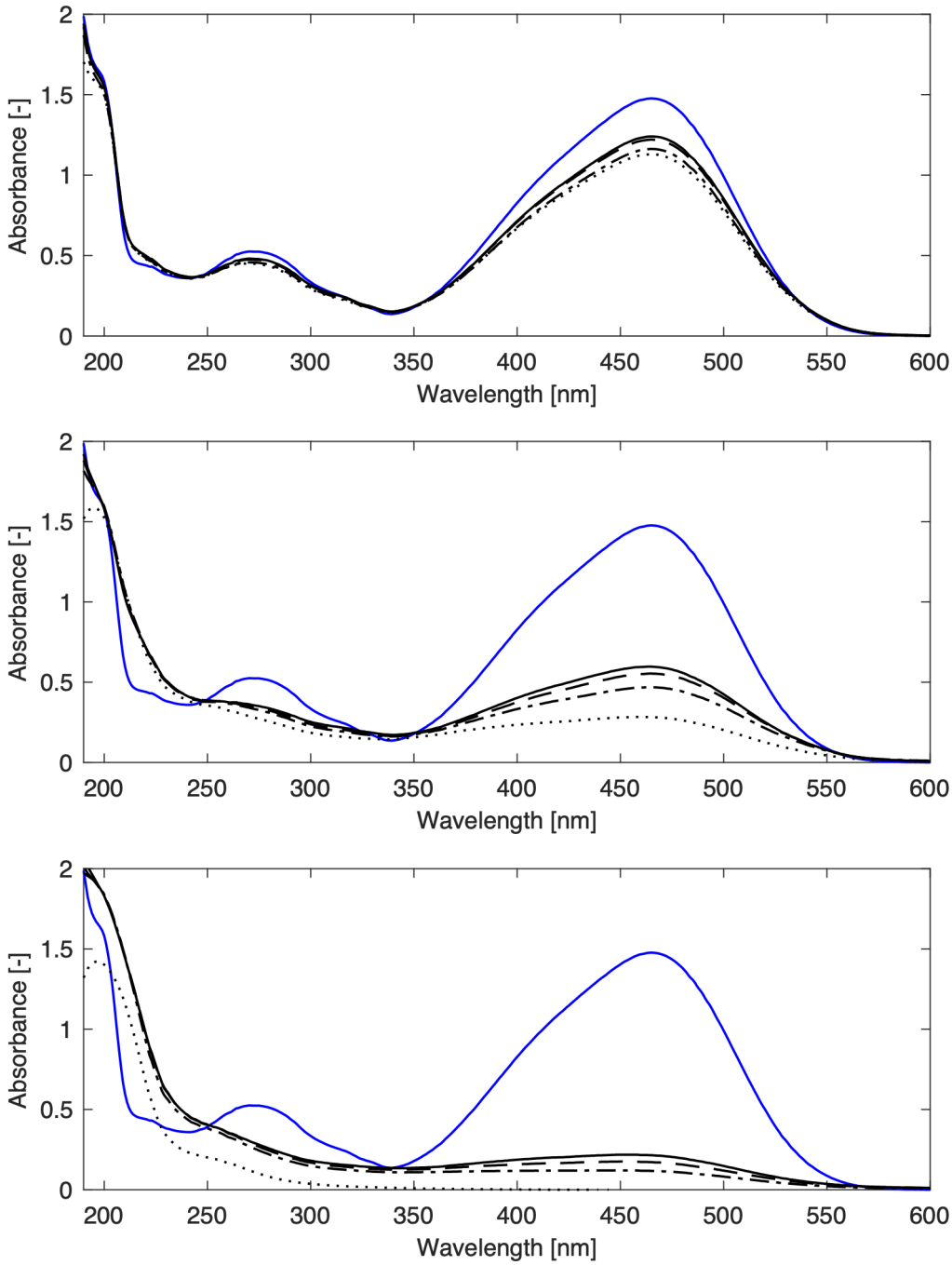


Figure A-9: Time resolved effects of cold atmospheric pressure helium plasma treatment of MO solution (20 µg/mL) for different plasma treatment times (top: 1 min; middle: 5 min; bottom: 10 min) Spectrum of MO (UV-visible), pre-plasma treatment (blue line); immediately after the plasma treatment (solid line); after 1 h (dashed line); after 24 h (dash-dotted line); after 5 days (dotted line)

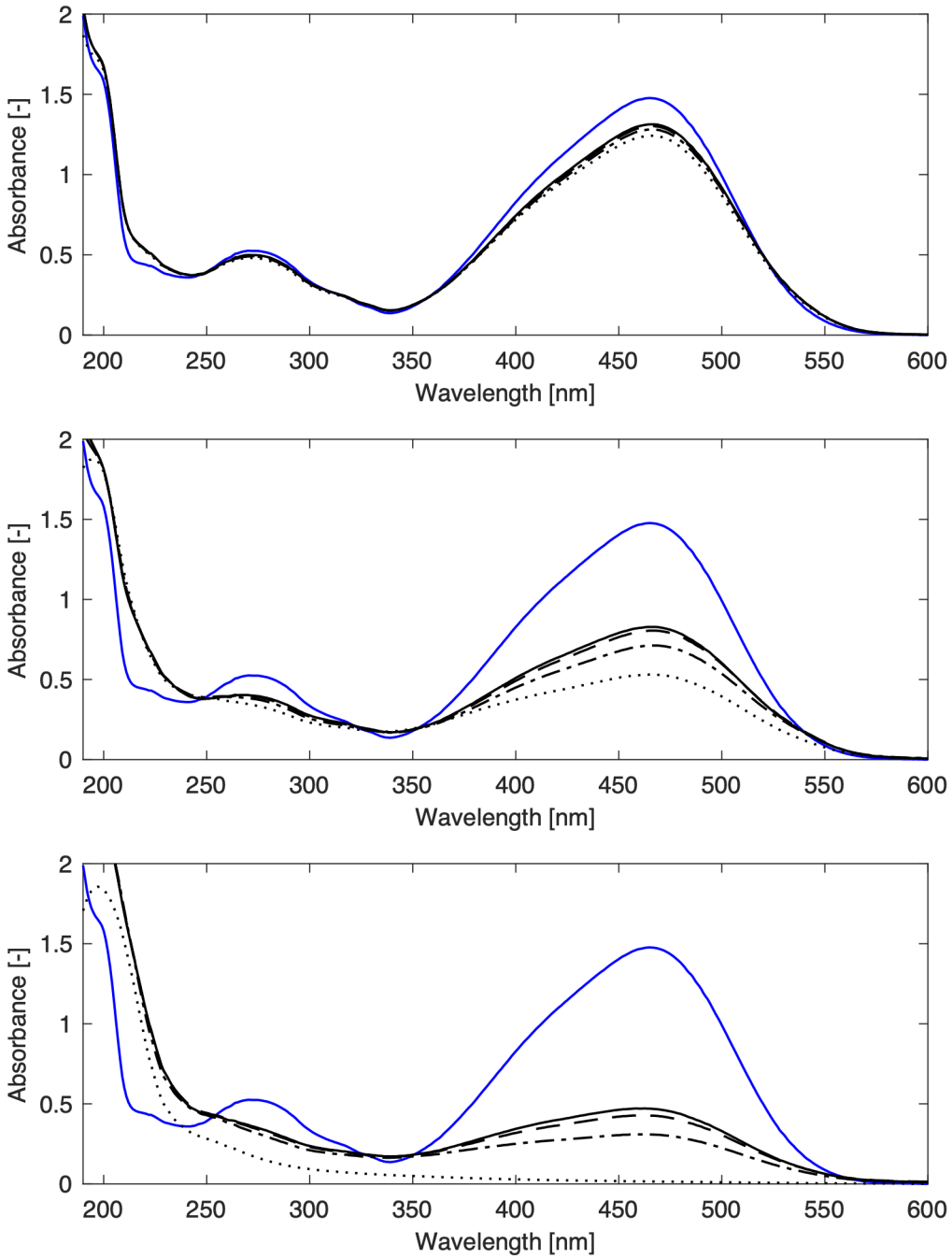


Figure A-10: Time resolved effects of cold atmospheric pressure He-$O_2$ (99.5%-0.5% v/v) plasma treatment of MO solution (20 µg/ mL) for different plasma treatment times (top: 1 min; middle: 5 min; bottom: 10 min)
Spectrum of MO (UV-visible), pre-plasma treatment (blue line); immediately after the plasma treatment (solid line); after 1 h (dashed line); after 24 h (dash-dotted line); after 5 days (dotted line)

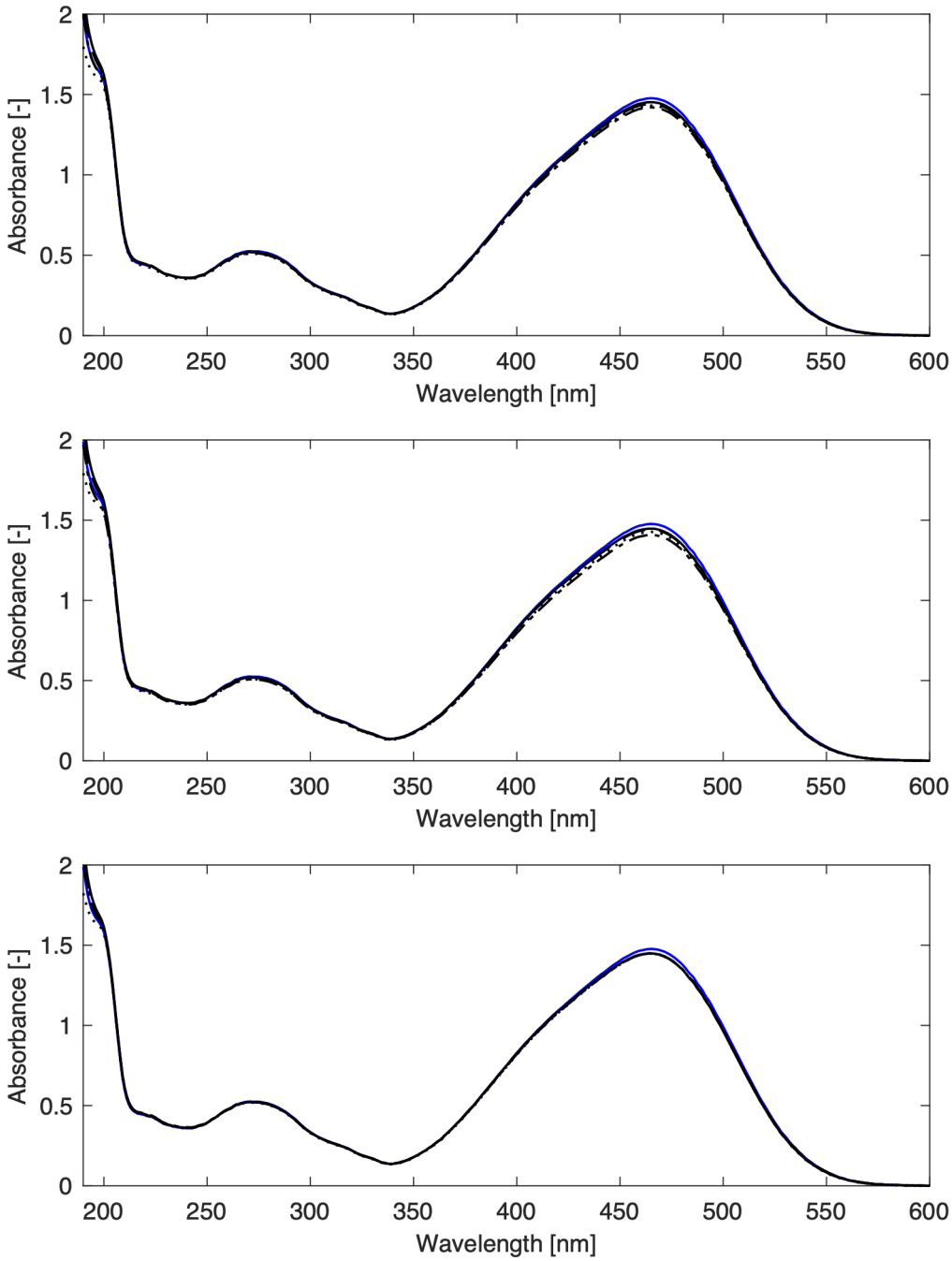


Figure A-11: Time resolved effects of cold atmospheric pressure oxygen plasma treatment of MO solution (20 µg/mL) for different plasma treatment times (top: 1 min; middle: 5 min; bottom: 10 min) Spectrum of MO (UV-visible), pre-plasma treatment (blue line); immediately after the plasma treatment (solid line); after 1 h (dashed line); after 24 h (dash-dotted line); after 5 days (dotted line)

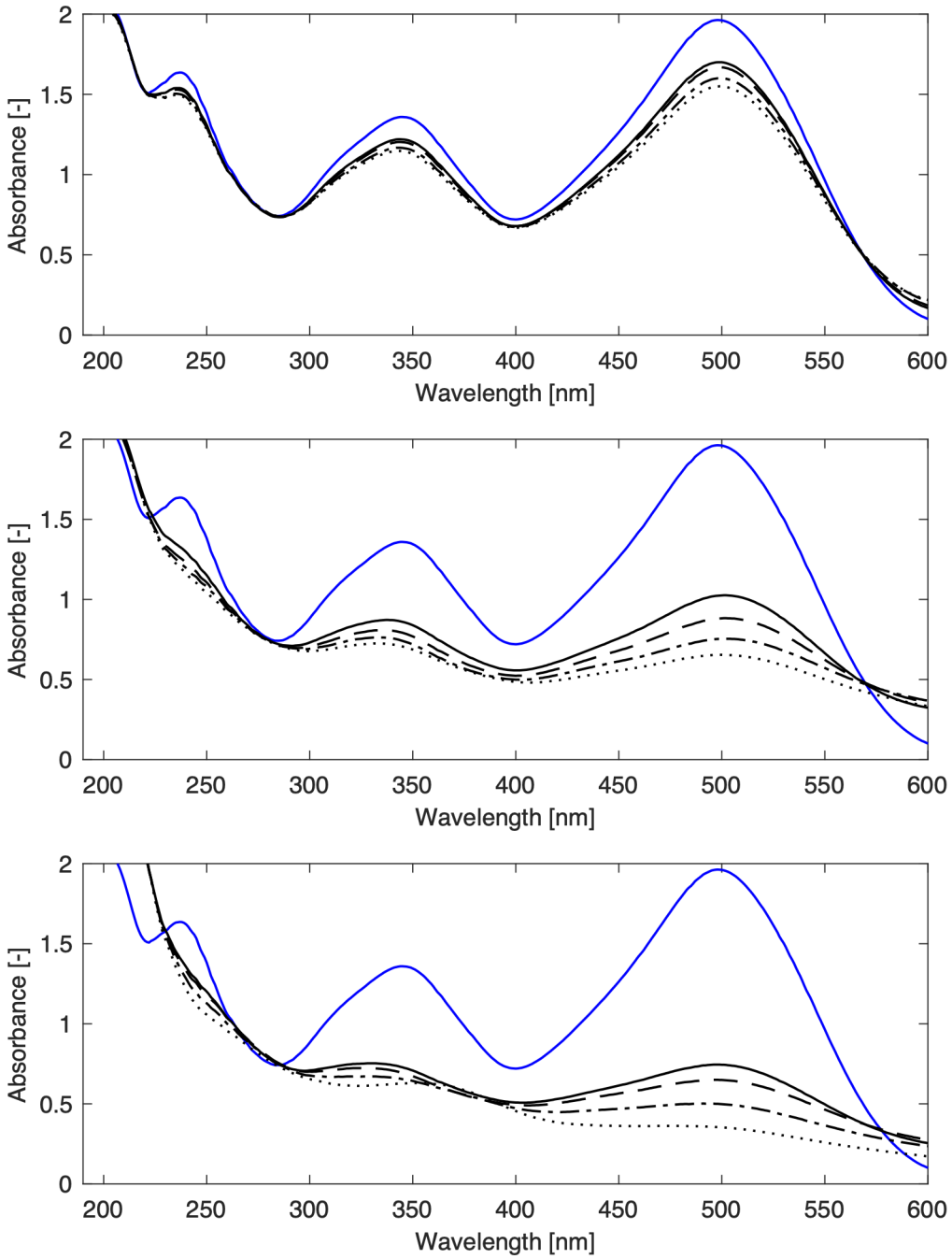


Figure A-12: Time resolved effects of cold atmospheric pressure helium plasma treatment of CR solution (1.073e-5 mol/L) for different plasma treatment times (top: 1 min; middle: 5 min; bottom: 10 min) Spectrum of CR (UV-visible), pre-plasma treatment (blue line); immediately after the plasma treatment (solid line); after 1 h (dashed line); after 24 h (dash-dotted line); after 5 days (dotted line)

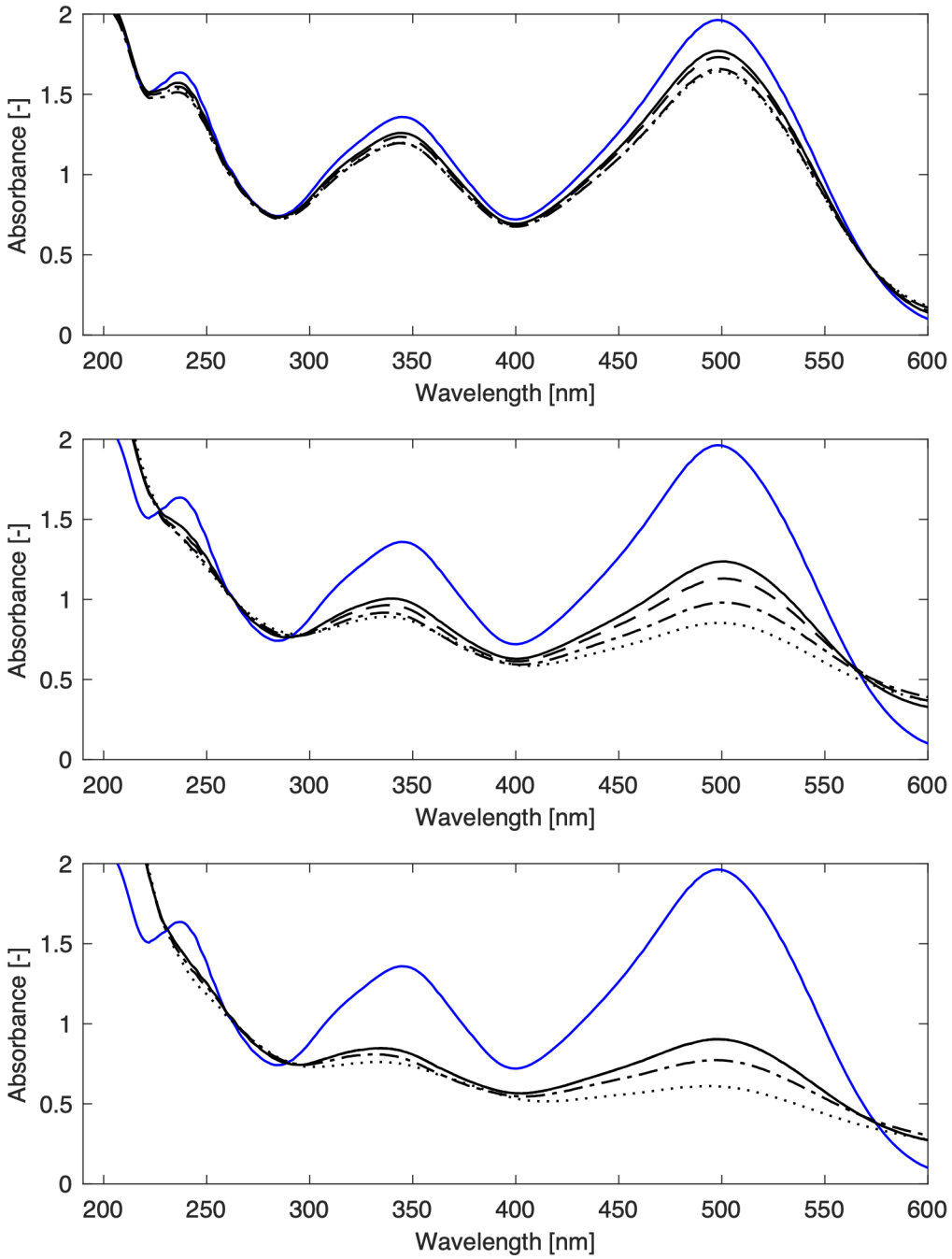


Figure A-13: Time resolved effects of cold atmospheric pressure He-$O_2$ (99.5%-0.5% v/v) plasma treatment of CR solution (1.073e-5 mol/L) for different plasma treatment times (top: 1 min; middle: 5 min; bottom: 10 min)
Spectrum of CR (UV-visible), pre-plasma treatment (blue line); immediately after the plasma treatment (solid line); after 1 h (dashed line); after 24 h (dash-dotted line); after 5 days (dotted line)

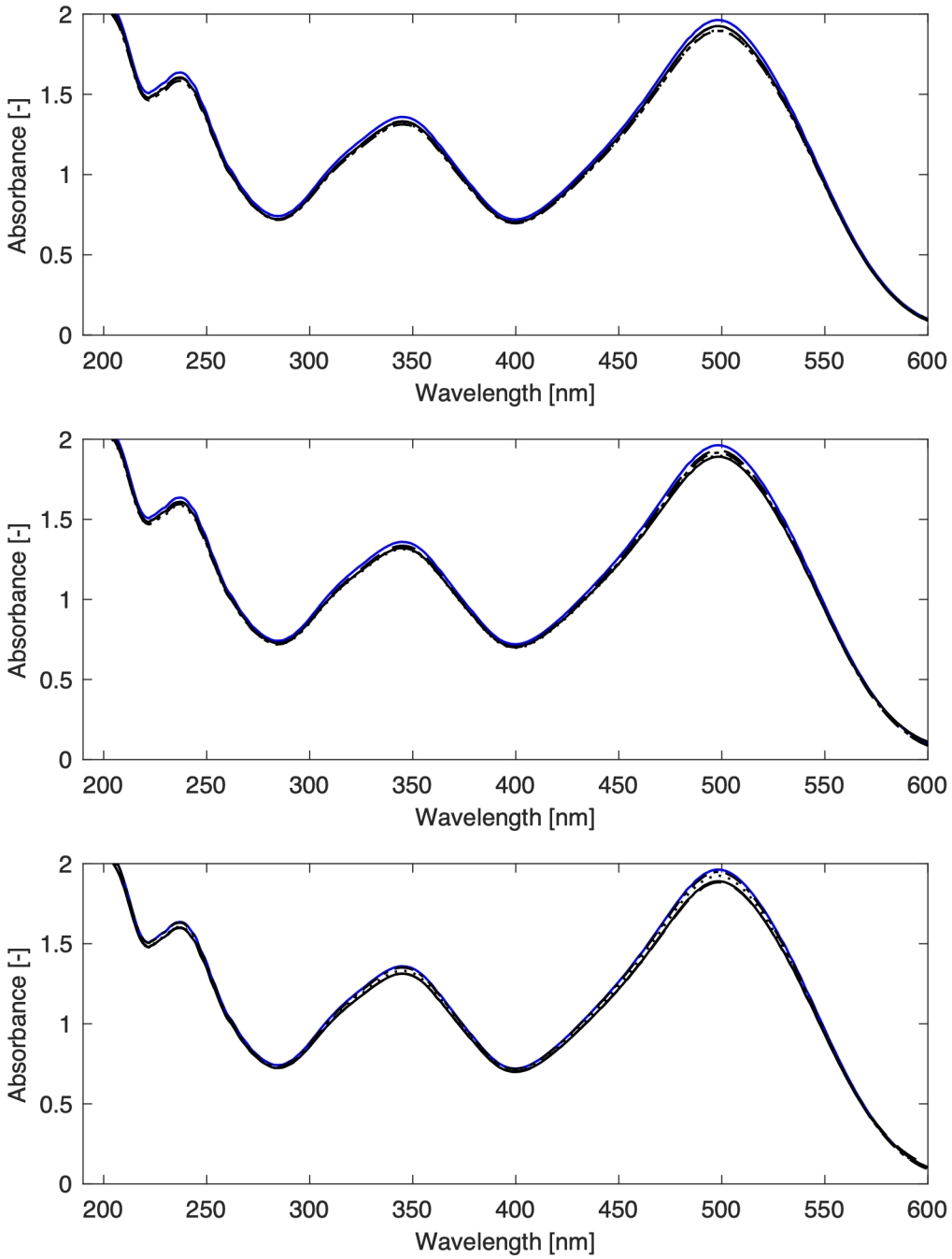


Figure A-14: Time resolved effects of cold atmospheric pressure oxygen plasma treatment of CR solution (1.073e-5 mol/L) for different plasma treatment times (top: 1 min; middle: 5 min; bottom: 10 min) Spectrum of CR (UV-visible), pre-plasma treatment (blue line); immediately after the plasma treatment (solid line); after 1 h (dashed line); after 24 h (dash-dotted line); after 5 days (dotted line)

## A 6. Protein binding isotherm of CC700

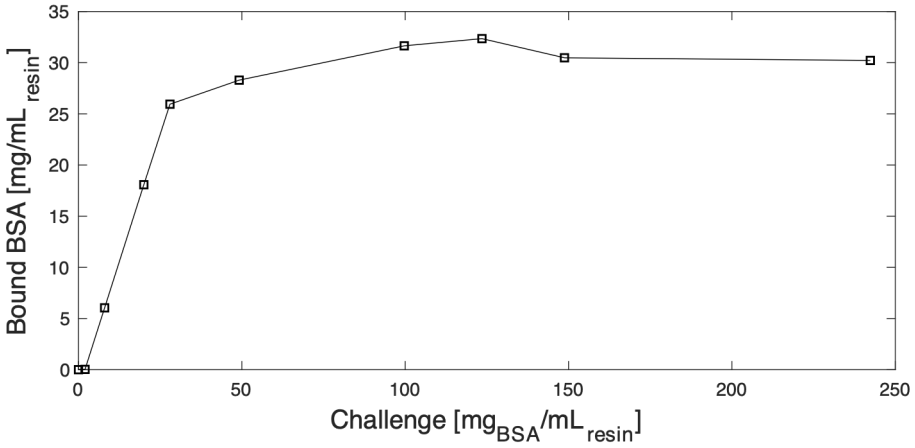


Figure A-15: BSA binding isotherm of CC700

# Bibliography


Abdulrahman, A. and Ghanem, A. (2018) 'Recent advances in chromatographic purification of plasmid DNA for gene therapy and DNA vaccines: A review', *Analytica Chimica Acta,* 1025, pp. 41-57.

Adielsson, P., Soderman, T. E. and Akerblom, A. 2018. Method for endotoxin removal. Google Patents.

Ager, K., Latulippe, D. R. and Zydney, A. L. (2009) 'Plasmid DNA transmission through charged ultrafiltration membranes', *Journal of Membrane Science,* 344(1), pp. 123-128.

Akhtar, S. (2005) 'Non-viral cancer gene therapy: Beyond delivery', *Gene Therapy,* 13, pp. 739.

Al-Dosari, M. S. and Gao, X. (2009) 'Nonviral gene delivery: principle, limitations, and recent progress', *The AAPS journal,* 11(4), pp. 671.

Al-Qaradawi, S. and Salman, S. R. (2002) 'Photocatalytic degradation of methyl orange as a model compound', *Journal of Photochemistry and Photobiology A: Chemistry,* 148(1), pp. 161-168.

Aldridge, S. (2006) 'Downstream processing needs a boost-Biomanufacturing trends and opportunities are meeting highlights', *Genetic Engineering News,* 26(1), pp. 1-+.

Allen, T. M. (1997) 'Liposomes', *Drugs,* 54(4), pp. 8-14.

Almeida, A. M., Queiroz, J. A., Sousa, F. and Sousa, A. (2015) 'Optimization of supercoiled HPV-16 E6/E7 plasmid DNA purification with arginine monolith using design of experiments', *J Chromatogr B Analyt Technol Biomed Life Sci,* 978-979, pp. 145-50.

Almog, R. and Shirey, T. L. (1978) 'A modified orcinol test for the specific determination of RNA', *Anal Biochem,* 91(1), pp. 130-7.

Altwaijry, N., Somani, S. and Dufes, C. (2018) 'Targeted nonviral gene therapy in prostate cancer', *Int J Nanomedicine,* 13, pp. 5753-5767.

Amemiya, T. (1994) *Introduction to statistics and econometrics.* Cambridge, Mass: Harvard University Press.

Ameskamp, N., Priesner, C., Lehmann, J. and Lutkemeyer, D. (1999) 'Pilot scale recovery of monoclonal antibodies by expanded bed ion exchange adsorption', *Bioseparation,* 8(1-5), pp. 169-88.

Anderson, W. F. (1990) 'Genetics and Human Malleability', *Hastings Center Report,* 20(1), pp. 21-24.

Andersson, R., Larm, O., Scholander, E. and Theander, O. (1980) 'Bromine oxidation of 1, 2-O-isopropylidene-α--Glucofuranose and sucrose', *Carbohydrate Research,* 78(2), pp. 257-265.

Aravindaram, K. and Yang, N. S. (2009) 'Gene gun delivery systems for cancer vaccine approaches', *Gene Therapy of Cancer*: Springer, pp. 167-178.

Arkhangelsky, E., Sefi, Y., Hajaj, B., Rothenberg, G. and Gitis, V. (2011) 'Kinetics and mechanism of plasmid DNA penetration through nanopores', *Journal of Membrane Science,* 371(1), pp. 45-51.

Arkhangelsky, E., Steubing, B., Ben-Dov, E., Kushmaro, A. and Gitis, V. (2008) 'Influence of pH and ionic strength on transmission of plasmid DNA through ultrafiltration membranes', *Desalination,* 227(1), pp. 111-119.

Arpanaei, A. (2008) *Improved Expanded Bed Adsorption Chromatography Systems.* PhD, Technical University of Denmark.

Arpanaei, A., Winther-Jensen, B., Theodosiou, E., Kingshott, P., Hobley, T. J. and Thomas, O. R. (2010) 'Surface modification of chromatography adsorbents by low temperature low pressure plasma', *J Chromatogr A,* 1217(44), pp. 6905-16.

Au, J. T., Mittra, A., Song, T. J., Cavnar, M., Jun, K., Carson, J., Gholami, S., Haddad, D., Gaujoux, S., Monette, S., Ezell, P., Wolchok, J. and Fong, Y. (2013) 'Irreversible electroporation facilitates gene transfer of a GM-CSF plasmid with a local and systemic response', *Surgery,* 154(3), pp. 496-503.

Axelsson, I. (1978) 'Characterization of proteins and other macromolecules by agarose gel chromatography', *Journal of Chromatography A,* 152(1), pp. 21-32.

Barbas, C. F., 3rd, Burton, D. R., Scott, J. K. and Silverman, G. J. (2007) 'Quantitation of DNA and RNA', *CSH Protoc,* 2007, pp. pdb ip47.

Beer, A. (1852) 'Bestimmung der Absorption des rothen Lichts in farbigen Flüssigkeiten', *Annalen der Physik,* 162(5), pp. 78-88.

Bellot, J. C. and Condoret, J. S. (1993) 'Modelling of liquid chromatography equilibria', *Process Biochemistry,* 28(6), pp. 365-376.

Belu, A. M., Graham, D. J. and Castner, D. G. (2003) 'Time-of-flight secondary ion mass spectrometry: techniques and applications for the characterization of biomaterial surfaces', *Biomaterials,* 24(21), pp. 3635-3653.

Berg, H. B., P.; Carlsson, M. (2003) *Chromatographic two-layer particles* Patent no. US20050242037A1. [Online].

Bergstrom, J. B., R.; Soderberg, L. (1997) *Process for introducing a functionality* Patent no. US6426315B1. [Online].

Biceroglu, S. and Memis, A. (2005) 'Gene therapy: applications in interventional radiology', *Diagn Interv Radiol,* 11(2), pp. 113-8.

Bicho, D., Caramelo-Nunes, C., Sousa, A., Sousa, F., Queiroz, J. A. and Tomaz, C. T. (2016) 'Purification of influenza deoxyribonucleic acid-based vaccine using agmatine monolith', *Journal of Chromatography B,* 1012-1013, pp. 153-161.

Bioinformatics (2017) http://www.bioinformatics.org/sms2/dna_mw.html. bioinformatics.org: Bioinformatics (Accessed: 23.01.2018 2018).

Biosciences, A. (2001) 'Use of sodium hydroxide for cleaning and sanitizing chromatography media and systems', *Process Chromatogr*.

BioToolomics (2018) *Negative Chromatography Antibody Purification (N-CAP) Technology*. http://www.biotoolomics.com/NCAPtec.htm (Accessed: 01.11. 2018).

Birnboim, H. C. and Doly, J. (1979) 'A rapid alkaline extraction procedure for screening recombinant plasmid DNA', *Nucleic Acids Res,* 7(6), pp. 1513-23.

Blanco, J. B., Vázquez, O., Martínez-Costas, J., Castedo, L. and Mascareñas, J. L. (2005) 'High affinity, sequence specific DNA binding by synthetic tripyrrole–peptide conjugates', *Chemistry–A European Journal,* 11(14), pp. 4171-4178.

Blom, H., Åkerblom, A., Kon, T., Shaker, S., van der Pol, L. and Lundgren, M. (2014) 'Efficient chromatographic reduction of ovalbumin for egg-based influenza virus purification', *Vaccine,* 32(30), pp. 3721-3724.

Bo, H., Wang, J., Chen, Q., Shen, H., Wu, F., Shao, H. and Huang, S. (2013) 'Using a single hydrophobic-interaction chromatography to purify pharmaceutical-grade supercoiled plasmid DNA from other isoforms', *Pharmaceutical biology,* 51(1), pp. 42-48.

Bonturi, N., Radke, V. S. C. O., Bueno, S. M. A., Freitas, S., Azzoni, A. R. and Miranda, E. A. (2013) 'Sodium citrate and potassium phosphate as alternative adsorption buffers in hydrophobic and aromatic thiophilic chromatographic purification of plasmid DNA from neutralized lysate', *Journal of Chromatography B,* 919, pp. 67-74.

Borujeni, E. E. and Zydney, A. L. (2014) 'Membrane fouling during ultrafiltration of plasmid DNA through semipermeable membranes', *Journal of Membrane Science,* 450, pp. 189-196.

Branovic, K., Forcic, D., Ivancic, J., Strancar, A., Barut, M., Gulija, T. K., Zgorelec, R. and Mazuran, R. (2004) 'Application of short monolithic columns for fast purification of plasmid DNA', *Journal of Chromatography B: Analytical Technologies in the Biomedical and Life Sciences,* 801(2), pp. 331-337.

Brenner, M., Hung, M.-C., Brenner, M. and Hung, M.-C. (2014) *Cancer Gene Therapy by Viral and Non-viral Vectors.* Somerset, US: Wiley.

Brown, T. A. (2010) *Gene cloning and DNA analysis : an introduction* Oxford; Hoboken, NJ: Wiley-Blackwell,.

Bruffaerts, N., Huygen, K. and Romano, M. (2014) 'DNA vaccines against tuberculosis', *Expert opinion on biological therapy,* 14(12), pp. 1801-1813.

Bruggeman, P. J., Kushner, M. J., Locke, B. R., Gardeniers, J. G. E., Graham, W. G., Graves, D. B., Hofman-Caris, R. C. H. M., Maric, D., Reid, J. P., Ceriani, E., Fernandez Rivas, D., Foster, J. E., Garrick, S. C., Gorbanev, Y., Hamaguchi, S., Iza, F., Jablonowski, H., Klimova, E., Kolb, J., Krcma, F., Lukes, P., Machala, Z., Marinov, I., Mariotti, D., Mededovic Thagard, S., Minakata, D., Neyts, E. C., Pawlat, J., Petrovic, Z. L., Pflieger, R., Reuter, S., Schram, D. C., Schröter, S., Shiraiwa, M., Tarabová, B., Tsai, P. A., Verlet, J. R. R., von Woedtke, T., Wilson, K. R., Yasui, K. and Zvereva, G. 2016. Plasma–liquid interactions: a review and roadmap.

Budelier, K. and Schorr, J. (1998) 'Purification of DNA by Anion-Exchange Chromatography', *Current Protocols in Molecular Biology,* 42(1), pp. 2.1.11-2.1.18.

Burton, K. (1956) 'A study of the conditions and mechanism of the diphenylamine reaction for the colorimetric estimation of deoxyribonucleic acid', *Biochem J,* 62(2), pp. 315-23.

CalcTool (2008) *Protein Size Calculator*. http://www.calctool.org/CALC/prof/bio/protein_size 2018).

Camus, A. (1942) *Le mythe de Sisyphe. Les Essais,* Paris: Gallimard.

Cano, T., Murphy, J. C., Fox, G. E. and Willson, R. C. (2005) 'Separation of genomic DNA from plasmid DNA by selective renaturation with immobilized metal affinity capture', *Biotechnology Progress,* 21(5), pp. 1472-1477.

Caramelo-Nunes, C., Bicho, D., Almeida, P., Marcos, J. C. and Tomaz, C. T. (2013) 'Dynamic binding capacity and specificity of 3,8-diamino-6-phenylphenanthridine-Sepharose

support for purification of supercoiled plasmid deoxyribonucleic acid', *J Chromatogr A,* 1307, pp. 91-8.
Caramelo-Nunes, C., Gabriel, M. F., Almeida, P., Marcos, J. C. and Tomaz, C. T. (2014) 'Negative pseudo-affinity chromatography for plasmid DNA purification using berenil as ligand', *J Chromatogr B Analyt Technol Biomed Life Sci,* 944, pp. 39-42.
Cardinaud, C. P., M; Tessier, P (2000) 'Plasma etching: principles, mechanisms, application to micro- and nano-technologies', *Applied Surface Science* 164, pp. 72-83.
Carlson, A., Signs, M., Liermann, L., Boor, R. and Jem, K. J. (1995) 'Mechanical disruption of Escherichia coli for plasmid recovery', *Biotechnology and Bioengineering,* 48(4), pp. 303-315.
Carlsson, K. and Åslund, N. (1987) 'Confocal imaging for 3-D digital microscopy', *Applied Optics,* 26(16), pp. 3232-3238.
Carnes, A. E., Hodgson, C. P. and Williams, J. A. (2006) 'Inducible Escherichia coli fermentation for increased plasmid DNA production', *Biotechnol Appl Biochem,* 45(Pt 3), pp. 155-66.
Casali, N. P., Andrew (2003) *E. coli Plasmid Vectors*: Humana Press.
Černigoj, U., Vidic, U., Barut, M., Podgornik, A., Peterka, M. and Štrancar, A. (2013) 'A multimodal histamine ligand for chromatographic purification of plasmid DNA', *Journal of Chromatography A,* 1281, pp. 87-93.
Chakrabarti, A., Sitaric, S. and Ohi, S. (1992) 'A procedure for large-scale plasmid isolation without using ultracentrifugation', *Biotechnology and applied biochemistry,* 16(2), pp. 211-215.
Chandra, G., Patel, P., Kost, T. A. and Gray, J. G. (1992) 'Large-scale purification of plasmid DNA by fast protein liquid chromatography using a Hi-Load Q Sepharose column', *Analytical biochemistry,* 203(1), pp. 169-172.
Chen, H. and Belfort, G. (1999) 'Surface modification of poly (ether sulfone) ultrafiltration membranes by low-temperature plasma-induced graft polymerization', *Journal of Applied Polymer Science,* 72(13), pp. 1699-1711.
Cheng, M. A., Farmer, E., Huang, C., Lin, J., Hung, C.-F. and Wu, T. C. (2018) 'Therapeutic DNA Vaccines for Human Papillomavirus and Associated Diseases', *Human Gene Therapy*.
Cherng, J.-Y., Talsma, H., Crommelin, D. J. and Hennink, W. E. (1999) 'Long term stability of poly ((2-dimethylamino) ethyl methacrylate)-based gene delivery systems', *Pharmaceutical research,* 16(9), pp. 1417-1423.
Choi, H., Rybkin, V., Titov, V., Shikova, T. and Ageeva, T. (2006) 'Comparative actions of a low pressure oxygen plasma and an atmospheric pressure glow discharge on the surface modification of polypropylene', *Surface and Coatings Technology,* 200(14-15), pp. 4479-4488.
Close, E. J., Salm, J. R., Iskra, T., Sorensen, E. and Bracewell, D. G. (2013) 'Fouling of an anion exchange chromatography operation in a monoclonal antibody process: Visualization and kinetic studies', *Biotechnol Bioeng,* 110(9), pp. 2425-35.
Coffin, J. M., Hughes, S. H. and Varmus, H. E. (1997) 'Principles of Retroviral Vector Design'.
Colote, S., Ferraz, C. and Liautard, J. (1986) 'Analysis and purification of plasmid DNA by reversed-phase high-performance liquid chromatography', *Analytical biochemistry,* 154(1), pp. 15-20.

Colpan, M. and Riesner, D. (1984) 'High-performance liquid chromatography of high-molecular-weight nucleic acids on the macroporous ion exchanger, nucleogen', *Journal of Chromatography A,* 296, pp. 339-353.

Corso, G., Mäger, I., Lee, Y., Görgens, A., Bultema, J., Giebel, B., Wood, M. J. A., Nordin, J. Z. and Andaloussi, S. E. L. (2017) 'Reproducible and scalable purification of extracellular vesicles using combined bind-elute and size exclusion chromatography', *Scientific Reports,* 7(1), pp. 11561.

Cunha, B., Silva, R. J. S., Aguiar, T., Serra, M., Daicic, J., Maloisel, J.-L., Clachan, J., Åkerblom, A., Carrondo, M. J. T., Peixoto, C. and Alves, P. M. (2016) 'Improving washing strategies of human mesenchymal stem cells using negative mode expanded bed chromatography', *Journal of Chromatography A,* 1429, pp. 292-303.

Dainiak, M. B., Galaev, I. Y. and Mattiasson, B. (2002a) 'Direct capture of product from fermentation broth using a cell-repelling ion exchanger', *J Chromatogr A,* 942(1-2), pp. 123-31.

Dainiak, M. B., Galaev, I. Y. and Mattiasson, B. (2002b) 'Polyelectrolyte-coated ion exchangers for cell-resistant expanded bed adsorption', *Biotechnol Prog,* 18(4), pp. 815-20.

Danko, J. R., Kochel, T., Teneza-Mora, N., Luke, T. C., Raviprakash, K., Sun, P., Simmons, M., Moon, J. E., De La Barrera, R., Martinez, L. J., Thomas, S. J., Kenney, R. T., Smith, L. and Porter, K. R. (2018) 'Safety and Immunogenicity of a Tetravalent Dengue DNA Vaccine Administered with a Cationic Lipid-Based Adjuvant in a Phase 1 Clinical Trial', *The American Journal of Tropical Medicine and Hygiene,* 98(3), pp. 849-856.

de Faria, H. D., de Carvalho Abrão, L. C., Santos, M. G., Barbosa, A. F. and Figueiredo, E. C. (2017) 'New advances in restricted access materials for sample preparation: A review', *Analytica chimica acta,* 959, pp. 43-65.

Deane, N. 2013. *RE: Email exchange regarding suggested RI of agarose based chromatography suppports* Type to J., M.

Deipolyi, A. R., Golberg, A., Yarmush, M. L., Arellano, R. S. and Oklu, R. (2014) 'Irreversible electroporation: evolution of a laboratory technique in interventional oncology', *Diagnostic and interventional radiology (Ankara, Turkey),* 20(2), pp. 147-154.

Deshmukh, N. R. and Lali, A. M. (2005) 'Adsorptive purification of pDNA on superporous rigid cross-linked cellulose matrix', *Journal of Chromatography B,* 818(1).

Diogo, M. M., Queiroz, J. A., Monteiro, G. A., Martins, S. A., Ferreira, G. N. and Prazeres, D. M. (2000) 'Purification of a cystic fibrosis plasmid vector for gene therapy using hydrophobic interaction chromatography', *Biotechnol Bioeng,* 68(5), pp. 576-83.

Diogo, M. M., Queiroz, J. A. and Prazeres, D. M. F. (2005) 'Chromatography of plasmid DNA', *Journal of Chromatography A,* 1069(1), pp. 3-22.

Diogo, M. M. Q., J. A.; Monteiro, G. A.; Prazeres, D. M. (1999) 'Separation and analysis of plasmid denatured forms using hydrophobic interaction chromatography', (0003-2697 (Print)).

Dobson, J. (2006) 'Gene therapy progress and prospects: magnetic nanoparticle-based gene delivery', *Gene therapy,* 13(4), pp. 283.

Du, C., Shi, T., Sun, Y. and Zhuang, X. (2008) 'Decolorization of Acid Orange 7 solution by gas-liquid gliding arc discharge plasma', *Journal of hazardous materials,* 154(1-3), pp. 1192-1197.

Dunbar, C. E., High, K. A., Joung, J. K., Kohn, D. B., Ozawa, K. and Sadelain, M. (2018) 'Gene therapy comes of age', *Science,* 359(6372), pp. eaan4672.
Edelstein, M. L. (2018) 'Gene Therapy Trials Worldwide'.
Egorov, A., Vakhabov, A. K. and Chernyak, V. Y. (1970) 'Isolation of agarose and granulation of agar and agarose gel', *Journal of Chromatography A,* 46, pp. 143-148.
Ellegren, H. and Laas, T. (1989) 'Size-exclusion chromatography of DNA restriction fragments. Fragment length determinations and a comparison with the behaviour of proteins in size-exclusion chromatography', *Journal of Chromatography,* 467(1), pp. 217-26.
Endres, H. N., Johnson, J. A. C., Ross, C. A., Welp, J. K. and Etzel, M. R. (2003) 'Evaluation of an ion-exchange membrane for the purification of plasmid DNA', *Biotechnology and Applied Biochemistry,* 37(3), pp. 259-266.
Eon-Duval, A. and Burke, G. (2004) 'Purification of pharmaceutical-grade plasmid DNA by anion-exchange chromatography in an RNase-free process', *J Chromatogr B Analyt Technol Biomed Life Sci,* 804(2), pp. 327-35.
Epstein, S. (1996) 'Addendum to the points to consider in human somatic cell and gene therapy (1991)', *Hum Gene Ther,* 7(9), pp. 1181-90.
Fasbender, A., Marshall, J., Moninger, T., Grunst, T., Cheng, S. and Welsh, M. (1997) 'Effect of co-lipids in enhancing cationic lipid-mediated gene transfer in vitro and in vivo', *Gene therapy,* 4(7), pp. 716.
Fasman, G. D., Handbook of, b. and molecular, b. (1989) *Practical handbook of biochemistry and molecular biology.*
Author (2007)*: Guidance for Industry Considerations for Plasmid DNA  Vaccines for Infectious Disease  Indications* http://www.fda.gov/cber/guidelines.htm.
*Current Good Manufacturing Practice (CGMP) Regulations 21CFR210.1* (21).
FDA (2017b) 'FDA approval brings first gene therapy to the United States', *News release. August,* 30.
Ferreira, G., Cabral, J. and Prazeres, D. (1997) 'A comparison of gel filtration chromatographic supports for plasmid purification', *Biotechnology techniques,* 11(6), pp. 417-420.
Ferreira, G. N., Cabral, J. M. and Prazeres, D. M. (1999) 'Development of process flow sheets for the purification of supercoiled plasmids for gene therapy applications', *Biotechnol Prog,* 15(4), pp. 725-31.
Ferreira, G. N., Cabral, J. M. and Prazeres, D. M. (2000a) 'Anion exchange purification of plasmid DNA using expanded bed adsorption', *Bioseparation,* 9(1), pp. 1-6.
Ferreira, G. N., Monteiro, G. A., Prazeres, D. M. and Cabral, J. M. (2000b) 'Downstream processing of plasmid DNA for gene therapy and DNA vaccine applications', *Trends Biotechnol,* 18(9), pp. 380-8.
Fisher, E. R. (2002) 'On the interplay between plasma ions, radicals and surfaces: who dominates the interaction?', *Plasma Sources Science and Technology,* 11(3A), pp. A105.
Freitas, S., Canário, S., Santos, J. A. L. and Prazeres, D. M. F. (2009a) 'Alternatives for the intermediate recovery of plasmid DNA: Performance, economic viability and environmental impact', *Biotechnology Journal,* 4(2), pp. 265-278.

Freitas, S. S., Santos, J. A. and Prazeres, D. M. (2009b) 'Plasmid purification by hydrophobic interaction chromatography using sodium citrate in the mobile phase', *Separation and Purification Technology,* 65(1), pp. 95-104.
Fridman, A. A. (2008) *Plasma chemistry.* Cambridge ; New York: Cambridge University Press.
Friedmann, T. and Roblin, R. (1972) 'Gene therapy for human genetic disease?', *Science,* 175(4025), pp. 949-55.
Gardlik, R., Palffy, R., Hodosy, J., Lukacs, J., Turna, J. and Celec, P. (2005) 'Vectors and delivery systems in gene therapy', *Med Sci Monit,* 11(4), pp. Ra110-21.
GE Healthcare (2012) 'Instructions Core Beads 28-9958-80 AC'.
GE Healthcare (2013) 'Instruction 29-0441-99 AB'.
Ge Healthcare (2018a) *Capto Core 400*. https://www.gelifesciences.com/en/ch/shop/chromatography/resins/multimodal/capto-core-400-p-09938 - order: GE Healthcare (Accessed: 20.11.2018 2018).
GE Healthcare (2018b) *Capto Core 700 multimodal chromatography resin*. https://www.gelifesciences.com/en/ch/shop/chromatography/resins/multimodal/capto-core-700-multimodal-chromatography-resin-p-05642 - order (Accessed: 11.08.2018 2018).
GE Healthcare (2018c) 'Multimodal Chromatography; Capto Core 400 Capto Core 400; Data file, 28-9983-07,AC'.
GE Healthcare (2018d) *Order Form Capto Core 700*. https://www.gelifesciences.com/en/gb/shop/chromatography/resins/multimodal/capto-core-700-multimodal-chromatography-resin-p-05642 - order (Accessed: 12.10. 2018).
GE Healthcare Bio-Science (2012) 'Capto Core 700 Data File, 28-9983-07, AA', (Accessed 10/2018).
Ge Healthcare Bio-Science (2013) *Multimodal Chromatography Handbook. 29-0548-08 AA* (Accessed: 11/2018).
GE Healthcare Bio-Science (2014) *Q Sepharose Fast Flow 18-1177-22 AE*. http://www.gelifesciences.com/webapp/wcs/stores/servlet/catalog/en/GELifeSciences-uk/products/AlternativeProductStructure_17466/17051001: GE Heathcare 2017).
GE Healthcare Bio-Science (2016) *Ion Exchange Chromatography. Principles and Methods* gelifesciences.com: GE HEalthcare.
GE Healthcare Bio-Science (2018) *Order Form Q Sepharose FF*. https://www.gelifesciences.com/en/gb/shop/chromatography/resins/ion-exchange/q-sepharose-fast-flow-p-04285 (Accessed: 12.10. 2018).
GE Healthcare Life Sciences 2012. Capto™ Core 700 and core bead technology: Overview. https://www.youtube.com/watch?v=YQRE9jdDmC8.
Gendimenico, G. J., Bouquin, P. L. and Tramposch, K. M. (1988) 'Diphenylamine-colorimetric method for DNA assay: A shortened procedure by incubating samples at 50°C', *Analytical Biochemistry,* 173(1), pp. 45-48.
Ghanem, A., Healey, R. and Adly, F. G. (2013) 'Current trends in separation of plasmid DNA vaccines: A review', *Analytica Chimica Acta,* 760(C), pp. 1-15.
Gilbert, P. 2018. Type to Professor O.R.T., T.
Ginn, S. L., Alexander, I. E., Edelstein, M. L., Abedi, M. R. and Wixon, J. (2013) 'Gene therapy clinical trials worldwide to 2012 - an update', *J Gene Med,* 15(2), pp. 65-77.

Ginn, S. L., Amaya, A. K., Alexander, I. E., Edelstein, M. and Abedi, M. R. (2018) 'Gene therapy clinical trials worldwide to 2017: An update', *The Journal of Gene Medicine,* 20(5), pp. e3015.

Glaser, V. (2013) 'Separation of Therapeutic Biomolecules: Mixed-Mode Chromatography. Layered Bead Designs, In Silico Modeling Used at Large Scale', *Genetic Engineering & Biotechnology News,* 33(9), pp. 33-34.

Glover, D. J., Lipps, H. J. and Jans, D. A. (2005) 'Towards safe, non-viral therapeutic gene expression in humans', *Nature Reviews Genetics,* 6(4), pp. 299.

Gonçalves, G. A. R. and Paiva, R. d. M. A. (2017) 'Gene therapy: advances, challenges and perspectives', *Einstein (Sao Paulo, Brazil),* 15(3), pp. 369-375.

Gregoriadis, G., McCormack, B., Obrenovich, M. and Perrie, Y. (2000) 'Entrapment of plasmid DNA vaccines into liposomes by dehydration/rehydration', *DNA Vaccines*: Springer, pp. 305-311.

Grunwald, A. G. and Shields, M. S. (2001) 'Plasmid purification using membrane-based anion-exchange chromatography', *Analytical biochemistry,* 1(296), pp. 138-141.

GSL Biotech LLC (2004) 'SnapGene®', 3.1.4.

Guo, J., Du, Y., Lan, Y. and Mao, J. (2011) 'Photodegradation mechanism and kinetics of methyl orange catalyzed by Fe(III) and citric acid', *Journal of Hazardous Materials,* 186(2), pp. 2083-2088.

Gustavsson, P. E., Lemmens, R., Nyhammar, T., Busson, P. and Larsson, P. O. (2004) 'Purification of plasmid DNA with a new type of anion-exchange beads having a non-charged surface', *J Chromatogr A,* 1038(1-2), pp. 131-40.

Hacein-Bey-Abina, S., Le Deist, F., Carlier, F., Bouneaud, C., Hue, C., De Villartay, J.-P., Thrasher, A. J., Wulffraat, N., Sorensen, R. and Dupuis-Girod, S. (2002) 'Sustained correction of X-linked severe combined immunodeficiency by ex vivo gene therapy', *New England Journal of Medicine,* 346(16), pp. 1185-1193.

Hagel, C., Laking, G., Laas, R., Scheil, S., Jung, R., Milde-Langosch, K. and Stavrou, D. K. (1996a) 'Demonstration of p53 protein and TP53 gene mutations in oligodendrogliomas', *Eur J Cancer,* 32A(13), pp. 2242-8.

Hagel, L., Östberg, M. and Andersson, T. (1996b) 'Apparent pore size distributions of chromatography media', *Journal of Chromatography A,* 743(1), pp. 33-42.

Haginaka, J. (1991) 'Drug determination in serum by liquid chromatography with restricted access stationary phases', *TrAC Trends in Analytical Chemistry,* 10(1), pp. 17-22.

Hale, G. M. and Querry, M. R. (1973) 'Optical constants of water in the 200-nm to 200-µm wavelength region', *Applied optics,* 12(3), pp. 555-563.

Hall, M., Berg, M., Eklind, I. and Kristiansson, S. 2018. Method for Chromatography. Google Patents.

Hayes, R., Ahmed, A., Edge, T. and Zhang, H. (2014) 'Core–shell particles: Preparation, fundamentals and applications in high performance liquid chromatography', *Journal of Chromatography A,* 1357, pp. 36-52.

He, L., de Val, N., Morris, C. D., Vora, N., Thinnes, T. C., Kong, L., Azadnia, P., Sok, D., Zhou, B., Burton, D. R., Wilson, I. A., Nemazee, D., Ward, A. B. and Zhu, J. (2016) 'Presenting native-like trimeric HIV-1 antigens with self-assembling nanoparticles', *Nature Communications,* 7, pp. 12041.

Heath, C. and Belfort, G. (1992) 'Synthetic membranes in biotechnology: realities and possibilities', *Bioseparation*: Springer, pp. 45-88.
Herweijer, H. and Wolff, J. A. (2007) 'Gene therapy progress and prospects: hydrodynamic gene delivery', *Gene Ther,* 14(2), pp. 99-107.
Higgins, N. P. and Vologodskii, A. V. (2015) 'Topological behavior of plasmid DNA', *Microbiology spectrum,* 3(2).
Hirabayashi, J. and Kasai, K.-i. (2000) 'Effects of DNA topology, temperature and solvent viscosity on DNA retardation in slalom chromatography', *Journal of Chromatography A,* 893(1), pp. 115-122.
Hirayama, K., Akashi, S., Furuya, M. and Fukuhara, K. (1990) 'Rapid confirmation and revision of the primary structure of bovine serum albumin by ESIMS and Frit-FAB LC/MS', *Biochem Biophys Res Commun,* 173(2), pp. 639-46.
Hjorth, R. (1997) 'Expanded-bed adsorption in industrial bioprocessing: recent developments', *Trends Biotechnol,* 15(6), pp. 230-5.
Holmes, D. S. and Quigley, M. (1981) 'A rapid boiling method for the preparation of bacterial plasmids', *Analytical biochemistry,* 114(1), pp. 193-197.
Horn, N., Marquet, M., Meek, J. and Budahazi, G. 1996. Process for reducing RNA concentration in a mixture of biological material using diatomaceous earth. Google Patents.
Horn, N. A., Meek, J. A., Budahazi, G. and Marquet, M. (1995) 'Cancer gene therapy using plasmid DNA: purification of DNA for human clinical trials', *Human Gene Therapy,* 6(5), pp. 565-573.
Horner, A. A., Van Uden, J. H., Zubeldia, J. M., Broide, D. and Raz, E. (2001) 'DNA-based immunotherapeutics for the treatment of allergic disease', *Immunological reviews,* 179(1), pp. 102-118.
Hubbuch, J. and Kula, M. R. (2008) 'Confocal laser scanning microscopy as an analytical tool in chromatographic research', *Bioprocess Biosyst Eng,* 31(3), pp. 241-59.
Hubbuch, J., Linden, T., Knieps, E., Thömmes, J. and Kula, M. R. (2002) 'Dynamics of protein uptake within the adsorbent particle during packed bed chromatography', *Biotechnology and Bioengineering,* 80(4), pp. 359-368.
Hubbuch, J. J., Brixius, P. J., Lin, D. Q., Mollerup, I. and Kula, M. R. (2006) 'The influence of homogenisation conditions on biomass-adsorbent interactions during ion-exchange expanded bed adsorption', *Biotechnol Bioeng,* 94(3), pp. 543-53.
Huber, H. B., W.; Diewok, J.; Ganja, R.; , Keller, D.; Urthaler, J.; Necina, R. (2008) 'Industrial Manufacturing of Plasmid DNA', *GEN (Genetic Engineering & Biotechnology news),* (no. 4).
Ioannidis, N., Bowen, J., Pacek, A. and Zhang, Z. (2012) 'Manufacturing of agarose-based chromatographic adsorbents--effect of ionic strength and cooling conditions on particle structure and mechanical strength', *J Colloid Interface Sci,* 367(1), pp. 153-60.
Iuliano, S., Fisher, J. R., Chen, M. and Kelly, W. J. (2002) 'Rapid analysis of a plasmid by hydrophobic-interaction chromatography with a non-porous resin', *Journal of chromatography. A,* 972(1), pp. 77-86.
Iwunze, M. O. (2010) 'Aqueous Photophysical Parameters of Congo Red', *Spectroscopy Letters,* 43(1), pp. 16-21.

Jahanshahi, M., Pacek, A. W., Nienow, A. W. and Lyddiatt, A. (2003) 'Fabrication by three-phase emulsification of pellicular adsorbents customised for liquid fluidised bed adsorption of bioproducts', *Journal of Chemical Technology & Biotechnology: International Research in Process, Environmental & Clean Technology,* 78(11), pp. 1111-1120.

Jahanshahi, M., Partida-Martinez, L. and Hajizadeh, S. (2008) 'Preparation and evaluation of polymer-coated adsorbents for the expanded bed recovery of protein products from particulate feedstocks', *J Chromatogr A,* 1203(1), pp. 13-20.

James, K. T., Cooney, B., Agopsowicz, K., Trevors, M. A., Mohamed, A., Stoltz, D., Hitt, M. and Shmulevitz, M. (2016) 'Novel High-throughput Approach for Purification of Infectious Virions', *Scientific Reports,* 6, pp. 36826.

Ji, Y., Tian, Y., Ahnfelt, M. and Sui, L. (2014) 'Design and optimization of a chromatographic purification process for Streptococcus pneumoniae serotype 23F capsular polysaccharide by a Design of Experiments approach', *Journal of Chromatography A,* 1348, pp. 137-149.

Jin, Y., Wu, Y., Cao, J. and Wu, Y. (2014) 'Optimizing decolorization of Methylene Blue and Methyl Orange dye by pulsed discharged plasma in water using response surface methodology', *Journal of the Taiwan Institute of Chemical Engineers,* 45(2), pp. 589-595.

Johansson, B. L., Andersson, M., Lausmaa, J. and Sjovall, P. (2004) 'Chemical characterisation of different separation media based on agarose by static time-of-flight secondary ion mass spectrometry', *J Chromatogr A,* 1023(1), pp. 49-56.

Jorge, S. and Dellagostin, O. A. (2017) 'The development of veterinary vaccines: a review of traditional methods and modern biotechnology approaches', *Biotechnology Research and Innovation,* 1(1), pp. 6-13.

Joseph, S. 2018- in preparation. Chapter II: Manufacture and Characterisation of Multifunctional Bi-Layered Materials. (in preparation).

Josic, D., Buchacher, A. and Jungbauer, A. (2001) 'Monoliths as stationary phases for separation of proteins and polynucleotides and enzymatic conversion', *Journal of Chromatography B: Biomedical Sciences and Applications,* 752(2), pp. 191-205.

Josić, D. and Štrancar, A. (1999) 'Application of membranes and compact, porous units for the separation of biopolymers', *Industrial and Engineering Chemistry Research,* 38(2), pp. 333-342.

Jungbauer, A. (2005) 'Chromatographic media for bioseparation', *Journal of Chromatography A,* 1065(1), pp. 3-12.

Jungbauer, A. and Hahn, R. (2004) 'Monoliths for fast bioseparation and bioconversion and their applications in biotechnology', *Journal of Separation Science,* 27(10-11), pp. 767-778.

Kaczmarski, K. and Bellot, J. C. (2003) 'Effect of particle-size distribution and particle porosity changes on mass-transfer kinetics', *Acta Chromatographica*, pp. 22-37.

Kanazawa, S., Kogoma, M., Moriwaki, T. and Okazaki, S. (1988) 'Stable glow plasma at atmospheric pressure', *Journal of Physics D: Applied Physics,* 21(5), pp. 838.

Karnchanasri, K. (2012) *Bi-layered chromatography matrices for the purification of biological nanoplexes.* PhD, University of Birmingham.

Kaushansky, K., Lichtman, M. A., Prchal, J. T., Levi, M., Press, O. W., Burns, L. J. and Caligiuri, M. A. (2016) *Williams hematology.* McGraw-Hill Education.

Kay, M. A. (2011) 'State-of-the-art gene-based therapies: the road ahead', *Nature Reviews Genetics,* 12(5), pp. 316.

Kepka, C., Lemmens, R., Vasi, J., Nyhammar, T. and Gustavsson, P.-E. (2004) 'Integrated process for purification of plasmid DNA using aqueous two-phase systems combined with membrane filtration and lid bead chromatography', *Journal of Chromatography A,* 1057(1), pp. 115-124.

Kim, H.-B., Hayashi, M., Nakatani, K., Kitamura, N., Sasaki, K., Hotta, J.-i. and Masuhara, H. (1996) 'In situ measurements of ion-exchange processes in single polymer particles: laser trapping microspectroscopy and confocal fluorescence microspectroscopy', *Analytical chemistry,* 68(3), pp. 409-414.

Knake, N., Reuter, S., Niemi, K., Schulz-von der Gathen, V. and Winter, J. (2008) 'Absolute atomic oxygen density distributions in the effluent of a microscale atmospheric pressure plasma jet', *Journal of Physics D-Applied Physics,* 41(19).

Kornberg, A. and Baker, T. (1992) *DNA replication.* 2nd edn. New York: W.H. Freeman.

Kotterman, M. A., Chalberg, T. W. and Schaffer, D. V. (2015) 'Viral vectors for gene therapy: translational and clinical outlook', *Annual review of biomedical engineering,* 17, pp. 63-89.

Krishnamoorthy, B., Karanam, V., Chellan, V. R., Siram, K., Natarajan, T. S. and Gregory, M. (2014) 'Polymersomes as an effective drug delivery system for glioma--a review', *J Drug Target,* 22(6), pp. 469-77.

Kudchodkar, S. B., Choi, H., Reuschel, E. L., Esquivel, R., Jin-Ah Kwon, J., Jeong, M., Maslow, J. N., Reed, C. C., White, S., Kim, J. J., Kobinger, G. P., Tebas, P., Weiner, D. B. and Muthumani, K. (2018) 'Rapid response to an emerging infectious disease – Lessons learned from development of a synthetic DNA vaccine targeting Zika virus', *Microbes and Infection*.

Labarca, C. and Paigen, K. (1980) 'A simple, rapid, and sensitive DNA assay procedure', *Anal Biochem,* 102(2), pp. 344-52.

Lagoutte, P., Mignon, C., Donnat, S., Stadthagen, G., Mast, J., Sodoyer, R., Lugari, A. and Werle, B. (2016) 'Scalable chromatography-based purification of virus-like particle carrier for epitope based influenza A vaccine produced in Escherichia coli', *Journal of Virological Methods,* 232, pp. 8-11.

Lahijani, R., Hulley, G., Soriano, G., Horn, N. A. and Marquet, M. (1996) 'High-yield production of pBR322-derived plasmids intended for human gene therapy by employing a temperature-controllable point mutation', *Human gene therapy,* 7(16), pp. 1971-1980.

Lai, W.-F. and Wong, W.-T. (2018) 'Design of Polymeric Gene Carriers for Effective Intracellular Delivery', *Trends in Biotechnology,* 36(7), pp. 713-728.

Larsson, M., Lindgren, J., Ljunglof, A. and Knuuttila, K. G. (2003) 'Ligand distributions in agarose particles as determined by confocal Raman spectroscopy and confocal scanning laser microscopy', *Appl Spectrosc,* 57(3), pp. 251-5.

Latt, S. A. and Stetten, G. (1976) 'Spectral studies on 33258 Hoechst and related bisbenzimidazole dyes useful for fluorescent detection of deoxyribonucleic acid synthesis', *J Histochem Cytochem,* 24(1), pp. 24-33.

Latulippe, D. and Zydney, A. (2009) *Elongational flow model for transmission of supercoiled plasmid DNA during membrane ultrafiltration.*

Latulippe, D. R. and Zydney, A. L. (2010) 'Radius of gyration of plasmid DNA isoforms from static light scattering', *Biotechnology and Bioengineering,* 107(1), pp. 134-142.

Lee, M. F. X., Chan, E. S. and Tey, B. T. (2014) 'Negative chromatography: Progress, applications and future perspectives', *Process Biochemistry,* 49(6), pp. 1005-1011.

Lee, S., Nguyen, M. T., Currier, M. G., Jenkins, J. B., Strobert, E. A., Kajon, A. E., Madan-Lala, R., Bochkov, Y. A., Gern, J. E. and Roy, K. (2016) 'A polyvalent inactivated rhinovirus vaccine is broadly immunogenic in rhesus macaques', *Nature communications,* 7, pp. 12838.

Lengsfeld, C. S. and Anchordoquy, T. J. (2002) 'Shear-Induced Degradation of Plasmid DNA', *Journal of Pharmaceutical Sciences,* 91(7), pp. 1581-1589.

Leonard, M. (1997) 'New packing materials for protein chromatography', *Journal of Chromatography B: Biomedical Sciences and Applications,* 699(1-2), pp. 3-27.

Levy, M. S., Collins, I. J., Yim, S. S., Ward, J. M., Titchener-Hooker, N., Ayazi Shamlou, P. and Dunnill, P. (1999) 'Effect of shear on plasmid DNA in solution', *Bioprocess Engineering,* 20(1), pp. 7-13.

Levy, M. S., O'kennedy, R. D., Ayazi-Shamlou, P. and Dunnill, P. (2000) 'Biochemical engineering approaches to the challenges of producing pure plasmid DNA', *Trends in Biotechnology,* 18(7), pp. 296-305.

Li, H., Bo, H., Wang, J., Shao, H. and Huang, S. (2011) 'Separation of supercoiled from open circular forms of plasmid DNA, and biological activity detection', *Cytotechnology,* 63(1), pp. 7-12.

Li, S.-D. and Huang, L. (2007) 'Non-viral is superior to viral gene delivery', *Journal of controlled release: official journal of the Controlled Release Society,* 123(3), pp. 181.

Li, Y., Dong, X.-Y. and Sun, Y. (2005) 'High-speed chromatographic purification of plasmid DNA with a customized biporous hydrophobic adsorbent', *Biochemical engineering journal,* 27(1), pp. 33-39.

Liebhafsky, H. A. (1939) 'The Hydrolysis of Bromine. The Hydration of the Halogens. The Mechanism of Certain Halogen Reactions', *Journal of the American Chemical Society,* 61(12), pp. 3513-3519.

Lin, D. Q., Thommes, J., Kula, M. R. and Hubbuch, J. J. (2004) 'The influence of biomass on the hydrodynamic behavior and stability of expanded beds', *Biotechnol Bioeng,* 87(3), pp. 337-46.

Listner, K., Bentley, L., Okonkowski, J., Kistler, C., Wnek, R., Caparoni, A., Junker, B., Robinson, D., Salmon, P. and Chartrain, M. (2006) 'Development of a highly productive and scalable plasmid DNA production platform', *Biotechnol Prog,* 22(5), pp. 1335-45.

Liu, Z.-M., Xu, Z.-K., Wang, J.-Q., Wu, J. and Fu, J.-J. (2004) 'Surface modification of polypropylene microfiltration membranes by graft polymerization of N-vinyl-2-pyrrolidone', *European polymer journal,* 40(9), pp. 2077-2087.

Ljunglof, A., Bergvall, P., Bhikhabhai, R. and Hjorth, R. (1999) 'Direct visualisation of plasmid DNA in individual chromatography adsorbent particles by confocal scanning laser microscopy', *J Chromatogr A,* 844(1-2), pp. 129-35.

Lodish, H. B., A.; Zipursky, S. L.; Matsudaira, P.; Baltimore, D.; Darnell, J. (2000) 'Section 4.1 Structure of Nucleic Acids', in Freeman, W.H. (ed.) *Molecular Cell Biology, 4th Edition.* 4th Edition ed. New York.

Loontiens, F. G., Regenfuss, P., Zechel, A., Dumortier, L. and Clegg, R. M. (1990) 'Binding characteristics of Hoechst 33258 with calf thymus DNA, poly[d(A-T)], and d(CCGGAATTCCGG): multiple stoichiometries and determination of tight binding with a wide spectrum of site affinities', *Biochemistry,* 29(38), pp. 9029-39.

Lowe, C. R., Lowe, A. R. and Gupta, G. (2001) 'New developments in affinity chromatography with potential application in the production of biopharmaceuticals', *Journal of Biochemical and Biophysical Methods,* 49(1-3), pp. 561-574.

Lumen 2018. structure and function of DNA. https://courses.lumenlearning.com/microbiology/chapter/structure-and-function-of-dna/.

Lv, H., Zhang, S., Wang, B., Cui, S. and Yan, J. (2006) 'Toxicity of cationic lipids and cationic polymers in gene delivery', *Journal of controlled release,* 114(1), pp. 100-109.

Lyddiatt, A. and O'Sullivan, D. A. (1998) 'Biochemical recovery and purification of gene therapy vectors', *Curr Opin Biotechnol,* 9(2), pp. 177-85.

Ma, G. and Su, Z.-G. (2013) *Microspheres and microcapsules in biotechnology: design, preparation and applications.* Pan Stanford.

Mali, S. (2013) 'Delivery systems for gene therapy', *Indian journal of human genetics,* 19(1), pp. 3-8.

Maloisel, J.-L., Busson, K., Lacki, K., Noren, B. and Skoglar, H. 2016. Separation matrices for purification of biological particles. Google Patents.

Manoj, S., Babiuk, L. A. and van Drunen Littel-van den Hurk, S. (2004) 'Approaches to enhance the efficacy of DNA vaccines', *Crit Rev Clin Lab Sci,* 41(1), pp. 1-39.

Marquet, M., Horn, N. A. and Meek, J. A. (1995) 'Process development for the manufacture of plasmid DNA vectors for use in gene therapy', *BIOPHARM-THE TECHNOLOGY & BUSINESS OF BIOPHARMACEUTICALS,* 8(7), pp. 26-&.

Matlschweiger, A., Engelmaier, H., Himmler, G. and Hahn, R. (2017) 'Secretory immunoglobulin purification from whey by chromatographic techniques', *Journal of Chromatography B,* 1060, pp. 53-62.

Matos, T., Queiroz, J. A. and Bülow, L. (2014) 'Plasmid DNA purification using a multimodal chromatography resin', *Journal of Molecular Recognition,* 27(4), pp. 184-189.

McCrudden, C. M. and McCarthy, H. O. (2013) 'Cancer gene therapy–key biological concepts in the design of multifunctional non-viral delivery systems', *Gene therapy-tools and potential applications*: InTech.

McCue, J. T. (2014) 'Use and application of hydrophobic interaction chromatography for protein purification', *Methods Enzymol,* 541, pp. 51-65.

McLaughlin, L. W. (1989) 'Mixed-mode chromatography of nucleic acids', *Chemical Reviews,* 89(2), pp. 309-319.

Merdan, T., Kopeček, J. and Kissel, T. (2002) 'Prospects for cationic polymers in gene and oligonucleotide therapy against cancer', *Advanced drug delivery reviews,* 54(5), pp. 715-758.

Meyer, V. R. (2013) *Practical high-performance liquid chromatography.* John Wiley & Sons.

MHRA 2017. Rules and Guidance for Pharmaceutical Manufacturers and Distributors (Orange Guide) 2017. Pharmaceutical Press.
Mihelič, I., Koloini, T., Podgornik, A. and Štrancar, A. (2000) 'Dynamic capacity studies of CIM (Convective Interaction Media)® monolithic columns', *HRC Journal of High Resolution Chromatography,* 23(1), pp. 39-43.
Millipore, E. (2016) 'Fractogel® EMD Chromatography Resin: Capture your target with speed and efficiency', Available: Merck KGaA.
Moreau, N., Tabary, X. and Le Goffic, F. (1987) 'Purification and separation of various plasmid forms by exclusion chromatography', *Analytical biochemistry,* 166(1), pp. 188-193.
Mountain, A. (2000) 'Gene therapy: the first decade', *Trends in biotechnology,* 18(3), pp. 119-128.
Müller, W. (1986) 'Fractionation of DNA restriction fragments with ion-exchangers for high-performance liquid chromatography', *European journal of biochemistry,* 155(1), pp. 203-212.
Mundle, S. T., Kishko, M., Groppo, R., DiNapoli, J., Hamberger, J., McNeil, B., Kleanthous, H., Parrington, M., Zhang, L. and Anderson, S. F. (2016) 'Core bead chromatography for preparation of highly pure, infectious respiratory syncytial virus in the negative purification mode', *Vaccine,* 34(32), pp. 3690-3696.
Murphy, J. C., Jewell, D. L., White, K. I., Fox, G. E. and Willson, R. C. (2003) 'Nucleic acid separations utilizing immobilized metal affinity chromatography', *Biotechnology Progress,* 19(3), pp. 982-986.
Murphy, J. C., Wibbenmeyer, J. A., Fox, G. E. and Willson, R. C. (1999) 'Purification of plasmid DNA using selective precipitation by compaction agents', *Nature Biotechnology,* 17(8), pp. 822.
Murphy, J. C. a. F., George E and Willson, Richard C (2003) 'Enhancement of anion-exchange chromatography of DNA using compaction agents', *Journal of chromatography. A,* 894.
Nestola, P., Peixoto, C., Villain, L., Alves, P. M., Carrondo, M. J. T. and Mota, J. P. B. (2015) 'Rational development of two flowthrough purification strategies for adenovirus type 5 and retro virus-like particles', *Journal of Chromatography A,* 1426, pp. 91-101.
Nethe-Jaenchen, R. (2001) *Genetik. Grundstudium Biologie* Heidelberg; Berlin: Spektrum, Akadem Verlag.
Newman, C. and Bettinger, T. (2007) 'Gene therapy progress and prospects: ultrasound for gene transfer', *Gene therapy,* 14(6), pp. 465.
Ng, P. K. and McLaughlin, V. (2007) 'Regeneration studies of anion-exchange chromatography resins', *BioProcess International,* 5(5), pp. 52.
Ninfa, A. J., Ballou, D. P. and Benore, M. (2010) *Fundamental laboratory approaches for biochemistry and biotechnology.* Hoboken, N.J
Chichester: Wiley.
Nishimura, A., Morita, M., Nishimura, Y. and Sugino, Y. (1990) 'A rapid and highly efficient method for preparation of competent Escherichia coli cells', *Nucleic Acids Res,* 18(20), pp. 6169.
Noel, R., O'Hare, W. and Street, G. (1996) 'Thiophilic nature of divinylsulphone cross-linked agarose', *Journal of Chromatography A,* 734(2), pp. 241-246.

Nussbaum, R. L., McInnes, R. R. and Willard, H. F. (2015) *Thompson & Thompson Genetics in Medicine E-Book.* Elsevier Health Sciences.

Nweke, M., Turmaine, M., Graham McCartney, R. and Bracewell, D. (2016) *Drying techniques for the visualisation of agarose-based chromatography media by scanning electron microscopy.*

Olszewski, P., Li, J. F., Liu, D. X. and Walsh, J. L. (2014) 'Optimizing the electrical excitation of an atmospheric pressure plasma advanced oxidation process', *Journal of Hazardous Materials,* 279, pp. 60-66.

Olszewski, P., Willett, T. C., Theodosiou, E., Thomas, O. R. T. and Walsh, J. L. (2013) 'In situ modification of chromatography adsorbents using cold atmospheric pressure plasmas', *Applied Physics Letters,* 102(20), pp. 204104.

Ongkudon, C. M., Pan, S. and Danquah, M. K. (2013) 'An innovative monolithic column preparation for the isolation of 25kilo base pairs DNA', *Journal of Chromatography A,* 1318, pp. 156-162.

Padilla-Zamudio, A., Lucero-Acuña, J., Guerrero-German, P., Ortega-López, J. and Tejeda-Mansir, A. (2017) 'Efficient Disruption of Escherichia coli for Plasmid DNA Recovery in a Bead Mill', *Applied Sciences,* 8(1), pp. 30.

Pall Life Sciences (2006) *BioSepra® Chromatography Media*. http://178.250.165.133/ex/downloads/flyer/chromatog_ss2pall.pdf [Online data sheet] (Accessed: 11.09. 2018).

Pappas, D., Bujanda, A., Demaree, J. D., Hirvonen, J. K., Kosik, W., Jensen, R. and McKnight, S. (2006) 'Surface modification of polyamide fibers and films using atmospheric plasmas', *Surface and Coatings Technology,* 201(7), pp. 4384-4388.

Park, G. Y., Hong, Y. J., Lee, H. W., Sim, J. Y. and Lee, J. K. (2010) 'A Global Model for the Identification of the Dominant Reactions for Atomic Oxygen in He/O-2 Atmospheric-Pressure Plasmas', *Plasma Processes and Polymers,* 7(3-4), pp. 281-287.

Parker, A. L., Newman, C., Briggs, S., Seymour, L. and Sheridan, P. J. (2003) 'Nonviral gene delivery: techniques and implications for molecular medicine', *Expert Rev Mol Med,* 5(22), pp. 1-15.

Patil, S. D., Rhodes, D. G. and Burgess, D. J. (2005) 'DNA-based therapeutics and DNA delivery systems: A comprehensive review', *The AAPS Journal,* 7(1), pp. E61-E77.

Pawley, J. (2006) *Handbook of Biological Confocal Microscopy.* 3rd Edition edn.: Springer Science+ Business Media LLC.

Pearson, S., Jia, H. and Kandachi, K. 2004. China approves first gene therapy. Nature Publishing Group.

Pereira, L. R., Prazeres, D. M. and Mateus, M. (2010) 'Hydrophobic interaction membrane chromatography for plasmid DNA purification: Design and optimization', *J Sep Sci,* 33(9), pp. 1175-84.

Pezzini, J., Cabanne, C. and Santarelli, X. (2009) 'Comparative study of strong anion exchangers: Structure-related chromatographic performances', *Journal of Chromatography B,* 877(24), pp. 2443-2450.

Phillips, A. J. (2001) 'The challenge of gene therapy and DNA delivery', *Journal of Pharmacy and Pharmacology,* 53(9), pp. 1169-1174.

Pieracci, J., Crivello, J. V. and Belfort, G. (1999) 'Photochemical modification of 10 kDa polyethersulfone ultrafiltration membranes for reduction of biofouling', *Journal of membrane science,* 156(2), pp. 223-240.

Pieracci, J., Wood, D. W., Crivello, J. V. and Belfort, G. (2000) 'UV-assisted graft polymerization of N-vinyl-2-pyrrolidinone onto poly (ether sulfone) ultrafiltration membranes: comparison of dip versus immersion modification techniques', *Chemistry of materials,* 12(8), pp. 2123-2133.

Pinkerton, T. C. (1991) 'High-performance liquid chromatography packing materials for the analysis of small molecules in biological matrices by direct injection', *Journal of Chromatography A,* 544, pp. 13-23.

Pinto, I., Aires-Barros, M. and Azevedo, A. (2015) *Multimodal chromatography: Debottlenecking the downstream processing of monoclonal antibodies.*

Pitarresi, T. M., Herzer, S. U., Kennedy, B. and Moore, P. (2004) '138. Purification of plasmid DNA on an anion exchange column without the use of RNase to process scale', *Molecular Therapy,* 9(S1), pp. S53.

Potschka, M. (1991) 'Size exclusion chromatography of DNA and viruses: properties of spherical and asymmetric molecules in porous networks', *Macromolecules,* 24(18), pp. 5023-5039.

Prather, K. J., Sagar, S., Murphy, J. and Chartrain, M. (2003) 'Industrial scale production of plasmid DNA for vaccine and gene therapy: plasmid design, production, and purification', *Enzyme and Microbial Technology,* 33(7), pp. 865-883.

Prazeres, D. (2011) *Plasmid biopharmaceuticals : basics, applications, and manufacturing.*

Prazeres, D. M., Ferreira, G. N., Monteiro, G. A., Cooney, C. L. and Cabral, J. M. (1999) 'Large-scale production of pharmaceutical-grade plasmid DNA for gene therapy: problems and bottlenecks', *Trends Biotechnol,* 17(4), pp. 169-74.

Prazeres, D. M., Monteiro, G. A., Ferreira, G. N., Diogo, M. M., Ribeiro, S. C. and Cabral, J. M. (2001) 'Purification of plasmids for gene therapy and DNA vaccination', *Biotechnol Annu Rev,* 7, pp. 1-30.

Prazeres, D. M., Schluep, T. and Cooney, C. (1998) 'Preparative purification of supercoiled plasmid DNA using anion-exchange chromatography', *J Chromatogr A,* 806(1), pp. 31-45.

Prazeres, D. M. F. and Monteiro, G. A. (2014) 'Plasmid Biopharmaceuticals', *Microbiol Spectr,* 2(6).

Privalov, P. L., Dragan, A. I., Crane-Robinson, C., Breslauer, K. J., Remeta, D. P. and Minetti, C. A. (2007) 'What drives proteins into the major or minor grooves of DNA?', *Journal of molecular biology,* 365(1), pp. 1-9.

PubChem-Substance-Database 2016. Sepharose, SID=319348051. https://pubchem.ncbi.nlm.nih.gov/substance/319348051: National Center for Biotechnology Information.

Quaak, S. G., Nuijen, B., Haanen, J. B. and Beijnen, J. H. (2009) 'Development and validation of an anion-exchange LC-UV method for the quantification and purity determination of the DNA plasmid pDERMATT', *J Pharm Biomed Anal,* 49(2), pp. 282-8.

Rago, R., Mitchen, J. and Wilding, G. (1990) 'DNA fluorometric assay in 96-well tissue culture plates using Hoechst 33258 after cell lysis by freezing in distilled water', *Anal Biochem,* 191(1), pp. 31-4.

Ramamoorth, M. and Narvekar, A. (2015) 'Non viral vectors in gene therapy- an overview', *Journal of clinical and diagnostic research : JCDR,* 9(1), pp. GE01-GE6.

Regnier, V., Tahiri, A., Andre, N., Lemaıtre, M., Le Doan, T. and Préat, V. (2000) 'Electroporation-mediated delivery of 3′-protected phosphodiester oligodeoxynucleotides to the skin', *Journal of controlled release,* 67(2-3), pp. 337-346.

Reule, A. G. (1976) 'Errors in Spectrophotometry and Calibration Procedures to Avoid Them', *JOURNAL OF RESEARCH of the National Bureau of Standards-A. Pllysics and Chemistry,* 80A(4), pp. 609-624.

Riesmeier, B., Kroner, K. and Kula, M.-R. (1989) 'Tangential filtration of microbial suspensions: filtration resistances and model development', *Journal of biotechnology,* 12(2), pp. 153-171.

Rosenberg, S. A., Aebersold, P., Cornetta, K., Kasid, A., Morgan, R. A., Moen, R., Karson, E. M., Lotze, M. T., Yang, J. C., Topalian, S. L. and et al. (1990) 'Gene transfer into humans--immunotherapy of patients with advanced melanoma, using tumor-infiltrating lymphocytes modified by retroviral gene transduction', *N Engl J Med,* 323(9), pp. 570-8.

Rouessac, F. and Rouessac, A. (2000) *Chemical analysis : modern instrumental methods and techniques.*

Sagar, S. W., M.; Lee, A. (2003) 'Chromatography-based purification of plasmid DNA', in Rathore, A.S.V., G. (ed.) *Scale-up and optimization in preprative chromatography: principles and biopharmaceutical applications.* New York: Marcel Dekker, pp. p. 251–72.

Santos, T., Proença, Z., Queiroz, J. A., Tomaz, C. and Cruz, C. (2017) 'Plasmid purification by using a new naphthalene tripodal support', *Separation and Purification Technology,* 188, pp. 81-89.

Saunders, K. C., Ghanem, A., Boon Hon, W., Hilder, E. F. and Haddad, P. R. (2009) 'Separation and sample pre-treatment in bioanalysis using monolithic phases: A review', *Analytica Chimica Acta,* 652(1), pp. 22-31.

Schleef, M. and Schmidt, T. (2004) 'Animal-free production of ccc-supercoiled plasmids for research and clinical applications', *The Journal of Gene Medicine: A cross-disciplinary journal for research on the science of gene transfer and its clinical applications,* 6(S1), pp. S45-S53.

Schluep, T. and Cooney, C. L. (1998) 'Purification of plasmids by triplex affinity interaction', *Nucleic Acids Research,* 26(19), pp. 4524-4528.

Schram, D. C., Th, H. J. B., Kroesen, G. M. W. and Hoog, F. J. d. (1987) 'Plasma surface modification and plasma chemistry', *Plasma Physics and Controlled Fusion,* 29(10A), pp. 1353.

Schram, D. C. B., T.H.J.; Kroesen, G.M.W.; de Hoog, F.J. (1987) 'Plasma surface modification and plasma chemistry', *Plasma Physics and Controlled Fusion,* 29(10A), pp. 1353-1364.

Schroeder, M. 2016. Purification of vwf. Google Patents.

Schromm, A. B., Brandenburg, K., Loppnow, H., Zähringer, U., Rietschel, E. T., Carroll, S. F., Koch, M. H. J., Kusumoto, S. and Seydel, U. (1998) 'The Charge of Endotoxin

Molecules Influences Their Conformation and IL-6-Inducing Capacity', *The Journal of Immunology,* 161(10), pp. 5464.
Selvam, S., Thomas, P. B., Hamm-Alvarez, S. F., Schechter, J. E., Stevenson, D., Mircheff, A. K. and Trousdale, M. D. (2006) 'Current status of gene delivery and gene therapy in lacrimal gland using viral vectors', *Advanced drug delivery reviews,* 58(11), pp. 1243-1257.
Shamlou, P. A. (2003) 'Scaleable processes for the manufacture of therapeutic quantities of plasmid DNA', *Biotechnology and Applied Biochemistry,* 37(3), pp. 207-218.
Shen, C. F., Jacob, D., Zhu, T., Bernier, A., Shao, Z., Yu, X., Patel, M., Lanthier, S. and Kamen, A. (2016) 'Optimization and scale-up of cell culture and purification processes for production of an adenovirus-vectored tuberculosis vaccine candidate', *Vaccine,* 34(29), pp. 3381-3387.
Shillitoe, E. J. (2009) 'Gene therapy: the end of the rainbow?', *Head & neck oncology,* 1(1), pp. 7.
Shirley, S. A., Heller, R. and Heller, L. C. (2014) 'Electroporation gene therapy', *Gene Therapy of Cancer*: Elsevier, pp. 93-106.
Shukla, A. A. and Yigzaw, Y. (2007) 'Modes of preparative chromatography', *BIOTECHNOLOGY AND BIOPROCESSING SERIES,* 31, pp. 179.
Silva-Santos, A. R., Alves, C. P. A., Prazeres, D. M. F. and Azevedo, A. M. (2016) 'Separation of plasmid DNA topoisomers by multimodal chromatography', *Analytical Biochemistry,* 503, pp. 68-70.
Silva-Santos, A. R., Alves, C. P. A., Prazeres, D. M. F. and Azevedo, A. M. (2017) 'A process for supercoiled plasmid DNA purification based on multimodal chromatography', *Separation and Purification Technology,* 182, pp. 94-100.
Sinden, R. R. (1994) *DNA structure and function.*
Singer, A., Eiteman, M. A. and Altman, E. (2009) 'DNA plasmid production in different host strains of Escherichia coli', *J Ind Microbiol Biotechnol,* 36(4), pp. 521-30.
Smrekar, V., Smrekar, F., Štrancar, A. and Podgornik, A. (2013) 'Single step plasmid DNA purification using methacrylate monolith bearing combination of ion-exchange and hydrophobic groups', *Journal of Chromatography A,* 1276, pp. 58-64.
Somasundaram, B., Chang, C., Fan, Y. Y., Lim, P.-Y., Cardosa, J. and Lua, L. (2016) 'Characterizing Enterovirus 71 and Coxsackievirus A16 virus-like particles production in insect cells', *Methods,* 95, pp. 38-45.
Sonnenfeld, A. and Thömmes, J. (2006) *Process scale bioseparations for the biopharmaceutical industry.* CRC Press, p. 59 ff.
Sousa, A., Bicho, D., Tomaz, C. T., Sousa, F. and Queiroz, J. A. (2011) 'Performance of a non-grafted monolithic support for purification of supercoiled plasmid DNA', *Journal of chromatography. A,* 1218(13), pp. 1701-1706.
Sousa, Â., Pereira, P., Sousa, F. and Queiroz, J. A. (2014) 'Binding mechanisms for histamine and agmatine ligands in plasmid deoxyribonucleic acid purifications', *Journal of Chromatography A,* 1366, pp. 110-119.
Sousa, A., Sousa, F. and Queiroz, J. A. (2012) 'Advances in chromatographic supports for pharmaceutical-grade plasmid DNA purification', *J Sep Sci,* 35(22), pp. 3046-58.

Sousa, F., Cruz, C. and Queiroz, J. A. (2010a) 'Amino acids–nucleotides biomolecular recognition: from biological occurrence to affinity chromatography', *Journal of Molecular Recognition,* 23(6), pp. 505-518.
Sousa, F., Matos, T., Prazeres, D. M. F. and Queiroz, J. A. (2008a) 'Specific recognition of supercoiled plasmid DNA in arginine affinity chromatography', *Analytical Biochemistry,* 374(2), pp. 432-434.
Sousa, F., Passarinha, L. and Queiroz, J. A. (2010b) 'Biomedical application of plasmid DNA in gene therapy: a new challenge for chromatography', *Biotechnology & genetic engineering reviews,* 26, pp. 83.
Sousa, F., Prazeres, D. M. F. and Queiroz, J. A. (2008b) 'Affinity chromatography approaches to overcome the challenges of purifying plasmid DNA', *Trends in Biotechnology,* 26(9), pp. 518-525.
Souverain, S., Rudaz, S. and Veuthey, J. L. (2004) 'Restricted access materials and large particle supports for on-line sample preparation: an attractive approach for biological fluids analysis', *Journal of Chromatography B,* 801(2), pp. 141-156.
Stadler, J., Lemmens, R. and Nyhammar, T. (2004) 'Plasmid DNA purification', *J Gene Med,* 6 Suppl 1, pp. S54-66.
Stocks, S. M. (2004) 'Mechanism and use of the commercially available viability stain, BacLight', *Cytometry A,* 61(2), pp. 189-95.
Strancar, A., Podgornik, A., Barut, M. and Necina, R. (2002) 'Short monolithic columns as stationary phases for biochromatography', *Advances in biochemical engineering/biotechnology,* 76, pp. 49-85.
Su, C.-H., Wu, Y.-J., Wang, H.-H. and Yeh, H.-I. (2012) 'Nonviral gene therapy targeting cardiovascular system', *American Journal of Physiology-Heart and Circulatory Physiology,* 303(6), pp. H629-H638.
Sudo, Y., Miyagawa, R. and Takahata, Y. (1998) 'Method for the preparation of restricted access media by low-temperature plasma treatment', *Journal of Chromatography B: Biomedical Sciences and Applications,* 705(1), pp. 55-62.
Sumita, C., Baba, Y., Hide, K., Ishimaru, N., Samata, K., Tanaka, A. and Tsuhako, M. (1994) 'Comparative study of non-porous anion-exchange chromatography, capillary gel electrophoresis and capillary electrophoresis in polymer solutions in the separation of DNA restriction fragments', *Journal of Chromatography A,* 661(1-2), pp. 297-303.
Summers, D. (2009) *The biology of plasmids.* John Wiley & Sons.
Svec, F. and Fréchet, J. M. J. (1995) 'Modified poly(glycidyl metharylate-co-ethylene dimethacrylate) continuous rod columns for preparative-scale ion-exchange chromatography of proteins', *Journal of Chromatography A,* 702(1-2), pp. 89-95.
Swartz, J. R. (2001) 'Advances in Escherichia coli production of therapeutic proteins', *Current opinion in biotechnology,* 12(2), pp. 195-201.
Tan, L., Lai, W.-B., Lee, C. T., Kim, D. S. and Choe, W.-S. (2007) 'Differential interactions of plasmid DNA, RNA and endotoxin with immobilised and free metal ions', *Journal of Chromatography A,* 1141(2), pp. 226-234.
Temmerman, E., Akishev, Y., Trushkin, N., Leys, C. and Verschuren, J. (2005) 'Surface modification with a remote atmospheric pressure plasma: dc glow discharge and surface streamer regime', *Journal of Physics D: Applied Physics,* 38(4), pp. 505.

Tennikova, T. B. and Svec, F. (1993) 'High-performance membrane chromatography: Highly efficient separation method for proteins in ion-exchange, hydrophobic interaction and reversed-phase modes', *Journal of Chromatography A,* 646(2), pp. 279-288.
Thatcher, D., Hitchcock, A., Hanak, J. and Varley, D. (1997) 'Method of plasmid Production and Purification', *International Patent Application WO/29190*.
Theodossiou, I., Collins, I., Ward, J., Thomas, O. and Dunnill, P. (1997) 'The processing of a plasmid-based gene from E. coli. Primary recovery by filtration', *Bioprocess engineering,* 16(3), pp. 175-183.
Theodossiou, I., Olander, M. A., Søndergaard, M. and Thomas, O. R. (2000) 'New expanded bed adsorbents for the recovery of DNA', *Biotechnology letters,* 22(24), pp. 1929-1933.
Theodossiou, I., Sondergaard, M. and Thomas, O. R. (2001) 'Design of expanded bed supports for the recovery of plasmid DNA by anion exchange adsorption', *Bioseparation,* 10(1-3), pp. 31-44.
Theodossiou, I. and Thomas, O. R. (2002) 'DNA-induced inter-particle cross-linking during expanded bed adsorption chromatography. Impact on future support design', *J Chromatogr A,* 971(1-2), pp. 73-86.
Thomas, C. M. S., D. (2008) 'Bacterial Plasmids', *eLS*.
Tiainen, P., Gustavsson, P.-E., Ljunglöf, A. and Larsson, P.-O. (2007a) 'Superporous agarose anion exchangers for plasmid isolation', *Journal of Chromatography A,* 1138(1), pp. 84-94.
Tiainen, P., Gustavsson, P.-E., Månsson, M.-O. and Larsson, P.-O. (2007b) 'Plasmid purification using non-porous anion-exchange silica fibres', *Journal of Chromatography A,* 1149(2), pp. 158-168.
Tiainen, P., Gustavsson, P. E., Ljunglof, A. and Larsson, P. O. (2007c) 'Superporous agarose anion exchangers for plasmid isolation', *J Chromatogr A,* 1138(1-2), pp. 84-94.
Tiainen, P., Gustavsson, P. E., Mansson, M. O. and Larsson, P. O. (2007d) 'Plasmid purification using non-porous anion-exchange silica fibres', *J Chromatogr A,* 1149(2), pp. 158-68.
Tichonovas, M., Krugly, E., Racys, V., Hippler, R., Kauneliene, V., Stasiulaitiene, I. and Martuzevicius, D. (2013) 'Degradation of various textile dyes as wastewater pollutants under dielectric barrier discharge plasma treatment', *Chemical Engineering Journal,* 229, pp. 9-19.
Tinnes, R. and Hoare, M. (1992) 'The biocontainment of a high speed disc bowl centrifuge', *Bioprocess Engineering,* 8(3-4), pp. 165-172.
Trombotto, S., Violet-Courtens, E., Cottier, L. and Queneau, Y. (2004) 'Oxidation of Two Major Disaccharides: Sucrose and Isomaltulose', *Topics in Catalysis,* 27(1), pp. 31-37.
Tseng, W. C., Jian, L. M. and Fang, T. Y. (2005) 'Effects of Buffer Ions on Isopropanol-Enhanced Plasmid Purification Using Q-Sepharose', *Separation science and technology,* 39(8), pp. 1761-1778.
Tseng, Y.-F., Weng, T.-C., Lai, C.-C., Chen, P.-L., Lee, M.-S. and Hu, A. Y.-C. (2018) 'A fast and efficient purification platform for cell-based influenza viruses by flow-through chromatography', *Vaccine,* 36(22), pp. 3146-3152.
Tyn, M. T. and Gusek, T. W. (1990) 'Prediction of diffusion coefficients of proteins', *Biotechnology and bioengineering,* 35(4), pp. 327-338.

Ulbricht, M. and Belfort, G. (1995) 'Surface modification of ultrafiltration membranes by low temperature plasma. I. Treatment of polyacrylonitrile', *Journal of applied polymer science,* 56(3), pp. 325-343.

uniQure 2012. uniQure's Glybera® First Gene Therapy Approved by European Commission. *First Gene Therapy Approved by European Commission.* https://web.archive.org/web/20121105033602/http://www.uniqure.com/news/167/182/uniQure-s-Glybera-First-Gene-Therapy-Approved-by-European-Commission.html.

Urthaler, J., Buchinger, W. and Necina, R. (2005a) 'Improved downstream process for the production of plasmid DNA for gene therapy', *Acta Biochim Pol,* 52(3), pp. 703-11.

Urthaler, J., Buchinger, W. and Necina, R. (2005b) 'Industrial Scale cGMP Purification of Pharmaceutical Grade Plasmid-DNA', *Chemical Engineering & Technology,* 28(11), pp. 1408-1420.

Urthaler, J., Schlegl, R., Podgornik, A., Strancar, A., Jungbauer, A. and Necina, R. (2005c) 'Application of monoliths for plasmid DNA purification: Development and transfer to production', *Journal of Chromatography A,* 1065(1), pp. 93-106.

Varley, D., Hitchcock, A., Weiss, A., Horler, W., Cowell, R., Peddie, L., Sharpe, G., Thatcher, D. and Hanak, J. (1999) 'Production of plasmid DNA for human gene therapy using modified alkaline cell lysis and expanded bed anion exchange chromatography', *Expanded Bed Chromatography*: Springer, pp. 209-217.

Verma, I. M. (2013) 'Gene Therapy That Works', *Science,* 341(6148), pp. 853.

Vickerman, J. C., Briggs, D. and SurfaceSpectra, L. (2001) *ToF-SIMS : surface analysis by mass spectrometry.*

Viloria-Cols, M. E., Hatti-Kaul, R. and Mattiasson, B. (2004) 'Agarose-coated anion exchanger prevents cell-adsorbent interactions', *J Chromatogr A,* 1043(2), pp. 195-200.

Walsh, J. L. and Kong, M. G. (2007) '10 ns pulsed atmospheric air plasma for uniform treatment of polymeric surfaces', *Applied Physics Letters,* 91(25), pp. 251504.

Watson, J. D. and Crick, F. H. (1953) 'Molecular structure of nucleic acids; a structure for deoxyribose nucleic acid', *Nature,* 171(4356), pp. 737-8.

Weigel, T., Solomaier, T., Peuker, A., Pathapati, T., Wolff, M. W. and Reichl, U. (2014) 'A flow-through chromatography process for influenza A and B virus purification', *Journal of Virological Methods,* 207, pp. 45-53.

Weitzhandler, M., Farnan, D., Horvath, J., Rohrer, J. S., Slingsby, R. W., Avdalovic, N. and Pohl, C. (1998) 'Protein variant separations by cation-exchange chromatography on tentacle-type polymeric stationary phases', *Journal of Chromatography A,* 828(1-2), pp. 365-372.

WHO (2007) *Quality assurance of pharmaceuticals.* WHO, 2007.

Williams, J. A., Luke, J., Langtry, S., Anderson, S., Hodgson, C. P. and Carnes, A. E. (2009) 'Generic plasmid DNA production platform incorporating low metabolic burden seed-stock and fed-batch fermentation processes', *Biotechnol Bioeng,* 103(6), pp. 1129-43.

Wils, P., Escriou, V., Warnery, A., Lacroix, F., Lagneaux, D., Ollivier, M., Crouzet, J., Mayaux, J. F. and Scherman, D. (1997) 'Efficient purification of plasmid DNA for gene transfer using triple-helix affinity chromatography', *Gene Therapy,* 4(4), pp. 323-330.

Wilson, J. M. (2005) 'Gendicine: The First Commercial Gene Therapy Product; Chinese Translation of Editorial', *Human Gene Therapy,* 16(9), pp. 1014-1015.

Wilson, J. M. (2009) 'A History Lesson for Stem Cells', *Science,* 324(5928), pp. 727.
Wolff, J. A., Malone, R. W., Williams, P., Chong, W., Acsadi, G., Jani, A. and Felgner, P. L. (1990) 'Direct gene transfer into mouse muscle in vivo', *Science,* 247(4949 Pt 1), pp. 1465-8.
Wu, N. and Ataai, M. M. (2000) 'Production of viral vectors for gene therapy applications', *Current Opinion in Biotechnology,* 11(2), pp. 205-208.
Xenopoulos, A. and Pattnaik, P. (2014) 'Production and purification of plasmid DNA vaccines: is there scope for further innovation?', *Expert Rev Vaccines,* 13(12), pp. 1537-51.
Xi, S. and Grandis, J. (2003) 'Gene therapy for the treatment of oral squamous cell carcinoma', *Journal of dental research,* 82(1), pp. 11-16.
Xiaogui, L., Chunsheng, R., Tengcai, M., Yan, F. and Dezhen, W. (2012) 'An atmospheric large-scale cold plasma jet', *Plasma Science and Technology,* 14(9), pp. 799.
Xu, D. Z. X., F. F. (2017) *Plasma surface metallurgy with double glow discharge technology.* New York, NY: Springer Berlin Heidelberg.
Yakovchuk, P., Protozanova, E. and Frank-Kamenetskii, M. D. (2006) 'Base-stacking and base-pairing contributions into thermal stability of the DNA double helix', *Nucleic acids research,* 34(2), pp. 564.
Yamakawa, H., Higashino, K.-i. and Ohara, O. (1996) 'Sequence-dependent DNA separation by anion-exchange high-performance liquid chromatography', *Analytical biochemistry,* 240(2), pp. 242-250.
Yan, Y., Zhang, Z., Stokes, J. R., Zhou, Q.-Z., Ma, G.-H. and Adams, M. J. (2009) 'Mechanical characterization of agarose micro-particles with a narrow size distribution', *Powder Technology,* 192(1), pp. 122-130.
Yang, B., Jeang, J., Yang, A., Wu, T. and Hung, C.-F. (2014) 'DNA vaccine for cancer immunotherapy', *Human vaccines & immunotherapeutics,* 10(11), pp. 3153-3164.
Yang, N.-S., Sun, W. H. and McCabe, D. (1996) 'Developing particle-mediated gene-transfer technology for research into gene therapy of cancer', *Molecular medicine today,* 2(11), pp. 476-481.
Yang, Y. and Geng, X. (2011) 'Mixed-mode chromatography and its applications to biopolymers', *Journal of Chromatography A,* 1218(49), pp. 8813-8825.
Yao, Y. and Lenhoff, A. M. (2004) 'Determination of pore size distributions of porous chromatographic adsorbents by inverse size-exclusion chromatography', *Journal of Chromatography A,* 1037(1), pp. 273-282.
Yin, H., Kanasty, R. L., Eltoukhy, A. A., Vegas, A. J., Dorkin, J. R. and Anderson, D. G. (2014) 'Non-viral vectors for gene-based therapy', *Nat Rev Genet,* 15(8), pp. 541-55.
Yin, H., Kauffman, K. J. and Anderson, D. G. (2017) 'Delivery technologies for genome editing', *Nature Reviews. Drug Discovery,* 16(6), pp. 387-399.
Zabicky, J. and Nutkovitch, M. (1986) 'Reactions of bromine and cyclohexene in aqueous media. Selectivity of bromohydrin vs. dibromo adduct formation', *Industrial & engineering chemistry product research and development,* 25(2), pp. 372-375.
Zeng, X. and Ruckenstein, E. (1999) 'Membrane chromatography: Preparation and applications to protein separation', *Biotechnology Progress,* 15(6), pp. 1003-1019.
Zhang, H., Kong, S., Booth, A., Boushaba, R., Levy, M. S. and Hoare, M. (2007) 'Prediction of shear damage of plasmid DNA in pump and centrifuge operations using an ultra scale-down device', *Biotechnology progress,* 23(4), pp. 858-865.

Zhang, L., Nolan, E., Kreitschitz, S. and Rabussay, D. P. (2002) 'Enhanced delivery of naked DNA to the skin by non-invasive in vivo electroporation', *Biochimica et Biophysica Acta (BBA)-General Subjects,* 1572(1), pp. 1-9.

Zhao, D., Sun, B., Jiang, H., Sun, S., Kong, F., Ma, Y., Jiang, L., Bai, L., Chen, X. and Yang, P. (2015) 'Enterovirus71 virus-like particles produced from insect cells and purified by multistep chromatography elicit strong humoral immune responses in mice', *Journal of applied microbiology,* 119(4), pp. 1196-1205.

Zhou, Q.-Z., Wang, L.-Y., Ma, G.-H. and Su, Z.-G. (2007) 'Preparation of uniform-sized agarose beads by microporous membrane emulsification technique', *Journal of colloid and interface science,* 311(1), pp. 118-127.

Zöchling, A., Hahn, R., Ahrer, K., Urthaler, J. and Jungbauer, A. (2004) 'Mass transfer characteristics of plasmids in monoliths', *Journal of Separation Science,* 27(10-11), pp. 819-827.

**完**